MANITOBA

INVEST. BUILD. GROW

REPORT OF ACTIVITIES 2018

Manitoba Geological Survey

Manitoba

REPORT OF ACTIVITIES
2018

Manitoba Growth, Enterprise and Trade
Manitoba Geological Survey

Manitoba

Manitoba Growth, Enterprise and Trade 2018: Report of Activities 2018; Manitoba Growth, Enterprise and Trade, Manitoba Geological Survey, 178 p.

Published by:
Manitoba Growth, Enterprise and Trade
Manitoba Geological Survey
360–1395 Ellice Avenue
Winnipeg, Manitoba
R3G 3P2 Canada

Telephone: 1-800-223-5215 (General Enquiry)
204-945-6569 (Publication Sales)
Fax: 204-945-8427
E-mail: minesinfo@gov.mb.ca
Website: manitoba.ca/minerals

ISBN No.: 978-0-7711-1591-2

The materials in this publication are available to download free of charge at manitoba.ca/minerals

Front cover photos:
Left: MGS geologist Kyle Reid analyzes drillcore at Snow Lake (GS2018-5, this volume).
Right: MGS geologist Tyler Hodder sampling Quaternary sediment exposed along a tributary to the Echoing River, northeast Manitoba (GS2018-13, this volume).

REPORT OF ACTIVITIES 2018

A message from the Minister:

As Minister of Growth, Enterprise and Trade, I am pleased to introduce the Manitoba Geological Survey's annual *Report of Activities*. This year's edition features 14 comprehensive professional geoscience reports, laying new groundwork and expanding the knowledge base for future investment decisions, exploration, and development of our province's valuable mineral resources.

This annual volume continues to raise the bar for geoscience excellence, with 2018 marking 50 years of annual reporting by the Manitoba Geological Survey, which also happens to turn 90 years old this year. Beginning in 1928, annual reports from the Mines Branch paved the way for the Survey's 1968 *Summary of Geological Field Work*, which featured reports and maps from Rice Lake, Wanipigow, Bissett, Pakwa and Pistol Lakes, Kettle Rapids in the Moose Lake area, Lake St. Martin, Turtle Mountain, and stratigraphic studies of southwest Manitoba. In 1976, the title changed to *Report of Field Activities*, which evolved again in 1990 into today's *Report of Activities*.

To accompany the information found in this volume, I encourage you to access the wealth of geoscience information found on the Survey's website at Manitoba.ca/minerals. There you will find hundreds of databases, reports, maps, and publications to assist you in your research and strategic planning.

Mining and petroleum continue to make up the largest primary resource industry of Manitoba's economy. By working together with First Nations and northern communities, industry representatives and other interest groups, I am confident we are on the path to a promising future of positive sustainability, renewal and growth.

Remember, in Manitoba there's *always* more to explore!

Honourable Blaine Pedersen
Minister of Growth, Enterprise and Trade

In Memoriam: Paul Gilbert

Paul Gilbert passed away in Winnipeg on December 16, 2017.

Paul was born in Piltdown, England on May 21, 1948 and completed a BSc in Geology at Bristol University, England in 1970. He and his wife Jeannie came to Canada in 1970 and made their home in Winnipeg.

Paul completed 43+ years of service as a geologist with the Manitoba Geological Survey (MGS), enjoyed rugged summer field seasons in Manitoba throughout his career, and authored or co-authored at least 163 publications. Major projects and milestones include:

- 1971–73: Paul's first mapping project on the Greenstone Project: Knee, Oxford and Gods lakes
- 1974–75: Karsakuwigamak Lake (NTS 64B5)
- 1976–82: Lynn Lake Project with E. Syme and H. Zwanzig plus mapping of eastern extension at Melvin, Barrington and Fraser lakes
- 1983–85: Island Lake project; also released final maps for the Greenstone Project which Paul compiled from the work of all the geologists who had contributed towards the project but had left the Survey
- 1986–91: Flin Flon North Flank Project: Tartan, Embury and Aimée lakes
- 1992–95: Wekusko Lake; 1993 final report for Melvin, Barrington and Fraser lakes
- 1996–99: Flin Flon North Flank Project: Lac Aimée, Naosap lakes
- 1999–2000: Max Lake—Aswapiswanan lakes area (Oxford House—Cross Lake area)
- 2001–04: Flin Flon North Flank Project: Wabishkok, Alberts and Blueberry lakes
- 2005: Wekusko Lake
- 2005–12: Bird River belt mapping
- 2012: Final report for Flin Flon North Flank Project
- 2013–2014: Bird River belt compilation

As for stories, there are many that relate to Paul's oneness of working and living in the bush, his great endurance, patience, maybe stubbornness, and always his kind helpfulness and boundless generosity. To pick one, as told by Ric Syme (MGS Director, 2000–2012):

Dave McRitchie (MGS Director, 1975-1997) was visiting Paul in the field one summer when Paul was recuperating from one of his inevitable knee problems. Paul always went so hard in the field that sooner or later he had a fall that caused him some pain for a week or two. Of course, Paul being Paul, he would not take it easy or seek medical care. Each time he was injured he simply got himself a suitable staff to lean on and continued work. On the occasion of Dave McRitchie's visit, Paul was walking with the aid of a staff and out they went, on a trip through Paul's field area. Dave McRitchie's way of operating was reminiscent of Paul's: go hard, find an outcrop, hammer the rocks into small piles. So he did, leaving the limping, staff-wielding Paul behind. As Dave told the story, he was busy sampling an outcrop at the bottom of a hill when he heard something, and looked up. There, backlit by the sun, was a vision truly from the Old Testament ... the dark form of a heavily bearded biblical prophet, unbrushed hair blowing in the wind, clothing in tatters, leaning on a tall staff, surrounded by a brilliant halo of sunbeams. Very nearly a religious experience for Dave, certainly one he repeated to us often.

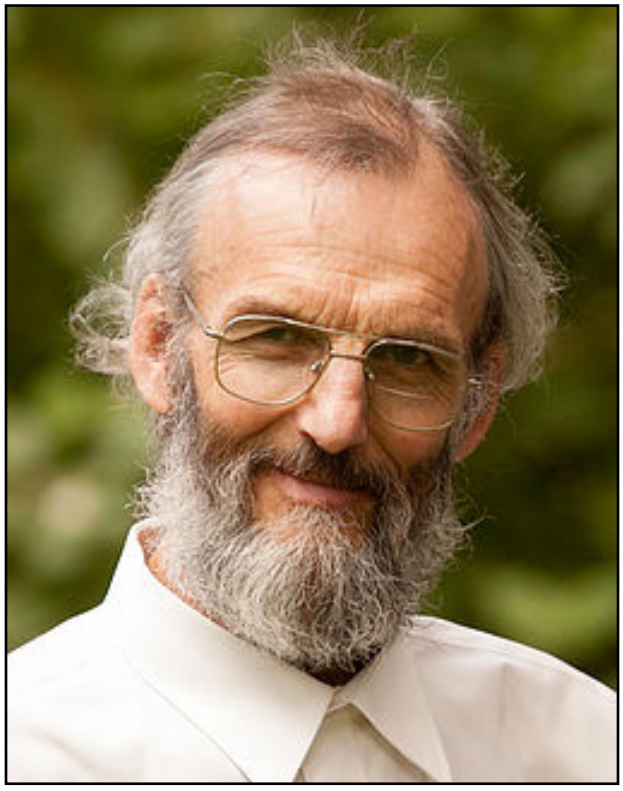

Paul was physically very fit and active, cycled wherever possible and enjoyed hiking and mountaineering trips in the Rockies. Paul was passionate about photography and choral singing. He believed strongly in animal welfare, and dogs especially held an important place in his life.

Paul was dedicated to his family and to helping others however he could.

In July 2014 he survived a severe cycling accident, and was quadriplegic and ventilator-dependent for the remainder of his life. Paul will be missed by friends and colleagues. We remain saddened by the loss of a most kind, generous and energetic member of the geological community. Paul will be remembered as the epitome of a gentleman. His gracious manner, gentle spirit, patient nature, and honest philosophy reflected in all he did. Paul is survived by his wife Jeannie, son Jonathan (Elliana) and grandchildren, and daughter Laura of Winnipeg, his sister Jancis (John Ham) of Lewes, England, and his brother Anthony, of Dalby, Australia.

In Memoriam: Clint Milligan

George Clinton Milligan died January 23, 2018 in Halifax, Nova Scotia, aged 98.

Clint was born at Tyne Valley, P.E.I. in 1919, as the son of Arthur Wesley and Fannie Isabelle (Brown) Milligan. He was educated at Prince of Wales College, Charlottetown, where he was the Governor-General's silver medalist in 1939; at Dalhousie University, Halifax (Dipl.Eng., BSc, MSc); and at Harvard University, Boston, Mass. (AM, PhD). A veteran of the Second World War, he served in England, as meteorological officer with HQ 1 Cdn Corps in Italy and the Netherlands.

From 1950 until 1957 Clint served as a geologist with the provincial Department of Mines and Natural Resources in Manitoba. During this time he worked on Precambrian geology and mineral resource projects in the Utik–Bear lakes area, northern Superior craton, in the Lower Seal River area, as well as in the Lynn Lake belt. The latter, which was also his PhD thesis at Harvard, is captured in Mines Branch Publication 57-1: Geology of the Lynn Lake District, including a series of beautiful, full-coloured (!) geological maps and sections still used by geologists today.

Between 1962 and 1967 Clint did geological survey work in the highlands of Cape Breton for the Province of Nova Scotia. From 1957 to 1985 he taught in the Geology Department of Dalhousie and was that department's advisor to undergraduate students. The student lounge in the Life Sciences Building, Dalhousie University was named in his honour in recognition of his dedication to undergraduates. Professor Milligan was Assistant Dean of Science from 1988 to 1990 when he retired.

Dr. Clint Milligan was a life member of the Association of Professional Engineers of Nova Scotia, and of the Canadian Institute of Mining, Metallurgy and Petroleum, a Fellow of the Geological Association of Canada, and a former president of

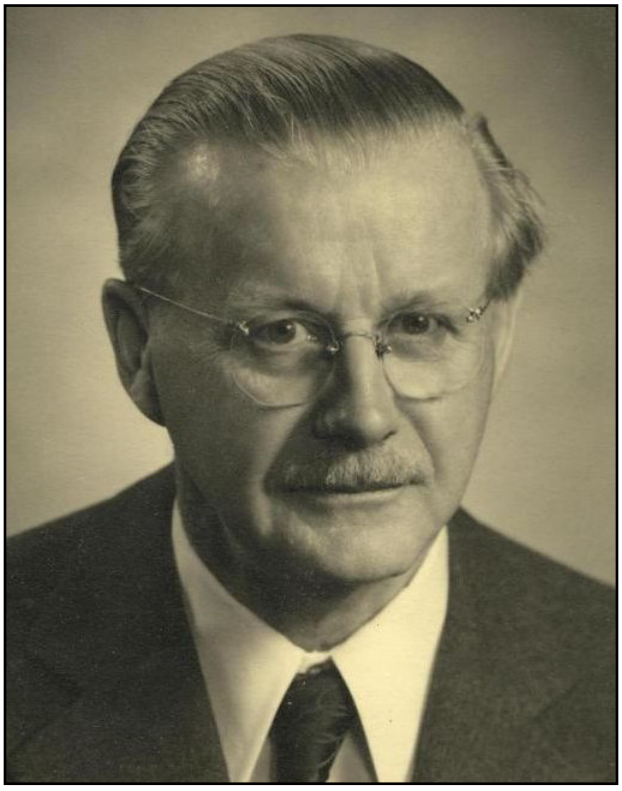

the Nova Scotian Institute of Science. He was a volunteer with UNICEF Canada, the Dartmouth Food Bank, the Nova Scotia Museum and with Scientists in the Schools. Clint is survived by his daughter, Marlene Davis, daughter Betty Ann Aaboe-Milligan and her husband Kim, his son Jayar Milligan and his wife Jenny, along with five grandchildren and five great-grandchildren.

Foreword

I am pleased to present the Manitoba Geological Survey's *Report of Activities 2018*.

This year marks the 90th anniversary of the Manitoba Geological Survey (MGS), a milestone that is significant and deserves celebration.

The MGS is the Province of Manitoba's centre of excellence for scientific research and mapping of Manitoba's key geological features and the public inventory of our vast mineral resources. The MGS team of geologists, technologists, and information managers are of the highest calibre and are held in great regard by academia, industry, communities, and other levels of government. This is a team that has demonstrated success in a most challenging year to deliver high quality results as presented in this 50th edition of the *Report of Activities*. I would like to thank each and every team member for their professional contributions and continued support for increasing the knowledge base of Manitoba's geological footprint.

The agility demonstrated by the MGS this year to deliver on project objectives in a time when government is focused on returning to a balanced budget has been exceptional and showcases the highest level of professional integrity. Manitoba is fortunate to have the commitment of this incredibly skilled team. Their dedication and passion for bringing forth new discoveries, and continuing to research existing bodies of knowledge, is how we will continue to build on the examination of Manitoba's geological composition.

It is of great importance to note that the MGS serves the people of Manitoba by providing a scientific, evidence-based approach to enhancing the geological picture through research and mapping, thereby supporting the responsible stewardship and development of our mineral resources, including oil and gas. This public inventory of geoscientific information is critical to stimulating investment, supporting responsible land use planning, and making strategic infrastructure decisions. Knowing what we have, where it is, and how it best serves Manitobans is of critical importance in making regulatory and tenure decisions regarding Manitoba's mineral resources.

It is also of significance that Manitoba is home to large areas of high mineral potential in remote, northern, and relatively underexplored regions. These regions represent a potential avenue for considerable economic growth in our province. The MGS is best positioned to move forward this agenda by focusing strategic efforts on the areas of the province where mineral development potential is greatest. This year, Manitoba has had a focus on increasing transparency and predictability of return on investment and ensuring a clear path forward on mineral development. As the Department focuses on increasing the participation of Indigenous communities in exploration and development projects, the support of the MGS to provide maps and expertise to decision makers has been critical.

Highlights for 2018 included a transformation of services, such as developing plans for the further integration of innovative technology into field work, and a focus on partnership and collaboration. It is recognized that our many partners have made this year's activities possible. In particular, we recognize collaboration with:

- Geological Survey of Canada
- Ontario Geological Survey
- Saskatchewan Geological Survey
- Canada-Nunavut Geoscience Office
- De Beers Group of Companies
- Hudbay Minerals Inc.
- Anglo American
- Vale Manitoba
- Alamos Gold Inc.
- Grid Metals Corp.
- Royal Nickel Corp.
- Rockcliff Metals Corp.
- Far Resources Ltd.
- Orix Geoscience Inc.
- Strider Resources Ltd.
- University of Manitoba
- Brandon University
- University of Calgary
- University of Waterloo
- University of Saskatchewan
- Western University
- University of Windsor
- Laurentian University
- University of Toronto
- University of New Brunswick
- University of Alberta
- Skidmore College (Saratoga Springs, NY)

The following acknowledges changes in the MGS over the past year:

- B. Lenton, Cartographer, retired in January 2018 with 27 years and 2 months of service
- P. Lenton, Manager, Geoscience Information section, retired in January 2018 with 43 years and 7 months of service

- M. Timcoe, Cartographer, retired in April 2018 with 37 years and 4 months of service
- N. Brandson, Field Support Manager, retired in September 2018 with 41 years and 4 months of service
- S. Anderson departed the MGS in August 2018 to pursue opportunities in the private sector after serving as Chief Geologist, Precambrian Geoscience section
- C. Bohm returned to Chief Geologist of the Precambrian Geoscience Section after serving on the Department's senior leadership team for service transformation

In conclusion, the results presented in this report are a representation of the hard work and dedication of the staff of the MGS. Should you have questions or be interested in more detailed information, please contact us at 204-945-1119.

Alisa Ramrattan

Acting Director, Mines Branch and Geological Survey

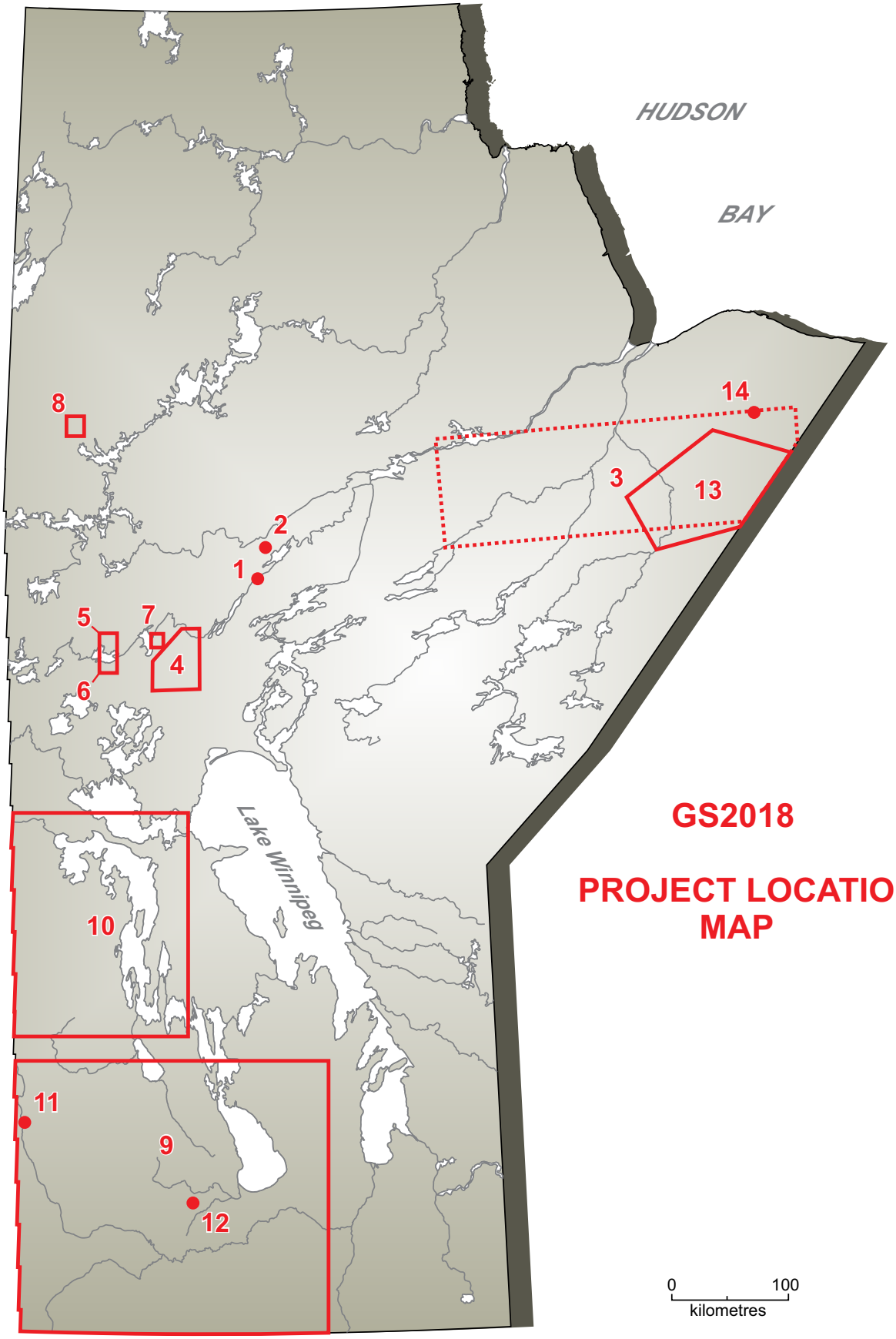

GS2018

PROJECT LOCATION MAP

Table of Contents

PRECAMBRIAN

PHANEROZOIC

QUATERNARY

PUBLICATIONS

GS2018-1

Re-examination of drillcore from southern Phillips Lake, and the possibility of a new nickel-mineralization–hosting sequence in the Thompson nickel belt, central Manitoba (part of NTS 63O1)

by C.G. Couëslan

In Brief:

- A mineralized ultramafic intrusion at southern Phillips Lake is hosted by a suite of metasedimentary rocks that appear to be distinct from the Ospwagan Group
- Metasedimentary rocks may have affinity with the Paleoproterozoic Paint sequence
- Ultramafic bodies hosted in Paint sequence rocks could be a viable exploration target for Ni-Cu deposits in the eastern Thompson nickel belt

Citation:
Couëslan, C.G. 2018: Re-examination of drillcore from southern Phillips Lake, and the possibility of a new nickel-mineralization–hosting sequence in the Thompson nickel belt, central Manitoba (part of NTS 63O1); *in* Report of Activities 2018, Manitoba Growth, Enterprise and Trade, Manitoba Geological Survey, p. 1–16.

Summary

A mineralized ultramafic intrusion at southern Phillips Lake, along the eastern Thompson nickel belt (TNB), is hosted by a suite of granulite-facies gneisses that have been variously interpreted as Archean orthogneiss, Proterozoic Ospwagan group rocks and, most recently, Proterozoic Paint sequence rocks. A simplified stratigraphy, from the structural hangingwall to the footwall, in the vicinity of the ultramafic body consists of the following: biotite-hornblende gneiss, interpreted as part of the Archean basement; multicomponent gneiss, consisting of a variety of gneissic phases typically interlayered on a scale <10 m and likely representing tectonically interleaved Archean and Proterozoic phases; metawacke, consisting of interlayered biotite-garnet and biotite-orthopyroxene gneisses with local layers of diffusely banded silicate-facies iron formation; calcsilicate and impure marble; peridotite with increasing sulphide content toward the structural footwall contact; additional metawacke; mafic gneiss, likely representing either an Archean layered mafic complex or volcanic suite; and a succession of disrupted metawacke with local layers of well-banded silicate-facies iron formation. All of the previously listed phases are intruded by granitic pegmatite and, with the exception of the peridotite, metadiabase dikes.

Normalized, multi-element profiles of the metawacke suggest an affinity to Paint sequence rocks. The geochemical affinity of the calcsilicate and impure marble remains unconstrained. Current models for the generation of Ni-Cu deposits in the TNB call for the intrusion of ultramafic magmas into sulphidic Ospwagan group rocks, leading to sulphur saturation of the magma and the precipitation and concentration of Ni-Cu sulphides. Preliminary results suggest the mineralized peridotite at southern Phillips Lake is hosted by Paint sequence rocks. This implies ultramafic intrusions in Paint sequence rocks could be viable exploration targets in the TNB; however, the calcareous rocks of unknown affinity could also indicate the presence of Ospwagan group rocks at southern Phillips Lake. Additional work is required to constrain the affinity of the calcareous rocks.

Introduction

Phillips Lake is located 60 km south-southwest of Thompson in the eastern TNB (Figure GS2018-1-1). Inco Ltd. (now Vale Canada Ltd.) conducted airborne and ground geophysical surveys, diamond-drilling and outcrop mapping in the southern Phillips Lake area from 1952 to 1975 (Assessment File 92118, Manitoba Growth, Enterprise and Trade, Winnipeg). Their work led to the discovery of one large, and several smaller, ultramafic bodies in the area. Drillcore logging and mapping also resulted in the recognition of metasedimentary rocks, including 'skarn' and iron formation, that were restricted to narrow bands in the enclosing gneiss. Later work by Falconbridge Ltd. (now Glencore plc) from 1980 to 1996 (Assessment Files 94497, 94506) delineated an ultramafic body with >1800 m strike length and significant Ni-mineralization along the footwall contact (Figure GS2018-1-2). Falconbridge geologists interpreted the ultramafic body to be hosted in Archean gneiss; however, regional compilation mapping by the Manitoba Geological Survey (MGS) suggested that the mineralized ultramafic body was hosted by a 'ghost succession' of the Ospwagan group (Figure GS2018-1-3; Macek et al., 2006; McGregor et al., 2006; Zwanzig et al., 2007). To date, all Ni deposits identified in the TNB have consisted of ultramafic

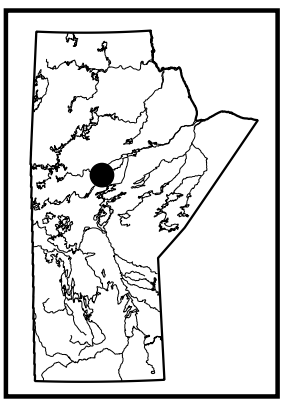

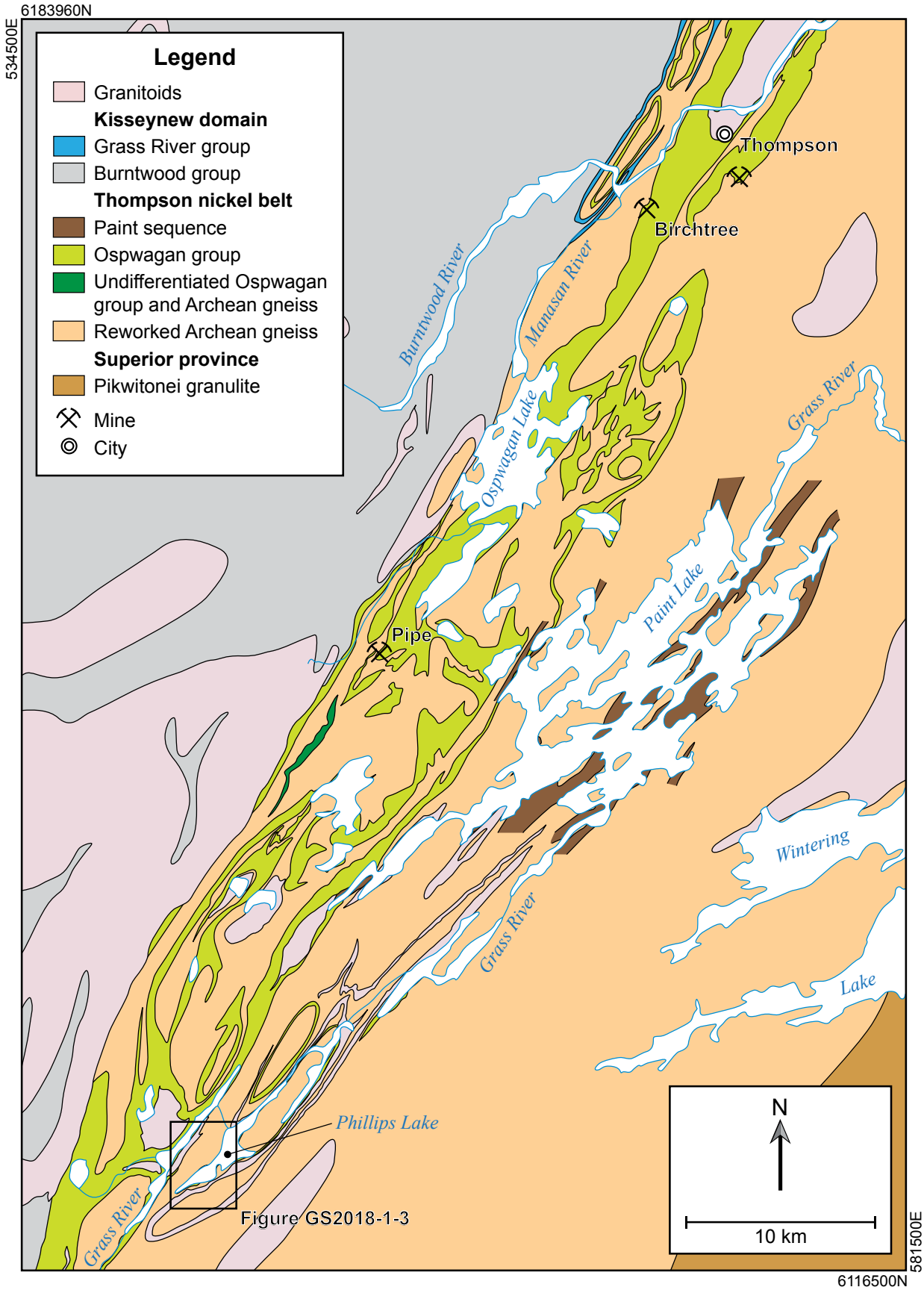

Figure GS2018-1-1: *Simplified geology of the central Thompson nickel belt (modified from Macek et al., 2006).*

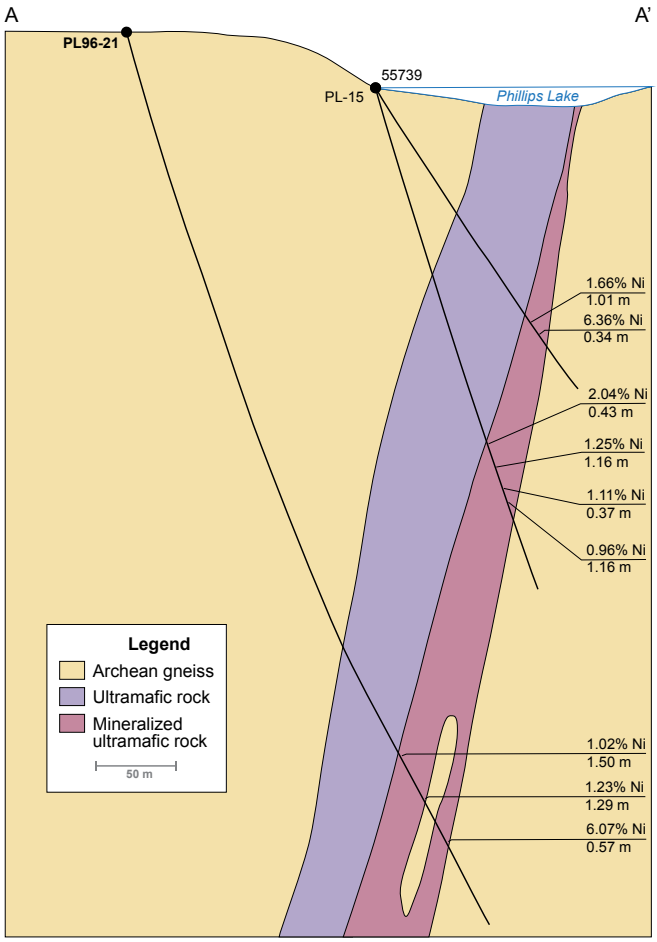

Figure GS2018-1-2: *Cross-section A–A', looking north through Falconbridge Ltd. drillholes PL-15 and PL96-21, and Inco Ltd. drillhole 55739 (modified from Assessment File 94497). The locations of drillholes and section A–A' are shown in Figure GS2018-1-3.*

bodies spatially associated with Ospwagan group rocks (Bleeker, 1990; Macek et al., 2006; Zwanzig et al., 2007).

Most recently, shoreline mapping by the MGS in 2012 suggested the presence of a newly recognized metasedimentary sequence, informally termed the 'Paint sequence', on the central islands and point, and along the west shore, of southern Phillips Lake (Figure GS2018-1-3; Couëslan, 2012, 2016). This suggests that Paint sequence rocks, rather than a ghost succession of Ospwagan group rocks, may host the mineralized ultramafic body. The objective of this study is to determine the affinity of the rocks that host the mineralized ultramafic intrusion in southern Phillips Lake (e.g., Ospwagan group, Paint sequence, or Archean gneiss?). If it is shown that rocks of the Paint sequence can also host mineralized ultramafic intrusions, it will generate a new exploration target for companies working in the TNB.

Regional geology

The TNB forms a segment of the Superior boundary zone, flanked to the northwest by the Kisseynew domain of the Trans-Hudson orogen and to the southeast by the Pikwitonei granulite domain (PGD) of the Superior craton. The TNB is underlain largely by reworked Archean gneiss of the Superior craton, which is typically quartzofeldspathic with enclaves of mafic to ultramafic rock; clearly recognizable paragneiss is rare. The gneiss is commonly migmatitic and characterized by complex internal structures that are the result of multiple generations of Archean and Paleoproterozoic deformation and metamorphism. It is interpreted to be derived from the adjacent PGD, which was subjected to amphibolite- to granulite-facies metamorphic conditions ca. 2720 to 2640 Ma (Hubregtse, 1980; Mezger et al., 1990; Heaman et al., 2011; Guevara et al., 2016a, b). The granulites of the PGD were exhumed and unconformably overlain by the Paleoproterozoic supracrustal rocks of the Ospwagan group (TNB) prior to intrusion of the Molson dike swarm and associated ultramafic intrusions ca. 1883 Ma (Bleeker, 1990; Zwanzig et al., 2007; Heaman et al., 2009; Scoates et al., 2017). The Archean basement gneiss and Ospwagan group were subjected to multiple generations

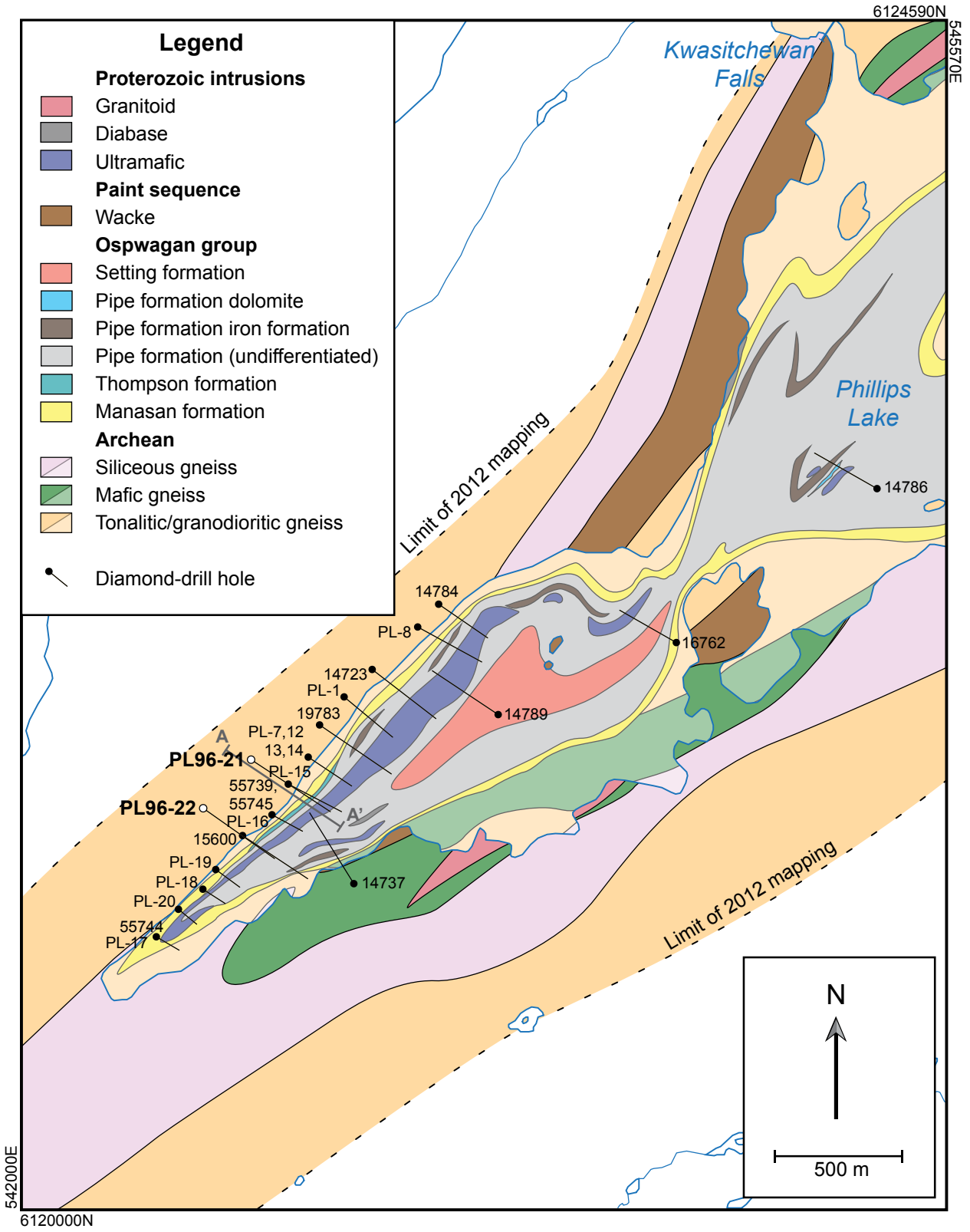

Figure GS2018-1-3: *Composite geology of southern Phillips Lake, showing the locations of diamond-drillholes by Inco Ltd. (five-digit numbers) and Falconbridge Ltd. (beginning with 'PL'). The geology underlying the lake is from Macek et al. (2006) and the shoreline geology is from Couëslan (2016). The section in Figure GS2018-1-2 is along line A–A' (in grey)*

of deformation and metamorphic conditions, ranging from middle-amphibolite facies to lower-granulite facies, during the Trans-Hudson orogeny (Bleeker, 1990; Burnham et al., 2009; Couëslan and Pattison, 2012).

The dominant phase of penetrative deformation is D_2, which affected the Ospwagan group and ca. 1883 Ma magmatic rocks. This deformation phase resulted in the formation of F_2 nappe structures, which incorporated the underlying Archean gneiss. The nappe structures have been interpreted as either east verging (Bleeker, 1990; White et al., 2002) or southwest verging (Zwanzig et al., 2007; Burnham et al., 2009). The recumbent folds are associated with regionally penetrative S_2 fabrics. The D_2 phase of deformation is interpreted to be the result of convergence between the Superior craton margin and the Reindeer zone of the Trans-Hudson orogen ca. 1830 to 1800 Ma. The D_3 phase of deformation resulted in isoclinal folds with vertical to steeply southeast-dipping axial planes (Bleeker, 1990; Burnham et al., 2009). Mylonite zones with subvertical stretching lineations parallel many of the regional F_3 folds. Tightening of D_3 structures continued during D_4, marked by localized retrograde greenschist-facies metamorphism along northeast-striking, mylonitic and cataclastic shear zones that commonly record southeast-side-up sinistral movement (Bleeker, 1990; Burnham et al., 2009).

Ospwagan group stratigraphy

The following summary of the Ospwagan group is sourced largely from Bleeker (1990) and Zwanzig et al. (2007). The Paleoproterozoic Ospwagan group unconformably overlies Archean basement gneiss in the TNB (Figure GS2018-1-4). The lowermost unit of the Ospwagan group is the Manasan formation, which consists of two members: the lower M1 member, consisting of layered to laminated sandstone with local conglomerate layers near the base; and the overlying M2 member, consisting of semipelitic rock. The Manasan formation is interpreted as a transgressive, fining-upward sequence deposited along a passive margin. This siliciclastic system grades into the overlying calcareous sedimentary rocks of the Thompson formation.

The Thompson formation consists of three members: the T1 member comprises a variety of calcareous–siliceous rocks, including chert, calcsilicate and impure marble; the T2 member is a semipelitic calcareous gneiss that is rarely present; and the T3 member consists of impure dolomitic marble with local horizons of calcsilicate. The Thompson formation represents a transition from a siliciclastic-dominated to a carbonate-dominated system.

The Pipe formation is subdivided into three members. The P1 member consists of a graphite-rich, sulphide-facies iron formation at the base (the locus of the Pipe II and Birchtree orebodies), overlain by a silicate-facies iron formation. The top of the P1 member consists of a reddish, laminated, siliceous rock. The P1 member grades into the overlying pelitic rocks of the P2 member, the top of which is marked by a sulphide-facies iron formation (the locus of the Thompson orebody). The overlying P3 member consists of a wide variety of rock types, including laminated, siliceous, sedimentary rocks; silicate-, carbonate- and local oxide-facies iron formations; and semipelitic rocks, calcsilicate and a local horizon of relatively pure dolomitic marble. The Pipe formation represents a mix of chemical sediments and fine to very fine siliciclastics that were deposited in either an open-marine environment (Zwanzig et al., 2007) or during the development of a foredeep basin (Bleeker, 1990).

The Setting formation is divided into two members and is defined to include all siliciclastic rocks above the uppermost iron formation of the P3 member. The S1 member consists of rhythmically interbedded quartzite and pelitic schist with local calcareous concretions, which are characteristic of the S1 member. The S2 member consists of thickly layered greywacke, with local horizons grading from conglomeratic at the base to pelitic at the top. No contact has been observed between the S1 and S2 members. It is possible that they represent a lateral facies change as opposed to a vertical succession. The Setting formation is interpreted to have been deposited by turbidity currents in a relatively deep-marine environment, possibly a foredeep basin (Bleeker, 1990). The coarse clastic material and thick turbidite bedding of the S2 member may record the shallowing of the basin, the onset of active tectonism or a lateral sedimentary facies change to a submarine-channel or upper-fan environment (Zwanzig et al., 2007).

At the top of the Ospwagan group is the Bah Lake assemblage, which consists of mafic to ultramafic volcanic rocks dominated by massive to pillowed basalt flows with local picrite and minor synvolcanic intrusions. The Bah Lake assemblage is dominated by a high-Mg suite (similar to normal mid-ocean–ridge basalt; N-MORB) that occurs throughout much of the main TNB, and an incompatible-element–enriched suite (similar to enriched mid-ocean–ridge basalt; E-MORB) that occurs in the northwestern Setting Lake area and along the margin of the Kisseynew domain (Zwanzig, 2005). The enriched suite is interpreted to overlie the high-Mg suite; however, it is uncertain if this represents a stratigraphic or tectonic relationship. The Bah Lake assemblage may suggest the onset of active rifting in the TNB (Zwanzig, 2005; Zwan-

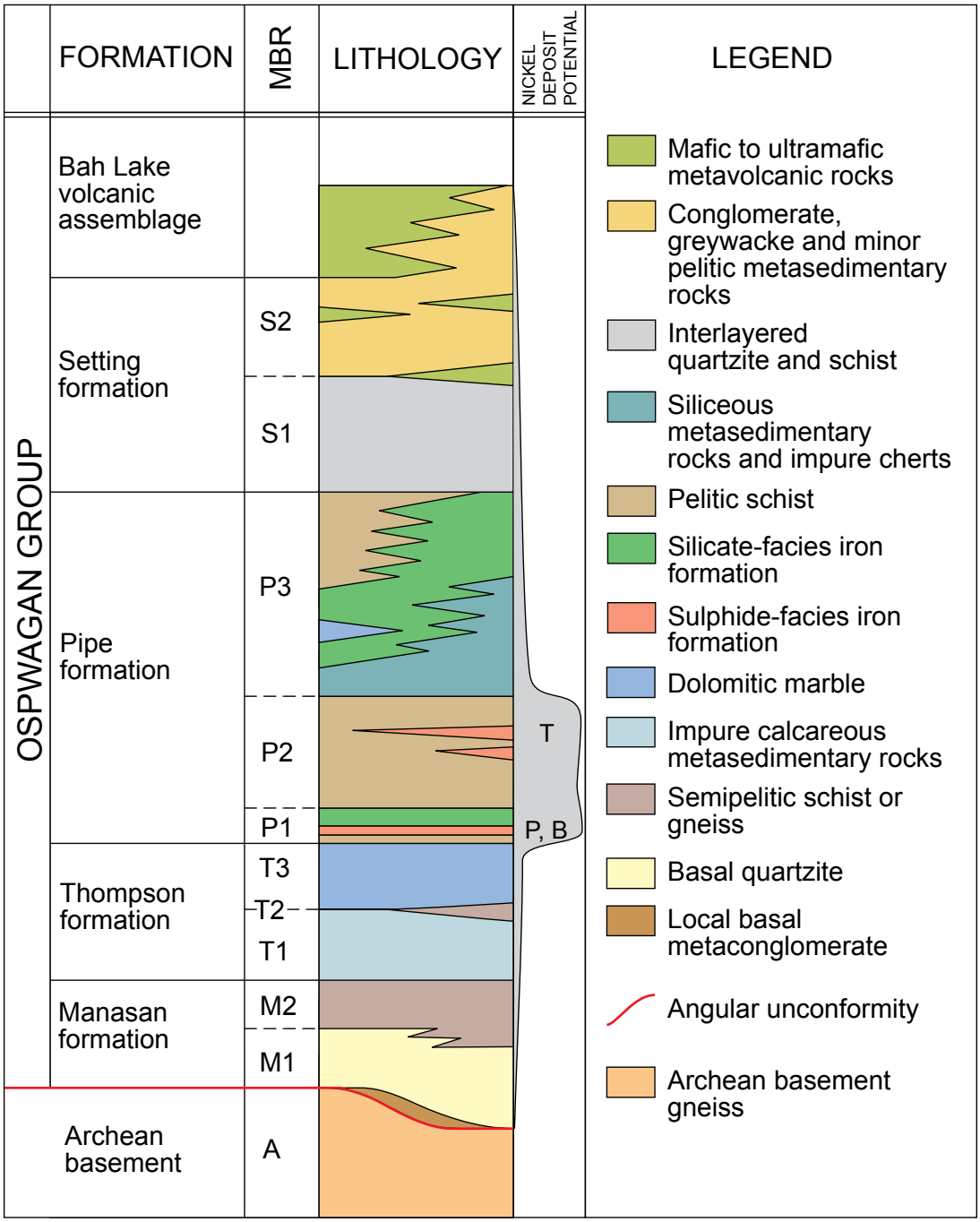

Figure GS2018-1-4: *Schematic lithostratigraphic section of the Ospwagan group (modified from Bleeker, 1990). Abbreviations: B, stratigraphic location of the Birchtree ore body; MBR, member; P, stratigraphic location of the Pipe II ore body; T, stratigraphic location of the Thompson ore body.*

zig et al., 2007), or that the foredeep was magmatically active (Bleeker, 1990).

A maximum age for the Ospwagan group is provided by a ca. 1974 Ma zircon recovered from Setting formation greywacke (Bleeker and Hamilton, 2001). A minimum age for the Ospwagan group is provided by crosscutting amphibolitized dikes interpreted to be part of the Molson dike swarm, and the possibly comagmatic Ni-ore–bearing ultramafic sills, which intruded the Ospwagan group at all stratigraphic levels ca. 1883 Ma (Bleeker, 1990; Zwanzig et al., 2007; Heaman et al., 2009; Scoates et al., 2017). Ospwagan group rocks yield crustal-residence Nd-model ages of ca. 3.22–2.82 Ga, which are typically younger than model ages obtained from the Archean basement (ca. 3.70–3.14 Ga; Böhm et al., 2007).

Granulite-facies assemblages in semipelitic and pelitic rocks of the Ospwagan group can become almost indistinguishable from the Archean basement gneiss; however, petrological end members such as marble, quartzite and iron formation remain recognizable at the highest metamorphic grades and can be used as marker horizons. Basement-like gneiss or migmatite successions between isolated but still recognizable marker horizons may represent 'ghost successions' of the Ospwagan group (Zwanzig et al., 2007). Distinguishing Archean from Ospwagan group rocks at high metamorphic grade may require the use of lithogeochemistry or Sm-Nd isotope geochemistry (Böhm et al., 2007; Zwanzig et al., 2007).

Paint sequence rocks

The 'Paint sequence' refers to three northeast-striking belts of metasedimentary rocks that occur in the Paint Lake area and appear to continue along strike to the Phillips Lake area (Couëslan, 2016). The stratigraphy of the Paint sequence is unconstrained but consists dominantly of wacke and psammite, with subordinate iron formation and pelite, and rare boudins of calcsilicate. To date, the Paint sequence has only been recognized in areas of granulite-facies metamorphism where primary textures and structures are all but obliterated save for centimetre-scale compositional layering. Wacke is the most abundant member of the sequence. It commonly contains centimetre- to decimetre-thick layers of psammite and iron formation. Pods of in situ to in-source leucosome are abundant. Outcrops of wacke are characterized by rusty weathered surfaces because of the presence of minor but ubiquitous pyrrhotite. The composition of the wacke and psammite are gradational into each other and they are commonly interbedded. The psammite is typically interlayered with centimetre- to metre-thick layers of wacke and rarely occurs interlayered with pelite. The iron formation occurs as discontinuous layers and lenses <3 m thick within the wacke. Iron formations are typically of the silicate facies; however, significant pyrrhotite and magnetite can be present. A maximum age for the Paint sequence is provided by five ca. 2436 Ma detrital zircon grains obtained from a sample of wacke (Couëslan, 2016). The Paint sequence rocks are intruded by relatively straight-walled mafic dikes, which are tentatively interpreted to be part of the Paleoproterozoic Molson dike swarm, suggesting a minimum age of ca. 1883 Ma for the sequence. The Paint sequence rocks contrast from the Ospwagan group rocks in having a distinct detrital zircon population, older crustal-residence Nd-model ages (ca. 3.57–3.23 Ga) and unique trace-element compositions (Couëslan, 2016).

Phillips Lake area

The Phillips Lake area is underlain by a highly attenuated basement dome (Burnham et al., 2009) consisting largely of Archean multicomponent gneiss, which comprises a mixture of tonalitic and granodioritic gneisses in varying proportions, with subordinate mafic and ultramafic phases (Macek et al., 2006; Couëslan, 2016). A thin sheet of Ospwagan group rocks mantles the dome and is thickened in the fold closure at the south end of Phillips Lake. Other, more discrete Archean units in the area include a mafic gneiss suite (Couëslan, 2016; amphibolitic gneiss), which could be derived from a layered gabbro complex (Macek, 1985) or possibly volcanic rocks (Couëslan, 2016); and a garnet- and magnetite-bearing siliceous gneiss unit. Rocks in the area attained granulite-facies metamorphic conditions during the Trans-Hudson orogeny, with orthopyroxene being a common constituent in rocks of felsic, intermediate and mafic bulk composition (Couëslan and Pattison, 2012).

Wacke and psammite, interpreted to be part of the Paint sequence, are exposed at Phillips Lake in the north arm, along the west shore south of Kwasitchewan Falls and in the central islands and the prominent point of the south basin (Figure GS2018-1-3; Couëslan, 2016). This is somewhat at odds with the mapping of Macek et al. (2006), which interpreted Ospwagan group rocks to underlie much of the south end of the lake, including the islands of the south basin. Several ultramafic bodies are hosted within the metasedimentary rocks. Discontinuous bodies and boudins of plagioclase amphibolite, ranging from centimetres to tens of metres across, are common in the area and are interpreted to represent metadiabase dikes. Intrusions of granodiorite and granitic pegmatite are also common, with pegmatite dikes present in almost all outcrops. The granitoid intrusions range in size from centimetres to tens of metres across and can be greater than 1 km in length (Couëslan, 2016).

Units

Two drillcores were selected for re-examination: PL96-21 and PL96-22. Both drillholes were collared in the hangingwall of the ultramafic body and drilled into the footwall (Figure GS2018-1-2). Units are described in order of intersection from top to bottom of the drillholes (Figure GS2018-1-5). All units are assumed to dip steeply to the west, and the stratigraphic younging direction is unknown. The core from each drillhole was laid out in its entirety, allowing for the entire sequence to be viewed and separated into petrographically distinct intervals. Each interval was described petrographically in the core logs, but they are presented here in a condensed, simplified

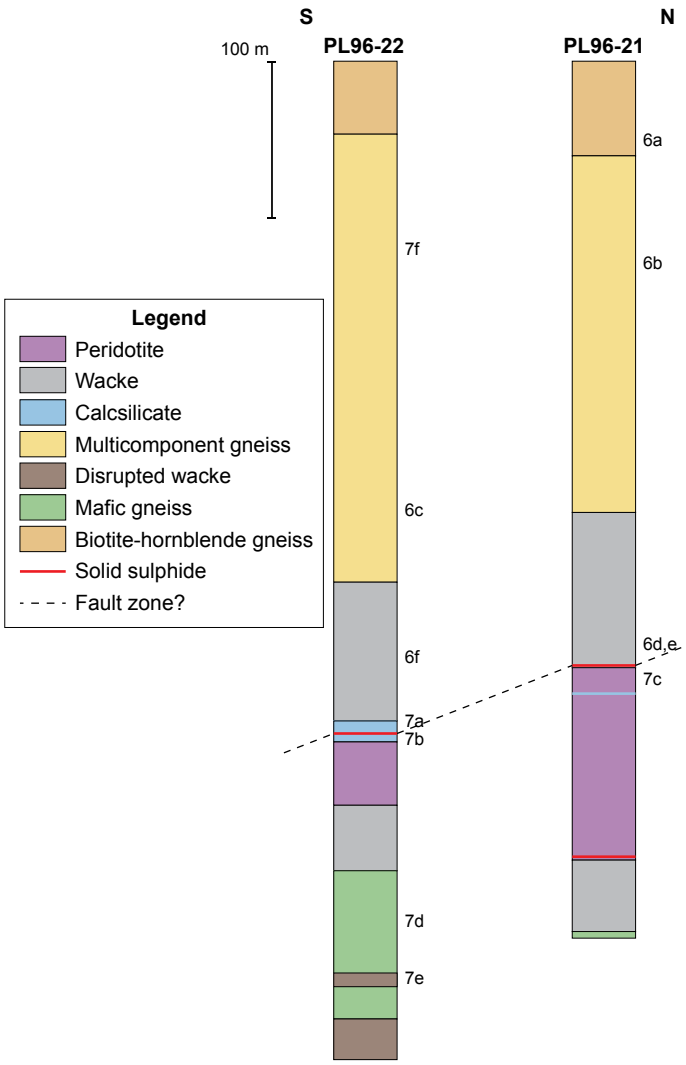

Figure GS2018-1-5: *Schematic logs of drillcores PL96-21 and PL96-22 in the southern Phillips Lake area; see Figure GS2018-1-3 for drillhole locations. The approximate locations of images in Figures GS2018-1-6 and GS2018-1-7 are indicated along the right-hand side of each column.*

form using protolith interpretation where appropriate. All rocks were metamorphosed to granulite facies, with orthopyroxene present in felsic, intermediate and mafic bulk compositions. All rocks, unless otherwise noted, are characterized by a well-developed penetrative foliation. Pods of leucosome, pegmatite injections and bands of plagioclase amphibolite are ubiquitous. Reported thicknesses are intersection lengths, not true thicknesses.

Biotite-hornblende gneiss

Both drillholes were collared in a 40–50 m thick interval of biotite-hornblende gneiss. The gneiss is grey to beige-grey and medium to coarse grained, and contains 3–5% hornblende and 7–15% biotite in a quartzofeldspathic groundmass (Figure GS2018-1-6a). Up to 3% garnet or 5% orthopyroxene is typically present, but they generally do not occur together. Interbanding of garnet-bearing and orthopyroxene-bearing gneisses typically occurs on a metre scale. This unit is tentatively interpreted as an orthogneiss and part of the Archean basement.

Multicomponent gneiss

Downhole from the biotite-hornblende gneiss is a 240–300 m thick interval of multicomponent gneiss. The gneiss is composed of a variety of phases, including various orthopyroxene-bearing gneisses likely derived from metamorphosed intrusive rocks; biotite-garnet and biotite-orthopyroxene gneisses likely derived from metamorphosed wackes; biotite-garnet and biotite-orthopyroxene gneisses of uncertain affinity; and a pink, orthopyroxene-free metasomatized gneiss. Although

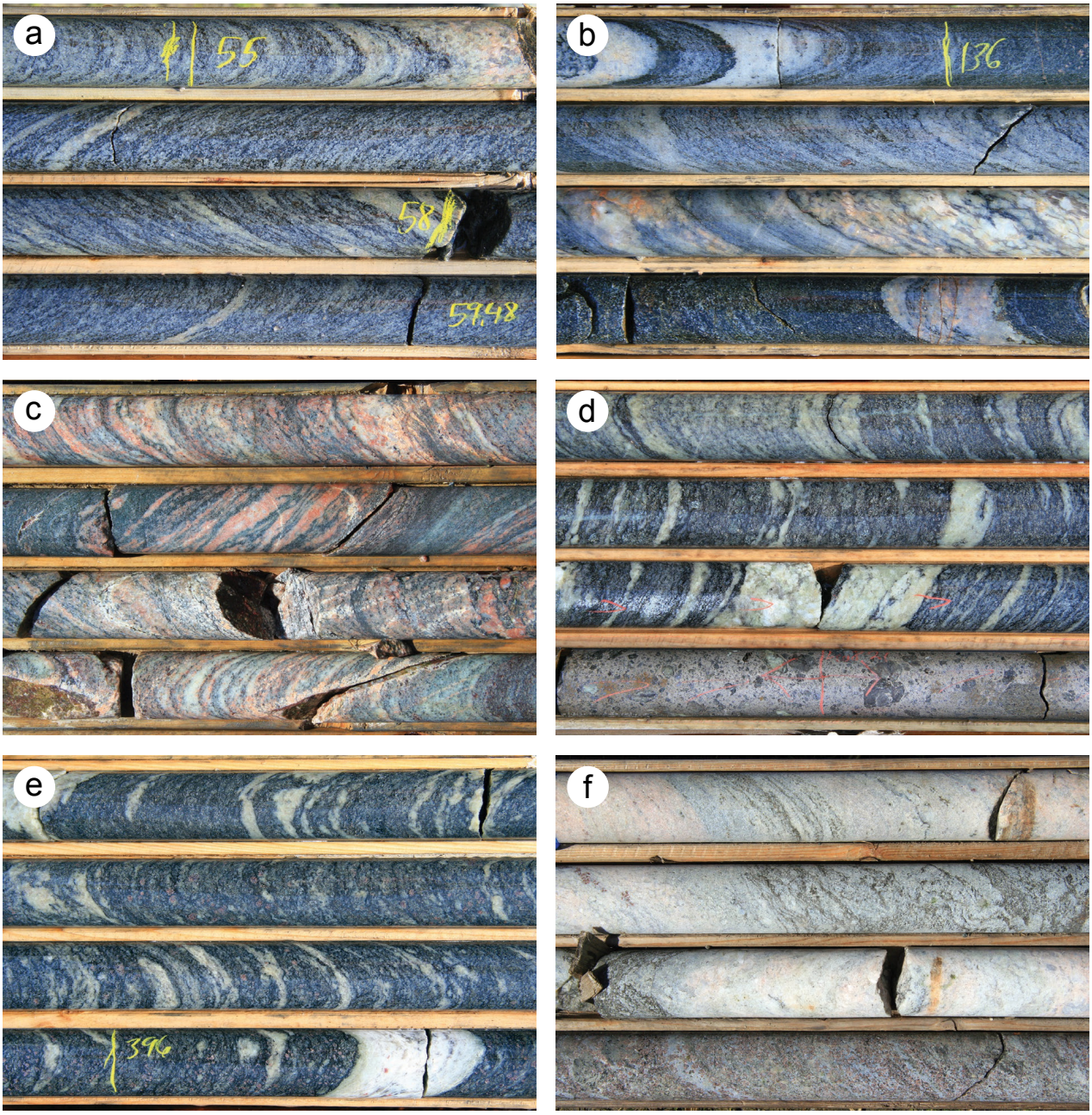

Figure GS2018-1-6: *Drillcore images from PL96-21 and PL96-22:* ***a)*** *biotite-hornblende gneiss (PL96-21, 54.9 m);* ***b)*** *multicomponent gneiss consisting of biotite-garnet gneiss of uncertain affinity (top two rows), sheared pegmatite (third row) and plagioclase amphibolite (bottom row; PL96-21, 135.7 m);* ***c)*** *metasomatized gneiss (PL96-22, 308.1 m);* ***d)*** *wacke-derived biotite-orthopyroxene gneiss (top three rows) with sulphide breccia (bottom row; PL96-21, 403.65 m);* ***e)*** *wacke-derived biotite-garnet gneiss (bottom three rows) and biotite-orthopyroxene gneiss (top row; PL96-21, 391.55 m);* ***f)*** *silicate-facies iron formation (bottom row) and pegmatite with schlieren of wacke-derived biotite-orthopyroxene gneiss (top three rows; PL96-22, 389.1 m). Drillcore is BQ with a diameter of 36.5 mm.*

intersections of discrete gneissic phases can be up to 81 m, as in the case for the metasomatized gneiss, the various gneissic phases are typically interlayered on a scale of <10 m. The gneisses are also intercalated with abundant layers of plagioclase amphibolite (<13 m) and granitic pegmatite (<56 m), and local layers of ultramafic amphibolite (<1.5 m; Figure GS2018-1-6b). The metasomatized gneiss appears to be an amphibolitized equivalent of the other gneiss varieties and may contain more abundant injections of granitic pegmatite (Figure GS2018-1-6c). The multicomponent gneiss likely represents a tectonic interleaving of various Archean and Proterozoic gneissic phases intruded by Paleoproterozoic diabase and granitic pegmatite intrusions. Intercala-

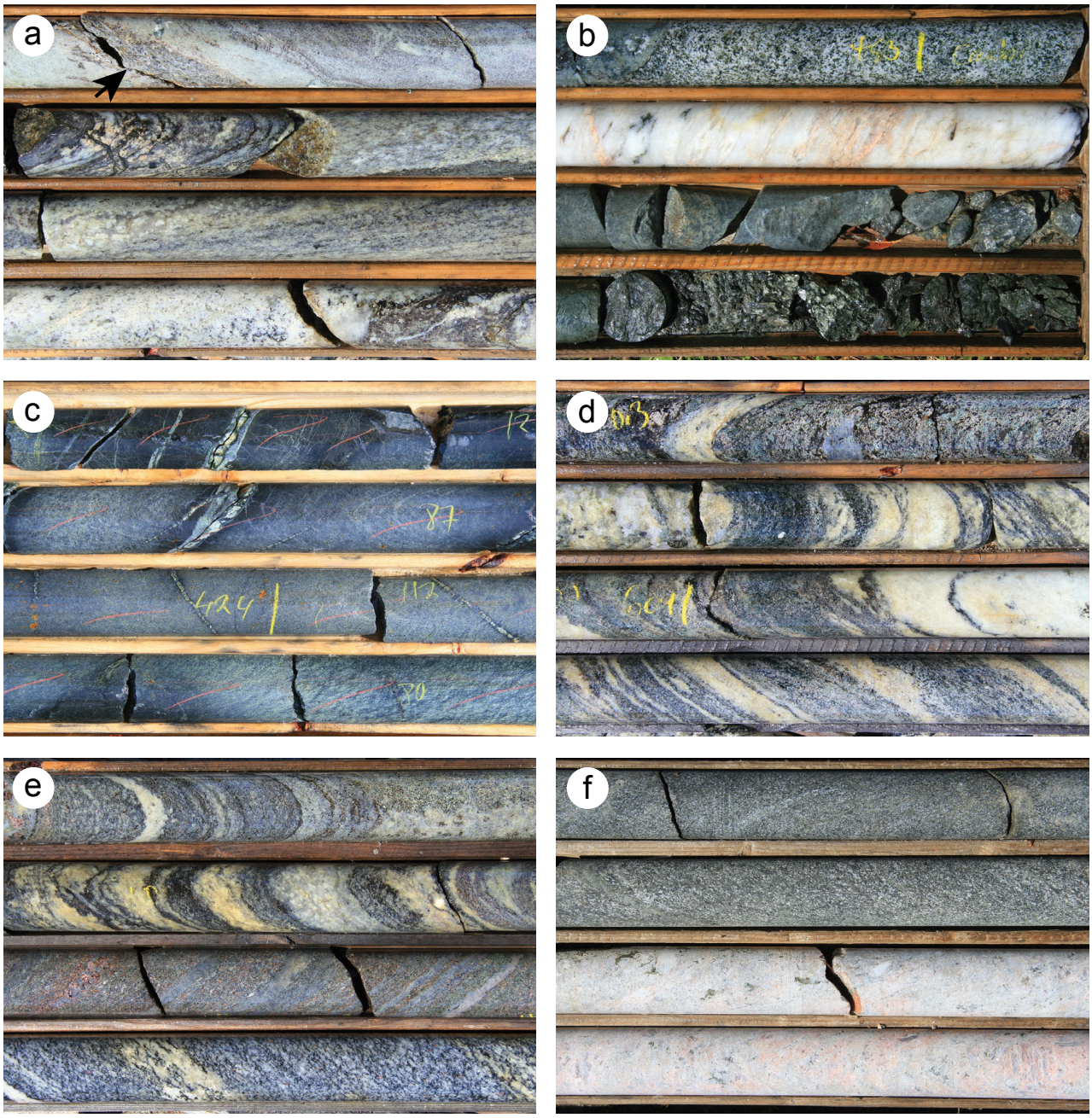

Figure GS2018-1-7: *Drillcore images from PL96-21 and PL96-22:* ***a)*** *calcsilicate with layer of phlogopite marble (arrow, top row) and sheared pegmatite (bottom three rows; PL96-22, 441 m);* ***b)*** *olivine marble (top row), sheared pegmatite (second row), serpentinized peridotite (third row) and ultramafic schist (bottom row; PL96-22, 452.8 m);* ***c)*** *serpentinized peridotite (PL96-21, 421.5 m);* ***d)*** *mafic gneiss (PL96-22, 601 m);* ***e)*** *disrupted wacke (biotite-garnet gneiss, top two rows), well-layered iron formation (third row) and garnet-bearing granodiorite (bottom row; PL96-22, 623 m);* ***f)*** *plagioclase amphibolite (top two rows) and pegmatite (bottom two rows; PL96-22, 122 m). Drillcore is BQ with a diameter of 36.5 mm.*

tions of the wacke-derived, biotite-orthopyroxene gneiss become increasingly abundant in the bottom 25 m of the multicomponent gneiss interval in drillhole PL96-21.

Wacke

Downhole from the multicomponent gneiss is a 95–107 m thick interval of wacke. The wacke consists of interlayered biotite-orthopyroxene gneiss (Figure GS2018-1-6d) and biotite-garnet gneiss (Figure GS2018-1-6e), with local intercalations of silicate-facies iron formation. The biotite-orthopyroxene gneiss is grey to beige and medium to coarse grained, with diffuse layering 2–5 cm thick. The gneiss contains 20–30% mafic minerals dominated by biotite with <10% orthopyroxene, and

rarely minor hornblende, in a quartzofeldspathic groundmass. Trace amounts of pyrrhotite and magnetite can also be present. The biotite-garnet gneiss is similar in overall appearance but contains <5% garnet. Intervals of wacke may be dominated by one variety of gneiss over the other, or they may occur in roughly equal proportions interlayered on a decimetre to metre scale.

Intercalations of silicate-facies iron formation <70 cm thick are present within the wacke-derived gneisses. The iron formation is dark purplish green, coarse grained and magnetic. It is relatively massive, with diffuse layering, <15 cm thick, defined by varying proportions of the mafic minerals that typically make up <50% of the rock. Mafic minerals are dominated by garnet and orthopyroxene, with <7% biotite and minor magnetite and pyrrhotite. The groundmass is relatively siliceous. Sparse chert layers are poorly developed and typically <1 cm thick (Figure GS2018-1-6f).

Calcsilicate and marble

A 14 m wide intersection of calcsilicate and marble occurs downhole from the wacke in the drillcore from PL96-22. The calcsilicate is light green and fine to coarse grained, with diffuse, <10 cm thick layering. The rock contains <12% phlogopite and 30–40% diopside in a groundmass of quartz, feldspar and carbonate. The calcsilicate contains sparse layers, <20 cm thick, of strongly foliated phlogopite marble (Figure GS2018-1-7a). A single 30 cm thick layer of olivine marble occurs toward the bottom of the interval (Figure GS2018-1-7b). The olivine marble is pale grey-green, medium grained and weakly foliated. It contains 10–20% serpentinized olivine and 5–7% phlogopite, with minor amounts of diopside.

Calcsilicate is also present as a 1.4 m wide band of tremolite-biotite gneiss hosted by peridotite in PL96-21. The gneiss is purplish grey and fine grained, with diffuse layering <3 cm thick. The gneiss appears to be quartzofeldspathic, with 10–20% tremolite and 5–7% biotite, and is interpreted as a xenolith within the ultramafic intrusion.

Sulphide breccia

A 70 cm thick zone of sulphide breccia occurs within the calcsilicate interval in PL96-22. The breccia consists of a near-solid pyrrhotite matrix surrounding 7–10% rounded to subangular quartzofeldspathic fragments <2 cm across, and 20–30% biotite schist fragments <10 cm across. The biotite schist fragments vary from rounded to angular and commonly display diffuse margins. A similar 1 m interval of sulphide breccia occurs within the wacke, immediately above the peridotite intrusion in PL96-21, and contains 3–5% ultramafic amphibolite fragments <2 cm across, 5–7% rounded graphite grains <1.5 cm across, and 7–10% rounded to subangular quartzofeldspathic fragments <2 cm across (Figure GS2018-1-6d). The sulphide breccia could be correlative between the two drillholes. Sheared to mylonitic rocks are associated with the breccia in both drillholes, suggesting the breccia likely represents structurally remobilized sulphide in a shear zone or fault. Falconbridge reported assays from both intervals to be barren (0.071% Ni in PL96-21, 0.095% Ni in PL96-22; Assessment File 94497).

Peridotite

The wacke is intruded by a 44–136 m thick interval of serpentinized peridotite (Figure GS2018-1-7c). The peridotite is black to green, medium to coarse grained and strongly magnetic. It contains serpentine and minor magnetite and sulphide. The sulphide generally occurs as fine disseminated grains; however, toward the bottom of the interval in PL96-21, the sulphide content increases to as much as 5% and occurs as segregations up to 1 cm across. Relict texture suggests that cumulate olivine were <1 cm across. Bands of ultramafic schist <1.5 m thick are common within the serpentinized peridotite (Figure GS2018-1-7b). The ultramafic schist is silvery grey-green, coarse grained and nonmagnetic. It consists of anthophyllite, with variable amounts of phlogopite, chlorite and clinoamphibole typically forming <40% of the rock. The ultramafic schist commonly occurs at the contacts of crosscutting pegmatite dikes. A 60 cm wide zone of solid sulphide near the base of the peridotite in PL96-21 yielded 6.07% Ni over 0.57 m in Falconbridge assays (Assessment File 94497). The solid sulphide consists dominantly of pyrrhotite, with 10–20% biotite, 5–7% pentlandite and 2–3% quartzofeldspathic fragments <10 cm across. A 43–51 m thick interval of wacke continues downhole from the ultramafic intrusion.

Mafic gneiss

Downhole from the wacke in PL96-22 is a 107 m thick package of mafic gneiss (Figure GS2018-1-7d). The gneiss is green-grey, medium to coarse grained and nonmagnetic, with diffuse banding <1 m thick. The rock is relatively heterogeneous, with abundant leucosome and a beige plagioclase-rich groundmass. Mafic mineral contents vary from 40–75%, consisting of varying proportions of orthopyroxene, clinopyroxene and green hornblende, along with minor biotite. Large portions of the interval are amphibolitized, with all mafic minerals reacted to form black hornblende±biotite, and the plagioclase becoming white in colour. Drillhole PL96-21 terminates in a similar,

largely amphibolitized unit that is likely correlative. The mafic gneiss is petrographically similar to the high-Mg amphibolitic gneiss previously described in the Paint and Phillips lakes area (Couëslan, 2016).

Disrupted wacke

A 7.8 m thick intersection of garnet-bearing wacke, with minor iron formation as bands <80 cm thick, occurs within the mafic gneiss interval in PL96-22 (Figure GS2018-1-7e). The wacke and iron formation appear texturally distinct from those previously described. The wacke is largely disrupted by leucosome and/or pegmatite injection, and the iron formation is well layered, with alternating ferruginous and cherty layers <7 cm thick. Ferruginous minerals make up 30–50% of the rock and consist of roughly equal proportions of magnetite and orthopyroxene, and <10% garnet. The iron formation also contains sparse grains of pyrrhotite <2 cm across. Disrupted wacke continues for another 30 m downhole, below the mafic gneiss.

Other intrusive phases

Intersections of plagioclase amphibolite <13 m thick are ubiquitous in the drillcore (Figure GS2018-1-7f). The amphibolite is dark green-grey, medium to coarse grained and relatively homogeneous. It contains 50–70% hornblende in a groundmass of plagioclase and quartz; orthopyroxene is locally present and garnet is rare. In a few locations, the amphibolite is zoned, with medium-grained margins and coarse-grained, more mafic cores (90–95% hornblende). The plagioclase amphibolite is interpreted as metamorphosed diabase and gabbro dikes, possibly related to the Molson dike swarm.

Intrusions of granitic pegmatite <56 m wide are also ubiquitous in the drillcore (Figure GS2018-1-6b, f; Figure GS2018-1-7a, b, f). The pegmatite is typically pink, with <2% biotite and rare garnet, orthopyroxene and magnetite. Locally derived schlieren are common. The pegmatite is often sheared to protomylonitic. Pegmatite associated with the calcsilicate, serpentinized peridotite and mafic gneiss is commonly white.

Geochemistry

Twenty-four samples, representing most of the major units, were collected for lithogeochemistry; however, this section will focus on the potential metasedimentary rocks (wacke, calcsilicate and iron formation). The samples were crushed and pulverized at the MGS's Midland Sample and Core Library, and the homogenized pulps were submitted to Activation Laboratories Ltd. (Ancaster, Ontario). The pulps were fused with lithium metaborate/tetraborate, followed by a nitric-acid digestion, and analyzed by inductively coupled plasma–emission spectrometry (ICP-ES) for the major elements and selected trace elements (Ba, Be, Sc, Sr, V, Y, Zr), and by inductively coupled plasma–mass spectrometry (ICP-MS) for the remaining trace elements and the rare-earth elements (REE). Samples of calcsilicate and marble were analyzed for carbon, and wacke and iron formation were analyzed for carbon and sulphur, through induction-furnace combustion and measurement of the release of CO_2 and SO_2 by infrared spectrometry.

Because of the high metamorphic grade, the wacke was subjected to intense partial melting. Therefore, wacke samples were selected that appear representative of the bulk composition in terms of proportion of leucosome to melanosome or mesosome, and care was taken to avoid apparent injected leucosome in favour of material that appeared to consist of in situ or in-source leucosome. The calcareous sedimentary rocks and iron formation underwent minimal partial melting, so care was taken to sample material with little to no leucosome.

The use of trace elements is restricted to those interpreted to be less mobile in the high-grade metamorphic environment, including selected transition metals (Sc, V, Cr, Ni), high-field-strength elements (HFSE; Ti, Zr, Nb), REE and Th. However, it should be noted that Th may partition into silicate melt, the removal of which could result in the depletion of Th.

Wacke

Whole-rock geochemical data for the wacke were normalized to the average P2 member pelite of the Pipe formation and plotted on multi-element diagrams, as outlined in Zwanzig et al. (2007). Normalized profiles for the Paint sequence wacke are relatively flat, with negative anomalies at Nb and Zr, and elevated V, Sc and especially Cr relative to the adjacent heavy rare-earth elements (HREE; Figure GS2018-1-8a). Thorium is characterized by significant variability, a potential consequence of intense partial melting. The majority of wacke samples from the Phillips Lake core show similar normalized profiles, although two samples have profiles with distinct negative slopes for the REE (Figure GS2018-1-8b). This contrasts with semipelitic to pelitic rocks of the Ospwagan group, which are characterized by relatively flat P2-normalized profiles, with some variability at Zr and Sc, and no positive anomalies at Cr (Figure GS2018-1-8c–e). The normalized profiles of the Phillips Lake wacke suggest a greater affinity to the Paint sequence wacke than to the pelitic to semipelitic rocks of the Ospwagan group. The elevated values for V, Sc and Cr in the Paint sequence and Phillips

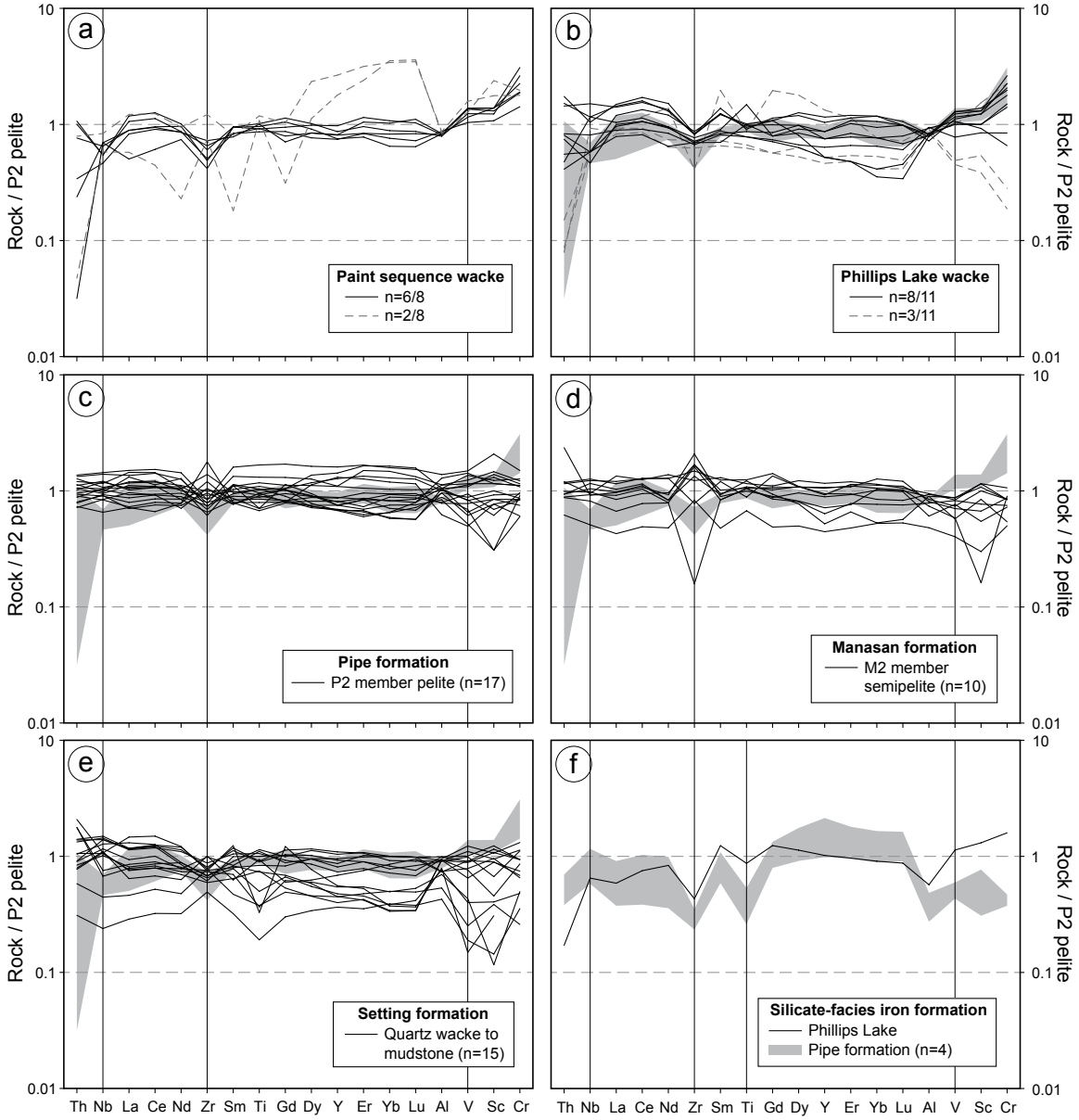

Figure GS2018-1-8: *Multi-element diagrams normalized to average P2 of Zwanzig et al. (2007):* ***a)*** *Paint sequence wacke from Paint Lake;* ***b)*** *wacke from Phillips Lake;* ***c)*** *Pipe formation P2 member pelite;* ***d)*** *Manasan formation M2 member semipelite;* ***e)*** *Setting formation quartz wacke to mudstone;* ***f)*** *Phillips Lake and Pipe formation silicate-facies iron formation. Dashed profiles are considered to be atypical. The grey fields in (b) to (e) denote typical Paint sequence wacke. Geochemical data for the Paint sequence wacke are from Couëslan (2016) and data for Ospwagan group rocks are from Zwanzig et al. (2007) and Couëslan (2016, unpublished data, 2012).*

Lake wackes could indicate a detrital source with a greater proportion of mafic rocks.

A sample of Phillips Lake silicate-facies iron formation, found interbedded with the wacke, has a P2-normalized profile that is concave down for the REE, with negative anomalies at Zr, Ti and Al, a positive anomaly at Nb, and elevated V, Sc, and Cr (Figure GS2018-1-8f). Normalized profiles for Pipe formation silicate-facies iron formation have slight positive slopes for the REE, negative anomalies at Zr, Ti and Al, and positive anomalies at Nb and Y. Values for V, Sc and Cr are below those of the HREE. The silicate-facies iron formation from Phillips Lake appears to be geochemically distinct from Pipe formation silicate-facies iron formation. The elevated V, Sc and Cr in the Phillips Lake iron formation are likely related to a siliciclastic component inherited from the same source as the wacke.

Calcsilicate and marble

The P2-normalized multi-element profiles for Phillips Lake calcsilicate are relatively flat to slightly concave

down for the REE, and characterized by negative anomalies at Th, Zr, Ti and Al, and a positive anomaly at Sc in one sample and Y in the other (Figure GS2018-1-9a). Normalized profiles for Thompson formation calcsilicate are relatively flat to slightly concave down for the REE, and characterized by positive anomalies at Zr and Sc, and a slight negative anomaly at Ti. The Phillips Lake phlogopite marble is characterized by a relatively flat to slightly concave-down profile, with a negative anomaly at Al and a positive anomaly at Sc (Figure GS2018-1-9b). Normalized profiles for Thompson formation phlogopite marble are also slightly concave down, generally with positive anomalies at Zr and Sc, a negative anomaly at Ti and depleted V, Sc and Cr relative to HREE. The Phillips Lake olivine marble is characterized by a profile with a positive slope, is depleted in Th, Nb, Ti, Al, V and Sc, and has a positive anomaly at Y (Figure GS2018-1-9c). Normalized profiles for the Thompson formation olivine marble are variable with generally positive slopes, a positive anomaly at Y and depletions in Ti, Al, V and Sc. Chromium was below detection limits in all of the olivine marble samples. Normalized profiles for Phillips Lake and Thompson formation calcareous rocks are similar overall, although slight differences do exist, most notably the lack of a positive Zr anomaly in the Phillips Lake calcsilicate and phlogopite marble; however, the sample size is too small for a statistically meaningful comparison. Additional work is required to determine the affinity of the calcsilicate rocks on Phillips Lake for either the Ospwagan group or the Paint sequence.

Economic considerations

The most widely accepted model for generating Ni-Cu deposits in the TNB invokes the intrusion of ultramafic magmas into sulphide-rich horizons of the Ospwagan group Pipe formation (Figure GS2018-1-4). The magmas then scavenged sulphide from the host sedimentary rocks, leading to sulphur saturation of the melt and the precipitation and concentration of sulphides enriched in Ni and Cu. As a result, ultramafic bodies hosted by Pipe formation rocks are considered the most likely to host mineralization and are therefore prime exploration targets in the TNB (Bleeker, 1990; Zwanzig et al., 2007). The recently recognized Paint sequence consists of sulphide-

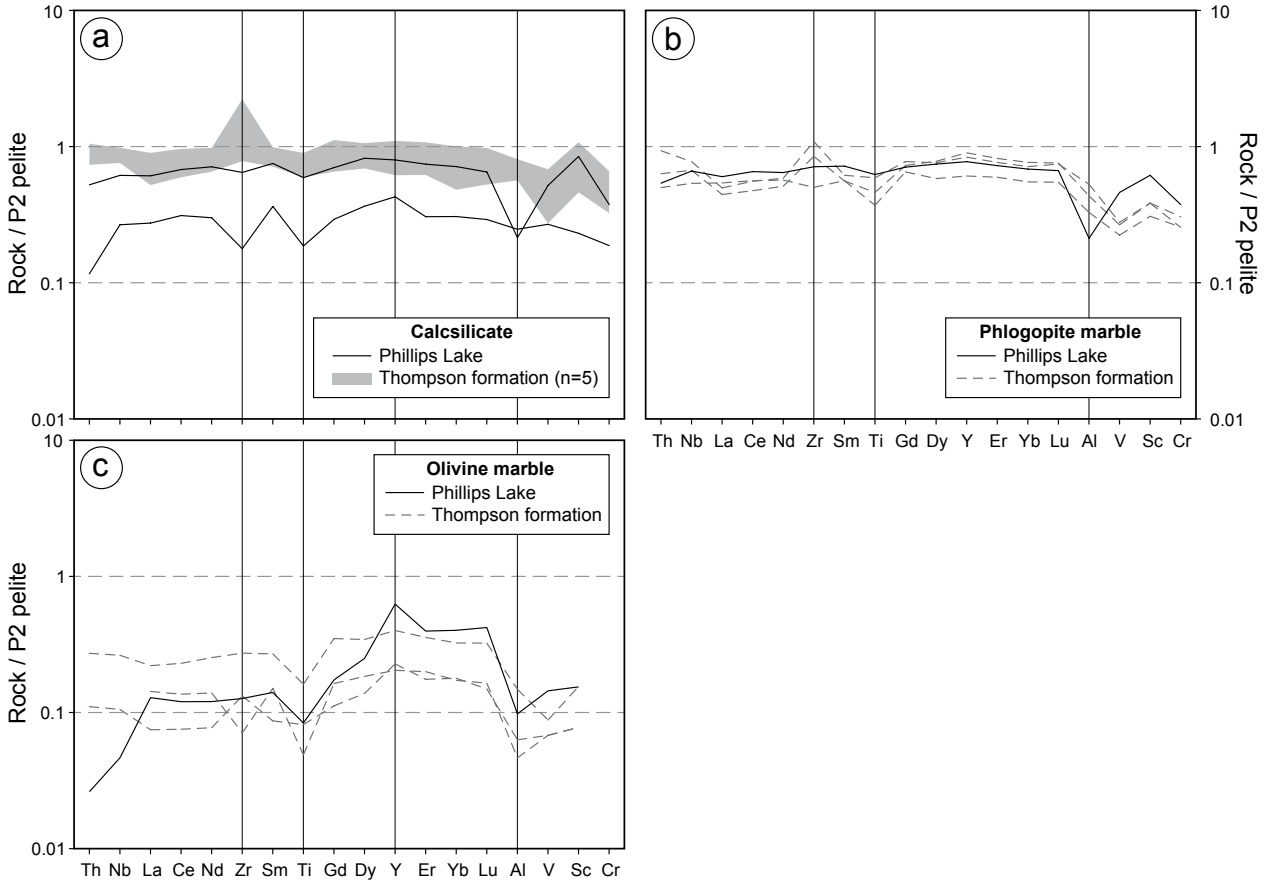

Figure GS2018-1-9: *Multi-element diagrams normalized to average P2 of Zwanzig et al. (2007):* ***a)*** *Phillips Lake and Thompson formation calcsilicates;* ***b)*** *Phillips Lake and Thompson formation phlogopite marbles;* ***c)*** *Phillips Lake and Thompson formation olivine marbles. Thompson formation geochemical data are from Couëslan (2003, 2016) and Zwanzig et al. (2007).*

bearing wacke and psammite with minor iron formation. The presence of sedimentary sulphide in this sequence suggests a notional potential to host mineralized ultramafic intrusions (Couëslan, 2016).

Preliminary results suggest that the wacke hosting the mineralized peridotite at Phillips Lake is likely part of the Paint sequence. This suggests that, in addition to the Ospwagan group, the Paint sequence is capable of hosting mineralized ultramafic intrusions; however, the matter is complicated by the presence of the calcareous sedimentary rocks of uncertain affinity. The two most likely scenarios for the calcareous rocks are that 1) they represent a tectonic sliver of Ospwagan group rocks spatially associated with the Paint sequence wacke, or 2) they are part of the Paint sequence. In the first scenario, the calcareous rocks could be part of the Thompson formation, with the spatially associated sulphide breccia potentially representing Pipe formation, P1 member sulphide-facies iron formation (Figures GS2018-1-4, -5). In this scenario, the mineralized peridotite is in direct contact with Ospwagan group rocks, at a similar stratigraphic level to that of the Pipe II and Birchtree ore bodies. The close spatial association of the Paint sequence wacke would in this case be coincidental and possibly of little consequence with respect to Ni mineralization. In the second scenario, the mineralized peridotite is hosted entirely in Paint sequence rocks, suggesting that ultramafic rocks hosted by the Paint sequence could be a new exploration target in the TNB. Rare boudins of calcsilicate are present in the Paint sequence rocks at Paint Lake, suggesting this could be a possibility. These preliminary results are ambiguous. It is hoped that the affinity of the calcareous rocks can be constrained through further lithogeochemical and Sm-Nd isotopic analyses.

Acknowledgments

Thanks go to A. Hutchins and J. Macek for assistance in moving, documenting and sampling the drillcore, and to N. Brandson and E. Anderson for logistical support. Sincere thanks go to K. Zhu and J. Stoness (CaNickel Mining Ltd.) for their hospitality in Wabowden and allowing full access to the drillcore and core-logging facilities. Thanks also go to C. Böhm and M. Rinne for reviewing previous drafts of this report.

References

Bleeker, W. 1990: Evolution of the Thompson Nickel Belt and its nickel deposits, Manitoba, Canada; Ph.D. thesis, University of New Brunswick, Fredericton, New Brunswick, 400 p.

Bleeker, W. and Hamilton, M.A. 2001: New SHRIMP U-Pb ages for the Ospwagan group: implications for the SE margin of the Trans-Hudson orogen; Geological Association of Canada–Mineralogical Association of Canada 2001, Joint Annual Meeting, St. John's, Newfoundland, May 27–30, 2001, Abstracts, v. 26, p. 15.

Böhm, C.O., Zwanzig, H.V. and Creaser, R.A. 2007: Sm-Nd isotope technique as an exploration tool: delineating the northern extension of the Thompson Nickel Belt, Manitoba, Canada; Economic Geology, v. 102, p. 1217–1231.

Burnham, O.M., Halden, N., Layton-Matthews, D., Lesher, C.M., Liwanag, J., Heaman, L., Hulbert, L., Machado, N., Michalak, D., Pacey, M., Peck, D.C., Potrel, A., Theyer, P., Toope, K. and Zwanzig, H. 2009: CAMIRO project 97E-02, Thompson Nickel Belt: final report, March 2002, revised and updated 2003; Manitoba Science, Technology, Energy and Mines, Manitoba Geological Survey, Open File OF2008-11, 434 p. plus appendices and GIS shape files for use with ArcInfo®.

Couëslan, C.G. 2003: Petrogenesis of the Thompson Formation T1 Member, Thompson Nickel Belt, Manitoba; B.Sc. thesis, Brandon University, Brandon, Manitoba, 126 p.

Couëslan, C.G. 2012: The Grass River Project: geological mapping at Phillips Lake, and new geochronological results from Paint Lake and Manasan Falls, Thompson Nickel Belt, central Manitoba (parts of NTS 63O1, 8, 9, 63P5, 12); *in* Report of Activities 2012, Manitoba Innovation, Energy and Mines, Manitoba Geological Survey, p. 68–78.

Couëslan, C.G. 2016: Geology of the Paint and Phillips lakes area, Thompson nickel belt, central Manitoba (parts of NTS 63O1, 8, 9, 63P5, 12); Manitoba Growth, Enterprise and Trade, Manitoba Geological Survey, Geoscientific Report GR2016-1, 44 p. and 1 colour map at 1:50 000 scale.

Couëslan, C.G. and Pattison, D.R.M. 2012: Low-pressure regional amphibolite-facies to granulite-facies metamorphism of the Paleoproterozoic Thompson Nickel Belt, Manitoba; Canadian Journal of Earth Sciences, v. 49, p. 1117–1153.

Guevara, V.E., Dragovic, B., Caddick, M.J., Kylander-Clark, A.R.C. and Couëslan, C.G. 2016a: Ultrahigh temperature metamorphism of the Archean Pikwitonei granulite domain; Geological Society of America, Annual Meeting, Denver, Colorado, September 25–28, 2016, Abstracts with Programs, v. 48, Paper 270-4, URL <https://gsa.confex.com/gsa/2016AM/webprogram/Paper284904.html> [October 2018].

Guevara, V., MacLennan, S.A., Schoene, B., Dragovic, B., Caddick, M.J., Kylander-Clark, A.R. and Couëslan, C.G. 2016b: Quantifying the timescales of Archean UHT metamorphism through U-Pb monazite and zircon petrochronology; American Geophysical Union, Fall Meeting, San Francisco, California, December 12–16, 2016, Abstract V51B-07, URL <https://agu.confex.com/agu/fm16/meetingapp.cgi/Paper/175259> [October 2018].

Heaman, L.M., Böhm, C.O., Machado, N., Krogh, T.E., Weber, W. and Corkery, M.T. 2011: The Pikwitonei Granulite Domain, Manitoba: a giant Neoarchean high-grade terrane in the northwest Superior Province; Canadian Journal of Earth Sciences, v. 48, p. 205–245.

Heaman, L.M., Peck, D. and Toope, K. 2009: Timing and geochemistry of 1.88 Ga Molson Igneous Events, Manitoba: insights into the formation of a craton-scale magmatic and metallogenic province; Precambrian Research, v. 172, p. 143–162, https://doi.org/10.1016/j.precamres.2009.03.015.

Hubregtse, J.J.M.W. 1980: The Archean Pikwitonei granulite domain and its position at the margin of the northwestern Superior Province (central Manitoba); Manitoba Energy and Mines, Manitoba Geological Survey, Geological Paper GP80-3, 16 p.

Macek, J.J. 1985: Geological investigations in the Phillips Lake area (part of 63O/12); *in* Report of Field Activities, Manitoba Energy and Mines, Geological Services, p. 181–182.

Macek, J.J., Zwanzig, H.V. and Pacey, J.M. 2006: Thompson Nickel Belt geological compilation map, Manitoba (parts of NTS 63G, J, O, P and 64A and B); Manitoba Science, Technology, Energy, and Mines, Manitoba Geological Survey, Open File Report OF2006-33, digital map on CD.

McGregor, C.R., Macek, J.J. and Zwanzig, H.V. 2006: Reinterpretation of Falconbridge Limited drillcore from the southern part of the exposed Thompson Nickel Belt, Manitoba (parts of NTS 63J, O, P and 64A), and criteria for recognizing lithologic units of the Ospwagan Group; Manitoba Science, Technology, Energy, and Mines, Manitoba Geological Survey, Open File Report OF2006-31, 1 DVD.

Mezger, K., Bohlen, S.R. and Hanson, G.N. 1990: Metamorphic history of the Archean Pikwitonei granulite domain and the Cross Lake subprovince, Superior Province, Manitoba, Canada; Journal of Petrology, v. 31, p. 483–517.

Scoates, J.S., Scoates, J.R.F., Wall, C.J., Friedman, R.M. and Couëslan, C.G. 2017: Direct dating of ultramafic sills and mafic intrusions associated with Ni-sulfide mineralization in the Thompson nickel belt, Manitoba, Canada; Economic Geology, v. 112, p. 675–692.

White, D.J., Lucas, S.B., Bleeker, W., Hajnal, Z., Lewry, J.F. and Zwanzig, H.V. 2002: Suture-zone geometry along an irregular Paleoproterozoic margin: the Superior boundary zone, Manitoba, Canada; Geology, v. 30, p. 735–738.

Zwanzig, H.V. 2005: Geochemistry, Sm-Nd isotope data and age constraints of the Bah Lake assemblage, Thompson Nickel Belt and Kisseynew Domain margin: relation to Thompson-type ultramafic bodies and a tectonic model (NTS 63J, O and P); *in* Report of Activities 2005, Manitoba Industry, Economic Development and Mines, Manitoba Geological Survey, p. 40–53.

Zwanzig, H.V., Macek, J.J. and McGregor, C.R. 2007: Lithostratigraphy and geochemistry of the high-grade metasedimentary rocks in the Thompson Nickel Belt and adjacent Kisseynew Domain, Manitoba: implications for nickel exploration; Economic Geology, v. 102, p. 1197–1216.

GS2018-2

Documentation of the Ospwagan group stratigraphy at the Pipe II open-pit mine, Thompson nickel belt, central Manitoba (part of NTS 63O8)

by C.G. Couëslan

In Brief:

- Classic Ospwagan group outcrops are beginning to flood at the Pipe II open-pit mine
- A project has been initiated to photographically document details of the remaining outcrops, including the use of an unmanned aerial vehicle (drone)
- A digital Open File report integrating detailed geological maps, aerial imagery, and outcrop photographs will be available as a resource for geologists and researchers working in the Thompson nickel belt

Citation:
Couëslan, C.G. 2018: Documentation of the Ospwagan group stratigraphy at the Pipe II open-pit mine, Thompson nickel belt, central Manitoba (part of NTS 63O8); *in* Report of Activities 2018, Manitoba Growth, Enterprise and Trade, Manitoba Geological Survey, p. 17–24.

Summary

One of the few continuous exposures of Ospwagan group stratigraphy in the Thompson nickel belt, including the type section for the Pipe formation, is beginning to flood at the Pipe II open-pit mine. The classic outcrops are located along the east shoulder of the open pit, which has been flooding naturally since its closure in 1984. Detailed aerial images of the outcrops were collected by unmanned aerial vehicle (drone), and the available outcrops were photographed to document details of the stratigraphy, structure and metamorphic assemblages. The final output proposed for this project is a digital Open File report integrating detailed geological maps, aerial imagery and detailed outcrop photographs. The Open File will be available as a learning resource for geologists and researchers working in the Thompson nickel belt.

Introduction

Supracrustal rocks of the Ospwagan group are spatially associated with all of the economic nickel deposits in the Thompson nickel belt (TNB). Much of our understanding of the stratigraphy and structure of the TNB stems from the detailed mapping of Ospwagan group rocks at the Pipe II open-pit mine in the late 1980s (Bleeker and Macek, 1988a–i; Macek and Bleeker, 1989). Since that time, the outcrops at 'Pipe pit' have been the focus of geological studies (Bleeker, 1990; Couëslan et al., 2011; Scoates et al., 2017) and countless formal and informal field trips for industry, academic and government geologists (Galley et al., 1990; Bleeker and Macek, 1996). It is the type locality for the Pipe formation and where geologists come to be initiated into the geology of the TNB.

The Pipe II deposit was discovered in 1957 at Pipe Lake, and dredging of silt and clay overburden began in 1967. Production from the open pit began in 1969 and ceased in 1984 at a depth of 245 m after removal of approximately 18 million tonnes of Ni-Cu ore (Bleeker and Macek, 1996). Since the cessation of mining, the pit has been allowed to slowly fill with water, largely through surface drainage. Recent imagery from Google Earth™ (Google, 2018) revealed that the water had risen above the northeast rim of the open pit and was beginning to flood the adjacent outcrops, including some of the classic exposures of Ospwagan group rocks (Figure GS2018-2-1). In June 2018, a project was initiated to photographically document the outcrops along the east and northeast shoulders of the Pipe pit before they become inundated. As an additional component, a drone was loaned by the Department of Geological Sciences at the University of Manitoba to capture high-resolution aerial imagery of these important outcrops.

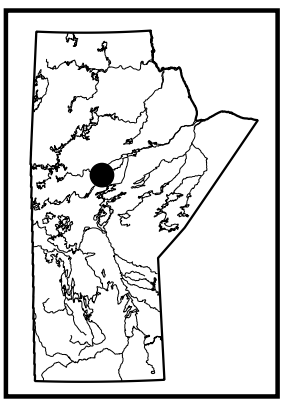

Ospwagan group

The following summary of the Ospwagan group is sourced largely from Bleeker (1990) and Zwanzig et al. (2007). The Paleoproterozoic Ospwagan group unconformably overlies Archean basement gneiss in the TNB (Figure GS2018-2-2). The lowermost unit of the Ospwagan group is the Manasan formation, a passive-margin, fining-upward siliciclastic sequence that consists of layered to laminated sandstone with local conglomerate layers near the base (M1 member) and overlying semipelitic rock (M2 member). This siliciclastic system grades into the overlying calcareous sedimentary rocks of the Thompson formation.

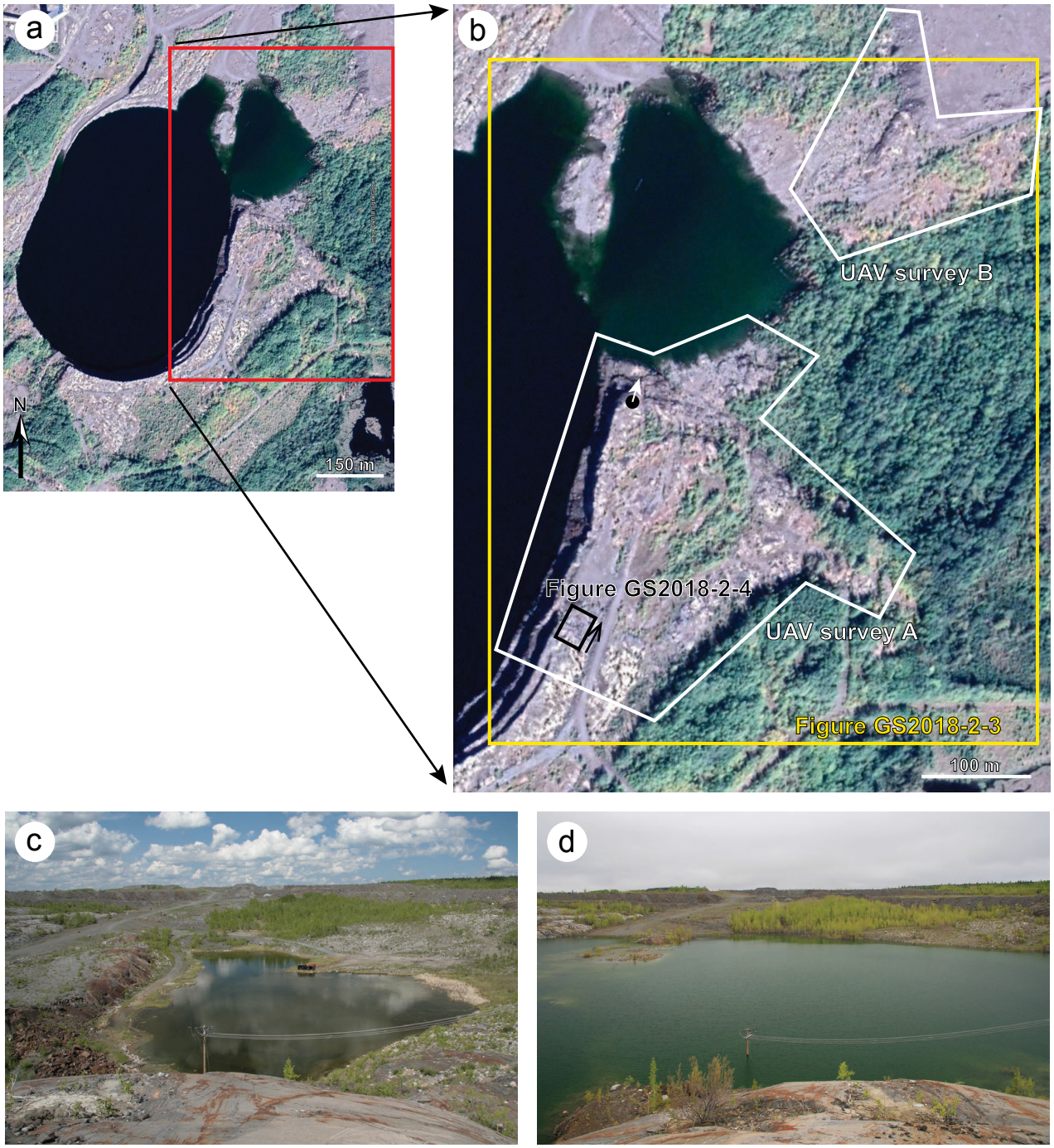

Figure GS2018-2-1: *Satellite imagery of the Pipe II open-pit mine* ***(a)*** *and outcrops along the east and northeast shoulders of the open pit (****b****; Google, 2018). The yellow outline indicates the approximate location of the geological map in Figure GS2018-2-3. The white outlines indicate the approximate locations of the two unmanned aerial vehicle (UAV) surveys. The black outline indicates the approximate location of the detailed aerial image in Figure GS2018-2-4 (the arrow indicates the top of the image). The black dot marks the vantage point of photos* ***(c)*** *and* ***(d)****, which were taken looking in the direction of the arrow. Photo* ***(c)*** *was taken during the summer of 2007 and photo* ***(d)*** *was taken in June 2018.*

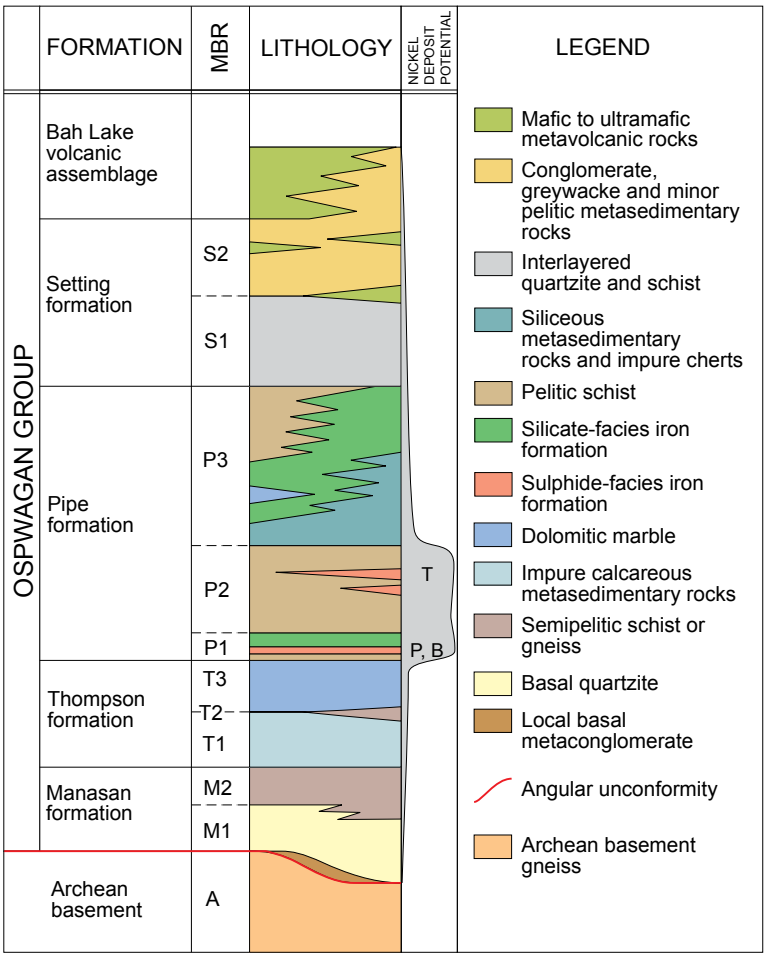

Figure GS2018-2-2: *Schematic lithostratigraphic section of the Ospwagan group (modified from Bleeker, 1990). Abbreviations: B, stratigraphic location of the Birchtree orebody; MBR, member; P, stratigraphic location of the Pipe II orebody; T, stratigraphic location of the Thompson orebody.*

The Thompson formation consists of a variety of calcareous–siliceous rocks, including chert, calcsilicate and impure marble (T1 member), and impure dolomitic marble with local horizons of calcsilicate (T3 member). The T2 member consists of a calcareous semipelitic rock that is rarely present. The Thompson formation represents a transition from a siliciclastic-dominated to a carbonate-dominated system.

The Pipe formation is subdivided into three members. The P1 member consists of a graphite-rich, sulphide-facies iron formation at the base (the locus of the Pipe II and Birchtree orebodies), overlain by a silicate-facies iron formation. The top of the P1 member consists of a reddish, laminated, siliceous rock. The P1 member grades into the overlying pelitic rocks of the P2 member, the top of which is marked by a sulphide-facies iron formation (the locus of the Thompson orebody). The overlying P3 member consists of a wide variety of rock types, including laminated, siliceous, sedimentary rocks; silicate-, carbonate- and local oxide-facies iron formations; and semipelitic rocks, calcsilicate and a local horizon of relatively pure dolomitic marble. The Pipe formation represents a mix of chemical sediments and fine to very fine siliciclastics that were deposited in either an open-marine environment (Zwanzig et al., 2007) or during the development of a foredeep basin (Bleeker, 1990).

The Setting formation is divided into two members and is defined to include all siliciclastic rocks above the uppermost iron formation of the P3 member. The S1 member consists of rhythmically interbedded quartzite and pelitic schist with local calcareous concretions, which are characteristic of the S1 member. The S2 member consists of thickly layered greywacke, with local horizons grading from conglomeratic at the base to pelitic at the top. The S2 member appears to be missing altogether in the area of the Pipe mine. The Setting formation is interpreted to have been deposited by turbidity currents in a relatively deep-marine environment, possibly a foredeep basin (Bleeker, 1990).

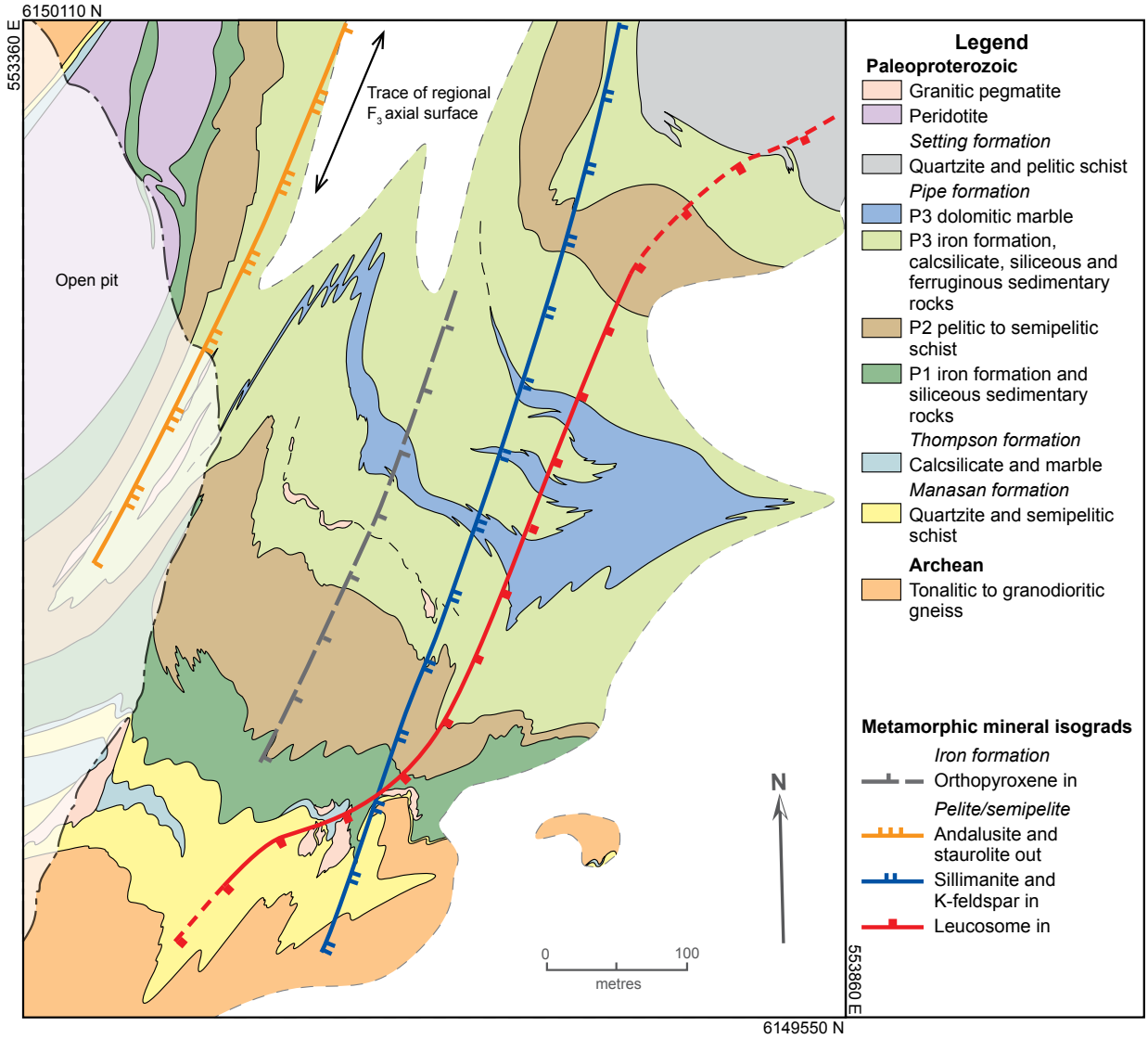

Figure GS2018-2-3: *Simplified geology of the east and northeast shoulders of the Pipe II open-pit mine (modified from Bleeker, 1990; Couëslan et al., 2011).*

At the top of the Ospwagan group is the Bah Lake assemblage, which consists of mafic to ultramafic volcanic rocks dominated by massive to pillowed basalt flows with local picrite and minor synvolcanic intrusions. Although present in the Pipe mine area, rocks of the Bah Lake assemblage are not present in the outcrops along the margin of the open pit. The Bah Lake assemblage may suggest the onset of active rifting in the TNB (Zwanzig, 2005; Zwanzig et al., 2007), or that the foredeep was magmatically active (Bleeker, 1990).

A maximum age for the Ospwagan group is provided by a ca. 1974 Ma zircon recovered from Setting formation greywacke (Bleeker and Hamilton, 2001). A minimum age for the Ospwagan group is provided by crosscutting amphibolitized dikes interpreted to be part of the Molson dike swarm, and the possibly comagmatic Ni-ore–bearing ultramafic sills that intruded the Ospwagan group at all stratigraphic levels ca. 1883 Ma (Bleeker, 1990; Zwanzig et al., 2007; Burnham et al., 2009; Heaman et al., 2009; Scoates et al., 2017). The interaction of these ultramafic intrusions with sulphide-rich horizons of the Pipe formation (Figure GS2018-2-2) led to sulphur saturation of the ultramafic magmas, and the precipitation and economic accumulation of Ni sulphides.

Geology of the Pipe II mine

The Pipe II mine is located approximately 35 km south of Thompson, Manitoba. Accessible outcrops along the east shoulder of the open pit provide one of the most complete successions of Ospwagan group

Figure GS2018-2-4: *Downsampled aerial image from the east shoulder of the Pipe II open-pit mine. Red rectangles mark the detailed outcrop images in Figure GS2018-2-5.*

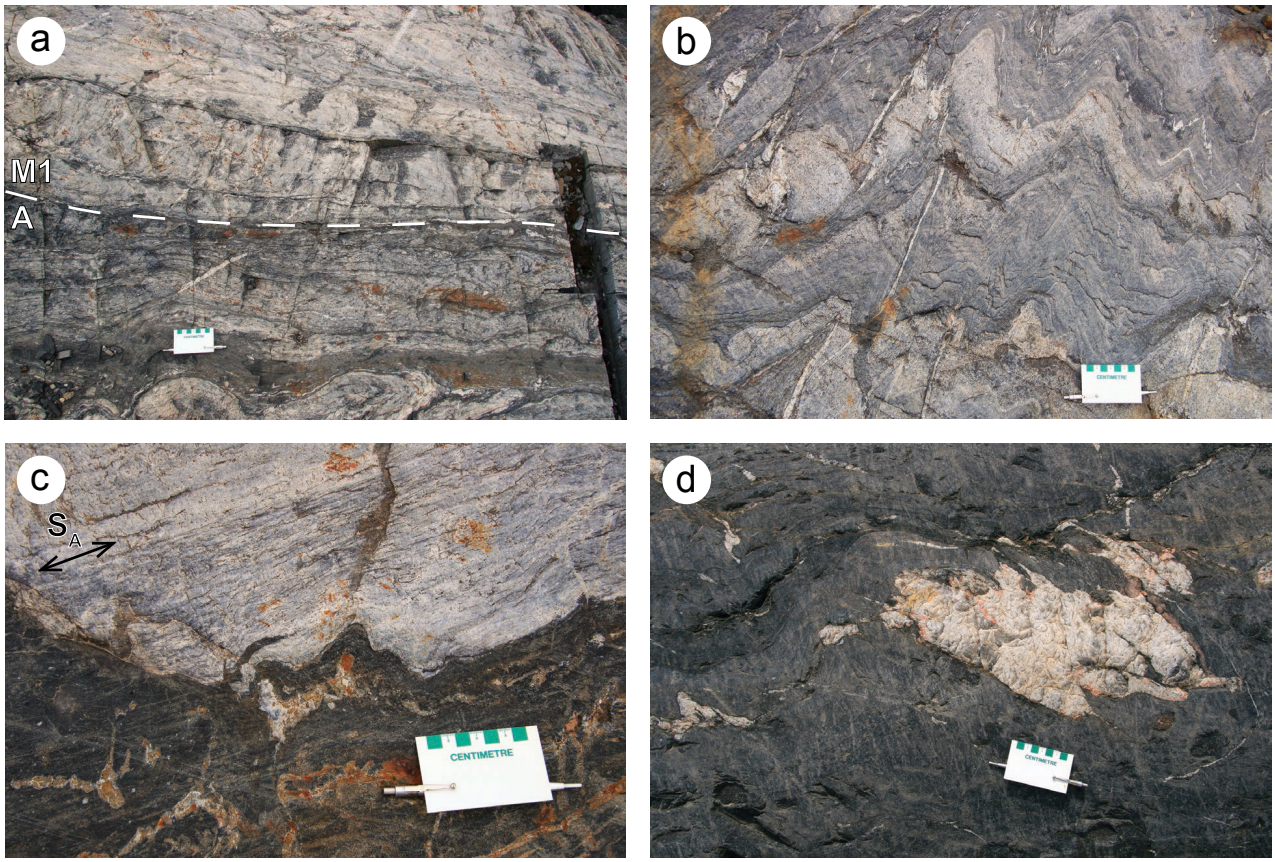

Figure GS2018-2-5: *Detailed images from the outcrop shown in Figure GS2018-2-4:* ***a)*** *unconformity between the Archean basement gneiss (A) and M1 member quartzite of the Manasan formation (M1);* ***b)*** *F_3 folds in graded beds of the M1 member;* ***c)*** *discordant relationship between Archean gneiss and a mafic dike, possibly related to the ca. 1883 Ma Molson swarm; S_A indicates the trace of the Archean gneissosity;* ***d)*** *a quartz-rich, likely subsolidus segregation in the M2 member semipelite of the Manasan formation.*

rocks in the TNB, and it is the type locality for the Pipe formation. The ore deposit is situated along the base of a serpentinized ultramafic body emplaced near the base of the Pipe formation (Bleeker, 1990). The ultramafic body is interpreted as a differentiated sill that comprises a base to top succession from dunite to peridotite to plagioclase-bearing orthopyroxenite. Intrusion of the ultramafic body occurred at 1880.2 ±1.4 Ma (Scoates et al., 2017). Simple quartz-feldspar pegmatite dikes up to tens of metres wide and hundreds of metres in length locally intrude both the Archean gneiss and Ospwagan group stratigraphy. Dikes of granitic pegmatite can be oriented subparallel to the stratigraphy or axial planar to F_3, or lack clear relationships to the stratigraphy or structures, and likely represent intrusions of various ages emplaced during metamorphism and deformation.

The rocks at the Pipe II mine are folded into a tight, northeast-trending F_3 synform that plunges steeply toward the east and has a steeply dipping axial plane (Figure GS2018-2-3; Fueten et al., 1986; Bleeker, 1990). The stratigraphy of the Ospwagan Group is upward facing and has been interpreted as the lower, upward-facing limb of an F_2 recumbent fold (Bleeker, 1990; Burnham et al., 2009). Metamorphic mineral assemblages in pelite and iron formation range from middle-amphibolite facies (585–600°C, 3.7–3.9 kbar) to upper-amphibolite facies (640–660°C, 3.0–3.6 kbar) and define a series of north-northeast-trending metamorphic mineral isograds subparallel to the trace of the F_3 axial surface. The mineral isograds suggest a metamorphic thermal gradient increasing toward the east-southeast across the Pipe mine area (Couëslan et al., 2011).

Methodology

Approximately 35 gigabytes of high-resolution aerial imagery was captured by unmanned aerial vehicle (UAV, drone; Figure GS2018-2-4). Individual images are approximately 24 megabytes each, with a resolution of 4000 by 3000 pixels, and were geospatially located with the onboard global positioning system (GPS). Surveys were flown over two separate areas as outlined in Figure

GS2018-2-1b. The surveys were flown at a height of 20 m above the approximate highest topographic point in each survey area. Attempts were made to get at least 80% overlap between adjacent images. Twelve control points were geospatially located with handheld GPS in the two survey areas (seven in area A and five in area B).

Approximately 200 detailed outcrop photographs were collected, each of which was spatially located by GPS. Attempts were made to document all of the units described in the preliminary maps of Bleeker and Macek (1988b–i), including representative images of the Archean basement, Ospwagan group and intrusive phases (Figure GS2018-2-5a–d). Images were also taken of structures, including the three main phases of folding, crosscutting relationships and late brittle faulting (Figure GS2018-2-5b, c); and of metamorphic mineral assemblages and features to document the west to east metamorphic field gradient (Figure GS2018-2-5d).

Planned outputs

The final output proposed for this project is a digital Open File report integrating a detailed geological map, high-resolution aerial imagery and detailed outcrop photographs in a geographic information system (GIS) format. The aerial imagery will be processed using structure-from-motion (SfM) photogrammetry to generate a 3-D point cloud and digital elevation model (DEM) based on the identification of matching features in multiple overlapping images (Turner et al., 2012; Westoby et al., 2012; Tavani et al., 2014). The UAV imagery and detailed geological map will then be overlain on the DEM. Detailed outcrop images of stratigraphy, structures and metamorphic assemblages will be linked to their locations projected on the map/aerial imagery surface. Processing of the UAV imagery is to begin in the autumn of 2018.

Economic considerations

A working knowledge of the Ospwagan group stratigraphy is key to successful exploration in the TNB. One must be able to recognize Ospwagan group stratigraphy in the drillcore, identify which part of the stratigraphy was intersected, and decide in which stratigraphic direction the most prospective horizons are located. In the mine environment, geologists must be able to recognize the stratigraphic and structural environment to vector-in on additional ore. The planned open file report will be available as a learning resource for geologists working in the TNB, as well as to researchers wishing to understand more about the belt.

Acknowledgments

Thanks go to N. Brandson and E. Anderson for logistical support, and A. Hutchins for assisting with fieldwork and flying a significant portion of the UAV survey. Sincere appreciation goes to R. Stewart and S. Kirby with Vale – Manitoba Operations for supporting the initial proposal of this project and providing access to the Pipe II mine site. A. Camacho, P. Durkin and D. Drayson from the Department of Geological Sciences, University of Manitoba graciously offered the use of, and provided training for, the department's drone. J. Macek provided a detailed tour of the Ospwagan group stratigraphy at the Pipe II mine, ensuring that no details were missed and all available parts of the sequence were documented. Thanks also go to S. Gagné and M. Rinne for reviewing previous drafts of this report.

References

Bleeker, W. 1990: Evolution of the Thompson Nickel Belt and its nickel deposits, Manitoba, Canada; Ph.D. thesis, University of New Brunswick, Fredericton, 400 p.

Bleeker, W. and Hamilton, M.A. 2001: New SHRIMP U-Pb ages for the Ospwagan group: implications for the SE margin of the Trans-Hudson orogen; Geological Association of Canada–Mineralogical Association of Canada, Joint Annual Meeting, St. John's, Newfoundland and Labrador, May 27–30, 2001, Program with Abstracts, v. 26, p. 15.

Bleeker, W. and Macek, J.J. 1988a: Thompson Nickel Belt Project – Pipe Pit mine; *in* Report of Field Activities 1988, Manitoba Energy and Mines, Minerals Division, p. 111–115.

Bleeker, W. and Macek, J.J. 1988b: Pipe open pit mine (part of NTS 63O/8NE); Manitoba Energy and Mines, Minerals Division, Preliminary Map 1988T-1, scale 1:400.

Bleeker, W. and Macek, J.J. 1988c: Pipe open pit mine (part of NTS 63O/8NE); Manitoba Energy and Mines, Minerals Division, Preliminary Map 1988T-2, scale 1:400.

Bleeker, W. and Macek, J.J. 1988d: Pipe open pit mine (part of NTS 63O/8NE); Manitoba Energy and Mines, Minerals Division, Preliminary Map 1988T-3, scale 1:400.

Bleeker, W. and Macek, J.J. 1988e: Pipe open pit mine (part of NTS 63O/8NE); Manitoba Energy and Mines, Minerals Division, Preliminary Map 1988T-4, scale 1:400.

Bleeker, W. and Macek, J.J. 1988f: Pipe open pit mine (part of NTS 63O/8NE); Manitoba Energy and Mines, Minerals Division, Preliminary Map 1988T-5, scale 1:400.

Bleeker, W. and Macek, J.J. 1988g: Pipe open pit mine (part of NTS 63O/8NE); Manitoba Energy and Mines, Minerals Division, Preliminary Map 1988T-6, scale 1:400.

Bleeker, W. and Macek, J.J. 1988h: Pipe open pit mine (part of NTS 63O/8NE); Manitoba Energy and Mines, Minerals Division, Preliminary Map 1988T-7, scale 1:400.

Bleeker, W. and Macek, J.J. 1988i: Pipe open pit mine (part of NTS 63O/8NE); Manitoba Energy and Mines, Minerals Division, Preliminary Map 1988T-8, scale 1:400.

Bleeker, W. and Macek, J.J. 1996: Evolution of the Thompson Nickel Belt, Manitoba: setting of Ni-Cu deposits in the western part of the Circum Superior Boundary Zone; Geological Association of Canada–Mineralogical Association of Canada, Joint Annual Meeting, Winnipeg, Manitoba, May 27–29, 1996, Field Trip Guidebook A1, 45 p.

Burnham, O.M., Halden, N., Layton-Matthews, D., Lesher, C.M., Liwanag, J., Heaman, L., Hulbert, L., Machado, N., Michalak, D., Pacey, M., Peck, D.C., Potrel, A., Theyer, P., Toope, K. and Zwanzig, H. 2009: CAMIRO project 97E-02, Thompson Nickel Belt: final report, March 2002, revised and updated 2003; Manitoba Science, Technology, Energy and Mines, Manitoba Geological Survey, Open File OF2008-11, 434 p. plus appendices and GIS shape files for use with ArcInfo®.

Couëslan, C.G., Pattison, D.R.M. and Tinkham, D.K. 2011: Regional low-pressure amphibolite-facies metamorphism at the Pipe II mine, Thompson nickel belt, Manitoba, and comparison of metamorphic isograds in metapelites and meta-iron formations; The Canadian Mineralogist, v. 49, p. 721–747.

Fueten, F., Robin, P.-Y.F. and Pickering, M.E. 1986: Deformation in the Thompson belt, central Manitoba: a progress report; *in* Current Research, Part B, Geological Survey of Canada, Paper 86-1B, p. 797–809.

Galley, A.G., Bailes, A.H., Syme, E.C., Bleeker, W., Macek, J.J. and Gordon, T.M. 1990: Geology and mineral deposits of the Flin Flon and Thompson belts, Manitoba; Geological Survey of Canada, Open File 2165 and the 8th International Association on the Genesis of Ore Deposits symposium, Ottawa, Ontario, August 12–28, 1990, Field Trip Guidebook 10, 136 p.

Google 2018: Google Earth™ satellite image of the Pipe II open-pit mine, Manitoba; Google, image, URL <http://earth.google.com> [©2018 Google – Imagery, © 2018 DigitalGlobe, July 2018].

Heaman, L.M., Peck, D. and Toope, K. 2009: Timing and geochemistry of 1.88 Ga Molson Igneous Events, Manitoba: insights into the formation of a craton-scale magmatic and metallogenic province; Precambrian Research, v. 172, p. 143–162, https://doi.org/10.1016/j.precamres.2009.03.015.

Macek, J.J. and Bleeker, W. 1989: Thompson Nickel Belt Project – Pipe Pit mine, Setting and Ospwagan lakes; *in* Report of Field Activities 1989, Manitoba Energy and Mines, Minerals Division, p. 73–87.

Scoates, J.S., Scoates, J.R.F., Wall, C.J., Friedman, R.M. and Couëslan, C.G. 2017: Direct dating of ultramafic sills and mafic intrusions associated with Ni-sulfide mineralization in the Thompson nickel belt, Manitoba, Canada; Economic Geology, v. 112, p. 675–692.

Tavani, S., Granado, P., Corradetti, A., Girundo, M., Iannace, A., Arbués, P., Muñoz, J.A. and Mazzoli, S. 2014: Building a virtual outcrop, extracting geological information from it, and sharing the results in Google Earth via OpenPlot and Photoscan: an example from the Khaviz Anticline (Iran); Computers in Geoscience, v. 63, p. 44–53.

Turner, D., Lucieer, A. and Watson, C. 2012: An automated technique for generating georectified mosaics from ultra-high resolution unmanned aerial vehicle (UAV) imagery, based on structure from motion (SfM) point clouds; Remote Sensing, v. 4, p. 1392–1410.

Westoby, M.J., Brasington, J., Glasser, N.F., Hambrey, M.J. and Reynolds, J.M. 2012: 'Structure-from-motion' photogrammetry: a low-cost, effective tool for geoscience applications; Geomorphology, v. 179, p. 300–314.

Zwanzig, H.V. 2005: Geochemistry, Sm-Nd isotope data and age constraints of the Bah Lake assemblage, Thompson Nickel Belt and Kisseynew Domain margin: relation to Thompson-type ultramafic bodies and a tectonic model (NTS 63J, O and P); *in* Report of Activities 2005, Manitoba Industry, Economic Development and Mines, Manitoba Geological Survey, p. 40–53.

Zwanzig, H.V., Macek, J.J. and McGregor, C.R. 2007: Lithostratigraphy and geochemistry of the high-grade metasedimentary rocks in the Thompson Nickel Belt and adjacent Kisseynew Domain, Manitoba: implications for nickel exploration; Economic Geology, v. 102, p. 1197–1216.

GS2018-3

Summary of key results and interpretations from the Fox River belt compilation project, northeastern Manitoba (parts of NTS 53M, N, O, 54B, C, D)

by M.L. Rinne

In Brief:

- Ca. 300 km long greenstone belt that forms part of the metallogenic circum-Superior belt
- Demonstrates potential for Ni (±Cu, PGE, Co, Cr) mineralization in widespread intrusive and volcanic units
- Proposed stratigraphic correlations with the Ospwagan group of the Thompson nickel belt

Citation:
Rinne, M.L., 2018: Summary of key results and interpretations from the Fox River belt compilation project, northeastern Manitoba (parts of NTS 53M, N, O, 54B, C, D); *in* Report of Activities 2018, Manitoba Growth, Enterprise and Trade, Manitoba Geological Survey, p. 25–36.

Summary

The Fox River belt forms a large but sparsely exposed segment of the circum-Superior belt in northeastern Manitoba and demonstrates potential to host Ni (±Cu, platinum-group elements, Co, Cr) mineralization of the same age as that in the Thompson nickel belt. This report summarizes the results of a recent geological compilation of the Fox River belt, incorporating the results of several past studies and more recent industry data.

Mafic–ultramafic intrusions and flows of the Fox River belt record high-volume, possibly mantle-plume–derived magmatism of the widespread Molson igneous event (ca. 1.88 Ga). Although the Fox River sill contains the highest Ni-Cu-platinum-group element (PGE) values sampled in the belt to date, the lower intrusions are also considered prospective for magmatic sulphide mineralization. Additional potential for mineralization in the mafic–ultramafic flows is proposed based on their cogenetic relationship with the locally mineralized intrusions, and on anomalous PGE contents in part of the Upper Volcanic formation.

Clastic sedimentary rocks of the Fox River belt are interpreted to have recorded marine sedimentation shed off the margin of the Superior craton. A regional stratigraphic correlation between rocks of the Lower and Middle Sedimentary formations (Fox River belt) and the Ospwagan group (Thompson nickel belt) is implied by their similar depositional and geodynamic environment, their shared regional detrital source (as reflected by similar trace-element characteristics and Archean Nd model ages that are distinct from rocks of the Kisseynew domain) and their deposition prior to Molson magmatism. From the perspective of mineral exploration, confirming an eastward extension of the Ospwagan group would further the potential for Ni mineralization in the Fox River belt.

Introduction

The Fox River belt (FRB) is a large (~6000 km^2) greenstone belt located along the northwestern margin of the Superior province (Figure GS2018-3-1a). Forming part of the circum-Superior belt, it records a sequence of Paleoproterozoic seafloor sedimentation and ca. 1883 Ma mafic-ultramafic magmatism (Heaman et al., 1986). As in other segments of the circum-Superior belt, the rocks were emplaced along the margins of the Superior craton prior to the closure of the Manikewan Ocean, culminating in the suture of the Superior and Churchill provinces (Baragar and Scoates, 1981; Corrigan et al., 2009). Circum-Superior segments both east and west of the FRB are host to significant magmatic sulphide mineralization: in the Cape Smith belt of northern Quebec, Ni-Cu±PGE deposits are hosted in ca. 1882–1881 Ma komatiite flows (Raglan horizon; Bleeker and Kamo, 2018); and in the Thompson nickel belt, magmatic sulphide deposits are hosted in (or were remobilized from) ca. 1883–1880 Ma ultramafic sills (Lightfoot et al., 2017; Scoates et al., 2017).

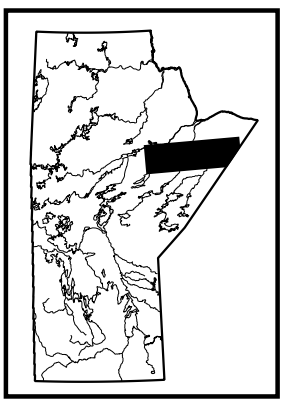

In 2015, the Manitoba Geological Survey (MGS) initiated a new geological compilation of the FRB. The aims of the project were to

- produce an up-to-date bedrock geology map of the FRB informed by a combination of previous mapping, detailed airborne magnetic surveys and drillcore data;
- provide an updated emplacement history and stratigraphic summary of the FRB; and
- investigate regional stratigraphic relationships between the FRB and the Thompson nickel belt.

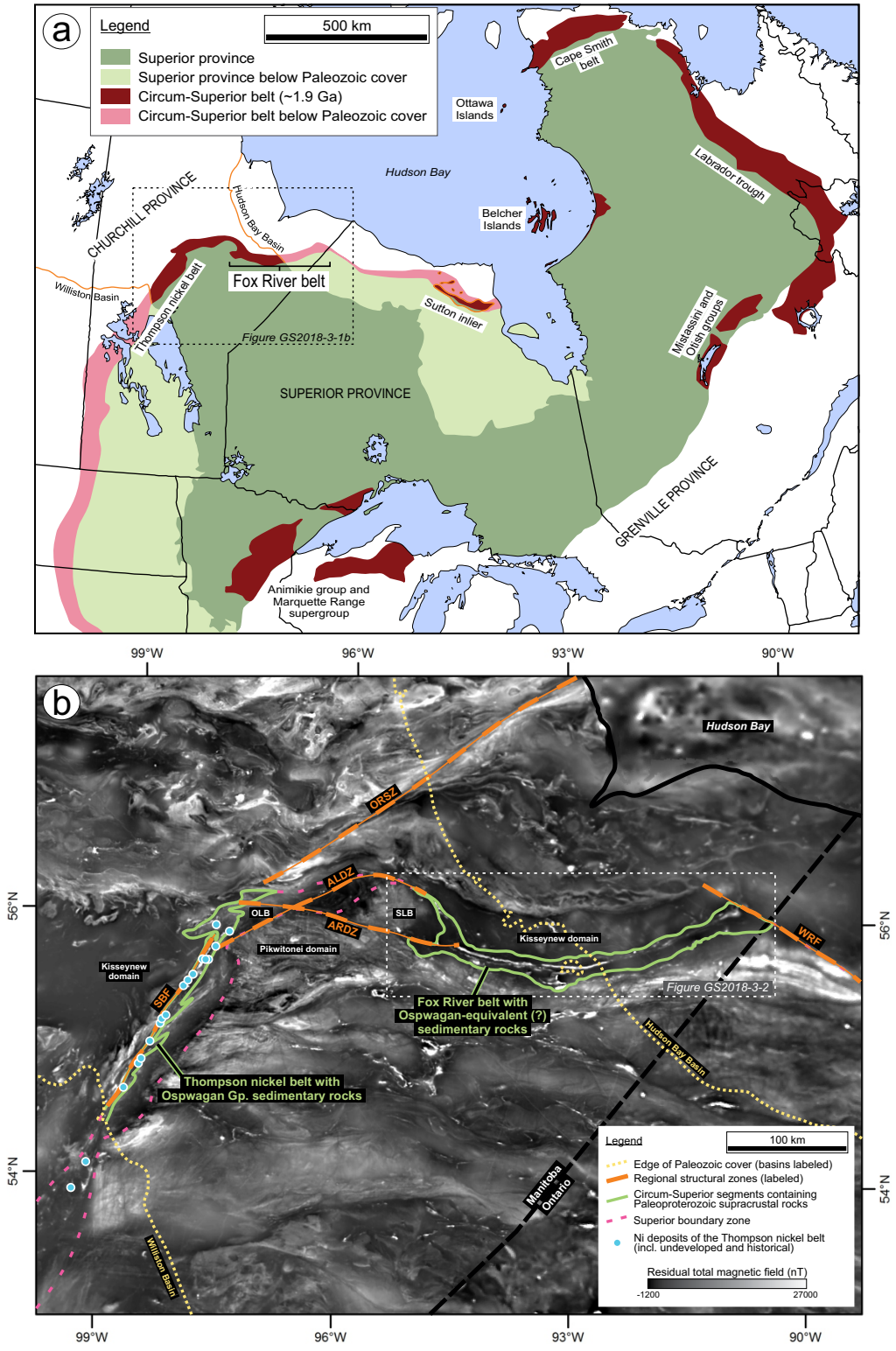

Figure GS2018-3-1: *Geological maps, showing* ***a)*** *the location of the Fox River belt along the circum-Superior belt, between the Ni deposits of the Thompson nickel belt and the Cape Smith belt (modified after Baragar and Scoates, 1981 and Minifie et al., 2013);* ***b)*** *an overview of the northwestern portion of the circum-Superior belt, northeastern Manitoba, extending from the buried portion of the Thompson nickel belt in the southwestern part of the map to the Fox River belt in the east. Major structural zones are shown over a greyscale map of the residual total magnetic field. The Superior boundary zone includes supracrustal segments of the circum-Superior belt as well as regions dominated by highly deformed Archean gneiss of the Superior province (such as the eastern portion of the Thompson nickel belt). Abbreviations: ALDZ, Assean Lake deformation zone; ARDZ, Aiken River deformation zone; OLB, Orr Lake block; ORSZ, Owl River shear zone; SBF, Superior boundary fault; SLB, Split Lake block; WRF, Winisk River fault.*

Exploration history

Following the first regional mapping in 1878 (Bell, 1879), the FRB was subject to several mineral exploration campaigns (Table GS2018-3-1). In addition to a number of airborne and ground magnetic and electromagnetic surveys, multimedia geochemical surveys and limited outcrop mapping, a total of 230 drillholes were collared within the FRB between 1955 and 2010. Approximately half of all drilling in the FRB was undertaken by the International Nickel Company of Canada Ltd. between 1955 and 1972 (Table GS2018-3-1). Approximately one quarter of drilling in the FRB was undertaken by Falconbridge Ltd. (later Xstrata Nickel Inc.) between 1977 and 2007, and the remainder by the companies identified in Table GS2018-3-1.

Geology of the Fox River belt

The dominantly east-striking FRB is approximately 15–20 km wide by 300 km long and consists of a series of mostly northward-younging and steeply north-dipping submarine sedimentary rocks, and mafic–ultramafic flows and intrusions. The belt is almost entirely drift covered; known outcrop locations are limited to the western part of the belt, mostly in river exposures (Figure GS2018-3-2).

Geological units of the FRB are described briefly in this section, moving up stratigraphy (Figure GS2018-3-3). More detailed geological descriptions are provided by Scoates (1981, 1990) and Desharnais (2005).

Southern gneiss domain (Superior province)

The Southern gneiss domain contains Archean quartz-feldspar-biotite gneiss, locally augen-bearing granite, granodiorite, and amphibolite dikes and rafts. The rocks outcrop near the southern edge of the FRB. Metamorphic grade is estimated to be middle amphibolite facies (Peck et al., 2000). Three samples of granitoid and granitoid gneiss, collected within 10 km of the southern margin of the FRB, yielded possibly reset K-Ar (biotite, hornblende) ages ranging from 2695 ±80 Ma to 2355 ±72 Ma (Wanless et al., 1968, 1973).

Lower Sedimentary formation

The Lower Sedimentary formation is a package of planar-bedded quartzofeldspathic to argillaceous mudstone and fine sandstone 4 km thick. The beds are normally graded and locally calcareous, with minor oxide-facies (magnetite±specular hematite) iron formation documented throughout the unit. Graphitic layers and sulphide-bearing horizons are also common in drillcore.

Rocks of the Lower Sedimentary formation are interpreted to have been deposited in a distal marine basin, consisting mostly of continent-derived turbidites (Baragar and Scoates, 1987). This is partly supported by a Nd model age of 2.86 Ga (Desharnais, 2005), consistent with material shed from the Archean Superior craton (i.e., the Southern gneiss domain). A possible northward-increasing abundance of iron formation in the Lower Sedimentary formation was interpreted by Peck et al. (2000) as recording the onset of rifting prior to emplacement of the overlying igneous units.

Mafic dikes

East-trending, locally well-layered dikes of gabbroic to dioritic composition have crosscut basement rocks of the Southern gneiss domain, along with the southernmost kilometre of the Lower Sedimentary formation. The dikes outcrop partly along the Stupart, Sipanigo and Bigstone rivers (Peck et al., 2000). One such dike has been dated at 1900 ±14 Ma (Heaman et al., 2009), indicating that they collectively form part of the ca. 1.88 Ga Molson igneous event, which includes the Molson dike swarm and Fox River sill (Heaman et al. 1986; Peck et al., 2000; Heaman et al., 2009).

Lower intrusions

The lower intrusions crosscut rocks of the Lower Sedimentary formation. Most of the intrusions are approximately parallel with the FRB stratigraphy, and occur near the contact between the Lower Sedimentary and Lower Volcanic formations (Figures GS2018-3-2, 3). Magnetic signatures and limited drill intersections indicate that the intrusions range from 50 to 500 m in thickness and up to tens of kilometres in length (Desharnais, 2005). Most of the intrusions exhibit cumulate segregation into a basal (southern) peridotite, a thin central pyroxenite layer and an upper gabbro.

The lower intrusions are mineralogically and geochemically identical to the later described Fox River sill. Although the lower intrusions have not been dated, Sm-Nd and La-Hf contents of least-contaminated samples plot along Nd and Hf 1883 Ma isochrons (Desharnais, 2005), further supporting a genetic relationship with the ca. 1883 Ma Fox River sill.

Lower Volcanic formation

The Lower Volcanic formation consists of up to 2.5 km of mafic–ultramafic (komatiitic basalt) flows with minor, locally sulphide-bearing interflow mudstone. Scoates (1981) subdivided the western part of the Lower Volcanic formation into three zones, namely the lower

Table GS2018-3-1: Summary of field and exploration work in the Fox River belt and adjacent areas, northeastern Manitoba.

Company / Organization	Dates	Summary of work
Geological Survey of Canada	1879-1955	Early regional surveys by Bell (1879), Brock (1911), Merritt (1925; first identification of ultramafic rocks), and Quinn (1955)
International Nickel Company of Canada Ltd.	1955-1972	Airborne (400 m) and ground geophysical surveys; river outcrop mapping; 116 holes drilled (30406 m; approximately half targeting the Fox River sill)
Sherritt Gordon Mines Ltd.	1956-1971	Airborne (800 m) and ground geophysical surveys; 8 holes drilled (1134 m)
Icon Syndicate Ltd.	1962	Airborne geophysical surveys (300 m); no documented follow-up
Selco Exploration Company Ltd. + Amax Exploration Inc.	1968	Airborne geophysical surveys (400 m); 2 holes drilled (387 m)
Manitoba Mineral Resources, Exploration Operations Branch	1976	Ground geophysical surveys; overburden drilling and basal till geochemistry (covering a small portion of the Fox River sill); regional glacial stratigraphic studies
Manitoba Geological Survey	1975-1977	Mapping of available river outcrop (1969, 1975, 1976, 1977 field seasons); extensive relogging of INCO drillcore; petrographic studies; detailed summaries published in 1981 and 1990
Falconbridge Nickel Mines Ltd.	1977-1981	Airborne and ground geophysical surveys; 12 holes drilled (2601 m)
BP Resources Canada Ltd. (Selco Division) + Platinum Exploration Canada Inc.	1985-1989	Airborne (115 m and 200 m) geophysical surveys (covering the western half of the Fox River sill), ground geophysical surveys; 13 holes drilled (2841 m)
Westminer Canada Ltd.	1991-1993	Lake sediment sampling (333 samples); ground geophysical surveys; 10 holes drilled (1921 m)
BHP Minerals Canada Ltd.	1998	Regional till sampling (KIM, Au, base metals; 503 samples collected, most south of the Fox River belt)
Manitoba Geological Survey	1999	Reconnaissance mapping in areas of known outcrop (in collaboration with Falconbridge); detailed mapping of volcanic stratigraphy in four river outcrop sections
Falconbridge Ltd.	1999-2000	Airborne (250 m) and ground geophysical surveys; reconnaissance mapping; 1:1000 scale mapping in the Great Falls area (with G. Desharnais); discovery of sulphide-bearing KO zone; 12 holes drilled (4123 m)
Marum Resources Inc.	2001	Ground geophysical surveys; 3 holes drilled (59 m; 2 collared in northwest corner of Fox River belt)
Falconbridge Ltd. + Rockwell Ventures Inc.	2001-2005	Airborne, ground, and borehole geophysical surveys; soil geochemical surveys; treetop biogeochemical surveys (482 samples); 9 holes drilled (1543 m)
Falconbridge Ltd. + Donner Minerals Ltd.	2003-2004	Airborne and ground geophysical surveys (mostly north as well as north and northwest of the Fox River belt); 10 holes drilled (2467 m)
Callinan Mines Ltd. + Bell Resources Ltd.	2002 - 2008	Airborne (200 m) and ground geophysical surveys (including gravity); snow hydrogeochemical survey; Mobile Metal Ion soil survey; till sampling; 18 holes drilled (4801 m)
Diamonds North Resources Ltd.	2004-2005	Airborne geophysical surveys (250 m; eastern end of the Fox River belt); till sampling (12 samples)
Pure Nickel Inc. + Xstrata Nickel	2007	Airborne geophysical surveys (150 m); 10 holes drilled (3506 m)
Auriga Gold Corp.	2010	1 hole drilled (562 m; targeting sulphide-bearing KO zone of Fox River sill)

Notes: Geophysical surveys refer to magnetic and electromagnetic methods unless otherwise specified. Bracketed distances for airborne surveys indicate flight line spacing. The table does not include all work on properties adjacent to the Fox River belt, such as a small ground geophysical survey by Inco Ltd. in 2006, and nearby till sampling programs by BHP Billiton World Exploration Ltd. (1999-2001), Indicator Explorations Ltd. (1999-2002) and Kennecott Canada Exploration Inc. (2000-2001).

Abbreviation: KIM, kimberlite-indicator mineral

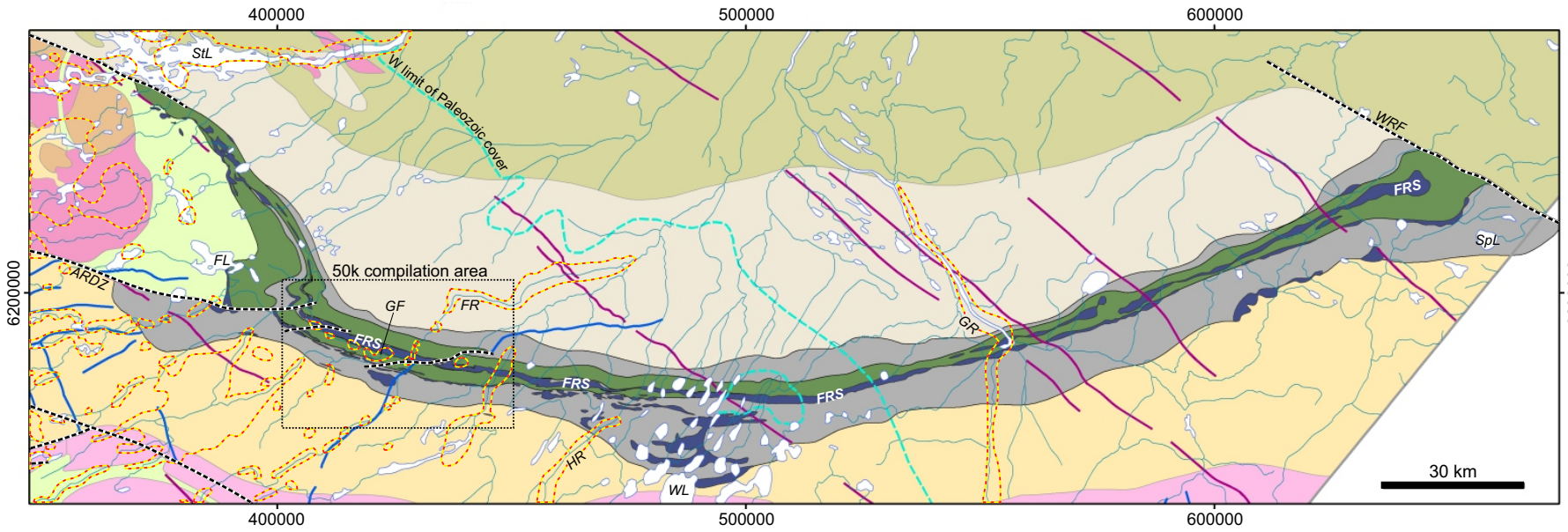

Figure GS2018-3-2: *Simplified geology of the Fox River belt, northeastern Manitoba. The dashed blue line marks the western edge of Paleozoic cover; units shown east of this line are projected through Paleozoic rock of the Hudson Bay Basin. Fox River belt units were drawn mostly on the basis of drillcore intercepts, known outcrop exposures, aeromagnetic data, and geological sections and map interpretations by Scoates (1981, 1990), and Hulbert and Scoates (2005). The figure area corresponds to a 1:250 000 scale compilation map with an expected release in early 2019, along with a 1:50 000 scale area over the western part of the belt (outlined area labeled). Abbreviations: ARDZ, Aiken River deformation zone; FL, Fox Lake; FR, Fox River; FRS, Fox River sill; GF, Great Falls outcrop area; GR, Gods River; HR, Hayes River; SpL, Spector Lake; StL, Stephens Lake; WL, Whitefish Lake; WRF, Winisk River fault. All co-ordinates are in UTM Zone 15 (NAD83).*

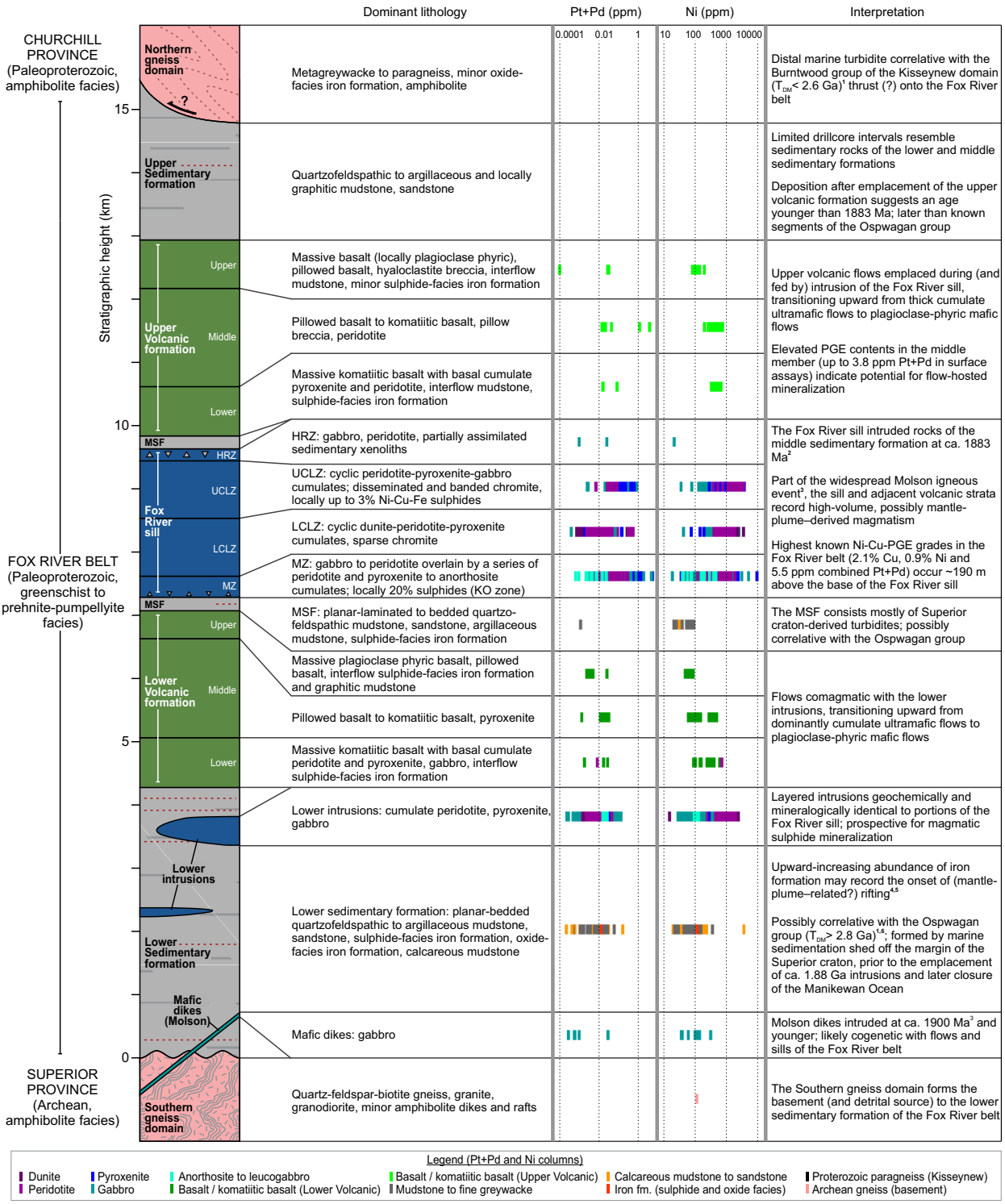

Figure GS2018-3-3: *Simplified stratigraphic summary of the Fox River belt, northeastern Manitoba. Red dashed lines in the stratigraphic column denote occurrences of iron formation in sedimentary strata. Platinum+Pd and Ni data are from sources compiled in Desharnais et al. (2004a) and assessment files (Assessment Files 73666, 73726, 73837, 73965, 74240, 93695, Manitoba Growth, Enterprise and Trade, Winnipeg). References cited with superscript numbers in the interpretation column are: 1) Böhm et al., 2007; 2) Heaman et al., 1986; 3) Heaman et al., 2009; 4) Scoates, 1981; 5) Peck et al., 2000; 6) Desharnais, 2005. Abbreviations: fm., formation; HRZ, hybrid roof zone; LCLZ, lower central layered zone; MSF, Middle Sedimentary formation; MZ, marginal zone; PGE, platinum-group elements; UCLZ, upper central layered zone.*

(dominantly massive), middle (dominantly pillowed) and upper (dominantly massive) zones (Figure GS2018-3-3). The plagioclase-phyric upper zone exhibits the most evolved composition, with elevated total rare-earth element concentrations compared to the lower and middle members (Scoates, 1981; Desharnais, 2005).

Flows of the Lower Volcanic formation vary from approximately 1 to 70 m in thickness (Syme et al., 1999). Well-preserved volcanic features consist of columnar jointing structures, northward-younging flow-top textures including pillows and flow-top hyaloclastite deposits, pyroxene and olivine spinifex textures, pillow shelves (Figure GS2018-3-4a), and cumulate layers (Scoates, 1981; Syme, 2010). In the lower zone, some thick flows are differentiated into a clinopyroxene-rich basal margin, a thick cumulate olivine centre, an upper gabbroic zone containing spherulitic and dendritic plagioclase and clinopyroxene, and a brecciated and vesiculated flow top (Scoates, 1981).

Middle Sedimentary formation

The Middle Sedimentary formation (MSF; Figure GS2018-3-3) occurs along both the northern and southern margins of the Fox River sill, with a total combined thickness of up to 800 m. It contains planar-laminated to bedded quartzofeldspathic mudstone to fine-grained sandstone (Figure GS2018-3-4b), argillaceous mudstone and minor calcareous mudstone (Figure GS2018-3-4c). Laminae and disseminated grains of pyrite and pyrrhotite occur throughout the unit. Hornfels texture has been documented in the MSF along both the southern

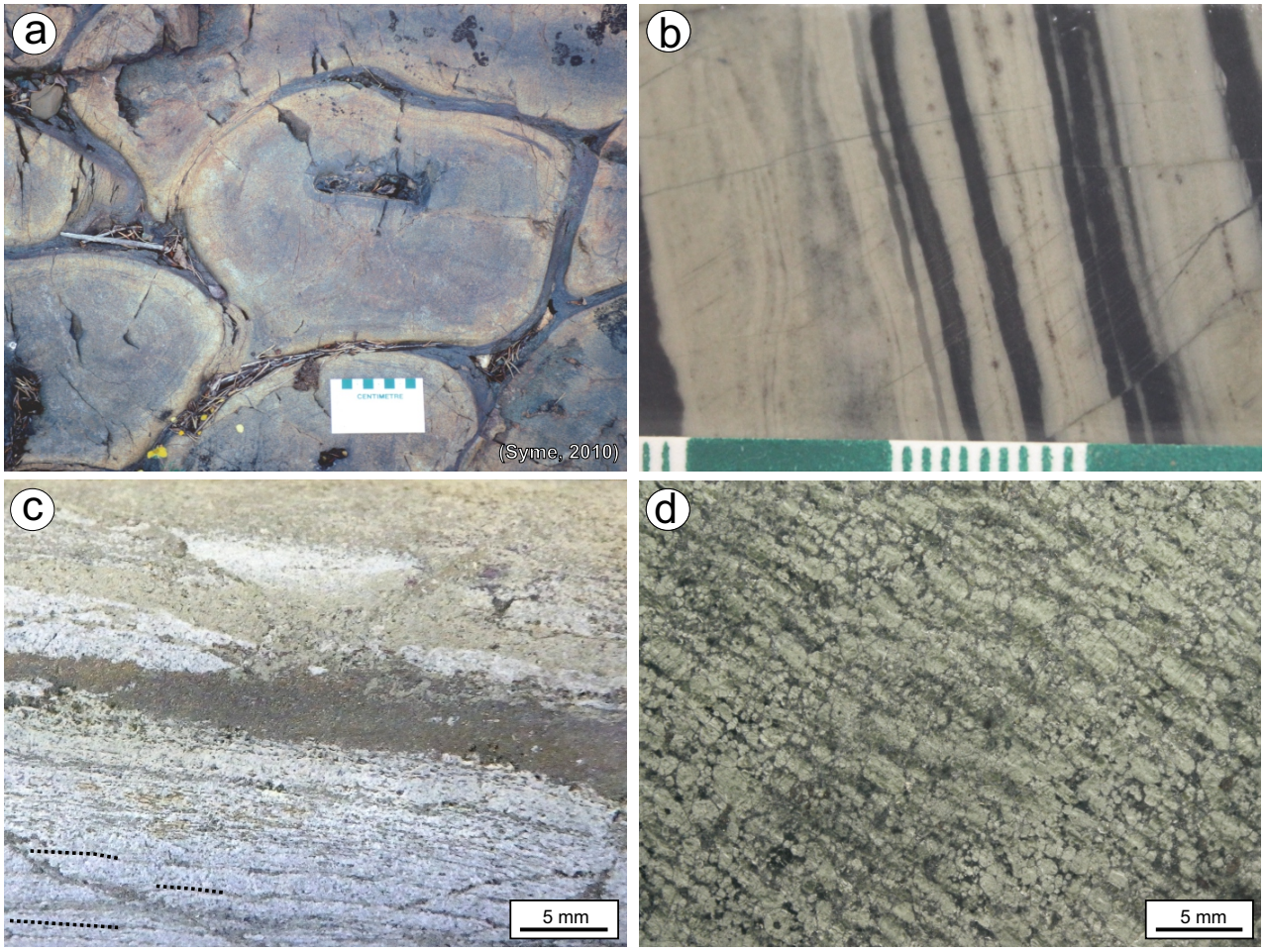

Figure GS2018-3-4: *Core and outcrop photos of stratigraphic units of the Fox River belt, northeastern Manitoba, showing* ***a)*** *well-preserved pillowed basalt of the Lower Volcanic formation, with dark grey selvages and an isolated shelf cavity at image centre (Syme, 2010, photo 5-30);* ***b)*** *planar-laminated to bedded quartzofeldspathic mudstone to fine-grained sandstone typical of the Lower and Middle sedimentary formations (International Nickel Company of Canada Ltd. hole 38512, 198 m depth);* ***c)*** *oxide-facies iron formation with magnetite laminae (bottom of image; partially indicated with dotted black lines), sulphide bed (centre) and calcareous mudstone (top) of the Middle Sedimentary formation (International Nickel Company of Canada Ltd. hole 38517, 82 m depth);* ***d)*** *medium-grained dunite cumulate of the Fox River sill, with elongated olivine cumulus crystals (Selco Exploration Company Ltd. hole FOX86-1, 144 m depth).*

and northern contacts of the Fox River sill (Hulbert and Scoates, 2005).

No material from either the Lower or Middle Sedimentary formations was found to be of suitable grain size for detrital zircon geochronology. However, as in the Lower Sedimentary formation, an Archean Nd model age (3.24 Ga; Desharnais, 2005) is consistent with the MSF originating from the Superior craton/Southern gneiss domain.

Fox River sill

The Fox River sill is among the largest of Earth's layered mafic–ultramafic intrusive complexes, with an average thickness of approximately 2 km, and an eastward strike of at least 250 km (based on its well-defined aeromagnetic anomaly). The sill complex has intruded rocks of the Middle Sedimentary formation, the latter entrained as variably assimilated xenoliths near the lower and upper contacts of the sill (Scoates, 1990). Olivine cumulates (peridotite, dunite) make up approximately 78% of the sill (Scoates, 1990), with MgO contents locally exceeding 50 wt. % (Figure GS2018-3-5a).

Scoates (1990) divided the Fox River sill into four zones (Figure GS2018-3-3), summarized in this section from south to north. Although much of the sill has been hydrothermally altered to serpentine- and magnetite-bearing assemblages, metamorphic rock names such as serpentinite are omitted from the following descriptions.

The lowermost portion of the sill, the marginal zone (MZ; Figure GS2018-3-3), is up to 275 m thick, but

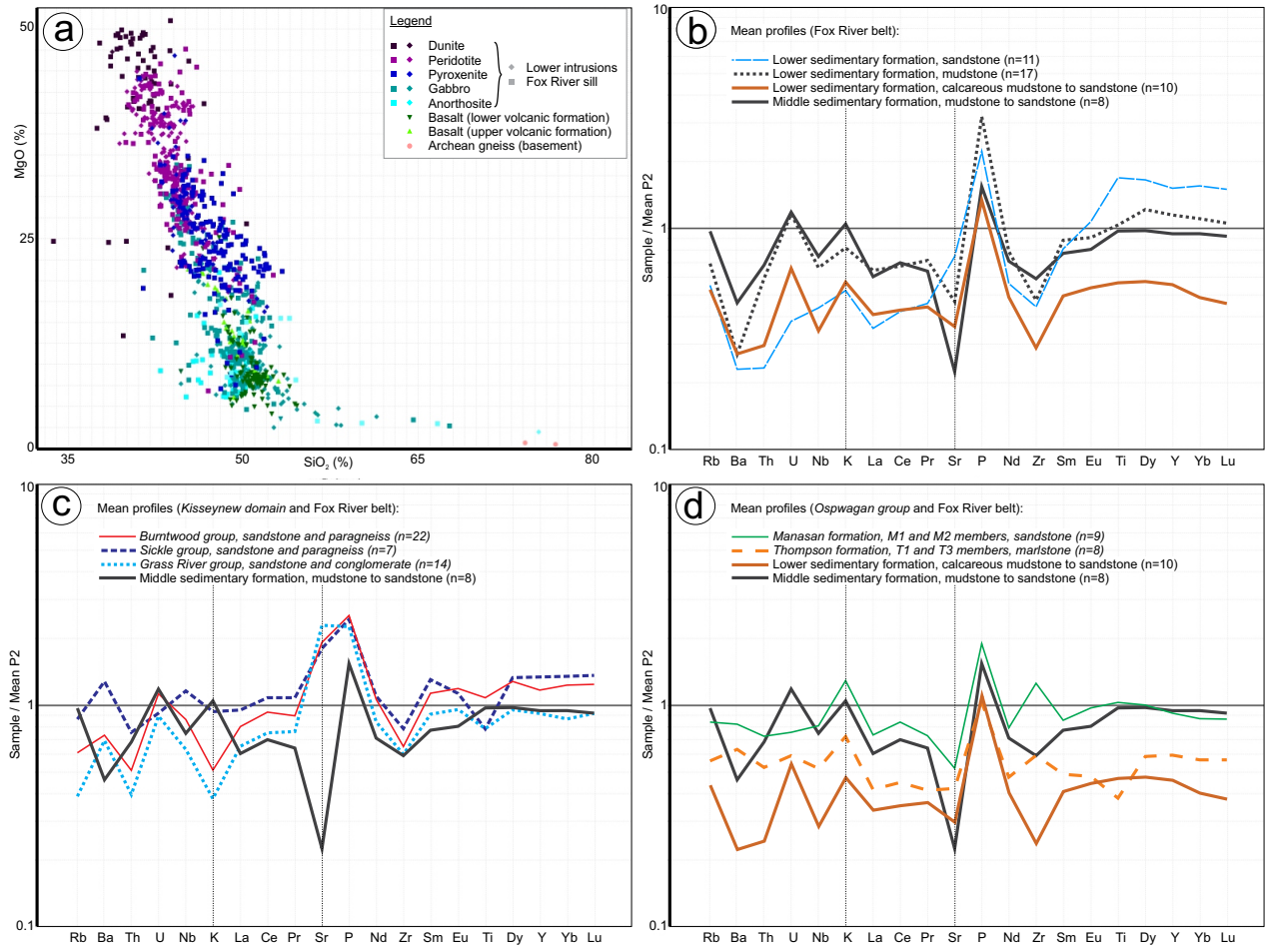

Figure GS2018-3-5: *Selected geochemical profiles of Fox River belt units, showing:* ***a)*** *MgO versus SiO_2, with an overall trend in intrusive samples corresponding to olivine abundance;* ***b)*** *mean P2 pelite-normalized profiles for all sampled sedimentary units of the Fox River belt (as applied by Zwanzig et al., 2007 to rocks of the Thompson nickel belt);* ***c)*** *mean profile of the Middle Sedimentary formation compared to metasedimentary rocks of the Kisseynew domain;* ***d)*** *mean profiles of the Middle and Lower Sedimentary formations compared to metasedimentary rocks of the Ospwagan group. Note greater similarity between profiles in panel d (e.g., relative enrichment in K, and relative depletion in Nb and Sr) compared to panel c. Along with comparable Nd model ages, these similarities are consistent with a regional stratigraphic correlation between the Ospwagan group (Thompson nickel belt) and the Lower and Middle Sedimentary formations (Fox River belt). Fox River belt data are mostly from Desharnais et al. (2004a), and Ospwagan and Kisseynew data are from Zwanzig et al. (2007) and C. Couëslan (pers. comm., 2017).*

is locally absent (Scoates, 1990; Peck et al., 1999). Its lower contact with (hornfelsed) mudstone is sharp and irregular. It contains locally pegmatitic and hornblende-bearing melagabbro overlain by two cyclic cumulate layers with sharp lower contacts, each grading upward from peridotite (±pyroxenite) to leucogabbro or anorthosite (Scoates, 1990; Peck et al., 1999). Heaman et al. (1986) reported a U-Pb zircon age of 1882.9 +1.5/-1.4 Ma from the marginal zone.

A discontinuous layer of stratabound sulphides occurs near the top of the MZ in the Great Falls outcrop area (Figure GS2018-3-2), approximately 190 m above the base of the Fox River sill. Termed the KO zone, this occurrence yields the best Ni-Cu-PGE grades in the FRB known to date (Figure GS2018-3-3; Desharnais et al., 2004b). Outcrops of the KO zone contain an average of 1–2% (locally <20%), dominantly disseminated (locally net-textured) pyrrhotite, chalcopyrite and pentlandite, typically concentrated along the scalloped lower contact of the overlying cyclic unit. The best-mineralized sample of the KO zone yielded 2.1% Cu, 0.9% Ni, 1 ppm Pt and 4 ppm Pd (Desharnais et al., 2004a).

The lower central layered zone (LCLZ; Figure GS2018-3-3), approximately 850 m thick, is made up of at least nine cyclic layers of thick olivine cumulates (peridotite to dunite) overlain by thin (<6 m) pyroxenite cumulates. Scoates (1990) interpreted each of the peridotite-pyroxenite pairs to be incomplete or 'beheaded' cyclic units in the Fox River sill; the LCLZ would therefore record at least nine injections of ultramafic magma. Up to 2% disseminated chromite occurs throughout the olivine cumulates, along with sparse bands of chromite (Scoates, 1990). Relict olivine cumulus crystals are commonly elongated parallel to the major unit contacts and chromite bands (Figure GS2018-3-4d), which Scoates (1990) interpreted as the result of magma flow during cumulus crystal settling.

The upper central layered zone (UCLZ; Figure GS2018-3-3) is approximately 900 m thick. Compared to the LCLZ, it contains thinner cumulate units of more variable composition, with an overall higher proportion of upper plagioclase cumulates and minor cumulus orthopyroxene (Scoates, 1990). Disseminated chromite is common and chromite bands occur locally. Sulphide contents and PGE tenor of the UCLZ are slightly higher than in the LCLZ, though generally low (<1 ppm Pt+Pd in the best metre assays; Figure GS2018-3-3). Weak mineralization in the UCLZ includes pyrrhotite, pentlandite, chalcopyrite, cubanite and mackinawite ($[Fe,Ni]_9S_8$), along with rare awaruite (Ni_3Fe) and heazlewoodite (Ni_3S_2; Scoates and Eckstrand, 1986; Scoates, 1990).

The uppermost portion of the Fox River sill, the hybrid roof zone (HRZ; Figure GS2018-3-3), is a thin (<100 m) zone of peridotite to gabbro with partially melted sedimentary xenoliths, quartz phenocrysts and granophyre patches (Scoates, 1990), in sharp intrusive contact with mudstone of the MSF. The character and spatial extent of the HRZ is constrained by drilling at only a few locations.

Upper Volcanic formation

As in the Lower Volcanic formation, the Upper Volcanic formation consists of a succession of mafic–ultramafic flows with minor interflow sedimentary units, demonstrating an overall upward trend from primitive, dominantly cumulate ultramafic flows to locally plagioclase-phyric mafic flows of more evolved composition. It contains the same variety of primary volcanic textures as in the Lower Volcanic formation, including columnar jointing structures, various flow-top textures (hyaloclastite, pillow shelves, spinifex) and cumulate layers (Scoates, 1981). However, vesicles are reportedly more common in the Upper Volcanic formation than in the Lower (Scoates, 1981).

The Upper Volcanic formation is interpreted by Scoates (1981) as the record of magmas expelled in stages from the Fox River sill magma chamber(s). Desharnais (2005) presented geochemical evidence for this comagmatic relationship, illustrating that the upward evolution of Upper Volcanic formation lavas may have been controlled by crystallization of cumulate phases (olivine, orthopyroxene, clinopyroxene and plagioclase) in the Fox River sill. Although historical drill logs also note rare felsic intervals within the Upper Volcanic formation, recent petrographic investigation of these intervals revealed sericite-altered basalt with relict pyroxene.

Two samples of the Upper Volcanic formation, collected by D. Peck (Peck et al., 1999) along the banks of the Fox River, returned 1.1 and 3.5 ppm Pd. These values significantly exceed background PGE contents (Figure GS2018-3-3), suggesting potential for flow-hosted magmatic sulphide mineralization in the Upper Volcanic formation.

Upper Sedimentary formation

The Upper Sedimentary formation forms the uppermost stratigraphic unit preserved in the FRB. Outcrops of the unit have not yet been identified. Based on the few intervals intersected in drillcore, it consists of up to 6 km of rocks resembling the Lower and Middle Sedimentary formations, with variably quartzofeldspathic to argillaceous and locally graphite-bearing beds dipping steeply to the north.

Northern gneiss domain (Churchill province)

The northern gneiss domain (previously termed the 'northern gneiss belt'; Scoates, 1990; Peck et al., 2000) is assigned to the Kisseynew domain of the Churchill province (Figure GS2018-3-1). It contains locally garnet-, staurolite- and hornblende-porphyroblastic metagreywacke and/or paragneiss, with minor iron formation. Unlike the weakly metamorphosed and relatively undeformed sedimentary units of the FRB, the northern gneiss domain exhibits amphibolite-facies metamorphism and south-dipping fold axes (Peck et al., 2000).

A sample of metagreywacke along the Fox River, from an outcrop located approximately 3.5 km north of the FRB, returned a Nd model age of 2.30 Ga (Böhm, pers. comm., 2000). This result indicates derivation from a source younger than the Superior craton and could imply correlation with the Burntwood group of the Kisseynew domain (T_{DM} <2.6 Ga; Böhm et al., 2007). Scoates (1981) proposed that the domain boundary between the northern gneiss domain and upper sedimentary formation is likely a north-dipping thrust fault (Figure GS2018-3-3).

Structure and metamorphism

Rocks of the FRB exhibit low-grade metamorphism, from lower greenschist facies in the south to prehnite-pumpellyite facies in the north (Scoates, 1981). In marked contrast to rocks of the Thompson nickel belt, the rocks record minimal structural complexity; nearly all of the FRB contains northward-younging and weakly strained units that dip ~80°N (Scoates, 1981). Exceptions occur in the buried northwestern part of the belt (between Stephens Lake and east of Fox Lake [also known unofficially as Atkinson lake]; Figure GS2018-3-2) where sparse drillcore intercepts reveal northwest-striking and steeply dipping units, and in the area along the northern shore of Whitefish Lake (Figure GS2018-3-2), where drill intercepts indicate possible near-horizontal bedding planes in the Lower Sedimentary formation. Dextral offsets interpreted from aeromagnetic data suggest the presence of east-northeast-trending dextral fault zones or shears through the FRB, including an eastward extension of the Aiken River deformation zone (Figures GS2018-3-1b, 2). The eastern boundary of the FRB is interpreted to correspond to the Winisk River fault (Figures GS2018-3-1b, 2).

Paleozoic and Quaternary cover

Marine and glaciomarine sedimentary rocks of the Hudson Bay Basin overlie the eastern part of the FRB, thickening toward Hudson Bay. Drill intercepts northeast of Whitefish Lake also delineate a zone of flat-lying Paleozoic cover currently interpreted as an outlier of the Hudson Bay Basin (Figure GS2018-3-2). Quaternary glacial material (dominantly glaciofluvial and glaciolacustrine) covers greater than 99% of the FRB, with sparse Precambrian outcrop limited to areas along and west of Hayes River, in addition to some Paleozoic outcrops along Gods River (e.g., Scoates, 1981; Peck et al., 2000; Desharnais, 2005).

Regional correlations and interpretations

Deposits of the Thompson nickel belt are primarily hosted by Paleoproterozoic sedimentary rocks of the Ospwagan group and are overlain, or were overthrust, by rocks of the Kisseynew domain (Bleeker, 1990; Zwanzig et al., 2007; Figure GS2018-3-1b). Delineating the extension of the Ospwagan group or identifying Ospwagan-equivalent units outside of the Thompson nickel belt is therefore applicable to nickel exploration in northern Manitoba (Böhm et al., 2007; Zwanzig et al., 2007).

Samples of the Lower and Middle Sedimentary formations of the FRB yield Nd model ages of 2.9 and 3.2 Ga (Desharnais, 2005), which are interpreted to indicate derivation from the Archean Superior province/Southern gneiss domain. Representative extended-element profiles of mudstone to sandstone samples of the Lower and Middle sedimentary formations, normalized to mean P2 pelite as in Zwanzig et al. (2007), show relative enrichments in K and depletions in Nb and Sr (Figure GS2018-3-5b). No geochemical data are available from the Upper Sedimentary formation.

Metasedimentary rocks of the Ospwagan group include both clastic and chemical components in a package up to 3 km thick (prior to deformation), metamorphosed to amphibolite- or granulite-facies conditions (Zwanzig et al., 2007; Couëslan and Pattison, 2012). The rocks are characterized by Nd model ages ranging from 2.8 to 3.2 Ga (Böhm et al., 2007), reflecting the Archean source material. Like the FRB sedimentary units—and unlike the overthrust rocks of the Kisseynew domain (Figure GS2018-3-5c)—most of the lower Ospwagan-group rocks show relative enrichments in K and depletions in Nb and Sr compared to P2 pelite (Figure GS2018-3-5d; Zwanzig et al., 2007).

Both the Ospwagan and FRB rocks are interpreted as passive marine sedimentary packages deposited on Superior cratonic basement. Both contain packages of quartzofeldspathic to argillaceous mudstone and sandstone, calcareous beds, and oxide- and sulphide-facies iron formation (Zwanzig et al., 2007). Although a maximum age has not been established for sedimentary rocks of the FRB, they share a minimum age with the Ospwagan group; both were deposited prior to the intrusion of

locally ore-forming, ca. 1883 Ma mafic–ultramafic magmas of the circum-Superior belt, followed by the closure of the Manikewan Ocean and related overthrusting by rocks of the Kisseynew domain.

Despite significant differences in strain and metamorphism, the above-described similarities suggest that sedimentary rocks of the Ospwagan group and the Lower and Middle Sedimentary formations of the Fox River belt could be stratigraphically equivalent. Although correlations at the formation level may not be possible (nor necessarily expected, given the likelihood of lateral facies variations between the Thompson nickel belt and Fox River belt), the identification of sulphide-bearing packages similar to the Pipe formation may be the key to nickel exploration in the Fox River belt.

Economic considerations

In addition to regional potential for diamonds and gold mineralization, the FRB remains prospective for magmatic Ni (±Cu, PGE, Co, Cr) deposits. A setting within the metallogenic circum-Superior belt, extensive ultramafic to mafic igneous rocks, a range of potential external sulphur sources, proposed stratigraphic correlations with the deposit-hosting Ospwagan group, and known occurrences of Ni-Cu-PGE sulphides in the FRB collectively support some prospect of economic mineralization. Renewed exploration strategies for magmatic sulphide deposits in the FRB may incorporate the following considerations

- Although intrusions were the main focus of past exploration, flows of the Upper and Lower Volcanic formations are also possible hosts to mineralization.
- A number of potential external sulphur sources have been documented throughout the sedimentary and volcanic stratigraphy, including sulphide-facies iron formation, widely disseminated sediment-hosted sulphide and discordant sulphide veins or alteration features (Syme et al., 1999).
- Previous workers have identified several ultramafic intrusive targets, including the MZ of the Fox River sill (containing the best known Ni-Cu-PGE mineralization discovered to date in the FRB), the LCLZ of the Fox River sill (wherein the 'beheaded' cyclic layers could imply a more prospective 'flow-through' as opposed to quiescent magma chamber) and the lower intrusions (containing geochemical evidence for assimilation of country rock and local chalcophile-element depletions; Desharnais, 2005).
- Large portions of the belt remain unexplored and include untested conductors identified in mafic–ultramafic-bearing stratigraphy (e.g., Hosain, 2003).
- Quaternary investigations, including till geochemical analyses, may prove an effective strategy for base-metal exploration in the extensively drift-covered belt.

Acknowledgments

R. Scoates' seminal work on the Fox River belt forms the basis for most of this work, in addition to valuable contributions by G. Desharnais, D. Peck and others. R. Scoates and G. Desharnais have both provided helpful advice and information at various stages of this compilation, along with J. Scoates, D. Benson and MGS staff, including C. Couëslan, T. Hodder, C. Böhm, C. Epp, T. Booth, S. Anderson and G. Keller. The author also thanks X.M. Yang and C. Couëslan for their reviews.

References

Baragar, W.A. and Scoates, R.J. 1981: The Circum-Ungava Belt: a Proterozoic plate margin?; *in* Precambrian Plate Tectonics, A. Kroner (ed.), Elsevier, Amsterdam, p. 297–330.

Baragar, W.A. and Scoates, R.J. 1987: Volcanic geochemistry of the northern segments of the Circum-Superior Belt of the Canadian Shield; Geological Society of London, Special Publications, v. 33, p. 113–131.

Bell, R. 1879: Report on the country between Lake Winnipeg and Hudson's Bay, 1878; Geological Survey of Canada, Report of Progress for 1877-78, 31 p.

Bleeker, W. 1990: New structural-metamorphic constraints on Early Proterozoic oblique collision along the Thompson nickel belt, Manitoba, Canada; *in* The Early Proterozoic Trans-Hudson Orogen of North America, J.F. Lewry and M.R. Stauffer (ed.), Geological Association of Canada Special Paper 37, p. 57–73.

Bleeker, W. and Kamo, S.L. 2018: Extent, origin, and deposit-scale controls of the 1883 Ma Circum-Superior large igneous province, northern Manitoba, Ontario, Quebec, Nunavut and Labrador; *in* Targeted Geoscience Initiative: 2017 report of activities, volume 2, N. Rogers (ed.); Geological Survey of Canada, Open File 8373, p. 5–14.

Böhm, C.O., Zwanzig, H.V. and Creaser, R.A. 2007: Sm-Nd isotope technique as an exploration tool: delineating the northern extension of the Thompson Nickel Belt, Manitoba, Canada; Economic Geology, v. 102, p. 1217–231.

Brock, R.W. 1911: The Hudson Bay route; *in* Summary Report of the Geological Survey Branch of the Department of Mines for the calendar year 1910; Sessional Paper 26, p. 14–26.

Corrigan, D., Pehrsson, S., Wodicka, N. and De Kemp, E. 2009: The Palaeoproterozoic Trans-Hudson Orogen: a prototype of modern accretionary processes; Geological Society of London, Special Publications, v. 327, p. 457–479.

Couëslan, C.G. and Pattison, D.R. 2012: Low-pressure regional amphibolite-facies to granulite-facies metamorphism of the Paleoproterozoic Thompson Nickel Belt, Manitoba; Canadian Journal of Earth Sciences, v. 49, p. 1117–1153.

Desharnais, G. 2005: Geochemical and isotopic investigation of magmatism in the Fox River Belt: tectonic and economic implications; Ph.D. thesis, University of Manitoba, Winnipeg, Manitoba, 207 p.

Desharnais, G., Peck, D.C., Halden, N.M., Scoates, R.J. and Hulbert, L.J. 2004a: Major- and trace-element analytical data for whole-rock samples from the Fox River Belt, northeastern Manitoba (NTS 53M15; 53M16); Manitoba Industry, Economic Development and Mines, Manitoba Geological Survey, Data Repository Item 2004001, Microsoft® Excel® file.

Desharnais, G., Peck, D.C., Scoates, R.J. and Halden, N.M. 2004b: The KO zone: a new model for PGE–Cu–Ni mineralization in the marginal zone of the Fox River sill, Northern Manitoba, Canada; The Canadian Mineralogist, v. 42, p. 291–302.

Heaman, L.M., Machado, N., Krogh, T.E. and Weber, W. 1986: Precise U-Pb zircon ages for the Molson dyke swarm and the Fox River Sill: constraints for the early Proterozoic crustal evolution in northeastern Manitoba, Canada; Contributions to Mineralogy and Petrology, v. 94, p. 82–89.

Heaman, L.M., Peck, D.C. and Toope, K. 2009: Timing and geochemistry of 1.88 Ga Molson Igneous Events, Manitoba: Insights into the formation of a craton-scale magmatic and metallogenic province; Precambrian Research, v. 172, p. 143–162.

Hosain, I.T. 2003: Summary of geophysical data from open assessment files of the Fox River Sill area, Manitoba (part of NTS 53N, 53M and 54D); Manitoba Industry, Trade and Mines, Manitoba Geological Survey, Open File Report 2001-7, 12 p. plus 11 maps at 1:50 000 scale.

Hulbert, L.J. and Scoates, R.J. 2005: Geology of the Fox River Belt, northern Manitoba; Geological Survey of Canada, Open File 4882, 1 map at 1:100 000 scale and 3 maps at 1:275 000 scale.

Lightfoot, P.C., Stewart, R., Gribbin, G. and Mooney, S.J. 2017: Relative contribution of magmatic and post-magmatic processes in the genesis of the Thompson Mine Ni-Co sulfide ores, Manitoba, Canada; Ore Geology Reviews, v. 83, p. 258–286.

Merritt, C.A. 1925: Bigstone and Fox Rivers area, northern Manitoba; *in* Geological Survey of Canada, Summary Report (1925), part B, p. 27–30.

Minifie, M.J., Kerr, A.C., Ernst, R.E., Hastie, A.R., Ciborowski, T.R., Desharnais, G. and Millar, I.L. 2013: The northern and southern sections of the western ca. 1880 Ma Circum-Superior Large Igneous Province, North America: the Pickle Crow dyke connection?; Lithos, v. 174, p. 217–235.

Peck, D.C., Huminicki, M., Wegleitner, C., Theyer, P., Olshefsky, K., Potter, L., Hulbert, L. and Scoates, R.J. 1999: Lithostratigraphic framework for platinum-group element-copper-nickel sulphide mineralization in the Marginal Zone of the Fox River Sill (parts of NTS 53M/16 and 53N/13); *in* Report of Activities 1999, Manitoba Industry, Trade and Mines, Geological Services, p. 46–50.

Peck, D.C., Potter, L., Desharnais, G., Scoates, R.J., Corkery, M.T. and Böhm, C.O. 2000: Geology of the western part of the Fox River Belt (parts of NTS 53M and 53N); *in* Report of Activities 2000, Manitoba Industry, Trade and Mines, Manitoba Geological Survey, p. 38–41.

Quinn, H.A. 1955: Knee Lake, Manitoba; Geological Survey of Canada, Map 55-8, 1:253 440 scale.

Scoates, R.J. 1981: Volcanic rocks of the Fox River Belt, northwestern Manitoba; Manitoba Energy and Mines, Mineral Resources Division, Geological Report GR81-1, 109 p. plus 1 map at 1:50 000 scale.

Scoates, R.J. 1990: The Fox River sill, northeastern Manitoba–a major stratiform intrusion; Manitoba Energy and Mines, Geological Services, Geological Report GR82-3, 192 p. plus 1 map at 1:50 000 scale.

Scoates, R.J. and Eckstrand, O.R. 1986: Platinum-group elements in the Upper Central Layered Zone of the Fox River Sill, northeastern Manitoba; Economic Geology, v. 81, p. 1137–1146.

Scoates, J.S., Scoates, R.J., Wall, C.J., Friedman, R.M. and Couëslan, C.G. 2017: Direct dating of ultramafic sills and mafic intrusions associated with Ni-sulfide mineralization in the Thompson Nickel Belt, Manitoba, Canada; Economic Geology, v. 112, p. 675–692.

Syme, E.C. 2010: Measured sections in the Lower and Upper volcanic formations, Fox River Belt, Manitoba (parts of NTS 53M16 and 53N13); Manitoba Innovation, Energy and Mines, Manitoba Geological Survey, Open File OF2010-1, 1 CD-ROM.

Syme, E.C., Peck, D.C. and Huminicki, M., 1999: Volcanic stratigraphy of selected sections on the Fox and Stupart rivers, Fox River Belt (parts of NTS 53M/16 and 53N/13); *in* Report of Activities 1999, Manitoba Industry, Trade and Mines, Geological Services, p. 51–60.

Wanless, R.K., Stevens, R.D., Lachance, G.R. and Edmonds, C.M. 1968: Age determinations and geological studies: K-Ar isotopic ages; *in* Report 8, Geological Survey of Canada, Paper 67-2, Part A, 141 p.

Wanless, R.K., Stevens, R.D., Lachance, G.R. and Delabio, R.N. 1973: Age determinations and geological studies: K-Ar isotopic ages; *in* Report 11, Geological Survey of Canada, Paper 73-2, 139 p.

Zwanzig, H.V., Macek, J.J. and McGregor, C.R. 2007: Lithostratigraphy and geochemistry of the high-grade metasedimentary rocks in the Thompson Nickel Belt and adjacent Kisseynew Domain, Manitoba: implications for nickel exploration; Economic Geology, v. 102, p. 1197–1216.

GS2018-4

Sub-Phanerozoic basement geology from drillcore observations in the Watts, Mitishto and Hargrave rivers area, eastern Flin Flon belt, west-central Manitoba (parts of NTS 63J5, 6, 11, 12, 13, 14)

by K.D. Reid

In Brief:

- Drillcore observation and geophysics define a new geological interpretation of the sub-Phanerozoic basement southeast of Wekusko Lake
- Previously unrecognized mafic to felsic volcanic rocks, typical of the Flin Flon belt, occur in the study area and significantly expand the exploration space for base-metal deposits

Citation:
Reid, K.D. 2018: Sub-Phanerozoic basement geology from drillcore observations in the Watts, Mitishto and Hargrave rivers area, eastern Flin Flon belt, west-central Manitoba (parts of NTS 63J5, 6, 11, 12, 13, 14); *in* Report of Activities 2018, Manitoba Growth, Enterprise and Trade, Manitoba Geological Survey, p. 37–47.

Summary

The Manitoba Geological Survey (MGS) is in the process of refining the geology of the Precambrian Flin Flon belt where it extends to the south beneath Phanerozoic cover rocks. New 1:50 000 scale geological maps are being developed from industry and government aeromagnetic, drillhole geochemistry and lithological log data. Domains with similar aeromagnetic signatures were investigated by examining drillcore from 31 holes during a three-week period in the summer of 2018.

Highlights of the summer's investigations include a new geological interpretation of the study area that encompasses metamorphosed sandstone and conglomerate, pelite and psammopelite, mafic to felsic volcanic rocks, and a variety of intrusive rocks from granite to gabbro. Middle- to upper-amphibolite facies peak metamorphic assemblages occur in pelitic rocks; a shift from sillimanite-bearing to migmatitic indicates a southeastward increase of the metamorphic grade. The recognition of volcanic rocks broadens the potential area for volcanogenic massive-sulphide (VMS) exploration in the region.

Introduction

The Flin Flon belt (FFB) is one of a series of volcanic-sedimentary belts that make up the internal Reindeer zone of the Paleoproterozoic Trans-Hudson orogen (Lewry and Collerson, 1990). Geological mapping of the exposed portion of the FFB demonstrates that a belt-wide stratigraphy is applicable from Flin Flon to Snow Lake. This stratigraphy involves ca. 1.9–1.8 Ga oceanic volcanic assemblages that include juvenile island-arc, juvenile ocean-floor/back-arc, and ocean-island basalts (Syme et al., 1999), which were tectonically accreted during closure of the Proterozoic Manikewan Ocean (e.g., Stauffer, 1984; Syme and Bailes, 1993). Postdating the accretion of the oceanic volcanic assemblages is the emplacement of 'successor'-arc plutons and the deposition of local subaerial volcanic rocks (1.87–1.83 Ga; e.g., Connors et al., 1999; Whalen et al., 1999). In addition, fluvial-alluvial sandstone and conglomerate of the Missi group (1.85–1.83 Ga) unconformably overlie older volcanic rocks and, in some cases, are intimately associated with 'successor'-arc volcanic rocks (e.g., Ansdell et al., 1992; Connors et al., 1999; Syme et al., 1999). Burntwood group (1.85–1.84 Ga) greywacke and argillite represent the deeper water lateral facies equivalents to the Missi group (e.g., Ansdell et al., 1995).

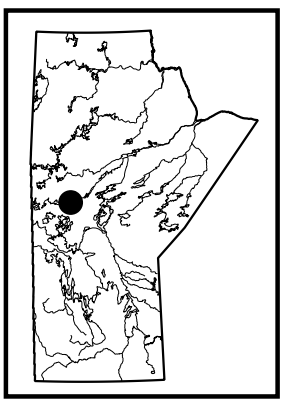

The FFB is one of the most well-endowed VMS camps in the world, with the majority of deposits hosted by juvenile-arc and arc-rift volcanic sequences (Syme et al., 1999). The development of deep-penetrating airborne geophysical surveys has expanded exploration in the FFB from the exposed areas to its sub-Phanerozoic extension to the south, and has resulted in the discovery of several VMS deposits since the mid-1990s (e.g., Watts River, Harmin, Fenton and Talbot). Several of the sub-Phanerozoic Cu-Zn massive-sulphide discoveries at the eastern end of the FFB are located on existing geological maps within Burntwood group sedimentary rocks (see Figure GS2017-7-1; Reid, 2017). This raises two important questions:

- Does the region contain volcanic rocks not previously identified?
- Alternatively, are these a new class of VMS deposit in the belt associated with dominantly sedimentary rocks?

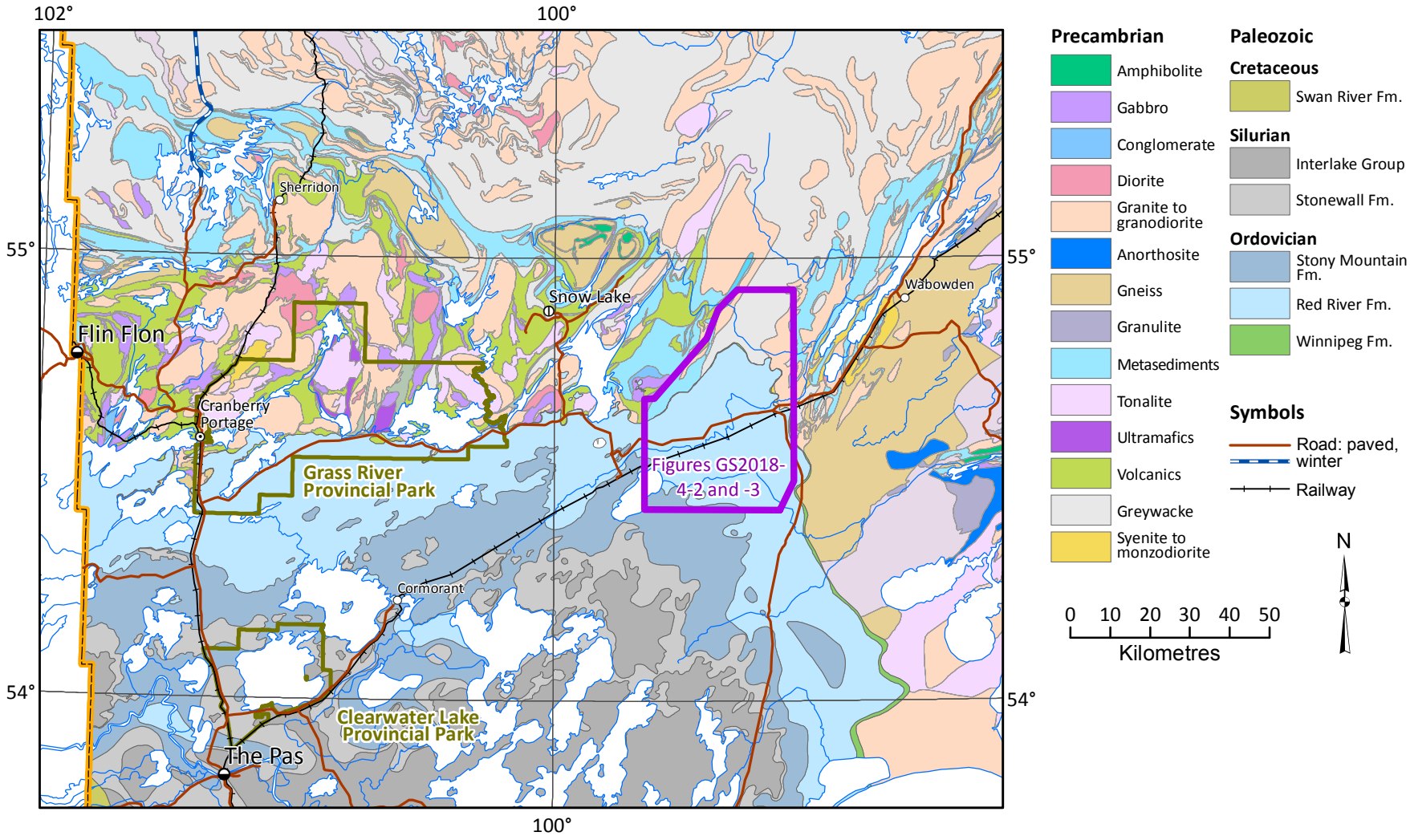

Figure GS2018-4-1: *Geology of the Flin Flon belt in west-central Manitoba, with the Watts, Mitishto and Hargrave rivers study area outlined in purple. Note the extent of Phanerozoic cover rocks. The rocks in the northern portion of the study area are poorly exposed.*

A better understanding of the sub-Phanerozoic geology of the eastern FFB is required, and part of this involves updating and refining geological maps for this region.

Previous work

Early geological work in the exposed FFB to the north of study area was completed by the Geological Survey of Canada and later by the MGS in the form of mapping in exposed areas to the northeast and north (e.g., Stockwell, 1937; Bailes, 1985). More recently, Leclair et al. (1997) subdivided the eastern sub-Phanerozoic portion of the FFB into three domains based on geophysical and drillcore data: the Cormorant batholith, the Clearwater domain and the East Kisseynew domain (see Figure GS2017-7-1; Reid, 2017). The increased metamorphic grade of the East Kisseynew domain complicates interpretation of protoliths; therefore, this area was only subdivided into two rock types: granitoids and pelites (Burntwood group). Reid (2017) reviewed drillcores from holes KUS356, KUS367 and KUS368 in 2017 but did not attempt to place these rocks into a new regional geological framework. Data from these drillholes, however, aided the geological interpretation given below.

Aeromagnetic data

Figure GS2018-4-2 shows a simplified geological interpretation based on compilation of drillcore and aeromagnetic data. Keating et al. (2012) compiled and leveled high-resolution government and industry aeromagnetic data for the Flin Flon–Snow Lake region and produced total magnetic intensity (TMI) and first vertical derivative (1st VD) maps of the magnetic field that are reduced to pole. The TMI provides the basis for defining domains of similar magnetic intensity, potentially identifying areas with similar rock types. A semitransparent hillshade directed from 290º adds depth to northeast-trending features in the TMI (Figure GS2018-4-3). In contrast, the 1st VD tends to define magnetic lineaments that help to delineate structures and internal complexity, and to better resolve contacts. Table GS2018-4-1 contains a summary of aeromagnetic signatures from stratigraphically constrained rocks in the exposed eastern FFB. The linework from Figure GS2018-4-2 is included on the TMI map in Figure GS2018-4-3 to aid interpretation.

Drillcore observations

The following summary of the drillcore observations makes it possible to test the interpretations made from geophysics. Middle-amphibolite facies and higher metamorphism affected all rocks in the study area, so the prefix 'meta' has been dropped for the sake of brevity. Industry drill logs refer to the rocks mainly as gneisses; however, not all rocks are gneissic in character and locally retain some primary textures. The preservation of primary textures depends largely on the extent of hydration, which is higher in hydrous pelitic rocks than in mature quartz-rich sandstone or unaltered rhyolite. More information regarding drillhole locations and associated assessment files can be found at https://web33.gov.mb.ca/mapgallery/mgm-md.html.

Sedimentary rocks

Psammite and conglomerate

Psammite and conglomerate occur in drillcores KUS342, KUS318, KUS378, and HAR195. These contain moderately to highly strained heterolithic (dominantly felsic rhyolite and minor granite) pebbles and cobbles within a quartz and feldspar sandstone matrix. Locally, millimetre- to centimetre-wide, weakly magnetic, dark layers are interpreted to represent heavy mineral–rich crossbeds (Figure GS2018-4-4a). Conglomeratic intervals in drillcore commonly display a striped appearance, with 2–10 mm of darker matrix between the flattened fragments. HAR195 contains a low-strain window where a subrounded rhyolitic cobble is present (Figure GS2018-4-4b). Sandstone and conglomerate in the northern half of the study area contain visible sillimanite as small white wisps in the matrix to the cobbles, whereas they contain abundant leucosome in the southwest. Magnetic susceptibility for these rocks is quite variable, ranging from 0.1 to 3 x 10^{-3} SI.

Pelite and psammopelite

Pelitic and psammopelitic rocks are recognized by their high biotite and garnet contents, which are generally above 30 and 10 modal percent in these rocks, respectively; changes in the amount of these minerals likely reflects minor compositional variations of the protolith. The magnetic susceptibility of these rocks in drillcore is typically less than 1 x 10^{-3} SI. Staurolite was not observed in these rocks; however, orange-brown staining around some garnets in KUS367 might reflect relict staurolite. Figure GS2018-4-2 shows the extent of biotite-garnet–bearing gneiss that contains visible wisps of sillimanite. Moving from west to east, sillimanite decreases or disappears and there is a notable increase of migmatite. Partial melting of pelite in HAR070 resulted in the development of quartzofeldspathic leucosome and biotite-garnet melanosome surrounded by paleosome (Figure GS2018-4-4c). Intervals 10–30 m wide containing graphite and sulphide (pyrrhotite and pyrite) were intersected

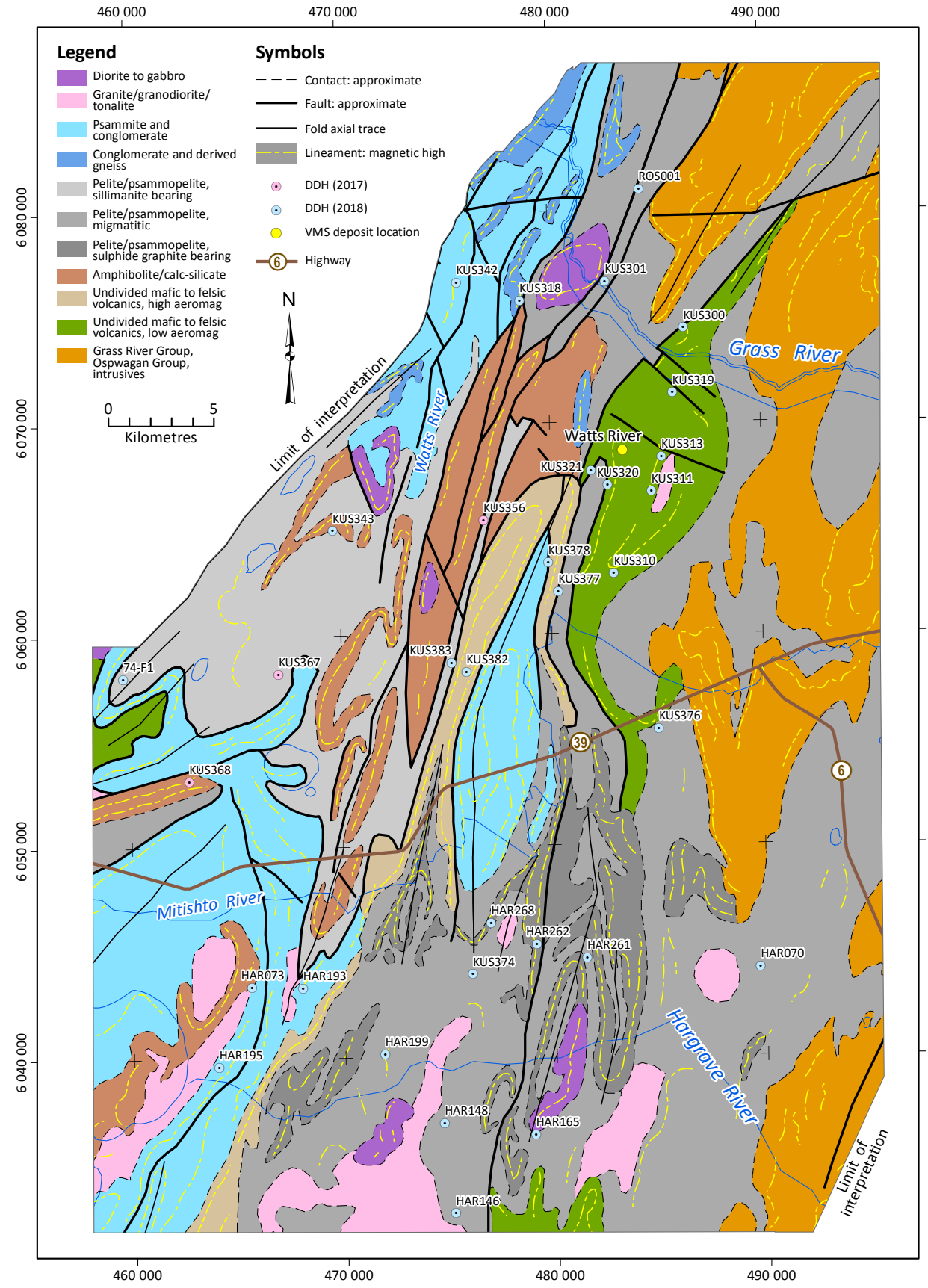

Figure GS2018-4-2: *Simple interpretation of the geology of the Watts, Mitishto and Hargrave rivers area from drillcore observations and aeromagnetic characteristics.*

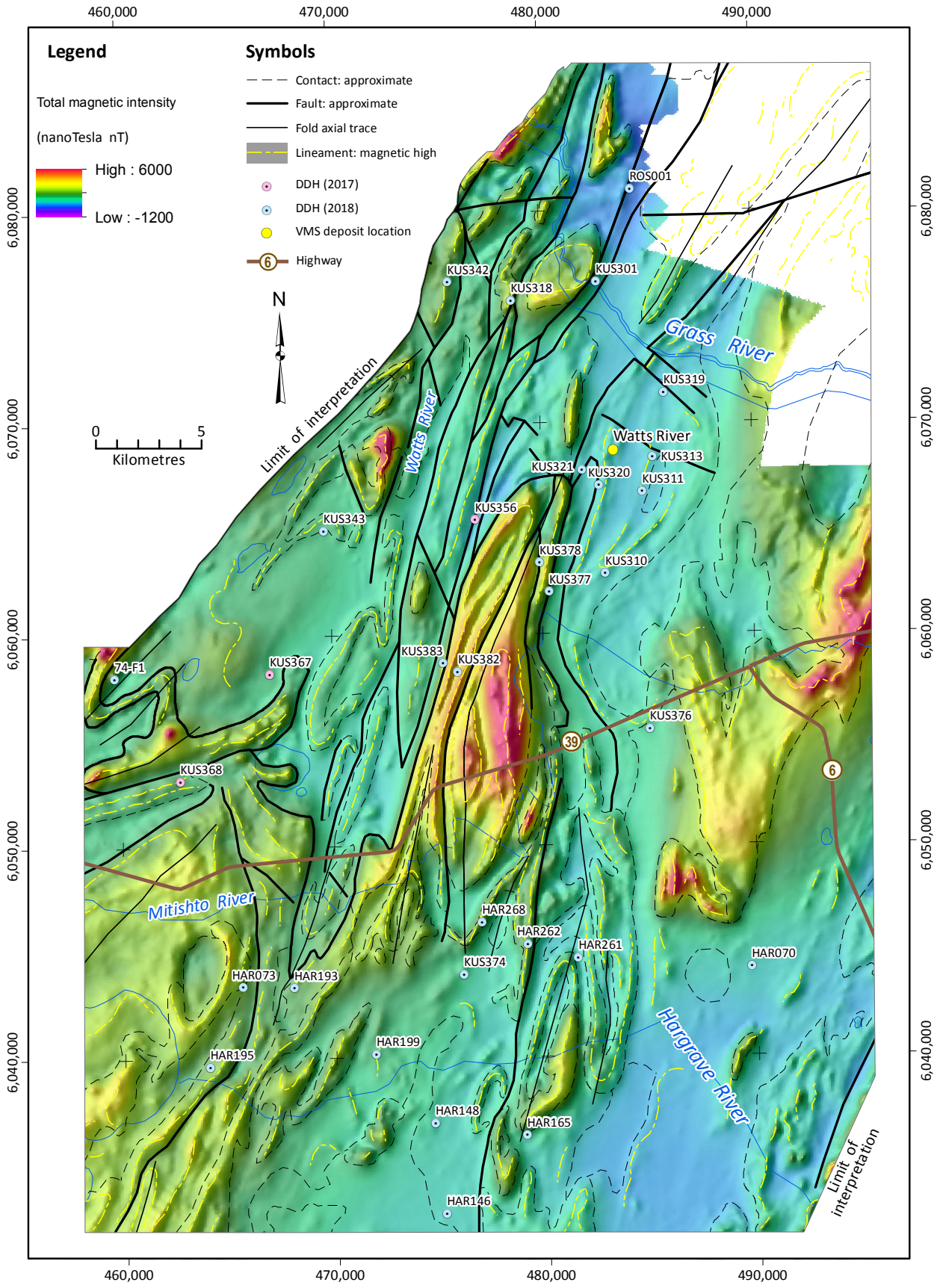

Figure GS2018-4-3: *Total magnetic intensity map of the Watts, Mitishto and Hargrave rivers study area, with a transparent hillshade (illuminated from 290°) and linework from Figure GS2018-4-2.*

Table GS2018-4-1: Aeromagnetic characteristics of stratigraphically constrained rocks in the exposed eastern Flin Flon belt.

	Rock type	Magnetic Intensity	Internal magnetic complexity	Electrical conductivity	Examples
'Successor-arc' intrusive rocks	Granite, granodiorite and tonalite	Low to moderate	Low complexity; circular to ovoid; cuts earlier fabrics	Low	Ham Lake and Wekusko Lake plutons
	Diorite and gabbro	Low to high, sill-like to layered complexes	Low complexity, circular to ovoid; earlier fabrics may be cut	Low	Rex Lake pluton, Rice Island gabbro
'Successor-arc' volcanic rocks	Basalt and andesite	Moderate to high	Moderately complex; contains folded stratigraphy	Low	Herb Lake arc-volcanic rocks
	Dacite and rhyolite	Low to moderate			
'Successor arc' basin deposits	Sandstone and conglomerate	High	Displays folding well, with magnetic highs and lows representing stratigraphy	Very low	Herb Lake sandstone and conglomereate
	Greywacke, mudstone and derived pelitic gneisses	Low	Monotonous with little complexity observed	Moderate to high	Wekusko Lake mudstone and siltstone
	Graphite-sulphide–bearing mudstone and pelite	Low to high (possibly dependent on metamorphic grade)	Prominent magnetic highs in broad magnetic lows; may or may not be complexly folded	High	
Ocean-floor basalt	Mainly mafic flows, pillows and minor tuff	Low-moderate to moderate	Variable; may contain magnetic highs due to sulphide- and oxide-facies iron formation	Moderate	Northeast Reed ocean-floor assemblage
Early arc-volcanic rocks	Mafic to felsic flows and volcanclastics with minor graphitic and sulphidic horizons	Low-moderate to moderate	Variable; may contain magnetic highs due to sulphide-facies iron formation	Low to high	Snow Lake juvenile-arc assemblage
Early arc-intrusive rocks	Gabbro to tonalite	Low-moderate to moderate	Lower complexity than surrounding volcanic rocks; may truncate stratigraphy	Low	Sneath and Richard plutons

in drillcores HAR261, HAR262 and HAR268 (see Figure GS2018-4-4d); magnetic susceptibility up to 30 x 10^{-3} SI coincides with narrow magnetic highs (Figure GS2018-4-3) and is the basis for extrapolation of this unit to other parts of the study area (Figure GS2018-4-2). Many of the drillholes that contain a graphite-sulphide interval also have an adjacent minor intersection of intermediate to felsic rocks of uncertain origin and relationship.

Volcanic rocks

The primary basis for discerning volcanic rocks is their fine-grained character relative to intrusive and sedimentary rocks, and their lower contents of biotite-garnet (<10% garnet) and in situ melt relative to pelitic and psammopelitic rocks. Features such as subtle compositional layering, which may represent volcaniclastic tuff, resedimented volcanic material or possible flow banding, were locally noted.

Amphibolite and calcsilicate-altered mafic rocks

Dark to light green, fine- to medium-grained amphibolite that often has centimetre-scale layering occurs in drillcores KUS343, KUS318, KUS356, KUS383 and HAR073. These mafic rocks do not show much compositional variability and are usually in sharp (possibly fault) contact with sedimentary rocks or are intruded by granitoids. Light green, centimetre-scale layering represents calcsilicate-altered domains (diopside) that were transposed by regional deformation and often contain remnant calcite (Figure GS2018-4-5a). In drillcore, these rocks have magnetic susceptibility readings lower than 2 x 10^{-3} SI; they are characterized by subtle magnetic highs when compared to pelite and psammopelite (Figure GS2018-4-3, Table GS2018-4-1).

Undivided mafic to felsic volcanic rocks with low aeromagnetic signature

Fine- to medium-grained rocks with <10% garnet that are mainly intermediate to felsic in composition occur in the area of the Watts River VMS deposit (Figure GS2018-4-2) and have a low aeromagnetic signature. Compositional layering, at the millimetre- to centimetre-scale, of intermediate rocks in KUS311 possibly reflects primary tuffaceous layering or a reworked volcanic sand-

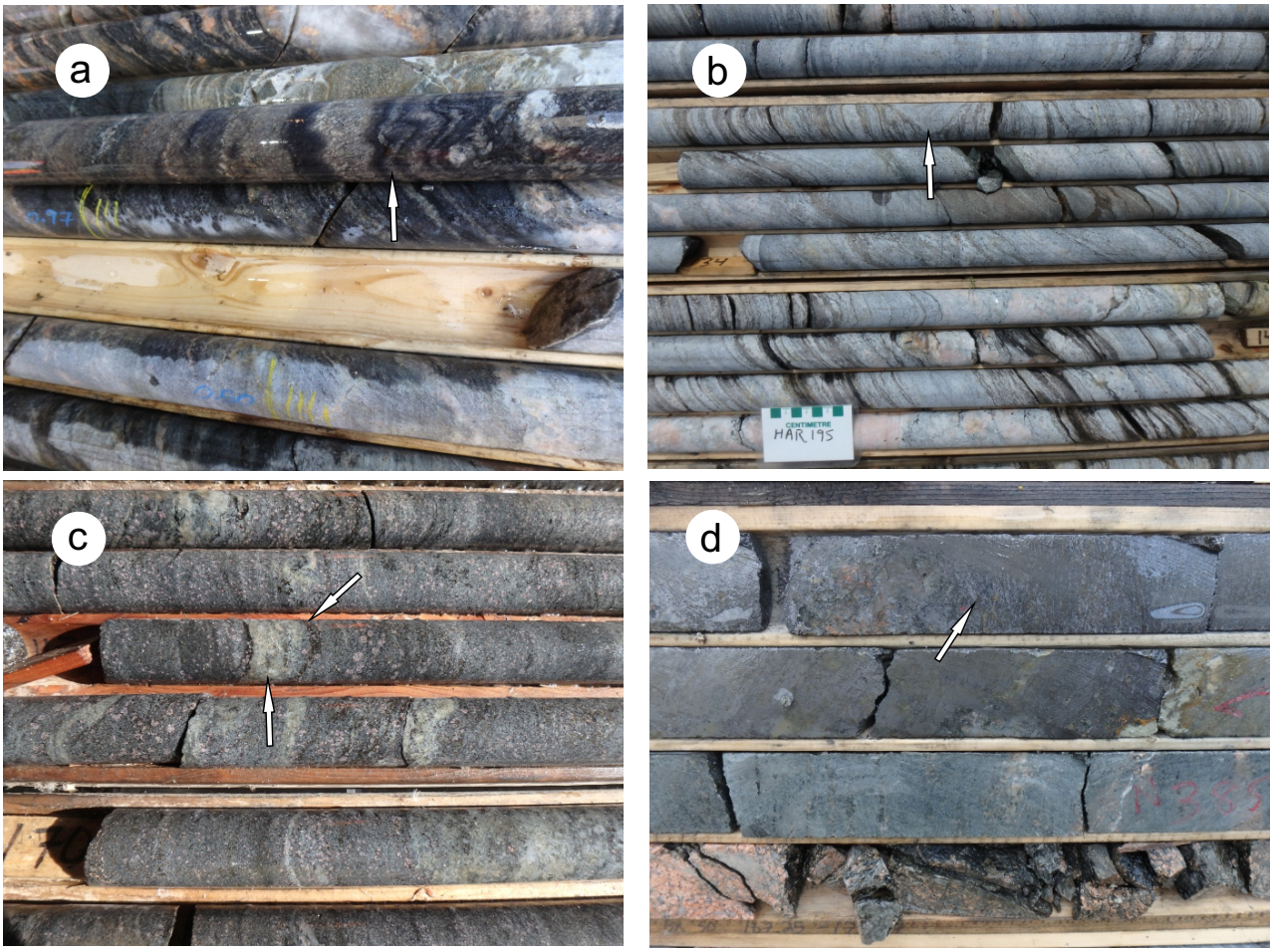

Figure GS2018-4-4: *Sedimentary rocks of the Watts, Mitishto and Hargrave rivers study area:* ***a)*** *dark, heavy-mineral layers (arrow) highlight primary bedding in a quartz-feldspar sandstone, drillcore KUS378;* ***b)*** *conglomerate interval with preserved subrounded felsic cobble (arrow), drillcore HAR195;* ***c)*** *biotite-garnet pelite with neosome (leucosome indicated by lower arrow and melanosome indicated by upper arrow) and paleosome, drillcore HAR070;* ***d)*** *graphite-sulphide–bearing interval in pelite (dull silvery wisps indicated by arrow are graphite), drillcore HAR261.*

stone (Figure GS2018-4-5b). Rare, subangular, lapilli-sized fragments are preserved; the example shown in Figure GS2018-4-5c contains local knots of sillimanite, suggesting possible hydrothermal alteration prior to metamorphism. A separate package of volcanic rocks with low aeromagnetic signature occurs along the western margin of the study area (immediately south of DDH 74-F1; Figure 2018-4-2), but no drillholes penetrate these rocks; instead they have been extrapolated from aeromagnetic data in the Wekusko Lake area, where they are interpreted as part of the Schist-Wekusko assemblage (Gilbert and Bailes, 2005).

Undivided mafic to felsic volcanic rocks with high aeromagnetic signature

These rocks have high TMI and display complex isoclinal folding (Figure GS2018-4-3) but lack textures characteristic of sandstone or conglomerate. Drillcore from hole KUS382 contains dark green, fine- to medium-grained amphibolite that contains scattered 4–10 mm garnet porphyroblasts and local calcsilicate alteration (Figure GS2018-4-5d); also present are lesser amounts of grey to light green, fine-grained intermediate rocks. What makes the amphibolite unit distinct, however, is its very high magnetic susceptibility (up to 161 x 10^{-3} SI), which is interpreted to correlate with the narrow pronounced aeromagnetic highs in the area (Figure GS2018-4-3). A potential analogue to this rock type could be strongly magnetic basalt flows and volcaniclastic rocks that occur to the northwest in the exposed Herb Lake volcanic block (e.g., Connors et al., 1999). Volcanic rocks of intermediate composition with moderate to high TMI are interpreted to occur in the southwestern portion of the study area; these have been extrapolated north from drillhole HAR253, the core from which was viewed in 2017 (see Figure GS2017-7-2 for the location of HAR253; Reid, 2017).

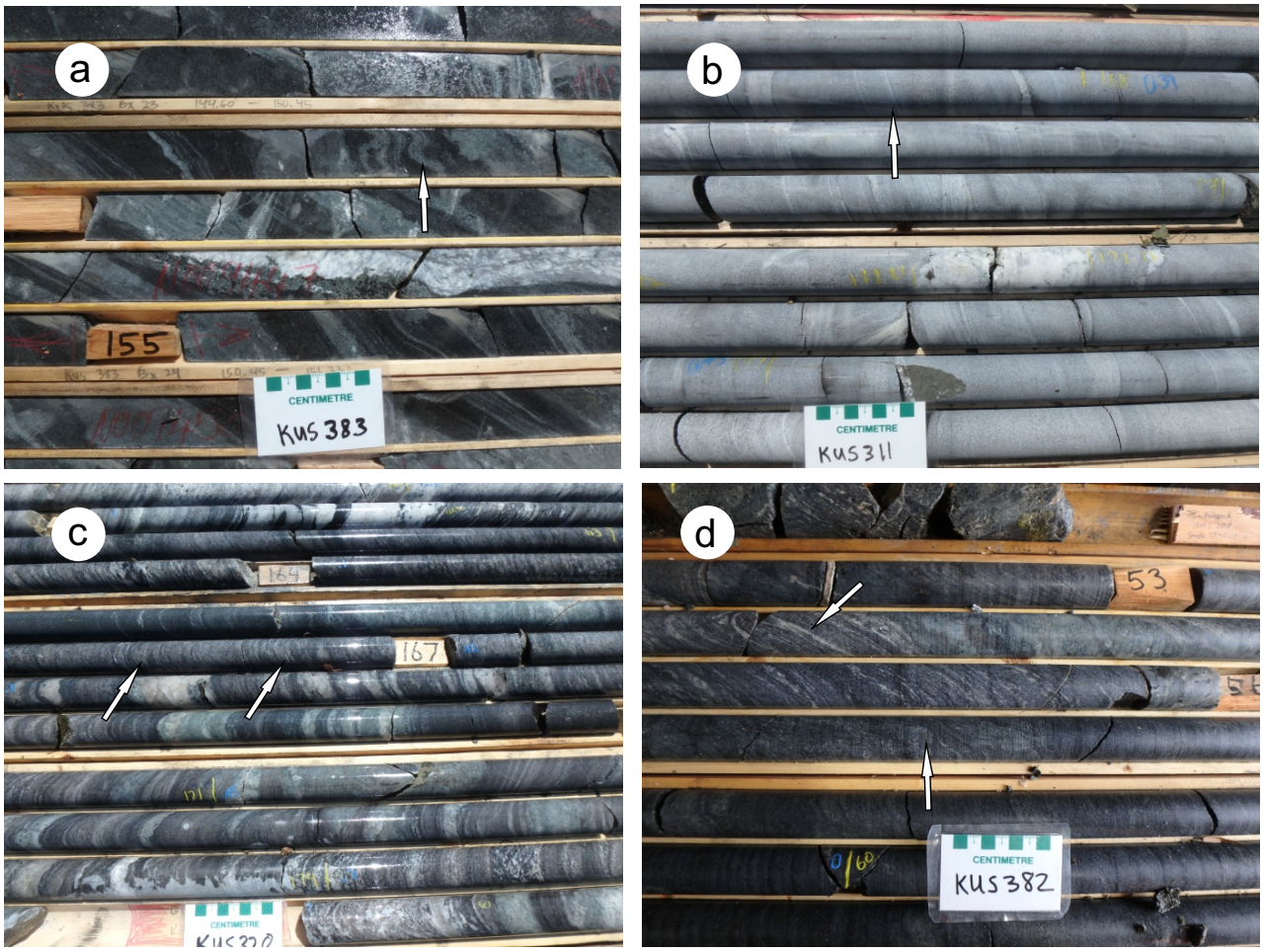

Figure GS2018-4-5*: Volcanic rocks of the Watts, Mitishto and Hargrave rivers study area:* ***a****) layered amphibolite with calcsilicate layer (arrow), drillcore KUS383;* ***b)*** *intermediate rock with centimetre-scale, subtle compositional layering (arrow), drillcore KUS311;* ***c)*** *light grey-green felsic rock with lapilli-sized fragments (left arrow) and local clots of sillimanite (right arrow), drillcore KUS320;* ***d)*** *highly magnetic carbonate- (upper arrow) and garnet-bearing (lower arrow) amphibolite, drillcore KUS382.*

Intrusive rocks

Pegmatite

Almost all drillcores examined contain numerous narrow (<3 m) intervals of leucocratic pegmatite; most of these have been affected to some extent by the latest stages of regional deformation, with contacts that parallel the foliation in the hostrock. Pegmatites typically have a relatively simple mineralogy, consisting of quartz, plagioclase, K-feldspar, minor biotite and occasionally muscovite. However, a noteworthy intersection occurs in drillcore KUS377 (continuous for 88 m, true width unknown) and multiple 3–5 m intervals are present in drillcore KUS310 (Figure GS2018-4-6a). These pegmatites both contain abundant macroscopic graphic textures that are interpreted to represent simultaneous crystallization and intergrowth of K-feldspar and quartz from a hydrous silicate melt (lower arrow in Figure GS2018-4-6a).

Granite, granodiorite and tonalite

Like pegmatite, granitoid rocks are present in nearly all drillholes and range from intersections of <1 m to most of the drillcore. Generally, the granitoid rocks are relatively homogeneous, leucocratic, medium to coarse grained and weakly to strongly foliated, and vary in colour from light grey to salmon pink (Figure GS2018-4-6a–c), depending largely on K-feldspar content. Contact relationships and primary features are mostly obliterated by ductile deformation (intrusive versus conformable), but the presence of what appear to be wallrock xenoliths indicates that granitoid rocks intruded the country rock (arrow in Figure GS2018-4-6b).

Diorite and gabbro

Mafic intrusive rocks are less abundant than felsic intrusives (see above). Mesocratic, dark green, massive

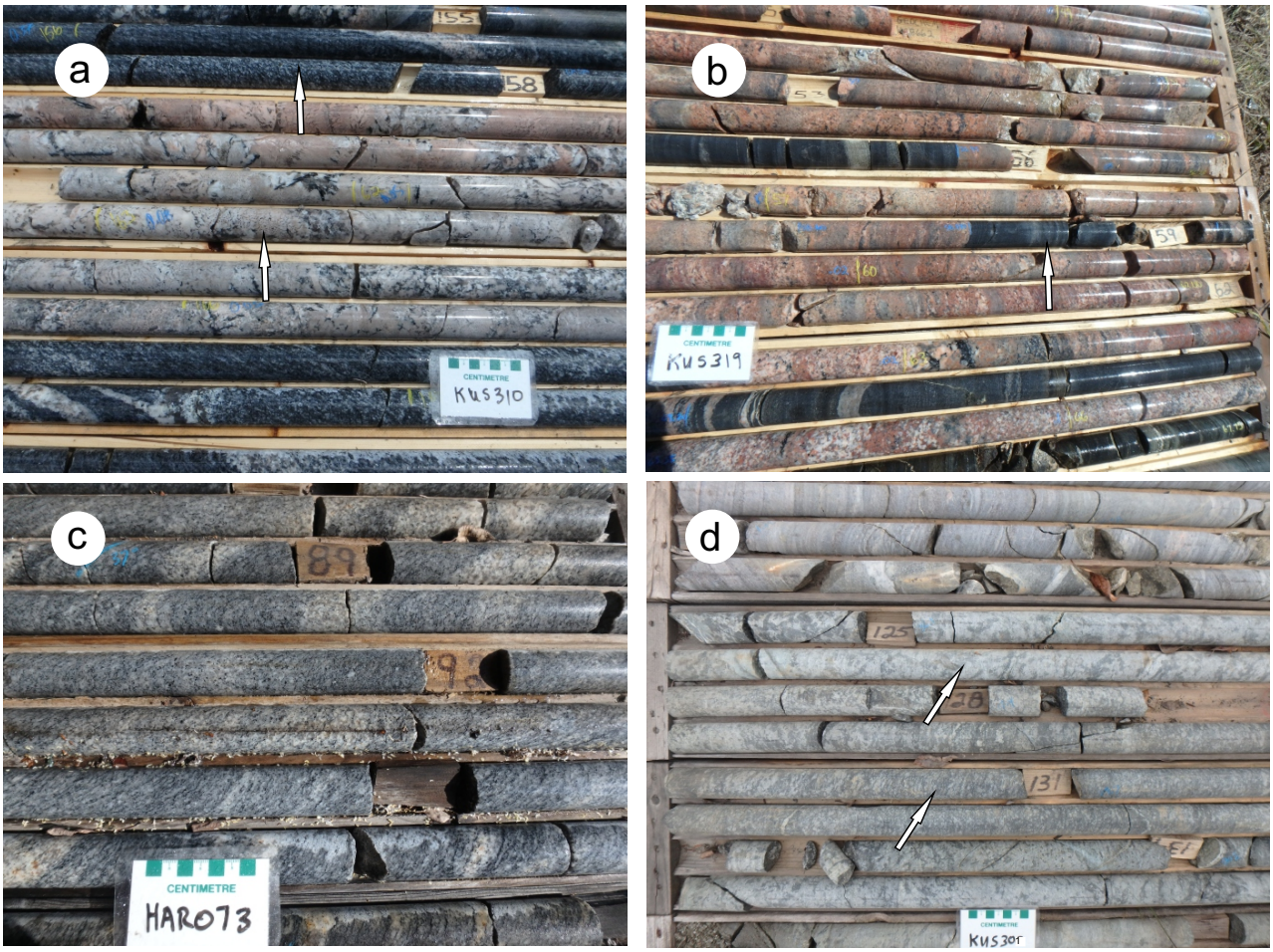

Figure GS2018-4-6: *Intrusive rocks of the Watts, Mitishto and Hargrave rivers study area:* ***a)*** *granodiorite (upper arrow) hosting significant interval of K-feldspar–rich pegmatite (graphic texture at lower arrow), drillcore KUS310;* ***b)*** *pink coarse-grained granite with xenoliths of intermediate volcanic rock (arrow), drillcore KUS319;* ***c)*** *well-foliated granite, drillcore HAR073;* ***d)*** *coarse-grained (lower arrow) to pegmatitic (upper arrow) gabbro, drillcore KUS301.*

to weakly foliated, coarse-grained to pegmatitic gabbro is present in drillcore KUS301 (Figure GS2018-4-6d). Its high magnetic susceptibility (~25 x 10^{-3} SI) is interpreted to correlate with the aeromagnetic high directly west of the drillhole location (Figure GS2018-4-3). A less conspicuous, melanocratic, moderately foliated, medium- to coarse-grained diorite occurs within volcanic rocks in drillcore KUS320. It should be noted that mafic intrusive rocks may be more abundant because fine- to medium-grained amphibolite and calcsilicate-altered amphibolite may represent high-level intrusions.

Grass River group, Ospwagan group and late intrusive rocks

Complexly folded rocks with high TMI near the intersection of Highways 39 and 6 (Figure GS2018-4-3) are surrounded by rocks with low aeromagnetic signature. These are interpreted to comprise undivided granitoid rocks; conglomerate and sandstone of the Grass River group; and pelite, calcsilicate, iron formation and volcanic rocks of the Ospwagan group. All of these rocks are surrounded by pelite and psammopelite of the Burntwood group. This interpretation rests largely on the fact that mapped examples are present in the Setting Lake area to the northeast (Zwanzig, 1999), where the Burntwood group is typically interpreted to be in thrust contact with rocks of the Ospwagan and Grass River groups (e.g., Zwanzig et al., 2007).

Metamorphic grade

Detailed petrographic studies have not been completed for rocks in the study area; tentative remarks, however, can be made based on macroscopic observations in pelitic and psammopelitic rocks. Biotite-garnet–bearing pelite underlying the Watts River area contains noticeable wisps of sillimanite, which is evidence that

these rocks were subjected to upper-amphibolite facies during peak metamorphism. Pelite in the southeast half of the study area rarely contains visual sillimanite but is migmatitic; less or no sillimanite may be related to compositional changes linked to a higher degree of partial melting, indicating that metamorphic grade increases southeastward.

Economic considerations

The Watts River base-metal deposit, located in the north half of the study area, is interpreted to be a VMS deposit associated with felsic volcanic and sedimentary rocks (Bailes, 2015). The recognition of additional volcanic rocks in drillholes KUS319, KUS320 and KUS321 extends prospective stratigraphy to the north and east (Figure GS2018-4-2). Drillcores KUS308, KUS310, KUS340, KUS348 and KUS349 all contain intercepts of subeconomic base (Cu, Zn) and precious (Au, Ag) metals, indicating that prospective stratigraphy extends for more than a kilometre (Assessment File 74696, Manitoba Growth, Enterprise and Trade, Winnipeg). Drillcore KUS374 contains subeconomic Cu (<0.1%) and Zn (<0.3%) values over a 13 m interval that includes a 3.09% Zn assay over 0.2 m (Assessment File 63J1142); these sulphides are associated with minor felsic rocks and may represent a prospective horizon worthy of further work.

Future work

Further investigation will focus on using whole-rock lithogeochemistry to determine the affinity and character of the volcanic and intrusive rocks. Petrographic studies may detail the metamorphic history. A zircon U-Pb age from felsic rocks hosting the Watts River VMS deposit is pending—this should provide some insight on whether this deposit is associated with early juvenile-arc volcanism or successor-arc volcanism.

Acknowledgments

The author thanks R. Colasuonno for providing enthusiastic field assistance, as well as N. Brandson and E. Anderson for thorough logistical support. C. Epp is thanked for thoughtful and thorough preparation of samples in the lab.

References

Ansdell, K.M., Kyser, K., Stauffer, M. and Edwards, G. 1992: Age and source of detrital zircons from the Missi Formation: a Proterozoic molasse deposit, Trans-Hudson Orogen, Canada; Canadian Journal of Earth Sciences, v. 29, p. 2583–2594.

Ansdell, K.M., Lucas, S.B., Connors, K. and Stern, R.A. 1995: Kisseynew metasedimentary gneiss belt, Trans-Hudson orogen (Canada): back-arc origin and collisional inversion; Geology, v. 23, p. 1039–1043.

Bailes, A.H. 1985: Geology of the Saw Lake area; Manitoba Energy and Mines, Manitoba Geological Survey, Geological Report GR83-2, 47 p.

Bailes, A.H. 2015: Geological setting of the Watts River base metal massive sulphide deposit; HudBay Minerals Inc., unpublished internal geological report, 70 p.

Connors, K.A., Ansdell, K.M. and Lucas, S.B. 1999: Coeval sedimentation, magmatism, and fold-thrust development in the Trans-Hudson Orogen: propagation of deformation into an active continental arc setting, Wekusko Lake area, Manitoba; Canadian Journal of Earth Sciences, v. 36, p. 275–291.

Gilbert, H.P. and Bailes, A.H. 2005: Geology of the southern Wekusko Lake area, Manitoba (NTS 63J12NW); Manitoba Industry, Economic Development and Mines, Manitoba Geological Survey, Geoscientific Map MAP2005-2, scale 1:20 000.

Keating, P., Pilkington, M. and Oneschuk, D. 2012: Geophysical Series, high-resolution aeromagnetic data compilation, Flin Flon and Snow Lake regions, Manitoba and Saskatchewan, NTS 63K and parts of NTS 63J, L, M, N and O; Geological Survey of Canada, Open File 7103, 2012, 2 sheets.

Leclair, A.D., Lucas, S.B., Broome, H.J., Viljoen, D.W. and Weber, W. 1997: Regional mapping of Precambrian basement beneath Phanerozoic cover in southeastern Trans-Hudson Orogen, Manitoba and Saskatchewan; Canadian Journal of Earth Sciences, v. 34, p. 618–634.

Lewry, J.F. and Collerson, K.D. 1990: Trans-Hudson Orogen: extent, subdivisions, and problems; *in* The Proterozoic Trans-Hudson Orogen of North America, J.F. Lewry and M.R. Stauffer (ed.), Geological Association of Canada, Special Publication 37, p. 1–14.

Reid, K.D. 2017: Sub-Phanerozoic basement geology south of Wekusko Lake, eastern Flin Flon belt, north-central Manitoba (parts of NTS63J5, 12, 63K8, 9): insights from drillcore observations and whole-rock geochemistry of mafic rocks; *in* Report of Activities 2017, Manitoba Growth, Enterprise and Trade, Manitoba Geological Survey, p. 65–77.

Stauffer, R.A. 1984: Manikewan: an early Proterozoic ocean in central Canada: its igneous history and orogenic closure; Precambrian Research, v. 25, p. 257–281.

Stockwell, C.H. 1937: Gold deposits of Herb Lake area, northern Manitoba; Geological Survey of Canada, Memoir 208, p. 46.

Syme, E.C. and Bailes, A.H. 1993: Stratigraphic and tectonic setting of early Proterozoic volcanogenic massive sulfide deposits, Flin Flon, Manitoba; Economic Geology, v. 88, no. 3, p. 566–589.

Syme, E.C., Lucas, S.B., Bailes, A.H. and Stern, R.A. 1999: Contrasting arc and MORB-like assemblages in the Paleoproterozoic Flin Flon Belt, Manitoba, and the role of intra-arc extension in localizing volcanic-hosted massive sulphide deposits; Canadian Journal of Earth Sciences, v. 36, p. 1767–1788.

Whalen, J.B., Syme, E.C. and Stern, R.A. 1999: Geochemical and Nd isotopic evolution of Paleoproterozoic arc-type magmatism in the Flin Flon Belt, Trans-Hudson Orogen, Canada; Canadian Journal of Earth Sciences, v. 36, p. 227–250.

Zwanzig, H.V. 1999: Mapping in the Setting Lake area (parts of NTS 63J15, 63O1, 63O2); *in* Report of Activities 1999, Manitoba Industry, Trade and Mines, Geological Services, p. 18–23.

Zwanzig, H.V., Macek, J.J. and McGregor, C.R. 2007: Lithostratigraphy and geochemistry of the high-grade metasedimentary rocks in the Thompson Nickel Belt and adjacent Kisseynew Domain, Manitoba: implications for nickel exploration; Economic Geology, v. 102, p. 1197–1216.

GS2018-5

Geochemistry, Sm-Nd isotopes and U-Pb geochronology of volcanic rocks from the North Star assemblage and the West Reed–North Star shear zone, Flin Flon belt, west-central Manitoba (parts of NTS 63K10, 15): implications for VMS prospectivity

by S. Gagné, S.D. Anderson, M. Hamilton[1], R.-L. Simard and M. Lazzarotto[2]

In Brief:

- The North Star assemblage represents a package of bimodal volcanic and volcaniclastic rocks with an arc-signature that has distinct geochemical and Sm-Nd isotopic characteristics
- A new U-Pb zircon age of 1895.9 ±1.6 Ma for a rhyolite from the North Star assemblage is similar in age to the main VMS-hosting volcanic sequences from the Flin Flon and Snow Lake areas
- The Rail deposit is interpreted to be part of the North Star assemblage

Citation:
Gagné, S., Anderson, S.D., Hamilton, M., Simard, R.-L. and Lazzarotto, M. 2018: Geochemistry, Sm-Nd isotopes and U-Pb geochronology of volcanic rocks from the North Star assemblage and the West Reed–North Star shear zone, Flin Flon belt, west-central Manitoba (parts of NTS 63K10, 15): implications for VMS prospectivity; *in* Report of Activities 2018, Manitoba Growth, Enterprise and Trade, Manitoba Geological Survey, p. 48–63.

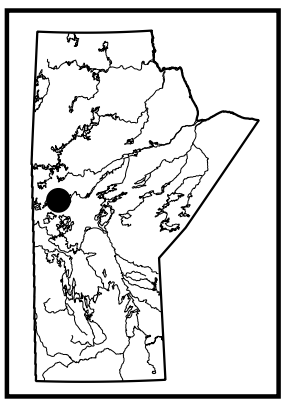

Summary

The West Reed–North Star shear zone (WRNS), traceable over a distance of 38 km west and northwest of Reed Lake in the Flin Flon belt, consists of layered tectonites hundreds of metres thick. The tectonites mark the boundary between two packages of bimodal volcanic and volcaniclastic rocks that host volcanogenic massive sulphides (VMS). The well-documented volcanic-arc/arc-rift rocks of the Fourmile Island assemblage (FIA) lie east of the WRNS and occur continuously along the entire trace of the WRNS. West of the WRNS lies another package of bimodal arc/arc-rift volcanic and volcaniclastic rocks termed the 'North Star assemblage' (NSA). The NSA is exposed along two main stretches separated by a 10 km gap. Geochemical investigation of the NSA rocks indicates that the northern and southern segments of the NSA are part of the same arc assemblage but have a complex volcanic history that includes generation of enriched mid-ocean ridge basalt (E-MORB), tholeiites with weak arc signatures and bimodal transitional to calc-alkaline magmatism. The distinct geochemical signatures of the NSA and FIA are both recognized in tectonized rocks within the WRNS. The Rail VMS deposit, interpreted to be located entirely within the WRNS, is hosted by rocks with a geochemical character similar to that of the NSA. Trace element signatures and Sm-Nd isotopic data show that NSA volcanism represents a more evolved sequence of juvenile-arc rocks, fed by a deeper magmatic source, compared to arc-volcanic rocks of the FIA.

Rhyolite at North Star Lake has been dated at 1895.9 +/-1.6 Ma and, considering it represents a significant volume of the NSA rocks, it is interpreted that the bulk of the arc assemblage was emplaced around 1896 Ma.

Introduction

Paleoproterozoic rocks in the Reed Lake area (Figure GS2018-5-1) are a component of a larger tectonic collage of volcano-plutonic and sedimentary rocks assembled during the closure of an ancient ocean (ca. 1.9–1.8 Ga) and collectively termed the 'Flin Flon belt' (FFB). The FFB contains numerous base-metal VMS deposits and is among the world's most prolific VMS districts (Syme et al., 1999). In the Reed Lake area and to the south beneath Phanerozoic sedimentary rocks, the FFB has significant potential to host additional VMS deposits. Despite the presence of several economic deposits, including the Reed Cu-Zn mine which ceased production in August 2018 after having depleted its reserves (Figure GS2018-5-1), the geological setting of VMS deposits in the Reed Lake area is not well understood. Previous workers recognized that significant stratigraphic, geochemical and isotopic differences exist between arc-volcanic rocks in the Flin Flon (Amisk collage) and Snow Lake areas, which suggested that these two segments of the FFB formed in distinct tectonic settings (Stern et al., 1995a; Lucas et al., 1996). Moreover, the Reed Lake area includes some major structural zones that resulted from the complex assembly of the FFB.

[1] Department of Earth Sciences, University of Toronto, 22 Russell Street, Toronto, ON M5S 3B1
[2] Department of Geosciences, University of Calgary, 2500 University Drive NW, Calgary, AB T2N 1N4

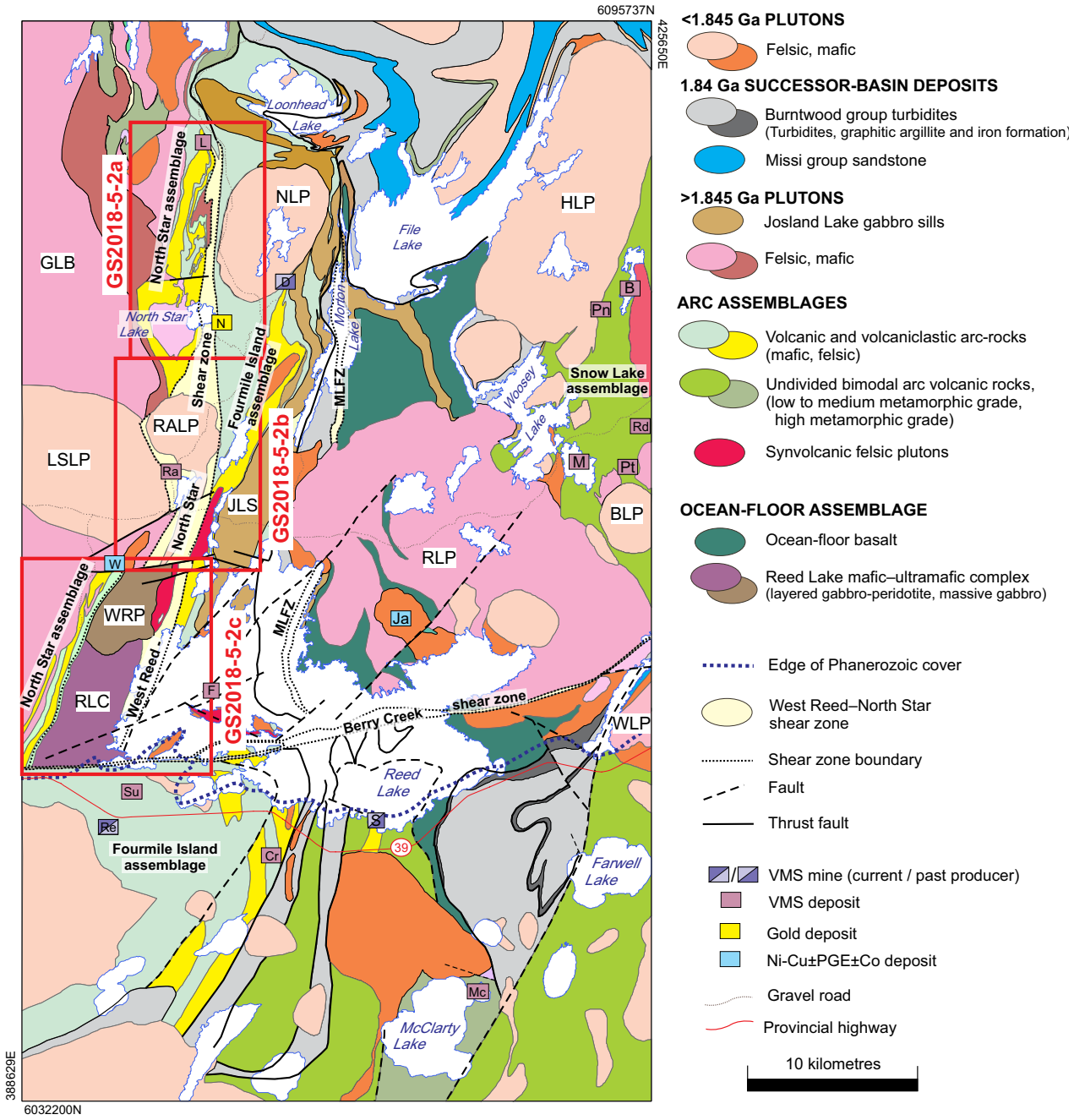

Figure GS2018-5-1: *Generalized geology of the Reed Lake area (compiled from Syme et al., 1995a; NATMAP Shield Margin Project Working Group, 1998; Gagné, 2017; Gagné et al., 2017). Intrusive rocks: BLP, Bujarsky Lake pluton; GLB, Gants Lake batholith; HLP, Ham Lake pluton; JLS, Josland Lake sills; LSLP, Little Swan Lake pluton; NLP, Norris Lake pluton; RALP, Rail Lake pluton; RLC, Reed Lake mafic–ultramafic complex; RLP, Reed Lake pluton; WLP, Wekusko Lake pluton; WRP, West Reed pluton. Structural feature: MLFZ, Morton Lake fault zone. Mines (active or closed), deposits and significant mineral occurrences: B, Bomber; Cr, Cowan River zone; D, Dickstone; F, Fourmile Island; Ja, Jackfish; L, Lon; M, Morgan; Mc, McClarty; N, North Star; Pn, Pen; Pt, Pot; Ra, Rail; Rd, Raindrop; Re, Reed; S, Spruce Point; Su, Super Zone; W, Wine. Other abbreviations: PGE, platinum-group elements; VMS, volcanogenic massive sulphide. Co-ordinates are in UTM Zone 14 (NAD83).*

One of these major structures, hundreds of metres wide, is the WRNS, which consists of tectonized mafic and felsic rocks that separate two sequences of bimodal volcanic rocks (Figure GS2018-5-1) that host VMS deposits. Rocks of the FIA occupy the eastern margin of the WRNS (Bailes, 1980; Syme et al., 1995b; Zwanzig and Bailes, 2010; Gagné, 2013; Gagné and Anderson, 2014a). Along the western margin of the WRNS, two segments of bimodal volcanic and volcaniclastic rocks are collectively referred to as the NSA (Figures GS2018-5-1, 2a, b, c). The northern

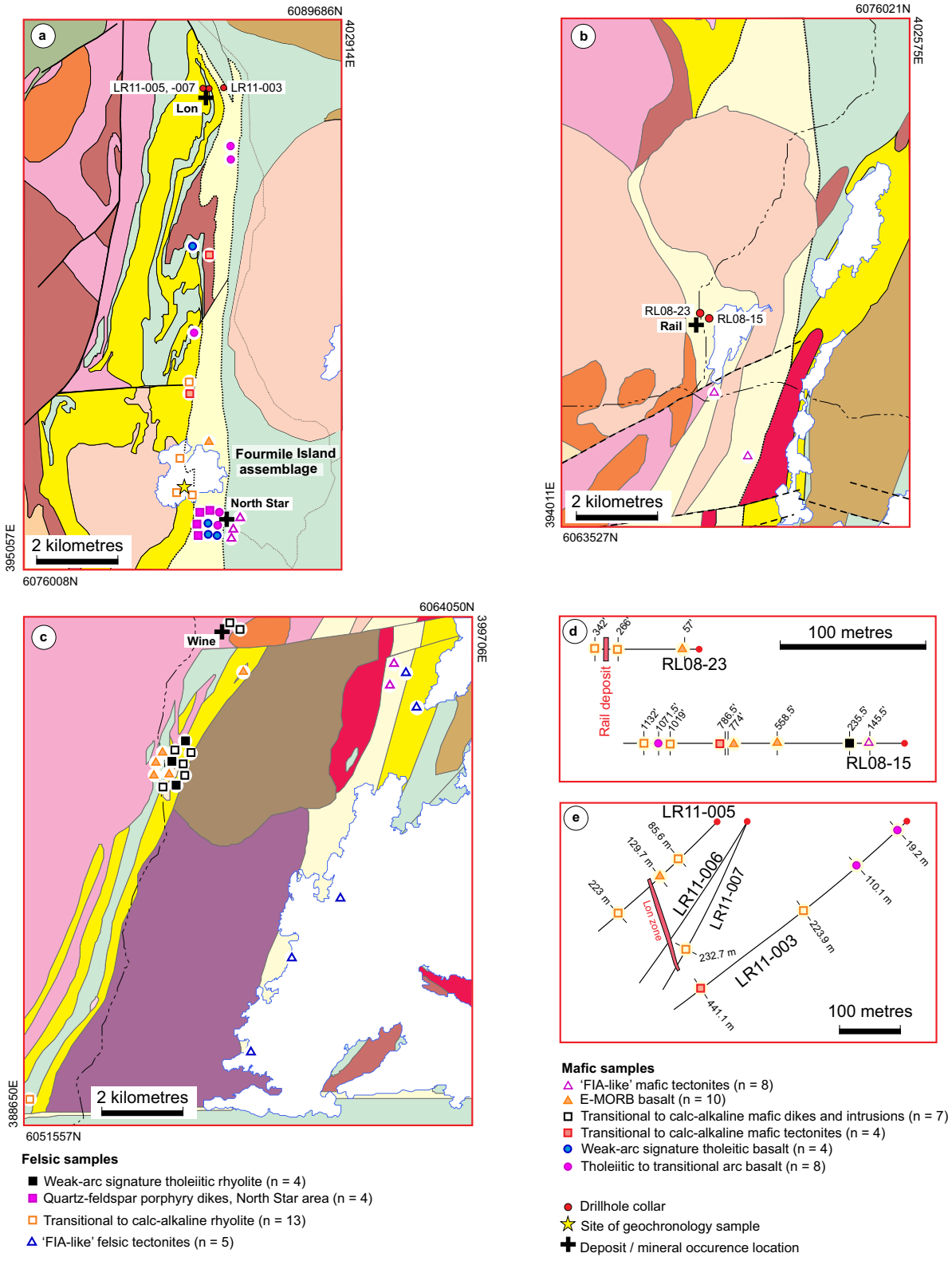

Figure GS2018-5-2: *Detailed geology of the three focus areas of the Flin Flon belt presented in this report, showing sample locations in* ***a)*** *the northern segment of the North Star assemblage (NSA);* ***b)*** *the Rail Lake area of the West Reed–North Star shear zone (WRNS);* ***c)*** *the southern segment of the NSA;* ***d)*** *the surface projection of the trace of two drillholes from the Rail deposit sampled by Simard et al. (2010), with sample locations indicated;* ***e)*** *an east-west vertical cross-section (looking north) along four drillholes that targeted the Lon volcanogenic massive sulphide deposit, with 2013 sample locations indicated. Geological units shown in a-c correspond to the legend in Figure GS2018-5-1. All NSA and WRNS geochemical samples are plotted on the map or along drillhole traces, with symbols reflecting their geochemical affinity.*

segment of the NSA extends northward from North Star Lake to southwest of Loonhead Lake over ~8 km and is host to the Lon VMS deposit (Figure GS2018-5-2a). The central portion of the WRNS is intruded by the Rail Lake pluton, lacks the less deformed NSA rocks along the western flank and is host to the Rail VMS deposit (Figure GS2018-5-2b). Figure GS2018-5-2c shows the southern portion of the NSA west of Reed Lake; Gagné and Anderson (2014a, b) described these rocks in detail. Detailed mapping and structural studies of the northern volcanic segment were conducted after the large 1989 Elbow Lake forest fire passed through the area. Detailed lithological descriptions and structural interpretations are provided in a series of Manitoba Geological Survey (MGS) Report of Activities (Norquay et al., 1991; Norquay et al., 1994) and a M.Sc. thesis (Norquay, 1997). However, no lithogeochemical analyses were published from these studies and very little work in terms of quantifying metamorphic petrology was done. These aspects are crucial to understanding the tectonometamorphic history of the supracrustal rocks of the NSA, and within the WRNS, and may provide vital information for assessing the mineral potential of the region.

This report provides the first geochemical characterization and Sm-Nd isotopic systematics of the rocks that form the NSA and the WRNS. In addition, the age of a rhyolite from the NSA is presented. New high-resolution geochemical data are presented here in combination with recent results from other MGS projects (Simard et al, 2010; Zwanzig and Bailes, 2010; Gagné and Anderson, 2014a) to provide a more comprehensive comparison. An update on metamorphic investigations in the North Star–Reed Lake–File Lake area, undertaken within the framework of a larger study of the metamorphism in the FFB conducted by M. Lazzarotto as part of his Ph.D. research at the University of Calgary (Lazzarotto et al., 2016, 2017), is presented in a companion paper (Lazzarotto et al., GS2018-6, this volume).

Regional geological framework

The exposed FFB contains several distinct juvenile-arc assemblages separated by major faults or intervening ocean-floor rocks, Burntwood group sedimentary rocks, plutonic rocks, or a combination of these. The volcanic assemblages are internally complex, commonly fault-bounded and folded, and typically bimodal suites (e.g., Bailes and Syme, 1989) with dominantly andesite/basalt and rhyolite/dacite flows, but also include a wide range of arc-related volcaniclastic and intrusive rocks (Bailes and Syme, 1989; Syme and Bailes, 1993; Stern et al., 1995a; Lucas et al., 1996; Bailes and Galley, 2007). The juvenile ocean-floor assemblages are composed mainly of mid-ocean–ridge basalt (MORB)–like basalt and related, layered, mafic–ultramafic plutonic complexes (Syme and Bailes, 1993; Stern et al., 1995b) that are kilometre-scale in width. Uranium-lead zircon ages for the ocean-floor assemblages in the exposed portion of the FFB indicate that ocean-floor magmatism was coeval with tholeiitic-arc volcanism around 1.9 Ga (Stern et al., 1995b).

The development of successor arcs resulted in the emplacement of voluminous plutons, coeval volcanism and deposition of sedimentary rocks. The successor-arc plutons were emplaced throughout the belt during three distinct magmatic stages (1878–1860 Ma, 1860–1844 Ma and 1843–1826 Ma; Whalen et al., 1999). Similar aged (ca. 1.88–1.83 Ga) volcanic, volcaniclastic and sedimentary rocks have been documented across the central and eastern parts of the exposed FFB and are interpreted as successor-basin deposits. They include the Schist–Wekusko assemblage, the Missi group and the Burntwood group. The fluvial–alluvial Missi group sedimentary deposits are characterized by thick packages of conglomerate, pebbly sandstone and massive sandstone. The marine turbidites of the Burntwood group include greywacke, siltstone, mudstone and rare conglomerate. In the low-grade metamorphic FFB, these sedimentary rocks are generally in fault contact with other units.

Exposed on the western shore of Reed Lake, the WRNS is a major, regionally extensive tectonite belt that lies between rocks of the FIA to the east and rocks of the NSA to the west (Figures GS2018-5-1, -2a–c). Collectively, rocks from the NSA, WRNS and FIA record a broad range of peak metamorphic conditions as discussed in Lazzarotto et al. (GS2018-6, this volume). For the sake of brevity, the prefix ‘meta-’ is not used in this report and the rocks are generally described in terms of their protoliths.

North Star assemblage

The NSA consists of two distinct segments, a northern and a southern segment (Figure GS2018-5-2a, c). According to Norquay (1997), the northern segment of the NSA (Figure GS2018-5-2a) comprises two intervals of rhyolitic rocks 600 and 100 m wide (Figure GS2018-5-3a) that host the Lon VMS deposit (Figure GS2018-5-3b, c). Two narrow successions of predominantly mafic volcanic rocks with lesser intermediate rock, minor siliciclastic intervals and iron formation are intercalated with the rhyolitic rocks and display a complex fold pattern. The felsic and mafic volcanic rocks of the northern segment of the NSA also include several zones of metamorphosed hydrothermal alteration exposed at surface

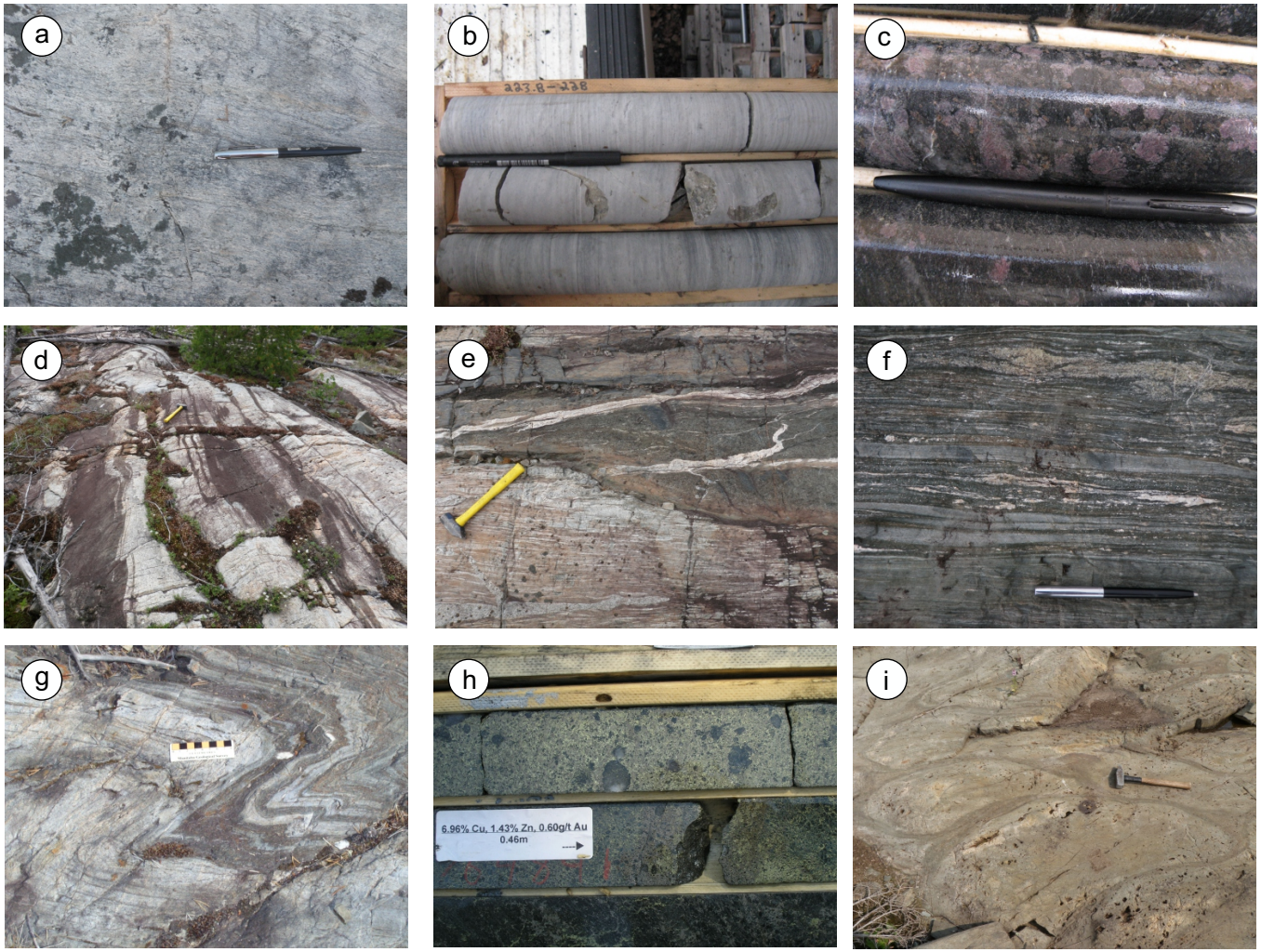

Figure GS2018-5-3: *Rock photographs showing* ***a)*** *strongly foliated, massive, homogeneous, quartz-phyric rhyolite of the northern North Star assemblage (NSA) segment on an island at North Star Lake (picture from sample 110-16-755 [399031E, 6077910N] analyzed for U-Pb geochronology);* ***b)*** *drillcore sample of rhyolite from the Lon deposit (LR-11-003 at 223 m; NQ core) in the northern NSA segment;* ***c)*** *drillcore sample of altered mafic gneiss containing abundant biotite and hornblende (black matrix minerals) with large garnet (pink) and staurolite (brown) porphyroblasts, from the Lon deposit (LR-11-003 at 85.3 m; NQ core) in the northern NSA segment;* ***d)****, rhyolite dikes in sparsely plagioclase-phyric basalt (392592E, 6060440N) from the southern NSA segment;* ***e)****, plagioclase-pyroxene–phyric dikes (dark coloured rocks) intruding felsic volcaniclastic rocks (392679E, 6061539N) from the southern NSA segment;* ***f)*** *mafic tectonites (400381E, 6073265N) from the West Reed–North Star assemblage (WRNS);* ***g)****, felsic tectonites interpreted as felsic tuff breccia (left) and intermediate crystal tuff (399801E, 6077439N) from the WRNS near North Star Lake;* ***h)*** *pyrrhotite-chalcopyrite solid sulphide horizons from diamond drill hole RL-08-23 at 93 m (NQ core) from the WRNS near the Rail deposit;* ***i)*** *large pillows from Preaston andesite (400381E, 6073265N) of the Fourmile Island assemblage. All co-ordinates are in UTM Zone 14 (NAD83). Drillcore diameter: NQ, 47.6 mm.*

and defined by the appearance or increasing abundance of porphyroblastic minerals, such as kyanite, staurolite, garnet and gahnite (Figure GS2018-5-3c). The southern segment of the NSA forms a narrow belt, some 300 to 500 m wide, consisting mainly of basaltic volcaniclastic rocks with intervals of mafic and felsic flows, and volcaniclastic rocks (Figure GS-2018-5-3d). The southern segment of the NSA is characterized by abundant syn- and postvolcanic dikes ranging in composition from mafic to felsic (Figure GS-2018-5-3e). Synvolcanic dikes, which are typically porphyritic with an aphanitic to fine-grained groundmass, are strongly foliated and transposed (Gagné and Anderson, 2014a).

West Reed–North Star shear zone

Felsic and mafic tectonites that form the WRNS extend for a strike length of 38 km along the western side of the FIA. The shear zone expands up to 1 km in width south of North Star Lake. Intense fabric within the mafic tectonite makes protolith determination difficult (Figure GS-2018-5-3f); however, in lower strain domains, possible remnant pillow selvages indicate that the protolith for this unit was, at least locally, mafic flows. The WRNS tectonites also include minor horizons of highly deformed felsic rocks of unknown precursor (Figure GS-2018-5-3g). The Rail VMS deposit is interpreted as being hosted within the WRNS (Figure GS-2018-5-3h).

Fourmile Island assemblage

West of Morton Lake, the FIA is 1.8 km thick and includes mafic to felsic volcanic rocks (Figures GS2018-5-1). The Preaston andesite at the base (Figure GS2018-5-3i) is stratigraphically overlain by the Dickstone rhyolite and, in turn, the Storozuk volcanic rocks, which are dominated by basalt (GS2018-5-2a-c). The Preaston andesite is found between the Dickstone rhyolite (felsic volcanic-arc rocks that extend southward from the Dickstone mine; Figures GS2018-5-1, 2a, b) and the eastern margin of the WRNS. The Storozuk mafic volcanic rocks extend along the eastern side of the Dickstone rhyolite and the Loonhead Lake area. The relatively thin (<330 m, not shown in Figures GS2018-5-1, 2) volcaniclastic Yakymiw formation forms the top of this succession (Bailes, 1980).

The FIA rocks were intruded by a compositionally zoned and highly fractionated mafic sill 1 km thick. The sill, part of the Josland Lake suite (Bailes, 1980), displays extreme iron fractionation and was dated at 1886 ±3 Ma (Zwanzig et al., 2001). This age indicates that the FIA volcanic rocks are part of the ca. 1.89 Ga juvenile-arc volcanic rocks that host the bulk of the VMS deposits in the FFB. The FIA is currently interpreted as a back-arc rift succession formed at about 1.89 Ga during opening of an ocean basin (Zwanzig and Bailes, 2010).

Sampling procedure and analytical methods

In order to characterize the geochemistry of the supracrustal rocks of the NSA and the tectonites of the WRNS, a suite of representative rock samples was collected for lithogeochemical analysis. The variations in trace-element chemistry and Sm-Nd isotopic composition can provide useful insight into the potential sources and geodynamic settings of magmatic rocks, and thus constrain regional-scale tectonic and metallogenic models. Major and trace-element compositions of all analyzed samples are available in Data Repository Item DRI2018003[3].

Whole-rock geochemistry

Sixty-seven drillcore, surface and underground samples provide regional coverage of the representative lithological units found within the NSA and WRNS (Figure GS2018-5-2). Where possible, samples were collected from the least altered rocks, but some include slightly altered material. All samples were trimmed to remove weathered surfaces, joints and veinlets; some samples may contain rare amygdules. Pulps were produced at the MGS rock laboratory using an agate mill. The pulps were then analyzed using the 4Lithores analytical package by Activation Laboratories Ltd. (Ancaster, Ontario). Major and minor elements were analyzed by inductively coupled plasma–emission spectrometry, and trace and rare-earth elements (REE) were analyzed using inductively coupled plasma–mass spectrometry (ICP-MS).

Sm-Nd isotopic analysis

Eight samples were submitted for Sm-Nd isotope geochemical analysis to the Radiogenic Isotope Facility of the University of Alberta (Edmonton, Alberta). Sampling and initial processing procedures were the same as those used for the lithogeochemical samples. Processing and analysis for $^{143}Nd/^{144}Nd$ and $^{147}Sm/^{144}Nd$ isotopic ratios followed the chromatographic and mass-spectrometry procedures described by Unterschutz et al. (2002) and Schmidberger et al. (2007). Samarium and Nd isotopic compositions were determined by multicollector ICP-MS

[3] MGS Data Repository Item DRI2018003 containing the data or other information sources used to compile this report is available online to download free of charge at https://www.gov.mb.ca/iem/info/library/downloads/index.html, or on request from minesinfo@gov.mb.ca, or by contacting the Resource Centre, Manitoba Growth, Enterprise and Trade, 360–1395 Ellice Avenue, Winnipeg, Manitoba R3G 3P2, Canada.

using an in-house Nd isotope standard (Schmidberger et al., 2007). Chemical-processing blanks were <200 pg for Nd and Sm. Neodymium isotope data are presented relative to a $^{143}Nd/^{144}Nd$ value of 0.511850 for the La Jolla Nd reference standard. Neodymium depleted-mantle model ages (T_{DM}) were calculated for samples with $^{147}Sm/^{144}Nd$ <0.14 using the model of DePaolo (1981), and present-day depleted-mantle values of $^{147}Sm/^{144}Nd$ = 0.2137 and $^{143}Nd/^{144}Nd$ = 0.513163. All epsilon Nd values (εNd) were calculated at the known or inferred age of crystallization (i.e., initial εNd values). They are reported relative to a chondritic uniform reservoir with present-day values of $^{147}Sm/^{144}Nd$ = 0.1967 (Jacobsen, 1980) and $^{143}Nd/^{144}Nd$ = 0.512638 (Goldstein et al., 1984).

U-Pb geochronology

Uranium-lead dating of the North Star rhyolite was carried out at the Jack Satterly Geochronology Laboratory at the University of Toronto. Sample preparation and analytical protocols generally followed those described in Bamburak et al. (2016).

Geochemistry

Mafic rocks

Mafic volcanic and selected intrusive samples from the NSA and the WRNS display five distinct geochemical signatures (Figure GS2018-5-4). For reference, analyses of the Preaston andesite and basalt flows (part of the FIA) from near the WRNS have been compiled from Zwanzig and Bailes (2010) and include unpublished samples collected by Gagné in 2013. Scatterplots show individual Preaston samples, but shaded areas reflect the unit's compositional range in the spider diagrams (Figure GS2018-5-4). Zwanzig and Bailes (2010) and Gagné and Anderson (2014a) discuss the geochemistry of the Preaston andesite in detail.

'FIA-like' mafic tectonites

Eight mafic tectonite samples mostly from the eastern side of the WRNS plot as basalt and andesite of distinctly tholeiitic affinity; these overlap closely with the Preaston andesite and basalt and are thus referred to as 'FIA-like' mafic tectonites (Figures GS2018-5-2, 4a, b). Mafic tectonite samples display a slightly enriched heavy REE (HREE) profile with a small negative Eu anomaly on a chondrite-normalized trace-element diagram (Figure GS2018-5-4c). On a primitive mantle–normalized, incompatible trace-element diagram (Figure GS2018-5-4d), the mafic rocks display distinct negative Nb anomalies and are depleted with respect to Ti. On a ternary Th-(Hf/3)-(Nb/16) diagram the rocks show a volcanic-arc affinity (Figure GS2018-10-4g), and on a Th/Nb versus Nb/Y diagram (Figure GS2018-5-4h) the FIA and 'FIA-like' mafic tectonites plot outside of the range of values of the Flin Flon arc rocks as compiled by Stern et al. (1995a). Mafic tectonite samples from the eastern margin of the WRNS appear to have very similar trace-element compositions to the Preaston andesite (Zwanzig and Bailes, 2010), indicating that the eastern portion of the WRNS is made up of FIA rocks caught up in the shear zone.

E-MORB

Ten samples of basalt with a tholeiitic to transitional affinity have slightly enriched light rare-earth-element (LREE) profiles and are referred to as 'E-MORB' (Figure GS2018-5-4a–c). On a primitive mantle–normalized incompatible trace-element diagram (Figure GS2018-5-4d), the basalt has an almost flat profile with samples showing either a weak positive or a weak negative Th signature and a weak negative Nb anomaly. On a ternary Th-(Hf/3)-(Nb/16) diagram (Figure GS2018-5-4g), the samples plot mostly in the E-MORB field. On a Th/Nb versus Nb/Y diagram (Figure GS2018-5-4h), the 'E-MORB' samples plot outside of the range of values of the Flin Flon arc rocks as compiled by Stern et al. (1995a) and overlap slightly with the compositional fields of both the N-MORB and E-MORB. Similar Th/Nb ratios (slightly elevated with respect to MORB) have also been documented within basalt of the Northeast Reed ocean-floor assemblage (Syme and Bailes, 1996) as well as in some basalt members of the Elbow–Athapapuskow ocean-floor assemblage (Stern et al. 1995b). Stern et al. (1995b) interpret these ratios as a subduction signature, rather than the result of crustal contamination; such MORB-like basalt with weak arc signatures suggests affinities with modern back-arc basin basalt.

Weak-arc tholeiitic basalt

Four samples mainly from the area immediately west of the North Star gold deposit plot as basalt with tholeiitic affinity and are referred to as 'weak-arc tholeiitic basalt' (Figures GS2018-5-2a and GS2018-5-4a, b). These show relatively flat REE profiles on a chondrite-normalized trace-element diagram (Figure GS2018-5-4e). On a primitive mantle–normalized incompatible trace-element diagram (Figure GS2018-5-4f), the 'weak-arc tholeiitic basalt' samples show almost flat profiles with weak to moderate relative depletions of Nb, Zr, Ti, V and Sc. On a ternary Th-(Hf/3)-(Nb/16) diagram (Figure GS2018-5-4g), the samples plot strictly in the arc-basalt field. These four samples plot close to the field of

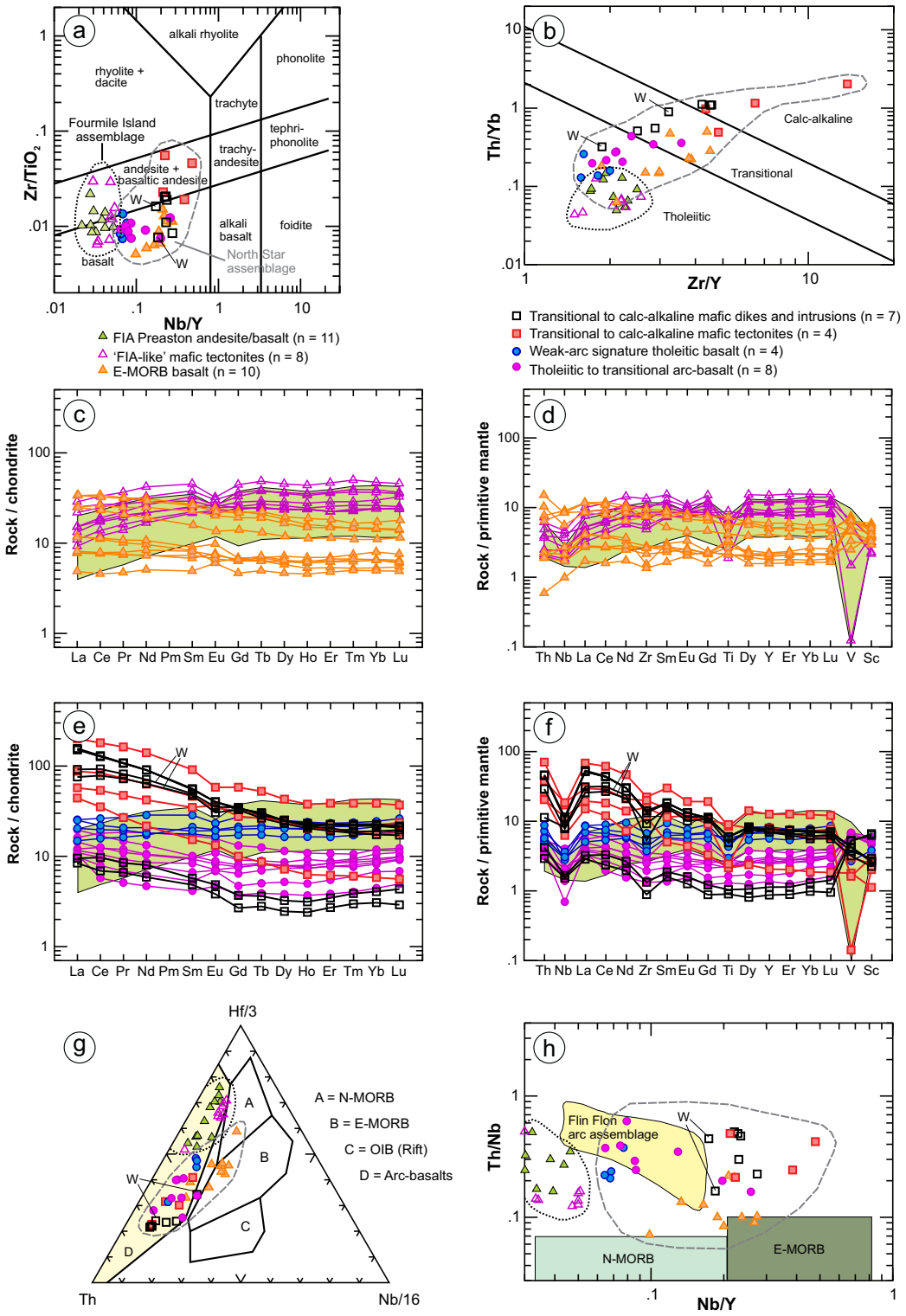

Figure GS2018-5-4: *Geochemical plots for mafic rocks of the North Star assemblage and West Reed–North Star shear zone areas:* ***a)*** *Zr/TiO_2 versus Nb/Y (modified from Winchester and Floyd, 1977);* ***b)*** *Th/ Yb versus Zr/Y (Ross and Bédard, 2009);* ***c)*** *and* ***e)*** *chondrite-normalized rare-earth element plots (normalizing values from McDonough and Sun, 1995);* ***d)*** *and* ***f)*** *primitive mantle–normalized incompatible trace-element plots (normalizing values from Sun and McDonough, 1989;* ***g)*** *Th-(Hf/3)-(Nb/16) ternary diagram after Wood (1980);* ***h)*** *Nb/Y versus Th/Nb discrimination diagram showing fields of primitive N-MORB and E-MORB (Saunders et al, 1988; Sun and McDonough, 1989), and Flin Flon assemblage arc rocks (from Stern et al., 1995a). Shaded areas in panels c–f indicate Preaston andesite compositions compiled from Zwanzig and Bailes (2010), and Gagné and Anderson (2014a). Abbreviations: E-MORB, enriched mid-ocean–ridge basalt; N-MORB, normal mid-ocean–ridge basalt; OIB, ocean-island basalt; W, Wine Ni-Cu-Co-PGE occurrence.*

the Flin Flon arc rocks on the Th/Nb versus Nb/Y diagram (Figure GS2018-5-4h).

Tholeiitic to transitional arc basalt

Eight samples, collected mostly from the northern NSA segment, are referred to as 'tholeiitic to transitional arc basalt' (Figure GS2018-5-2a). These plot as basaltic in the Zr/TiO_2 versus Nb/Y diagram (Figure GS2018-5-4a) and have a tholeiitic to transitional magmatic affinity (Figure GS2018-5-4b). The 'tholeiitic to transitional arc basalt' displays a slightly negative slope on a chondrite-normalized trace-element diagram (Figure GS2018-5-4e), with LREE enrichment and a flat to weak positive Eu anomaly. On a primitive mantle–normalized incompatible trace-element diagram (Figure GS2018-5-4f), the basalt samples show moderate negative Nb anomalies and positive V and Sc anomalies. On a ternary Th-(Hf/3)-(Nb/16) diagram (Figure GS2018-5-4g), the samples plot in the arc-basalt field. The 'tholeiitic to transitional arc basalt' samples plot mostly within the field of the Flin Flon arc rocks on the Th/Nb versus Nb/Y diagram (Figure GS2018-5-4h).

Transitional to calc-alkaline mafic rocks

Two subsets of samples, 'transitional to calc-alkaline mafic dikes and intrusions' and 'transitional to calc-alkaline mafic tectonites', have similar basaltic to andesitic composition based on the Zr/TiO_2 versus Nb/Y diagram (Figure GS2018-5-4a) and a transitional to calc-alkaline magmatic affinity (Figure GS2018-5-4b). The 'mafic dikes and intrusions' subset includes drillcore samples from the gabbro intrusion hosting the Wine Ni-Cu-Co-PGE occurrence (Figure GS2018-5-2c). These samples show strong LREE enrichment on a chondrite-normalized trace-element diagram (Figure GS2018-5-4e), with variation in overall enrichment interpreted as the result of magmatic differentiation from mafic to intermediate (49.4–65.0 SiO_2 wt. %). On a primitive mantle–normalized incompatible trace-element diagram (Figure GS2018-5-4f), the samples show strong negative slopes with strong negative Nb anomalies, moderate Zr depletions, flat to weakly depleted Ti, and variable V and Sc anomalies. On a ternary Th-(Hf/3)-(Nb/16) diagram (Figure GS2018-5-4g), the samples plot in the arc-basalt field. On the Th/Nb versus Nb/Y diagram (Figure GS2018-5-4h), these two subsets show higher ratios of Nb/Y than the FIA, NSA and Flin Flon arc rocks.

Felsic rocks

The geochemical characteristics of felsic supracrustal rocks from the NSA and the WRNS display three distinct geochemical signatures. For reference, a set of analyses including the Dickstone rhyolite (felsic flows from the FIA that lie closest to the WRNS) has been compiled from Zwanzig and Bailes (2010) and includes unpublished samples collected by Gagné in 2013. Scatterplots show individual Dickstone rhyolite samples, and the shaded areas reflect the unit's compositional range in the spider diagrams (Figure GS2018-5-5). Zwanzig and Bailes (2010) and Gagné and Anderson (2014a) discuss the geochemistry of the Dickstone rhyolite in detail.

'FIA-like' felsic tectonites

Samples of variably strained felsic tectonites from the eastern margin of the WRNS, 'FIA-like' felsic tectonites in Figure GS2018-5-2c and -5, plot in the rhyolite/dacite field on a Zr/TiO_2 versus Nb/Y diagram (Figure GS2018-5-5a) and have a tholeiitic magmatic affinity (Figure GS2018-5-5b). The rhyolite samples display slightly enriched HREE profiles, with weak negative Eu anomalies on a chondrite-normalized trace-element diagram (Figure GS2018-5-5c). On a primitive mantle–normalized incompatible trace-element diagram (Figure GS2018-5-5d), the samples display positive Th and negative Nb anomalies, and strongly depleted Ti. On a Nb versus Y discrimination diagram (Figure GS2018-5-5g), the felsic rocks all distinctly plot in the ocean-ridge field. The above-described geochemical characteristics are similar to the Dickstone rhyolite, indicating that the felsic tectonites along the eastern margin of the WRNS represent highly-strained FIA rocks entrained in the shear zone. On the La/Yb_{CN} versus Yb_{CN} diagram (Figure GS2018-5-5h), the 'FIA-like' felsic tectonites plot below the FIII rhyolite compositional range and show higher Yb_{CN} values than the FIV rhyolites from Hart et al (2004).

Weak-arc signature tholeiitic rhyolite

Four felsic samples from the southern segment of the NSA and the Rail deposit, referred to as 'weak-arc signature tholeiitic rhyolite', have a lower content of high-field-strength elements (HFSE), including Zr values of 30 to 49 ppm, and all plot in the andesite field on the Zr/TiO_2 versus Nb/Y diagram (Figure GS2018-5-2, -5a). Syme and Bailes (1993) and Bailes (1997) reported other examples of rhyolite that have similarly low HFSE content for the FFB. The samples all have a LOI (loss on ignition) of less than 1.2 wt. % and range from 70.9 to 78.9 wt. % SiO_2. The low-Zr rhyolite samples have a tholeiitic to transitional magmatic affinity (Figure GS2018-5-5b) and flat to slightly HREE-enriched chondrite-normalized profiles with flat to negative Eu anomalies (Figure GS2018-5-5c). Primitive mantle–normalized incompatible trace-element profiles have variable anomalies in Nb, Zr, Eu and

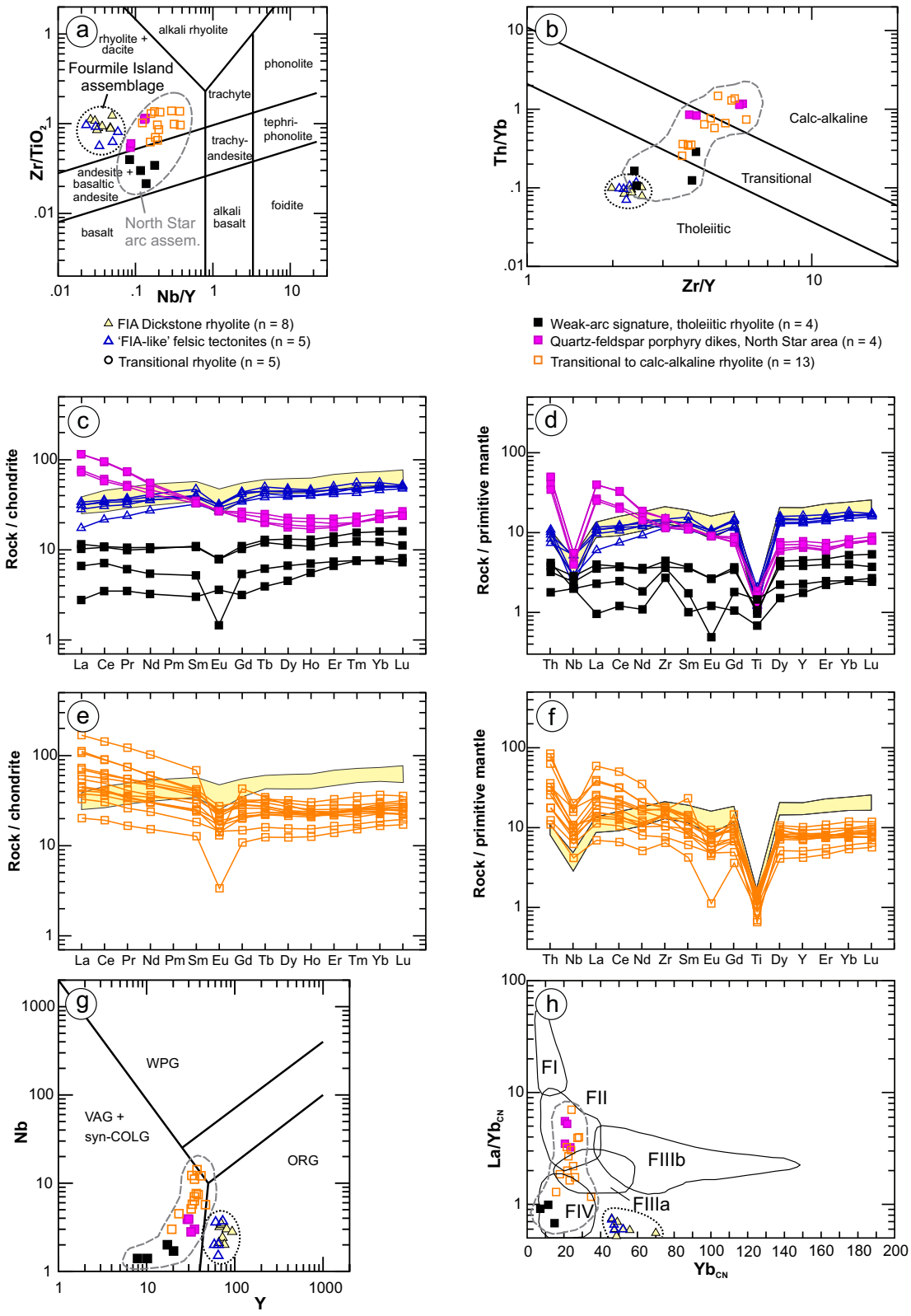

Figure GS2018-5-5: *Geochemical plots for felsic rocks of the North Star assemblage and West Reed–North Star shear zone areas:* ***a)*** *Zr/TiO_2 versus Nb/Y (modified from Winchester and Floyd, 1977);* ***b)*** *Th/ Yb versus Zr/Y (Ross and Bédard, 2009);* ***c)*** *and* ***e)*** *chondrite-normalized rare-earth-element plots (normalizing values from McDonough and Sun, 1995);* ***d)*** *and* ***f)*** *primitive mantle–normalized incompatible trace-element plots (normalizing values from Sun and McDonough, 1989;* ***g)*** *Nb versus Y (Pearce et al.,1984) and* ***h)*** *La/Yb_{CN} versus Yb_{CN} (Hart et al., 2004) discrimination diagrams. Shaded areas in panels c–f indicate Dickstone rhyolite compositional ranges compiled from Zwanzig and Bailes (2010), and Gagné and Anderson (2014a). Abbreviations: ORG, ocean-ridge granite; SynCOLG, syncollisional granite; VAG, volcanic-arc granite; WPG, within-plate granite.*

Ti (Figure GS2018-5-5d). The spread of data may be the result of synvolcanic alteration or metasomatic alteration during the development of the WRNS. The Nb versus Y diagram (Figure GS2018-5-5g) shows that the felsic rocks plot in the syncollisional volcanic-arc field. On the La/Yb_{CN} versus Yb_{CN} diagram (Figure GS2018-5-5h), the low-Zr rhyolite samples plot within the field of FIV rhyolite from Hart et al (2004).

Transitional to calc-alkaline rhyolite and quartz-feldspar porphyry dikes

Two sets of felsic samples share several geochemical characteristics, namely the 'transitional to calc-alkaline rhyolite' and 'quartz-feldspar porphyry dikes' (Figure GS2018-5-5). All samples plot as rhyolite/dacite (Figure GS2018-5-5a) and have a transitional to calc-alkaline magmatic affinity (Figure GS2018-5-5b). On a chondrite-normalized trace elements plot (Figure GS2018-5-5c, e), all samples display a similar negative slope. Many of the 'transitional to calc-alkaline rhyolite' samples show a moderate to strong negative Eu anomaly, unlike the porphyry dikes (Figure GS2018-5-5c, e). Primitive mantle–normalized incompatible trace elements show positive Th and negative Nb anomalies, and strong Ti depletion (Figure GS2018-5-5d, f). The samples plot in the syncollisional volcanic-arc field (Figure GS2018-5-5g). The rhyolite and porphyry dikes plot mostly in the FII and FIIIa field of Hart et al. (2004) on the La/Yb_{CN} versus Yb_{CN} diagram (Figure GS2018-5-5h).

Sm/Nd isotopes

Four rhyolite and three basalt samples from the NSA and WRNS were analyzed for Sm/Nd isotopes. The results span a narrow range of εNd values from +2.76 to 3.99 (Table GS2018-5-1), indicating that the rocks were derived from a juvenile-arc magma source. More specifically, they formed from depleted mantle in an oceanic environment or on recently evolved Paleoproterozoic crust with little or no influence of older (Archean) continental crust (Stern et al., 1995a, b; Whalen et al., 1999). These εNd values are distinctly lower than the published values of +4.61 and +6.72 for the Preaston andesite and the Dickstone rhyolite, respectively (Zwanzig and Bailes, 2010, Table 15).

U-Pb geochronology

Sample 110-16-755 (see Data Repository Item DRI-2018003), a sparsely quartz-phyric, massive, homogeneous and strongly foliated rhyolite from an island near the southern shore of North Star Lake (Figure GS2018-5-2a), was collected for U-Pb zircon age determination using isotope dilution–thermal ionization mass spectrometry at the Jack Satterly Geochronology Laboratory, University of Toronto.

Table GS2018-5-1: Samarium-neodymium isotope results for selected samples from the North Star assemblage and West Reed–North Star shear zone areas.

SAMPLE	UNIT	Geochemical grouping	LITHOLOGY	Nd ppm	Sm ppm	$^{147}Sm/^{144}Nd$	$^{143}Nd/^{144}Nd0$	UNCERT	TMA	εNdT
110-14-596-A01	North Star arc assemblage, northern segment	Transitional to calc-alkaline rhyolite	rhyolite	23.8	5.89	0.1495	0.51223	0.00001	1900	3.48
105-10-RL08-15-1019	North Star arc assemblage, Rail deposit area	Transitional rhyolite	Aphyric rhyolite	12.21	3.09	0.1528	0.5122	0.00001	1890	2.76
96-14-98-B1	North Star arc assemblage, southern segment	Low Zr rhyolite	rhyolite	5.12	1.67	0.1971	0.5128	0.00001	1890	3.98
105-10-RL08-15-235.5	North Star arc assemblage, Rail deposit area	Low Zr rhyolite	Qtz-phyric +/-chloritized rhyolite	4.54	1.51	0.2012	0.5129	0.00001	1890	3.99
105-10-RL08-15-1071.5	North Star arc assemblage, Rail deposit area	Tholeiitic to transitional arc-basalt	andesite, epidotized	4.62	1.26	0.1653	0.5124	0.00001	1890	3.07
105-10-RL08-15-558.5	North Star arc assemblage, Rail deposit area	E-MORB basalt	fine-grained andesite	14.07	3.89	0.1672	0.5125	0.00001	1890	3.52
96-14-92-A1	North Star arc assemblage, southern segment	E-MORB basalt	basalt	3.59	1.08	0.1827	0.5126	0.00001	1890	2.84

Several kilograms of rhyolite sample 110-16-755 yielded a modest amount of zircon, mostly elongated euhedral or subhedral, clear to cloudy, colourless crystals with length to breadth ratios of up to 4:1, but generally flat. The maximum dimension of the best quality grains is typically <200 μm, but rare, more clouded and altered grey grains reach up to ~300 μm (Figure GS2018-5-6a).

Four chemically abraded single zircon grain fractions were analyzed; U-Pb results are presented in Table GS2018-5-2 and displayed graphically in Figure GS2018-5-6b. Uranium concentrations in these fractions was relatively low, ranging from approximately 30–100 ppm, with Th/U ratios between 0.38 and 0.53. Most data overlap with or plot only slightly below concordia (0.5–1.6% discordant), yielding model $^{207}Pb/^{206}Pb$ ages between 1886–1896 Ma, although three of the fractions are colinear (Z1, Z2 and Z3) and give a weighted average $^{207}Pb/^{206}Pb$ age of 1895.9 ±1.6 Ma (2σ; mean square of weighted deviates [MSWD] = 0.25, probability of fit = 78%). A fourth fraction is displaced to the left of the main array of data and likely reflects minor secondary Pb loss. The age of 1895.9 ±1.6 Ma is interpreted to represent the primary age of eruption of the North Star rhyolite.

As reported in Stern et al. (1995b), juvenile-arc felsic volcanic rocks of the Flin Flon belt are difficult to date due to their low HFSE concentrations resulting in little zircon. As only a few rhyolite samples have been directly dated in the FFB, this newly obtained age of 1895.9 ±1.6 Ma for the North Star Lake rhyolite is significant. It confirms that the NSA represents a juvenile oceanic arc and that it formed around the time most VMS deposits of the FFB were produced. Recent geochronological results on four samples from the Flin Flon block by Rayner (2010) indicate that the bulk of the volcanism and associated VMS mineralization occurred ca. 1890 Ma. The significance of the 1903 +7/-5 Ma age from Stern et al. (1999, sample FF92-1) remains unclear. The timing of VMS mineralization in the Snow Lake arc assemblage is also ca. 1890 Ma. Two synvolcanic intrusions, the Richard Lake pluton and the Sneath Lake pluton, interpreted as the heat source for the VMS-hosting Anderson and Chisel sequences, have been respectively dated at 1886 +17/-9 Ma and at 1889 +8/-6 (Bailes et al., 1991; Bailes and Galley, 1999). The only U-Pb date from the host volcanic succession in the Snow Lake arc assemblage comes from a felsic volcaniclastic bed that provided a maximum age of 1892 +/-3 Ma (David et al., 1996) for the Anderson sequence.

Discussion

The geochemical data show that felsic and mafic volcanic rocks of similar geochemical signature occur both within the northern NSA segment and the southern NSA segment, indicating that both segments belong to the NSA (Figure GS2018-5-2a, c). The NSA has a trace-element geochemical signature that is distinct from the FIA but shares some features with the Flin Flon bimodal juvenile-arc sequences (Figures GS2018-5-4, -5). Further

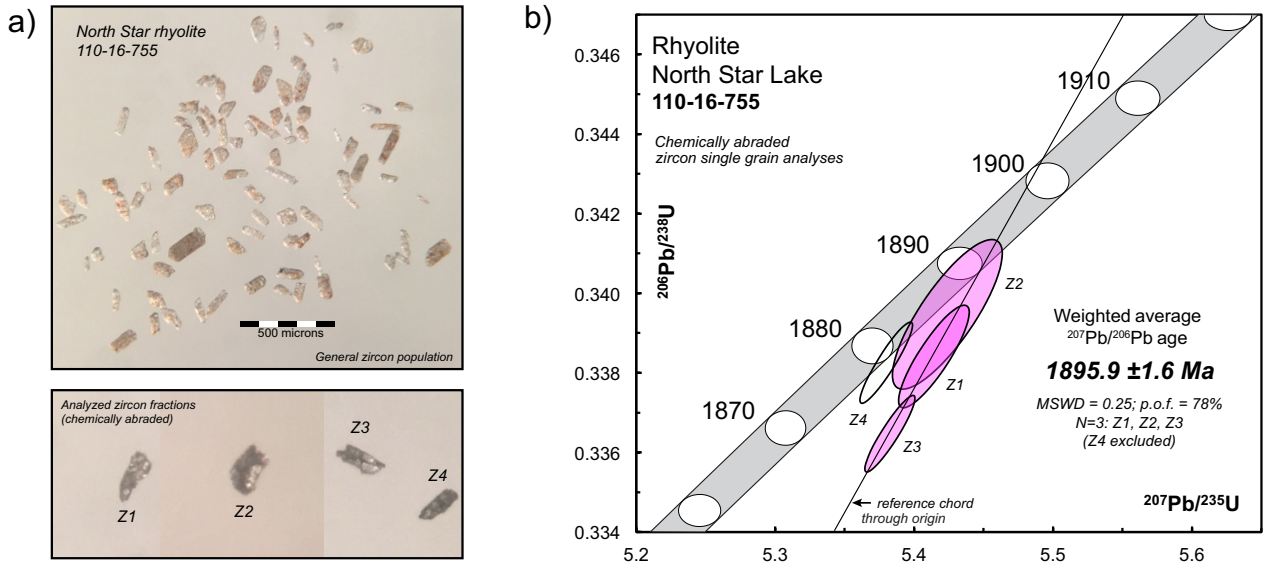

Figure GS2018-5-6: *Zircon grain images and concordia plots for rhyolite sample 110-16-755 (UTM Zone 14, 399031E, 6077910N [NAD83]) from the North Star Lake area:* ***a)*** *transmitted light photomicrographs of representative zircon grains; the lower image shows chemically abraded (annealed and etched) grain fragments selected for U-Pb analysis;* ***b)*** *concordia diagram showing U-Pb analytical results for zircon grains from rhyolite sample 110-16-755. Error ellipses are shown at the 2σ level of uncertainty. Calculated age shown is a weighted average of results for fractions Z1, Z2 and Z3 only; fraction Z4 (unshaded ellipse) is excluded. Concordia 'band' reflects uncertainties in U decay constants. Abbreviations: MSWD, mean square of weighted deviates; p.o.f., probability of fit.*

Table GS2018-5-2: Uranium-lead analytical results for zircon from a rhyolite sample from the North Star Lake area.

Sample Fraction	Description	Weight (mg)	U (ppm)	Th/U	Pb* (pg)	Pb_c (pg)	$^{206}Pb/^{204}Pb$	$^{206}Pb/^{238}U$	± 2σ	$^{207}Pb/^{235}U$	± 2σ	$^{207}Pb/^{206}Pb$	± 2σ
110-16-755 Rhyolite, North Star Lake													
Z1	1 cldy, cls, el frag	0.8	45	0.52	16.66	0.33	2957	0.33835	0.001060	5.41389	0.02055	0.11605	0.000225
Z2	1 cldy, cls brkn frag	1.1	27	0.38	9.51	0.40	1453	0.33941	0.001536	5.42345	0.03230	0.11589	0.000406
Z3	1 cldy and clr, cls,brkn el, crk	0.9	95	0.53	34.81	0.20	10377	0.33640	0.000785	5.38214	0.01467	0.11604	0.000124
Z4	1 dk grey, cldy el frag	0.7	69	0.44	24.95	0.21	7118	0.33819	0.000838	5.37972	0.01563	0.11537	0.000132

Sample Fraction	$^{206}Pb/^{238}U$ Age (Ma)	± 2σ	$^{207}Pb/^{235}U$ Age (Ma)	± 2σ	$^{207}Pb/^{206}Pb$ Age (Ma)	± 2σ	Disc. (%)
110-16-755 Rhyolite, North Star Lake							
Z1	1878.7	5.1	1887.1	3.3	1896.2	3.5	1.1
Z2	1883.8	7.4	1888.6	5.1	1893.8	6.3	0.6
Z3	1869.3	3.8	1882.0	2.3	1896.0	1.9	1.6
Z4	1878.0	4.0	1881.6	2.5	1885.7	2.1	0.5

Notes:
All analyzed fractions represent best quality zircon grains.
Abbreviations: brkn, broken; cldy, cloudy; clr, clear; cls, colourless; crk, cracked; dk, dark; el, elongated; frag, fragment.
Fraction weights (in micrograms) are estimated from digitally measured grain dimensions and the density of zircon (realistic errors are on the order of ± 20%)
Pb* is total amount (in picograms) of radiogenic Pb.
Pb_c is total measured common Pb (in picograms) assuming the isotopic composition of laboratory blank: $^{206/204}$ - 18.221; $^{207/204}$ - 15.612; $^{208/204}$ - 39.360 (errors of 2%).
Pb/U atomic ratios are corrected for spike, fractionation, blank, and, where necessary, initial common Pb; $^{206}Pb/^{204}Pb$ is corrected for spike and fractionation.
Th/U is model value calculated from radiogenic $^{208}Pb/^{206}Pb$ ratio and $^{207}Pb/^{206}Pb$ age assuming concordance.
Disc. (%) - per cent discordance for the given $^{207}Pb/^{206}Pb$ age.

geochemical sampling of the WRNS tectonites may allow to delineate more precisely the boundary between FIA rocks and NSA rocks.

Drillcore samples collected from the Rail deposit show the same geochemical character as the NSA rocks; the Rail deposit is therefore interpreted as belonging to the NSA. The rhyolite found within the host sequences of both the Rail and Lon VMS deposits (Figure GS2018-5-2d, e) are interpreted to be correlative to the North Star rhyolite; the deposits are interpreted to have formed around the time of crystallization of the North Star rhyolite at ca. 1896 Ma.

The presence of E-MORB, weak-arc tholeiites and bimodal transitional to calc-alkaline rocks within the NSA sequence suggests a complex magmatic history. The presence of E-MORB and the positive εNd values (+2.76–3.99; Table GS2018-5-1) indicates that the NSA was derived from a juvenile source, with magmatic contribution from an enriched mantle. Compared to the FIA, felsic samples from the NSA show depletions in HREE and lower Yb_{CN} and Y contents (Figure GS2018-5-5g, h), which is interpreted to suggest a deeper magmatic source for the NSA. However, other factors such as source composition and fractionation processes cannot be discounted given the available data.

Economic considerations

Base-metal potential

The recognition that the WRNS juxtaposes two packages of juvenile bimodal volcanic-arc sequences that host VMS and that these packages can be distinguished geochemically within the WRNS tectonites significantly expands the area prospective for base-metal mineralization. The shear zone itself should not be overlooked, given that the Rail deposit occurs in the western part of the WRNS and that this study demonstrates that the WRNS tectonites consist mostly of bimodal juvenile-arc volcanic rocks (host sequence characteristics that are broadly favourable for VMS mineralization; e.g., Syme and Bailes, 1993). In addition, the presence of prospective bimodal juvenile-arc rocks on the western margin of

the WRNS warrants further investigation along the full strike length of the structure.

Orogenic Au

The WRNS must represent a major crustal structure, as it separates two packages of arc rocks that have evolved in distinct tectonic environments. Such major crustal structures provide favourable pathways for deeply sourced, gold-bearing hydrothermal fluids and are prospective for orogenic gold mineralization. The WRNS is host to several significant Au showings in the North Star Lake area. Iron-enriched mafic rocks (such as the tholeiitic units found both in the FIA and NSA) near the WRNS may have served as a chemical trap for the sulfur-bearing fluids often associated with orogenic gold deposits (Dubé and Gosselin, 2007). The major structures associated with Au mineralization in the North Star Lake area extend southward to the Reed Lake area, which is considered to have similar potential for shear-hosted Au mineralization.

Magmatic Ni-Cu-Co-PGE mineralization

The Wine Ni-Cu-Co-PGE occurrence (Figure GS2018-5-2c) was discovered through drilling of a ground geophysical anomaly by Hudson Bay Exploration and Development Company Limited in the early 1980s. The mineralization is described as disseminated sulphides and stringers associated with a mafic magmatic breccia hosted by leucogabbro (Assessment Files 94660, 94667, 94669, Manitoba Growth, Enterprise and Trade, Winnipeg). Two samples collected from the gabbroic intrusion hosting the Wine occurrence display a transitional to calc-alkaline signature (Figure GS2018-5-4). Several other samples within the NSA and along the western margin of the WRNS share the same geochemical character (see 'transitional to calc-alkaline dikes and mafic intrusion' and 'transitional to calc-alkaline mafic tectonites' in Figure GS2018-5-4), which suggests that the western flank of the WRNS should be further tested for Ni-Cu-Co-PGE mineralization. Of particular interest is a folded gabbroic intrusion south of the Lon deposit, where one sample displayed a geochemical signature almost identical to that of the gabbro hosting the Wine occurrence. Three diabase/gabbro dike samples from the southern segment of the NSA also have the Wine gabbro geochemical signature.

Acknowledgments

The authors thank M. Rich, D. Campbell, S. Bawden, S. Kuschner, R. Green and R. Ponto for enthusiastic field assistance, as well as N. Brandson and E. Anderson for thorough logistical support. Thanks also go to K. Reid, C. Böhm and M. Rinne for reviewing this manuscript. They also thank G. Benger, V. Varga and C. Epp for their preparation of samples and thin sections.

References

Bailes, A.H. 1980: Geology of the File Lake area; Manitoba Energy and Mines, Mineral Resources Division, Geological Report GR78-1, 134 p.

Bailes, A.H. 1997: Geochemistry of Paleoproterozoic metavolcanic rocks in the Photo Lake area, Snow Lake, Flin Flon Belt; *in* Report of Activities 1997, Manitoba Energy and Mines, Geological Services, p. 61–72.

Bailes, A.H. and Galley, A.G. 1999: Evolution of the Paleoproterozoic Snow Lake arc assemblage and geodynamic setting for associated volcanic-hosted massive sulphide 88 deposits, Flin Flon Belt, Manitoba, Canada; Canadian Journal of Earth Science, v. 36, p. 1789–1805.

Bailes, A.H. and Galley, A.G. 2007: Geology of the Chisel–Anderson lakes area, Snow Lake, Manitoba (NTS areas 63K16SW and west half of 63J13SE); Manitoba Science, Technology, Energy and Mines, Manitoba Geological Survey, Geoscientific Map MAP2007-1, scale 1:20 000.

Bailes, A.H. and Syme, E.C. 1989: Geology of the Flin Flon–White Lake area; Manitoba Energy and Mines, Geological Services, Geological Report GR87-1, 313 p.

Bailes, A.H., Hunt, P.A. and Gordon, T.M. 1991: U-Pb zircon dating of possible synvolcanic plutons in the Flin Flon belt at Snow Lake, Manitoba; Radiogenic Age and Isotopic Studies: Report 4, Geological Survey of Canada, Paper 91-2, p. 35–43.

Bamburak, J.D., Hamilton, M. and Heaman, L.M. 2016: Geochronology of Late Cretaceous bentonite beds in southwestern Manitoba: 2016 update; *in* Report of Activities 2016, Manitoba Growth, Enterprise and Trade, Manitoba Geological Survey, p. 168–175.

David, J., Bailes, A.H. and Machado, N. 1996: Evolution of the Snow Lake portion of the Paleoproterozoic Flin Flon and Kisseynew belts, Trans-Hudson Orogen, Manitoba, Canada; Precambrian Research, v. 80, p. 107–124.

DePaolo, D.J. 1981: Neodymium isotopes in the Colorado Front Range and crust-mantle evolution in the Proterozoic; Nature, v. 291, p. 193–196.

Dubé, B. and Gosselin, P. 2007: Greenstone-hosted quartz-carbonate vein deposits; *in* Mineral Deposits of Canada: a Synthesis of Major Deposit-Types, District Metallogeny, the Evolution of Geological Provinces, and Exploration Methods, W.D. Goodfellow (ed.), Geological Association of Canada, Mineral Deposits Division, Special Publication no. 5, p. 49–73.

Gagné, S. 2013: Geological investigations in the Rail Lake–Sewell Lake area, Flin Flon–Snow Lake greenstone belt, west-central Manitoba (parts of NTS 63K10, 15); *in* Report of Activities 2013, Manitoba Mineral Resources, Manitoba Geological Survey, p. 95–105.

Gagné, S. 2017: Sub-Phanerozoic geology of the Reed Lake area, Flin Flon belt, west-central Manitoba (parts of NTS 63K7, 8, 9, 10); Manitoba Growth, Enterprise and Trade, Manitoba Geological Survey, Preliminary Map PMAP2017-2, scale 1:30 000.

Gagné, S. and Anderson, S.D. 2014a: Update on the geology and geochemistry of the west Reed Lake area, Flin Flon greenstone belt, west-central Manitoba (part of NTS 63K10); *in* Report of Activities 2014, Manitoba Mineral Resources, Manitoba Geological Survey, p. 77–93.

Gagné, S. and Anderson, S.D. 2014b: Bedrock geology west of Reed Lake, Flin Flon greenstone belt, Manitoba (part of NTS 63K10); Manitoba Mineral Resources, Manitoba Geological Survey, Preliminary Map PMAP2014-5, scale 1:20 000.

Gagné, S., Anderson, S.D., Hamilton, M., Simard, R.-L. and Lazzarotto, M. 2018: Geochemistry data of selected samples of volcanic and volcaniclastic rocks of the North Star assemblage, the West Reed–North Star shear zone and the Fourmile Island assemblage, Flin Flon belt, west-central Manitoba (parts of NTS 63K10, 15); Manitoba Growth, Enterprise and Trade, Manitoba Geological Survey, Data Repository Item DRI2018003, Excel® file.

Gagné, S., Syme, E.C., Anderson, S.D. and Bailes, A.H. 2017: Geology of the exposed basement in the Reed Lake area, Flin Flon belt, west-central Manitoba (parts of NTS 63K9, 10, 15, 16); Manitoba Growth, Enterprise and Trade, Manitoba Geological Survey, Preliminary Map PMAP2017-1, scale 1:30 000.

Goldstein, S.L., O'Nions, R.K. and Hamilton, P.J. 1984: A Sm-Nd study of atmospheric dusts and particulates from major river systems; Earth and Planetary Science Letters, v. 70, p. 221–236.

Hart, T.R., Gibson, H.L. and Lesher, C.M. 2004: Trace element geochemistry and petrogenesis of felsic volcanic rocks associated with volcanogenic massive Cu-Zn-Pb sulfide deposits; Economic Geology, v. 99, p. 1003–1013.

Jacobsen, S.B. 1980: Sm-Nd isotopic evolution of chondrites; Earth and Planetary Science Letters, v. 50, p. 139–155.

Lazzarotto, M., Gagné, S. and Pattison, D.R.M. 2016: Tectonometamorphic investigations in the Athapapuskow Lake area, west-central Manitoba (part of NTS 63K12); *in* Report of Activities 2016, Manitoba Growth, Enterprise and Trade, Manitoba Geological Survey, p. 87–98.

Lazzarotto, M., Pattison, D.R.M. and Gagné, S. 2017: Prehnite-pumpellyite– to amphibolite-facies metamorphism in the Athapapuskow Lake area, west-central Manitoba (parts of NTS 63K12, 13); *in* Report of Activities 2017, Manitoba Growth, Enterprise and Trade, Manitoba Geological Survey, p. 104–116.

Lucas, S.B., Stern, R.A., Syme, E.C., Reilly, B.A. and Thomas, D.J. 1996: Intraoceanic tectonics and the development of continental crust; 1.92–1.84 Ga evolution of the Flin Flon Belt, Canada; Geological Society of America Bulletin, v. 108, no. 5, p. 602–629.

McDonough, W.F. and Sun, S.-S. 1995: The composition of the Earth; *in* Chemical Evolution of the Mantle, W.F. McDonough, N.T. Arndt and S. Shirey (ed.), Chemical Geology, v. 120, p. 223–253.

NATMAP Shield Margin Project Working Group 1998: Geology, NATMAP Shield Margin Project area, Flin Flon belt, Manitoba/Saskatchewan; Geological Survey of Canada, Map 1968A, scale 1:100 000.

Norquay, L.I. 1997: Structural and metamorphic evolution of the North Star Lake area, Manitoba; M.Sc. thesis, University of Manitoba, 244 p.Norquay. L.I., Prouse, D.E., Bieri, M. and Gale, G.H. 1991: Geology of a part of the North Star Lake area (NTS 63K/15); *in* Report of Activities 1991, Manitoba Energy and Mines, Minerals Division, p. 31–40.

Norquay, L.I., Prouse, D.E. and Gale., G.H. 1994: The North Star Lake project (NTS 63K/15); *in* Report of Activities 1994, Manitoba Energy and Mines, Minerals Division, p. 83–84.

Pearce, J.A., Harris, N.B.W. and Tindle, A.G. 1984: Trace element discrimination diagrams for the tectonic interpretation of granitic rocks; Journal of Petrology, v. 25, p. 956–983.

Rayner, N.M. 2010: New U-Pb zircon ages from the Flin Flon Targeted Geoscience Initiative Project 2006-2009: Flin Flon and Hook Lake blocks, Manitoba and Saskatchewan, Geological Survey of Canada, Current Research (Online) no. 2010-4, 12 p., doi:10.4095/261489

Ross, P.-S. and Bédard, J.H. 2009: Magmatic affinity of modern and ancient sub-alkaline volcanic rocks determined from trace-element discriminant diagrams; Canadian Journal of Earth Sciences, v. 46, p. 823–839.

Saunders, A.D., Norry, M.J. and Tarney, J. 1988: Origin of MORB and chemically-depleted mantle reservoirs: trace element constraints; Journal of Petrology, Special Volume 1, p. 415–445.

Schmidberger, S.S., Heaman, L.M., Simonetti, A., Creaser, R.A. and Whiteford, S. 2007: Lu-Hf, in-situ Sr and Pb isotope and trace element systematics for mantle eclogites from the Diavik diamond mine: evidence for Paleoproterozoic subduction beneath the Slave craton, Canada; Earth and Planetary Science Letters, v. 254, p. 55–68.

Simard, R.-L., McGregor, C.R., Rayner, N. and Creaser, R.A. 2010: New geological mapping, geochemical, Sm-Nd isotopic and U-Pb age data for the eastern sub-Phanerozoic Flin Flon Belt, west-central Manitoba (parts of NTS 63J3–6, 11, 12, 14, 63K1–2, 7–10); *in* Report of Activities 2010, Manitoba Innovation, Energy and Mines, Manitoba Geological Survey, p. 69–87.

Stern, R.A., Machado, N., Syme, E.C., Lucas, S.B. and David, J. 1999: Chronology of crustal growth and recycling in the Paleoproterozoic Amisk collage (Flin Flon Belt), Trans-Hudson Orogen, Canada; Canadian Journal of Earth Sciences, v. 36, p. 1807–1827.

Stern, R.A., Syme, E.C., Bailes, A.H. and Lucas, S.B. 1995a: Paleoproterozoic (1.90–1.86 Ga) arc volcanism in the Flin Flon Belt, Trans-Hudson Orogen, Canada; Contributions to Mineralogy and Petrology, v. 119, no. 2–3, p. 117–141.

Stern, R.A., Syme, E.C. and Lucas, S.B. 1995b: Geochemistry of 1.9 Ga MORB- and OIB-like basalts from the Amisk collage, Flin Flon Belt, Canada: evidence for an intra-oceanic origin; Geochimica et Cosmochimica Acta, v. 59, no. 15, p. 3131–3154.

Sun, S.-S. and McDonough, W.F. 1989: Chemical and isotopic systematics of oceanic basalts: implication for mantle composition and processes; The Geological Society of London, Special Publications, v. 42, p. 313–345.

Syme, E.C. and Bailes, A.H. 1993: Stratigraphic and tectonic setting of early Proterozoic volcanogenic massive sulfide deposits, Flin Flon, Manitoba; Economic Geology, v. 88, no. 3, p. 566–589.

Syme, E.C. and Bailes, A.H. 1996: Geochemistry of arc and ocean-floor metavolcanic rocks in the Reed Lake area, Flin Flon belt; *in* Report of Activities 1996, Manitoba Energy and Mines, Geological Services, p. 52–65.

Syme, E.C., Bailes, A.H. and Lucas, S.B. 1995a: Reed Lake, parts of NTS 63K/9, 63K/10; Manitoba Energy and Mines, Geological Services, Preliminary Map 1995F-1, scale 1:50 000.

Syme, E.C., Bailes, A.H. and Lucas, S.B. 1995b: Geology of the Reed Lake area (parts of NTS 63K/9 and 10); *in* Report of Activities 1995, Manitoba Energy and Mines, Geological Services, p. 42–60.

Syme, E.C., Lucas, S.B., Bailes, A.H. and Stern, R.A. 1999: Contrasting arc and MORB-like assemblages in the Paleoproterozoic Flin Flon Belt, Manitoba, and the role of intra-arc extension in localizing volcanic-hosted massive sulphide deposits; Canadian Journal of Earth Sciences, v. 36, p. 1767–1788.

Unterschutz, J.L.E., Creaser, R.A., Erdmer, P., Thompson, R.I. and Daughtry, K.L. 2002: North American margin origin of Quesnel terrane strata in the southern Canadian Cordillera: inferences from geochemical and Nd isotopic characteristics of Triassic metasedimentary rocks; Geological Society of America Bulletin, v. 114, p. 462–475.

Whalen, J.B., Syme, E.C. and Stern, R.A. 1999: Geochemical and Nd isotopic evolution of Paleoproterozoic arc-type granitoid magmatism in the Flin Flon Belt, Trans-Hudson Orogen, Canada; Canadian Journal of Earth Sciences, v. 36, p. 227–250.

Winchester, J.A. and Floyd, P.A. 1977: Geochemical discrimination of different magma series and their differentiation products using immobile elements; Chemical Geology, v. 20, no. 4, p. 325–343.

Wood, D.A. 1980: The application of a Th-Hf-Ta diagram to problems of tectonomagmatic classification and to establishing the nature of crustal contamination of basaltic lavas of the British Tertiary volcanic province; Earth and Planetary Science Letters, v. 50, p. 11–30.

Zwanzig, H.V. and Bailes, A.H. 2010: Geology and geochemical evolution of the northern Flin Flon and southern Kisseynew domains, Kississing–File lakes area, Manitoba (parts of NTS 63K, N); Manitoba Innovation, Energy and Mines, Manitoba Geological Survey, Geoscientific Report GR2010-1, 135 p.

Zwanzig, H.V., Bailes, A.H. and Böhm, C.O. 2001: Josland Lake Sills: U-Pb age and tectonostratigraphic implications (parts of NTS 63K and 63N); *in* Report of Activities 2001, Manitoba Industry, Trade and Mines, Manitoba Geological Survey, p. 28–32.

GS2018-6

Metamorphism of volcanic rocks from the North Star Lake and the Fourmile Island assemblages, west-central Manitoba (parts of NTS 63K10, 15)

by M. Lazzarotto[1], D.R.M. Pattison[1] and S. Gagné

In Brief:

- Detailed petrography on metabasites from the North Star and Fourmile Island assemblages has identified a series of six mineral isograds
- Regional metamorphic grade increases from greenschist facies in the south to garnet-amphibolite facies in the north
- The West Reed-North Star shear zone is a pre-metamorphic structure that does not disrupt the continuous succession of metamorphic zones and isograds

Citation:
Lazzarotto, M., Pattison, D.R.M. and Gagné, S. 2018: Metamorphism of volcanic rocks from the North Star Lake and the Fourmile Island assemblages, west-central Manitoba (parts of NTS 63K10, 15); *in* Report of Activities 2018, Manitoba Growth, Enterprise and Trade, Manitoba Geological Survey, p. 64–78.

Summary

The Reed Lake–North Star Lake area is part of a tectonic collage in the Flin Flon greenstone belt, west-central Manitoba. It consists of accreted terranes of metamorphosed ocean-floor and island-arc assemblages that are unconformably overlain by sedimentary rocks and intruded by successor-arc plutons. The area is characterized by the north-trending West Reed–North Star shear zone (WRNS), which juxtaposes two packages of bimodal volcanic and volcaniclastic rocks. The well-documented volcanic-arc/arc-rift rocks of the Fourmile Island assemblage (FIA) lie east of the WRNS and can be followed continuously along the entire trace of the WRNS. The North Star assemblage (NSA), another package of bimodal volcanic and volcaniclastic rocks, lies on the west side of the WRNS.

Rocks in the area have experienced both regional and contact metamorphism. The regional metamorphic grade generally increases northward across the Flin Flon greenstone belt from lower-greenschist–facies rocks in the south, to amphibolite-facies rocks in the north. Rocks in contact metamorphic aureoles around plutons record amphibolite-facies conditions.

A sequence of regional metamorphic zones was established through field observations and thermodynamic modelling of mafic volcanic rocks. Six isograds were identified separating seven metamorphic zones. From south to north, these isograds are hornblende-in, albite-out, actinolite-out, garnet-in, epidote-out and chlorite-out. The metamorphic mineral assemblage and isograd map demonstrates that the metamorphic grade increases toward the north, from lower-greenschist facies at Reed Lake to garnet-amphibolite facies north of North Star Lake. The WRNS does not seem to disrupt the continuous metamorphic succession of zones and isograds. It is suggested that the WRNS may have been an important pathway for the transport and concentration of precious metals within metamorphic fluids.

Introduction

In 2015, a project involving the tectonic and metamorphic study of parts of the Flin Flon greenstone belt (FFB) was initiated by the University of Calgary in collaboration with the Manitoba Geological Survey. Greenstone belts are zones of variably metamorphosed bimodal volcanic sequences, associated sedimentary rocks and granitoid to gabbroic intrusive bodies that occur within Precambrian cratons. The rocks in such belts commonly record events of regional metamorphism, contact metamorphism and hydrothermal alteration. In addition to providing insight into the tectonic evolution of the area, the study of these rocks allow for the better understanding of metamorphic processes, such as the behaviour of rocks and minerals at the transition from greenschist facies to amphibolite facies, which results in the release of hydrothermal fluids. Identifying these transitions, and understanding the associated fluid release, helps researchers better understand the transport and concentration mechanisms of precious and base metals. An improved understanding of the metamorphic and alteration events that affected these areas may help to constrain exploration models for volcanogenic massive-sulphide (VMS) and orogenic gold deposits in the region.

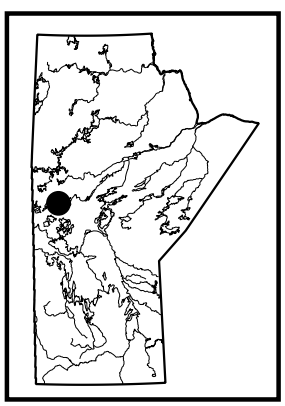

[1] Department of Geosciences, University of Calgary, 2500 University Drive NW, Calgary, AB T2N 1N4

This metamorphic investigation is part of a larger study of the metamorphic and tectonic evolution in the FFB conducted by M. Lazzarotto as part of his Ph.D. research at the University of Calgary (Lazzarotto et al., 2016, 2017). Future research will focus on the relationships between metamorphosed mafic volcanic rocks and metamorphosed sedimentary rocks along a north-south transect in the File and North Star lakes area and building an integrated metamorphic map of the whole Flin Flon greenstone belt.

Regional geological framework

The Reed Lake–North Star Lake area is situated in the eastern-central FFB, Manitoba. The FFB is part of the Reindeer zone of the Trans-Hudson orogen, which formed through the closure of the Manikewan Ocean and convergence of the Hearne, Superior and Sask cratons (Hoffmann, 1988).

The exposed FFB contains several distinct juvenile-arc assemblages juxtaposed on ocean-floor rocks, with interlayered sedimentary and intrusive units separated by major faults (Figure GS2018-6-1; Stern et al., 1995a, b; Syme et al., 1999; Whalen et al., 2016). The arc assemblages are internally complex, comprising numerous fault-bounded and folded volcanic suites (e.g., Bailes and Syme, 1989) that are typically bimodal and include a wide range of volcanic, volcaniclastic and intrusive rocks (Bailes and Syme, 1989; Syme and Bailes, 1993; Stern et al., 1995a; Lucas et al., 1996; Bailes and Galley, 2007). The juvenile ocean-floor assemblages are composed mainly of rock similar to mid-ocean–ridge basalt (MORB) and related kilometre-scale, layered, mafic–ultramafic plutonic complexes (Syme and Bailes, 1993; Stern et al., 1995b).

Uranium-lead zircon ages for the ocean-floor assemblages in the exposed portion of the FFB indicate that the ocean-floor magmatism was coeval with tholeiitic-arc volcanism at ca. 1.90 Ga (Stern et al., 1995b). Voluminous successor-arc magmatism and deposition of sedimentary rocks occurred between ca. 1.88 and 1.83 Ga (Lucas et al., 1996). Large plutons were emplaced throughout the belt during three distinct magmatic stages. They are lithologically and geochemically variable with alkaline, calcalkaline and shoshonitic affinities. Volcanic, volcaniclastic and sedimentary rocks with ages of ca. 1.88–1.83 Ga are documented across the central and eastern parts of the exposed FFB and are termed successor-basin deposits (Ansdell et al., 1995; Lucas et al., 1996). They include the Schist-Wekusko assemblage, the Missi group and the Burntwood group. The fluvial-alluvial Missi group sedimentary deposits are characterized by thick packages of conglomerate, pebbly sandstone and massive sandstone. The marine turbidites of the Burntwood group include greywacke, siltstone, mudstone and rare conglomerate. In the low-grade metamorphic FFB, these sedimentary rocks are generally in fault contact with other units.

The Reed Lake area is characterized by a major, regionally extensive tectonite belt exposed on western Reed Lake; the WRNS, which juxtaposes rocks of the FIA on the east; and the NSA on the west (Figure GS2018-6-2). Rocks from the NSA, WRNS and FIA record a broad range of peak metamorphic conditions and will be discussed in further detail later in this report. For the sake of brevity, the prefix 'meta-' is not used in this report and the rocks are described in terms of their protoliths.

Metamorphism

With the exception of the Phanerozoic rocks south of Reed Lake, all rocks in the Reed Lake–North Star Lake area are metamorphosed. Two distinct types of metamorphism are observed: regional metamorphism and contact metamorphism. The regional metamorphic grade increases to the north from lower-greenschist facies on Reed Lake, to garnet-amphibolite facies north of North Star Lake. This work focuses on the metamorphism of mafic volcanic rocks with only limited work performed on Burntwood group sedimentary rocks and successor-arc intrusive rocks.

Metamorphic mineral assemblage and isograd map

Figure GS2018-6-3 shows a metamorphic mineral assemblage and isograd map for the Reed Lake–North Star Lake area. The map was compiled using data from Bailes and McRitchie (1978), Bailes (1980), Norquay (1997), Zwanzig and Bailes (2010) and mapping performed by the authors in recent years (e.g., Lazzarotto et al., 2016, 2017). The plotted mineral assemblages only include the diagnostic minerals used to define the metamorphic zones, which include actinolite, hornblende, albite, Ca-bearing plagioclase (oligoclase, andesine), chlorite, epidote and garnet (full mineral assemblages including nondiagnostic minerals are summarized in Table GS2018-6-1). Six isograds were identified separating seven metamorphic zones. From south to north, these isograds are hornblende-in, albite-out, actinolite-out, garnet-in, epidote-out and chlorite-out. The metamorphic mineral assemblage and isograd map demonstrates that the metamorphic grade increases toward the north, from lower-greenschist facies at Reed Lake to garnet-amphibolite facies north of North Star Lake.

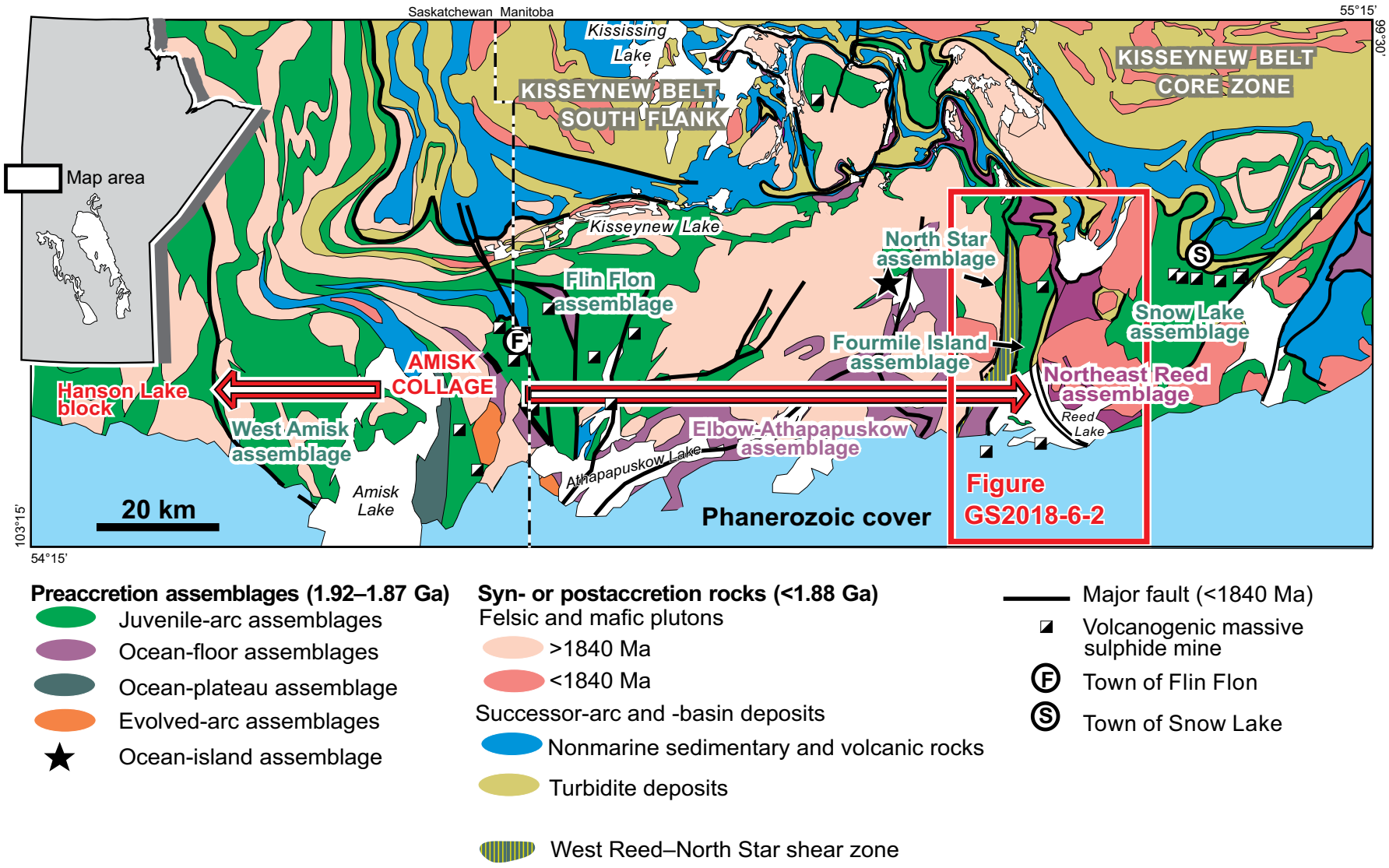

Figure GS2018-6-1: *Simplified geology of the Flin Flon greenstone belt (modified from NATMAP Shield Margin Project Working Group, 1998). The box outlined in red shows the study area (Figure GS2018-6-2).*

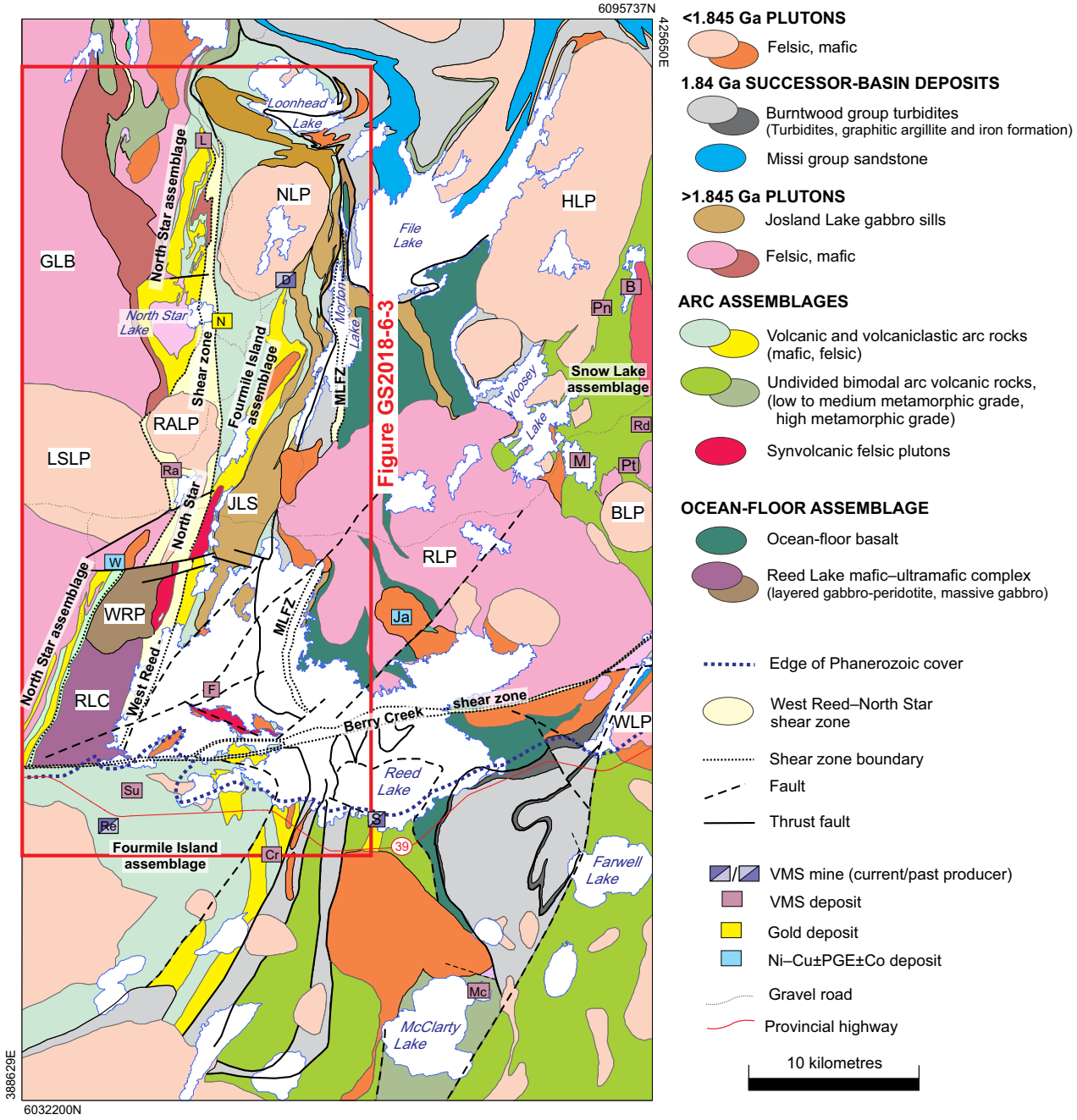

Figure GS2018-6-2: *Geology of the Reed Lake area, compiled from Syme et al. (1995a), NATMAP Shield Margin Project Working Group (1998), Gagné (2017) and Gagné et al. (2017). The box outlined in red shows the area of Figure GS2018-6-3. Intrusive rocks: GLB, Gants Lake batholith; HLP, Ham Lake pluton; JLS, Josland Lake sills; LSLP, Little Swan Lake pluton; NLP, Norris Lake pluton; RALP, Rail Lake pluton; RLC, Reed Lake complex; RLP, Reed Lake pluton; WLP, Wekusko Lake pluton; WRP, West Reed pluton. Structural feature: MLFZ, Morton Lake fault zone. Mines (active or closed), deposits and significant mineral occurrences: B, Bomber; Cr, Cowan River zone, D, Dickstone; F, Fourmile Island; Ja, Jackfish; L, Lon, M, Morgan; Mc, McClarty; N, North Star; Pn, Pen; Pt, Pot; Ra, Rail; Rd, Raindrop; Re, Reed; S, Spruce Point; Su, Super zone, W, Wine. Other abbreviations: PGE, platinum-group elements; VMS, volcanogenic massive sulphide.*

The WRNS does not appear to disrupt the continuous succession of metamorphic zones and isograds (Syme et al., 1995b; Zwanzig and Bailes, 2010). No late brittle structures disrupt the sequence either, in contrast to observations in the Athapapuskow Lake area further to the west (Lazzarotto et al., 2017).

Igneous remnants and metamorphic textures

Greenschist-facies samples show random orientations of metamorphic minerals and igneous fabrics that are well preserved; however, the preservation of igneous textures is less common in amphibolite-facies samples. The distribution of metamorphic-mineral assemblages

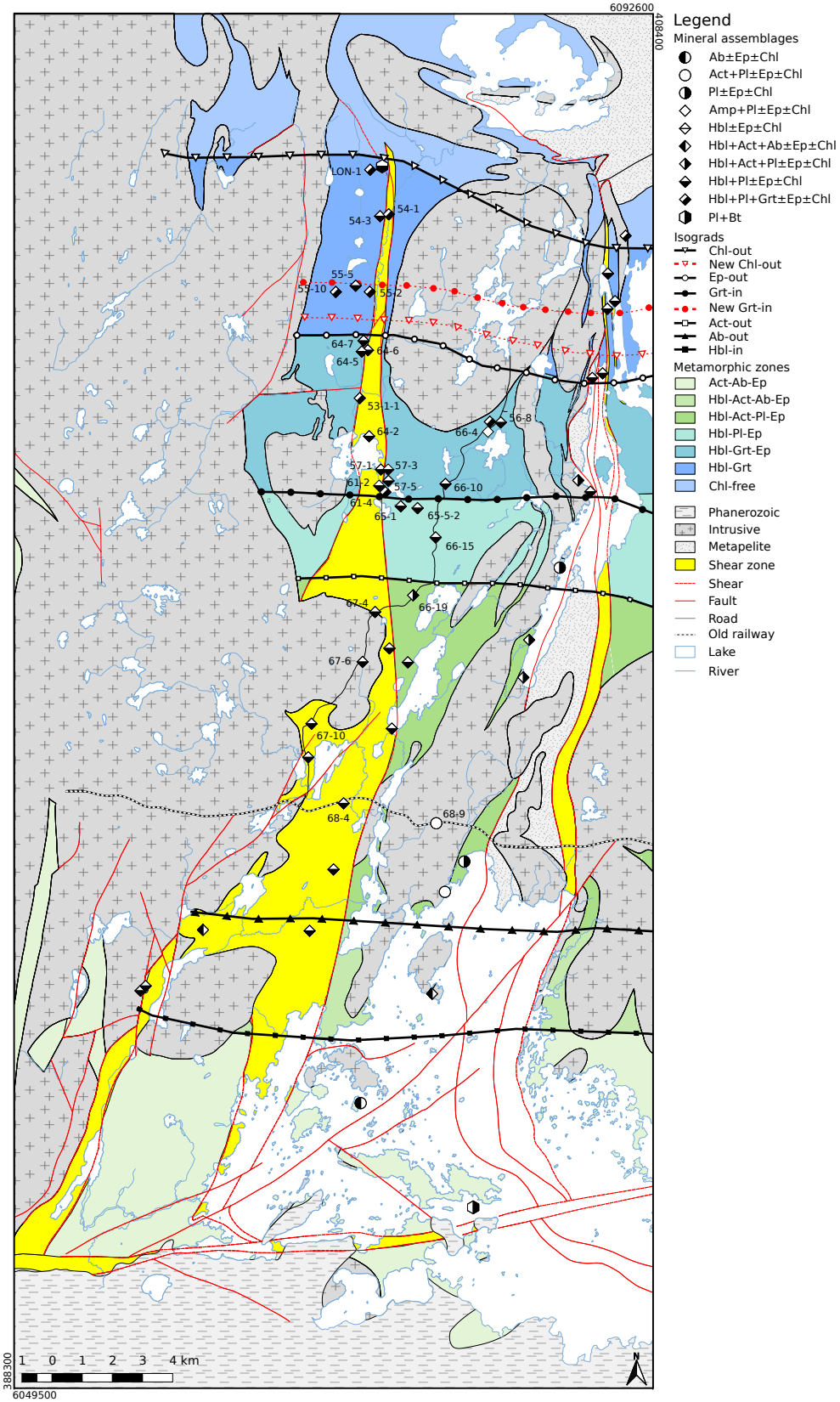

Figure GS2018-6-3: *Metamorphic mineral assemblage and isograd map of the Reed Lake–North Star Lake area; zones are coloured according to regional metamorphic grade and exclude contact metamorphic aureoles. Data compiled from Bailes and McRitchie (1978), Bailes (1980), Norquay (1997), Zwanzig and Bailes (2010) and samples collected by the authors (e.g., Lazzarotto et al., 2016, 2017). Abbreviations: Ab, albite; Act, actinolite; Amp, amphibole; Bt, biotite; Chl, chlorite; Ep, epidote; Grt, garnet; Hbl, hornblende; Pl, plagioclase.*

Table GS2018-6-1: Full metamorphic mineral assemblages recorded for the samples of the Reed Lake–North Star Lake area. Abbreviations: Ab, albite; Ap, apatite; Act, actinolite; Bt, biotite; Cb, carbonate mineral; Chl, chlorite; Ep, epidote; Grt, garnet; Hbl, hornblende; Ilm, ilmenite; Ms; white mica; Opq, opaque mineral; Pl, plagioclase; Qz, quartz; St, staurolite; Ttn, titanite; x, present; ?, uncertain (due to the fine-grained nature of the rocks).

Station number	UTM (Easting)	UTM (Northing)	Pl	Ab	Act	Hbl	Chl	Ep	Opq	Ilm	Ttn	Cb	Ap	Bt	Ms	Grt	St	Qz
0105-10-01	402693	6050881	x	?					x									x
0105-10-05	399284	6056942	x	x			x	x	x			x		x				x
110-13-009-A01	400846	6071549	x			x		x			?							x
110-13-013-A01	400235	6072013	x			x		x		x	x							x
110-13-104-A01	403565	6079523	x			x		x				x		x		x		x
110-13-136-A01	400316	6069354	x			x	x	x										x
110-15-EEL300-492	403012	6053487	x	x								x		x				x
53-1	399252	6080302	x			x	x		x			?		x		x		x
54-1	400212	6086398	?			x			x							x		x
54-3	399926	6086334	x			x			x	x				?				x
55-10	398415	6083803	x	x								x		x				x
55-2	399596	6083847	x			x	x		x	x		x		x	x	x		x
55-5	399119	6084030	x			x			x	x				?		x		x
56-8	403927	6079500	?			x						x		x				x
57-1	399952	6077937	x			x	x		x	x				?		x		x
57-3	400095	6077882	x			x			x									x
57-5	400203	6077562	?			x			x			x						x
59-1	404855	6072183	x		x	?	?	x	x									x
59-2	404717	6071218	x		?	x			x									x
59-5	405948	6074665	?						x					x				x
59-6	406854	6077196	x			x			x			x						x
59-8	406401	6077826			?	x	x		x					x				x
60-2	407534	6083331	x			x			x			x		x				x
60-3	407644	6083587	?			x			x			x						x
60-4	407412	6084555	x			x			x					x				x
60-5	407222	6084625	x			x	?		x									x
61-2	400011	6077365	?			x		x	x									x
61-4	400100	6077188	?			x			x					x		x		x
62-4	408083	6085858	?			x			x					x		x		x
63-1	402715	6064946	x											x				x
63-4	402075	6063941	x		x			x		x	x							x
63-9	401652	6060563	x	?	x	?	x	x	x			x						x
64-2	399564	6079041	x			x				x	x			x				x
64-5	399320	6081848	x			x				x	x	?		x		?		x
64-6	399522	6081893	x			x			x					x		x		x
64-7	399380	6082203	?			x		x				x		x				x
65-1	400612	6076720	?			x		x	x			x						x
65-5	401169	6076659	x			x		x	x									x
66-10	402095	6077461	?			x			x						?			x
66-15	401770	6075689	x		x	x		x	x	x								x
66-19	401022	6073769	x		x	x		x	x	x	x	x						x
66-4	403542	6079421	x		x	x		x	x	x	x							x
67-10	397654	6069515	?			x			x									x

Table GS2018-6-1 (continued): Full metamorphic mineral assemblages recorded for the samples of the Reed Lake–North Star Lake area. Abbreviations: Ab, albite; Ap, apatite; Act, actinolite; Bt, biotite; Cb, carbonate mineral; Chl, chlorite; Ep, epidote; Grt, garnet; Hbl, hornblende; Ilm, ilmenite; Ms; white mica; Opq, opaque mineral; Pl, plagioclase; Qz, quartz; St, staurolite; Ttn, titanite; x, present; ?, uncertain (due to the fine-grained nature of the rocks).

Station number	UTM (Easting)	UTM (Northing)	Pl	Ab	Act	Hbl	Chl	Ep	Opq	Ilm	Ttn	Cb	Ap	Bt	Ms	Grt	St	Qz
67-14	397546	6068402	x			x			x				x					x
67-4	399761	6073217	?			x						x		x				x
67-6	399348	6071563	x			x		x										x
68-4	398717	6066876	x		?	x	x	x		x	x	?		x	?			x
68-9	401790	6066216	x		x	x	x	x		x	x							
96-14-061-A2	398383	6064685	?	x		x			x									x
96-14-116-A2	392153	6060825	?	x		x												x
96-14-117-A2	391986	6060665	x	?		x		x										x
96-14-130-A2	394055	6062681			?	x		x										x
96-14-46-A2	397589	6062651	?	x		x		x		x	x			x				x
96-14-92-A2	392137	6060679	x	x		x		x	x					x				x
LON-1	399761	6087963	?			x	?		x	x	x		x	x		x		x
LON-2	399829	6087988	?				x							x		x	x	x

in samples is controlled by relict igneous textures such as phenocrysts and amygdules, which are common in metamorphosed basalt flows and pillows found throughout the study area. No igneous minerals are preserved. Pyroxene is generally replaced by actinolite and/or hornblende, and chlorite depending on metamorphic grade. Igneous calcic plagioclase is not present in any sample. Plagioclase is replaced by albite (<An_{10}, with minor epidote) in lower-greenschist–facies samples, whereas it is replaced by intermediate plagioclase (<An_{50}, with minor albite, epidote and carbonate) at higher metamorphic grades. In both cases these pseudomorphs generally vary in size from <0.1 to 10 mm. Amygdules are generally filled with quartz, epidote and carbonate. They are rounded to subrounded and range in size from <0.1 to 10 mm. The matrix is usually composed of finer grained crystals of the same composition as the phenocrysts or amygdules.

At outcrop scale, massive flows and pillow basalt form the best-preserved igneous structures. Typically, pillow cores are light in colour, rich in epidote and contain a few small amygdules; rims are dark coloured and contain more chlorite, actinolite and hornblende, and occasionally abundant large amygdules (e.g., Figure GS2018-6-4e). At lower metamorphic grade, plagioclase and/or pyroxene phenocrysts replaced as pseudomorphs are often aligned, preserving trachytic textures typical of magmatic flow. Igneous structures become deformed (e.g., Figure GS2018-6-4a, e) and metamorphic minerals such as amphibole or biotite define a foliation in areas of high strain (e.g., Figure GS2018-6-4c, d, g).

Regional metamorphism

Greenschist facies: actinolite-albite-epidote zone

The actinolite-albite-epidote zone is bounded to the south by the Phanerozoic sedimentary rocks of the Western Canadian Sedimentary Basin, and to the north by the hornblende-in isograd (Figure GS2018-6-3). Characteristic metamorphic minerals in this assemblage are actinolite+albite+epidote+chlorite+quartz±biotite±titanite±apatite ±opaque minerals, which is typical of greenschist-facies rocks.

Primary igneous textures are usually well preserved within samples of this zone. Pyroxene and plagioclase phenocrysts are pseudomorphed by actinolite and albite (with minor chlorite, epidote and white mica), respectively. Amygdules are typically filled with fine-grained quartz, granular or radial epidote, chlorite and carbonate. Fine-grained acicular actinolite, fine-grained albite, granular epidote, interstitial chlorite and quartz make up the bulk of the matrix. Minor titanite, carbonate, apatite and opaque minerals are also found as part of the matrix. Very fine grained biotite is present in some samples. In most cases the biotite-bearing rocks contain no actinolite.

Lower-amphibolite facies: hornblende-actinolite-albite-epidote zone

The hornblende-actinolite-albite zone is defined as the area between the hornblende-in and the albite-out isograds (Figure GS2018-6-3). The zone is characterized by the mineral assemblage hornblende+actinolite+albite

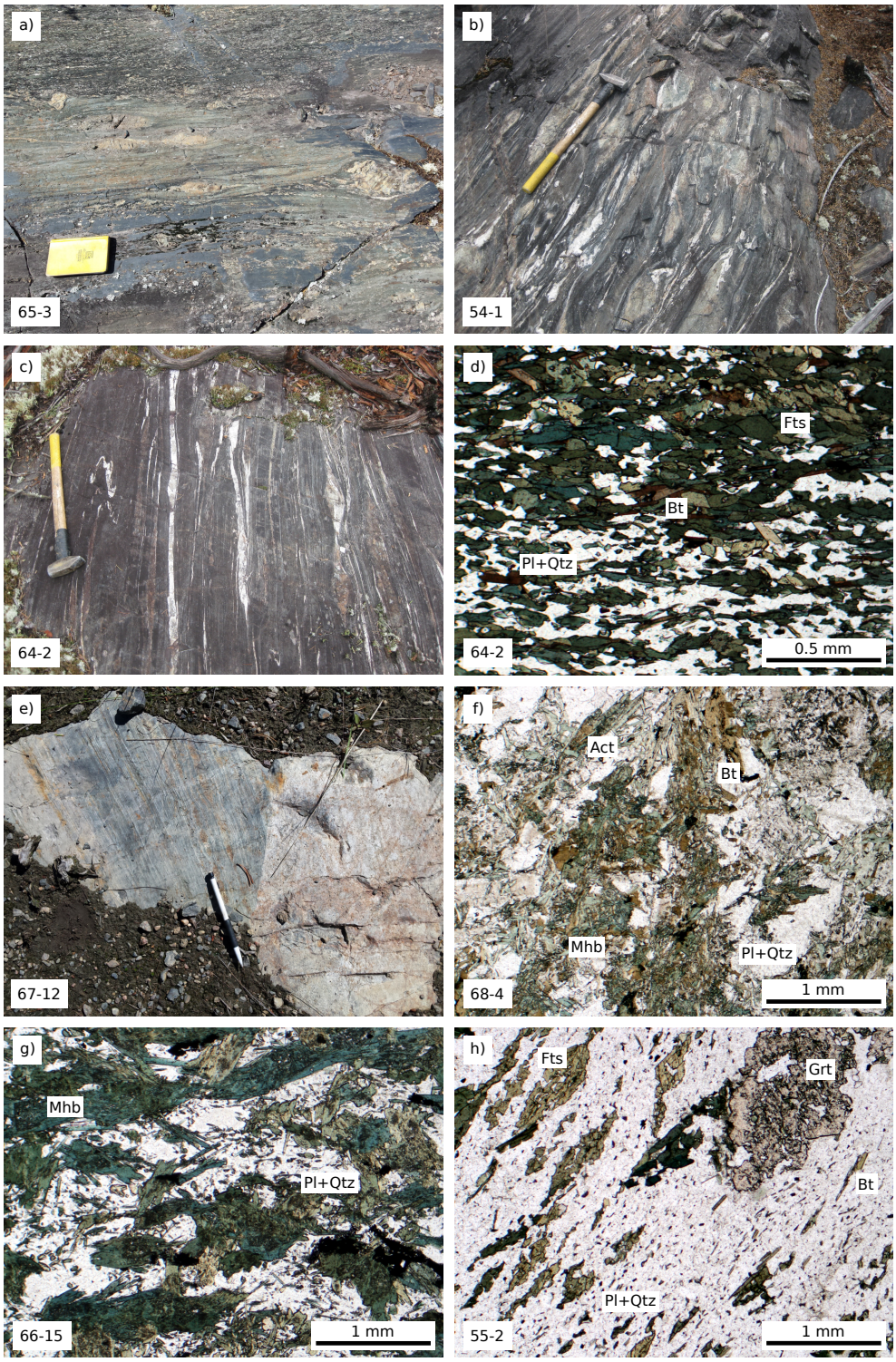

Figure GS2018-6-4: *Outcrop photo and photomicrographs of metamorphic zones in the study area:* ***a)*** *amphibolite with preserved epidotized pillow cores from the Hbl-Pl-Ep zone (station 65-3, UTM Zone 14, 400803E 6076677N [NAD 83]);* ***b)*** *amphibolite with stretched pillows of the Hbl-Grt zone (station 54-1, UTM Zone 14, 400212E 6086389N [NAD 83]);* ***c)*** *amphibolite from the Hbl-Grt-Ep zone (station 64-2, UTM Zone 14, 399565E 6079040N [NAD 83]);* ***d)*** *Fts and Bt from the Hbl-Grt-Ep zone (plane-polarized light, sample 64-2, UTM Zone 14, 399565E 6079040N [NAD 83]);* ***e)*** *strongly foliated amphibolite from the Hbl-Act-Pl-Ep zone (station 67-12, UTM Zone 14, 397404E 6069111N [NAD 83]);* ***f)*** *Mhb, Act, Bt and Pl from the Hbl-Act-Pl-Ep zone (plane-polarized light, sample 68-4, UTM Zone 14, 398720E 6066907N [NAD 83]);* ***g)*** *Mhb and Pl from the Hbl-Pl-Ep zone (plane-polarized light, sample 66-15, UTM Zone 14, 401766E 6075689N [NAD 83]);* ***h)*** *Fts, Grt and Bt from the Hbl-Grt zone (plane-polarized light, sample 55-2, UTM Zone 14, 399598E 6083847N [NAD 83]). Abbreviations: Act, actinolite; Bt, biotite; Ep, epidote; Fts, ferro-tschermakite; Grt, garnet; Hbl, hornblende; Mhb, magnesiohornblende; Pl, plagioclase; Qz, quartz.*

+epidote+chlorite+quartz±titanite±biotite±apatite ±opaque minerals.

Several textural relationships between actinolite and hornblende have been identified in all zones where these minerals coexist, including distinct grains, patchy intergrowths and core-rim microstructures. Even though the typical assemblage contains both hornblende and actinolite, assemblages containing only one of the two minerals are common. Hornblende occurs as rare, small blebs in samples from the southern part of the zone and is rich in Mg. The modal percent of hornblende increases toward the north. A similar trend is observed for the grain size. Close to the albite-out isograd, hornblende is characterized by dark green needles, needle aggregates or blades, up to 0.5 mm long. Actinolite persists throughout the zone and typically consists of pale green to green needle aggregates that vary in size depending on whether it is part of the matrix or replacing phenocrysts. Plagioclase phenocrysts are replaced by albite, which is also found as a fine-grained component within the matrix. Granular epidote, chlorite and fine-grained quartz are common in the matrix and within amygdules and fractures. Accessory titanite, apatite and opaque minerals are found as part of the matrix assemblage.

Lower-amphibolite facies: hornblende-actinolite-plagioclase-epidote zone

The area between the albite-out and actinolite-out isograds delimits the hornblende-actinolite-plagioclase-epidote zone (Figure GS2018-6-3). The characteristic metamorphic mineral assemblage observed in this zone is hornblende+actinolite+plagioclase+epidote+chlorite +quartz±biotite±ilmenite±titanite±apatite±opaque minerals, typical for lower-amphibolite–facies rocks (Figure GS2018-6-4h).

As in the hornblende-actinolite-albite zone there are textural relationships between actinolite and hornblende. Generally, the amphibole grains are too small to be visible in hand sample; however, hornblende is occasionally identifiable as fine black needles up to 1 mm long. The hornblende crystals are rich in Mg and show a slight enrichment in Si and Fe toward the north. Biotite (Mg# = Mg/[Mg+Fe] = 0.5) is present as platy and elongate, green to brown grains up to 1 mm long. Elongate hornblende, actinolite and biotite are intricately intergrown with fine-grained interstitial plagioclase (An_{50}), acicular chlorite and skeletal epidote. Ilmenite is the main Ti-bearing phase, often mantled by late (retrograde?) titanite.

Amphibolite facies: hornblende-plagioclase-epidote zone

The hornblende-plagioclase-epidote zone is defined as the area between the actinolite-out and the garnet-in isograds (Figure GS2018-6-3). The typical metamorphic-mineral assemblage is hornblende+plagioclase+epidote +chlorite+quartz±biotite±ilmenite±titanite±apatite ±opaque minerals (Figure GS2018-6-4f).

Plagioclase of intermediate composition (An_{20}–An_{30}) is common and occurs interstitial to fairly coarse grained, dark green, hornblende blades or needle aggregates up to 1 mm long. The hornblende in this area is transitional between Mg- and Fe-hornblende. Skeletal epidote, usually <0.5 mm across, and acicular or fibrous chlorite are also interstitial to the hornblende. Brown to green biotite (Mg# = 0.4) is present in most of the samples as plates or blades of variable size associated with hornblende. Ilmenite is commonly rimmed by (retrograde?) titanite.

Upper-amphibolite facies: hornblende-garnet-epidote zone

The zone up-grade of the garnet-in isograd and down-grade of the epidote-out isograd is defined as the hornblende-garnet-epidote zone (Figure GS2018-6-3). The key mineral assemblage observed in rocks from this zone is hornblende+plagioclase+garnet+epidote+chlorite+ quartz±biotite±ilmenite±titanite±apatite± opaque minerals and is characteristic of upper-amphibolite–facies mafic rocks (Figure GS2018-6-4d).

Rocks in this zone consist of up to 60–70% hornblende (Fe-tschermakite). Hornblende grains are subhedral, exhibit the typical 120°/60° cleavage and display light green/brown to dark green pleochroism. Grain sizes range between a few micrometres up to 1 mm. Euhedral brown biotite with Mg# = 0.3 occurs as flakes and blades up to 0.2 mm long and is found throughout the zone. Hornblende and biotite define a foliation resulting from strain along the WRNS. Garnet porphyroblasts are subhedral and rich in Fe (Alm_{60}). The garnet grains range from 50 µm to 1 mm and contain inclusions of ilmenite and quartz. Some garnet porphyroblasts overgrow the foliation in high-strain zones proximal to the WRNS. The observed plagioclase is of intermediate composition (An_{30}–An_{40}) and does not show any sign of late alteration. It is usually present as an interstitial phase together with quartz. Small grains of skeletal epidote, usually <0.1 mm across, and fibrous chlorite are part of the remaining matrix. Accessory ilmenite (sometimes rimmed by late titanite) is common.

Upper amphibolite facies: hornblende-garnet zone

The zone between the epidote-out and the chlorite-out isograds is defined as the hornblende-garnet zone (Figure GS2018-6-3). The characteristic metamorphic-mineral assemblage in samples from this zone is hornblende+plagioclase+garnet+chlorite+quartz±biotite±ilmenite±titanite±apatite±opaque minerals (Figure GS2018-6-4b).

Hornblende crystals are green/brown to dark green in colour and are chemically classified as Fe-tschermakites. Grains range in size from a few micrometres to 1 mm, are typically euhedral to subhedral and display 120°/60° cleavage. Hornblende generally makes up half of the rock volume. Biotite is usually associated with hornblende and has a relatively low magnesium content (Mg# = 0.25). The biotite grains display brown to green pleochroism, are euhedral to subhedral and range in size from <10 µm to 200 µm. Anhedral to subhedral garnet porphyroblasts and grain aggregates reach up to several millimetres in diameter and have locally overgrown the amphibole- and biotite-defined foliation. They are rich in Fe (Alm_{55}–Alm_{65}) and zoning can be present with relatively Ca-rich rims (Grs_{32}/Alm_{55}) and Ca-poor cores (Grs_{23}/Alm_{65}). Grains are several hundreds of micrometres across and contain inclusions of quartz, ilmenite, apatite and rare magnetite/hematite. Interstitial plagioclase of intermediate composition (An_{20}–An_{40}) is the major component in the matrix, together with quartz, ilmenite, titanite (late?) and minor chlorite. Chlorite mantling biotite and hornblende is probably a product of retrograde metamorphism.

Upper-amphibolite facies: chlorite-free zone

The chlorite-free zone is located between the chlorite-out isograd to the south and where the Kisseynew gneisses overlie the volcanic units to the north (Figure GS2018-6-3). This zone is characterized by the absence of chlorite, with a key mineral assemblage of hornblende+plagioclase+garnet+quartz±biotite±ilmenite±titanite±apatite±opaque minerals.

Hornblende (Fe-tschermakite) occurs as green subhedral blades a few hundreds of micrometres to several millimetres long with typical 120°/60° cleavage. The plagioclase is intermediate in composition (An_{40}) and is usually interstitial to the amphibole. Several samples contain brown to green biotite (Mg# = 0.25) as plates or blades varying from <0.1 mm to 0.5 mm. Garnets are anhedral to subhedral, unzoned and rich in Fe (Alm_{55}–Alm_{65}), with inclusions of quartz and ilmenite. Ilmenite is also present in the matrix and is often enveloped by titanite.

Contact metamorphism

Contact metamorphism is recognized in low-grade metamorphic zones (i.e., greenschist facies) by the presence of hornblende in mafic rocks. In high-grade metamorphic areas (i.e., amphibolite facies), the distinction between contact and regional metamorphism becomes difficult. Limited data on contact aureoles in the Reed Lake–North Star Lake area is available; based on previous work (e.g., Zwanzig and Bailes, 2010; Syme, 2015; Lazzarotto et al., 2017), they are observed to extend approximately 1 km outward from the margins of intrusions.

Contact metamorphic aureoles in mafic volcanic units are recognized in the field by a darkening of the fresh and weathered surfaces, sometimes associated with an increase in the grain size of porphyroblasts such as hornblende. Usually the rocks within these units are very fine grained and the mineral assemblages are difficult to identify in hand sample or with a petrographic microscope. It is possible to unravel contact metamorphic assemblages within aureoles with the aid of electron probe microanalyses of the samples.

Contact aureoles generally consist of dark grey to black weathering massive or pillow basalt. Fresh surfaces are dark green, with lighter epidotized patches. Igneous textures such as phenocrysts and pillow or flow structures are preserved in low-strain areas. Primary igneous minerals are replaced with pseudomorphs: pyroxene is usually replaced by actinolite and/or hornblende, whereas calcic plagioclase is replaced by more sodic varieties of plagioclase (<An_{50}). The typical mineral assemblage observed in thin section is hornblende±actinolite+plagioclase+quartz±biotite±epidote±chlorite±opaque minerals. Discrete actinolite grains are intergrown with hornblende where both amphiboles co-exist. Prograde replacement locally results in actinolite cores mantled by hornblende. Granular epidote, acicular or fibrous chlorite and fine-grained quartz occur in veins, amygdules or as part of the matrix. Biotite is present as small, brown to green, platy grains. Local red to purple garnet porphyroblasts <1 mm in diameter occur within domains of pre-metamorphic alteration (interaction with fluids?).

Thermodynamic modelling

A phase-equilibrium diagram (Figure GS2018-6-5) was calculated for a representative, juvenile-arc rock (whose bulk composition is seen in Table GS2018-6-2), to estimate peak metamorphic pressure and temperature conditions. The Gibbs free energy minimization software suite Theriak-Domino (de Capitani and Brown, 1987; de Capitani and Petrakakis, 2010) was used in conjunction with the thermodynamic dataset of Holland and Powell

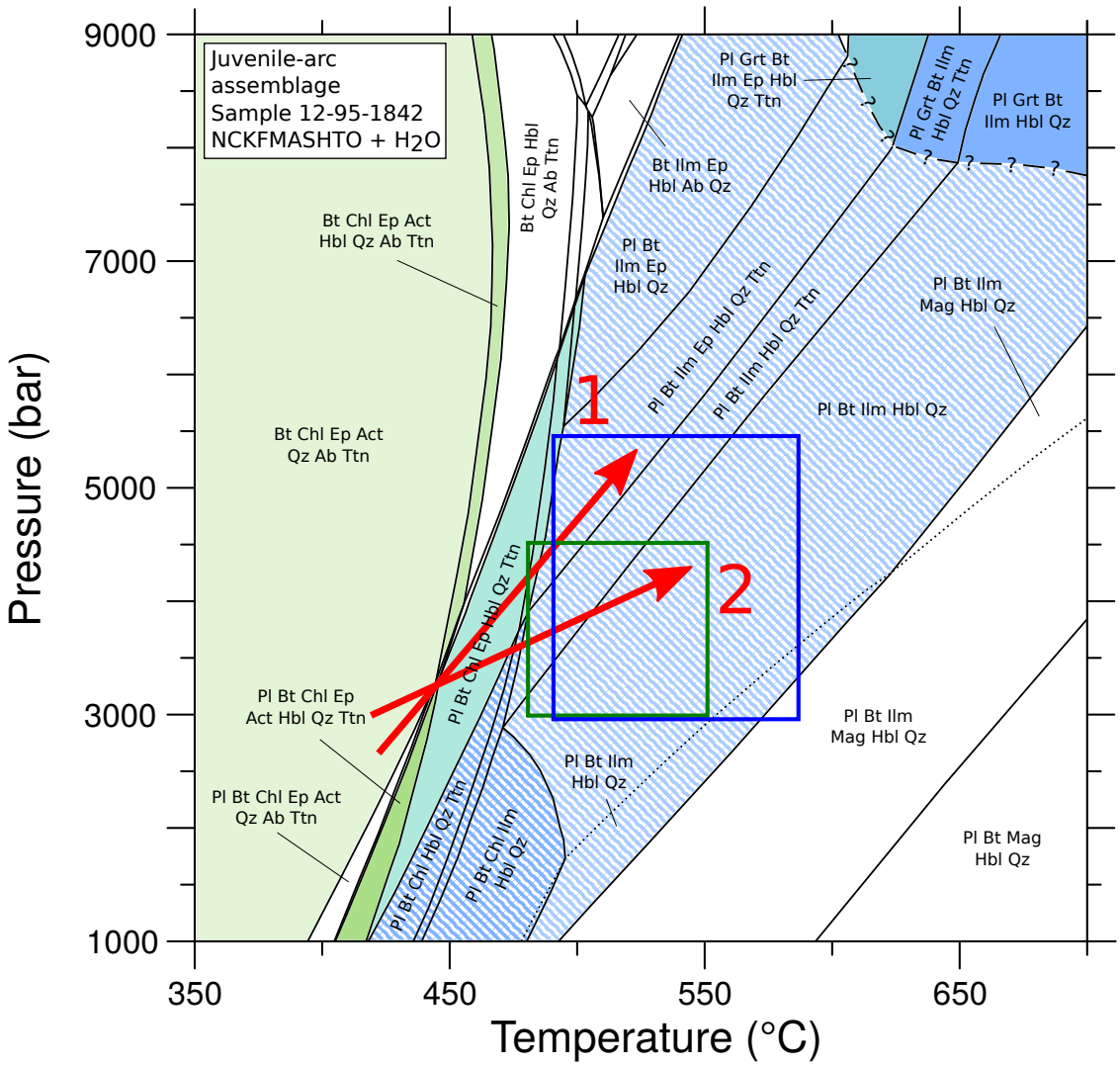

Figure GS2018-6-5: *Equilibrium phase diagram constructed for a representative juvenile-arc assemblage bulk composition in the Na_2O-CaO-K_2O-FeO-MgO-Al_2O_3-SiO_2-H_2O-TiO_2-Fe_2O_3 (NCKFMASHTO) chemical system (sample 12-95-1842; Table GS2018-6-2). Assemblage fields use the same colour scheme as Figure GS2018-6-3. The red arrows represent possible metamorphic field gradients as discussed in the text. Abbreviations: Ab, albite; Act, actinolite; Bt, biotite; Chl, chlorite; Ep, epidote; Hbl, hornblende; Ilm, ilmenite; Mag, magnetite; Pl, plagioclase; Qz, quartz; Ttn, titanite.*

Table GS2018-6-2: Whole-rock geochemical data for sample 12-95-1842 used to calculate the phase-equilibrium diagram of Figure GS2018-6-5.

Sample 12-95-1842	SiO_2	TiO_2	Al_2O_3	Fe_2O_3	FeO	MnO	MgO	CaO	Na_2O	K_2O	P_2O_5	LOI	Total
wt. %	56.40	0.68	15.20	1.47	9.25	0.00	2.78	7.84	3.09	0.23	0.00	0.45	97.39

(1998; updated to version ds5.5). Activity-composition models (a-X models) for clinoamphibole (Diener et al., 2007, revised by Diener and Powell, 2012), clinopyroxene (Green et al., 2007; Diener and Powell, 2012), garnet (White et al., 2007), chloritoid (White et al., 2000), chlorite (Holland et al., 1998), white mica (Coggon and Holland, 2002), biotite (White et al., 2007), epidote (Holland and Powell, 1998), spinel (White et al., 2002), ilmenite-hematite (White et al., 2000) and feldspar (Cbar1 field; Holland and Powell, 2003) were used. Calculations were performed in the Na_2O-CaO-K_2O-FeO-MgO-Al_2O_3-SiO_2-H_2O-TiO_2-Fe_2O_3 (NCKFMASHTO) chemical system. This system is a good approximation of the analyzed composition of the rocks. Ferric iron oxide (Fe_2O_3) was estimated as 15% of the total Fe, based on the presence of accessory Fe-bearing phases (magnetite), wet titration

of selected samples and iterative T-XFe^{3+} and pressure-temperature (P-T) equilibrium modelling for different ferric to ferrous iron ratios and pressures. Investigations of the influence of ferric iron on the calculated phase-diagram section topology shows that by increasing the amount of Fe_2O_3 by 5%, the equilibration-pressure range of the observed assemblage is lowered by more than 1 kbar. Similarly, decreasing the amount of Fe_2O_3 by 5% yields a pressure increase of more than 1 kbar; therefore, interpreting the results of phase-equilibria modelling of rocks containing ferric and ferrous iron warrants caution. Garnet is the main phase incorporating Mn, which often results in overstabilization of the mineral in the modelled P-T space. Manganese was, therefore, not incorporated into the chemical system due to its relatively low abundance (usually MnO <0.1 wt. %) and to prevent the calculation of stable garnet in unlikely portions of P-T space. All P is assumed to be contained in apatite and Ca was subtracted from the bulk composition at a molar ratio of 5Ca:3P. The system was oversaturated in H_2O over the calculated P-T range.

Figure GS2018-6-5 shows the phase-equilibrium diagram for a representative juvenile-arc bulk composition (sample 12-95-1842) in the NCKFMASHTO chemical system. The colours used to highlight the various assemblage fields correspond to the colours of the metamorphic mineral assemblage and isograd map (Figure GS2018-6-3) and represent areas with the same key mineral assemblage.

The greenschist facies is represented by a large field containing the assemblage actinolite+albite+chlorite+epidote+biotite+quartz+titanite and occurs below 450°C. Just up-grade of this field are two relatively narrow fields (<20°C wide) representing the transition into amphibolite-facies assemblages. The lower pressure field has co-existing albite and plagioclase and is followed by a band of coexisting hornblende and actinolite spanning the full calculated pressure range. The epidote-out reaction occurs up-temperature of the actinolite-out and albite-out reactions between 1 and 6.5 kbar. It delimits a 30°C wide area where hornblende and epidote coexist in the assemblage hornblende+plagioclase+chlorite+biotite+epidote+quartz+titanite. Down-temperature of the chlorite-out reaction (approximately 500°C) and below 4 kbar is an assemblage field with coexisting plagioclase, hornblende and chlorite, with no epidote. A dashed line indicates the stability field of an additional amphibole phase upgrade of the chlorite-out reaction. This phase is an amphibole with a calculated composition, created to handle structural order-disorder of Fe, Mg and Al where the partitioning of these elements is unknown (camo1 and camo2; see Holland and Powell, 2006; Diener et al., 2007). In the sequences discussed in this paper, no amphibole other than actinolite and hornblende are present. The amphibole calculated up-grade of the dashed line is therefore interpreted as hornblende. At pressures <6.5 kbar and temperatures >500°C, magnetite is stable. Biotite is stable over the entire P-T range.

Discussion and conclusion

Comparison of the calculated phase-equilibrium diagram with the sequence of isograds observed in the field allows for the approximation of two possible metamorphic field gradients (red arrows in Figure GS2018-6-5). The observed sequence of reactions is hornblende-in, albite-out, actinolite-out, garnet-in, epidote-out and chlorite-out. The garnet-in reaction occurs at noticeably higher grade (above 7.5 kbar and 600°C, up-grade of the chlorite-out reaction) in the modelled phase-equilibrium section. Calculated garnet compositions at 700°C and 8 kbar correspond to the measured compositions in samples from the study area (Alm_{50}–Alm_{60}). Slight variations in the Fe content, Ca content and Fe^{2+}/Fe^{3+} ratio do not change the stability of garnet. The chlorite-out isograd was mapped as the northernmost (highest temperature) reaction. The location of this isograd is uncertain because it is difficult to distinguish prograde from retrograde chlorite within the rock matrix. If the chlorite-out reaction was to occur down-grade of the garnet-in reaction ('New Chl-out' and 'New Grt-in' in Figure GS2018-6-3), the sequence of observed mineral assemblages and reactions would correspond to the calculated phase-equilibrium diagram with a field gradient approximated by arrow 1 (Figure GS2018-6-5); however, a relatively large jump in pressure and temperature occurs between the chlorite-out and garnet-in reactions (4 kbar and 150°C). This suggests that the garnet a-X model is very sensitive to modelling. Calculations incorporating Mn result in garnet being stable over the entire P-T range, whereas without Mn, garnet is stable only at a P that is too high.

Independent pressure-temperature constraints from different calibrations of the hornblende-plagioclase thermobarometer (Holland and Blundy, 1994; Zenk and Schulz, 2004; Bhadra and Bhattacharya, 2007) and the garnet-biotite Fe-Mg exchange thermometer (Ferry and Spear, 1978; Hodges and Spear, 1982) yield pressures of 3–4.5 kbar and temperatures of 480–550°C for samples from the Hbl-Grt-Ep zone (green box in Figure GS2018-6-5), and pressures of 3–5.5 kbar and temperatures of 490–590°C for samples from the Hbl-Grt zone (blue box in Figure GS2018-6-5). These independent constraints partially agree with the calculated phase equilibrium

diagram and are believed to better depict the stability of garnet.

Garnet porphyroblasts and aggregates are oriented with the foliation defining amphibole and biotite in most samples (Figure GS2018-6-4b). This suggests that the garnet grains grew before (or during) the deformation phase and were subjected to the strain developed by the WRNS. The garnet is interpreted to be coeval with the metamorphic amphibole and biotite. Nevertheless, it is possible that not all garnet is part of the metamorphic peak assemblage. In sample 55-5, metamorphic hornblende and biotite define the foliation, suggesting that they formed before, or during, the phase of deformation. Garnet porphyroblasts in this sample overgrow the foliation, suggesting that their growth postdates deformation along the WRNS, and therefore the interpreted timing of peak metamorphism. If garnet from areas south of sample 55-5 are of later origin and not part of the metamorphic peak assemblage, the location of the garnet-in isograd shifts up-grade of the epidote-out reaction. Dashed, garnet-free fields that otherwise match the sequence of mapped metamorphic mineral assemblages are depicted in the phase-equilibrium diagram and allow for a different field gradient indicated by arrow 2 (Figure GS2018-6-5). Late garnet could be a product of fluid infiltration along the WRNS.

Economic considerations

Volcanogenic massive-sulphide deposits

The Flin Flon greenstone belt is host to several volcanogenic massive-sulphide deposits (VMS), which form by seafloor venting of metalliferous hydrothermal fluids in active volcanic settings (e.g., Galley et al., 2007). The Reed Lake–North Star Lake area contains bimodal volcanic successions of mafic and felsic rocks that are characteristic of extensional tectonic regimes, are similar to the volcanic sequence that hosts the Flin Flon and Callinan VMS deposits (e.g., Bailes and Syme, 1989; Syme and Bailes, 1993) and indicate excellent exploration potential. These deposits are overprinted, and in some cases strongly remobilized via metamorphic and deformational processes because they formed early in the tectonic evolution of the region. Recognizing the effects of metamorphism on these deposits and the effect and extension of the associated alteration is important for exploration.

Orogenic gold deposits

Orogenic gold deposits form later with respect to regional deformation, magmatism and metamorphism, and the associated release of fluids. The controls on orogenic gold deposits are thus strongly related to metamorphic and tectonic processes. For example, dehydration reactions at the transition from greenschist to amphibolite facies in metabasites have been interpreted to provide fluids for the transport of gold (e.g., Phillips and Powell, 1993). In addition, crustal-scale shear zones can create pathways and/or traps for the transport and deposition of gold in solution (e.g., Dubé and Gosselin, 2007). The WRNS hosts several significant gold showings in the NSA. The major structures associated with gold mineralization extend continuously southward to the Reed Lake area, which is considered to have similar potential for shear-hosted (i.e., orogenic) gold mineralization.

Acknowledgments

The authors thank R. Ponto for enthusiastic field assistance, N. Brandson and E. Anderson for efficient logistical support, as well as all the staff at the Midland Rock Preparation Laboratory for sample preparation. Thanks also go to K. Reid and C. Couëslan for reviewing earlier versions of this manuscript.

References

Ansdell, K.M., Lucas, S.B., Connors, K. and Stern, R.A. 1995: Kisseynew metasedimentary gneiss belt, Trans-Hudson Orogen (Canada): backarc origin and collisional inversion; Geology, v. 23, p. 1039–1043.

Bailes, A.H. 1980: Geology of the File Lake area; Manitoba Department of Energy and Mines, Mineral Resources Division, Geological Report GR78-1, 134 p.

Bailes, A.H. and Galley, A.G. 2007: Geology of the Chisel–Anderson lakes area, Snow Lake, Manitoba (NTS areas 63K16SW and west half of 63J13SE); Manitoba Science, Technology, Energy and Mines, Manitoba Geological Survey, Geoscientific Map MAP2007-1, scale 1:20 000.

Bailes, A.H. and McRitchie, W.D. 1978: The transition from low to high grade metamorphism in the Kisseynew sedimentary gneiss belt, Manitoba; *in* Metamorphism in the Canadian Shield, J.A. Fraser and W.W. Heywood (ed.), Geological Survey of Canada, Paper 7E-10, p. 155–177.

Bailes, A.H. and Syme, E.C. 1989: Geology of the Flin Flon–White Lake area; Manitoba Energy and Mines, Minerals Division, Geological Report GR87-1, 313 p.

Bhadra, S. and Bhattacharya, A., 2007: The barometer tremolite+tschermakite+2 albite=2 pargasite+8 quartz: constraints from experimental data at unit silica activity, with application to garnet-free natural assemblages; American Mineralogist, v. 92, no. 4, p. 491–502.

Coggon, R. and Holland, T.J.B. 2002: Mixing properties of phengitic micas and revised garnet-phengite thermobarometers; Journal of Metamorphic Geology, v. 20, no. 7, p. 683–696.

de Capitani, C. and Brown, T.H. 1987: The computation of chemical equilibrium in complex systems containing non-ideal solutions; Geochimica et Cosmochimica Acta, v. 51, no. 10, p. 2639–2652.

de Capitani, C.D. and Petrakakis, K. 2010: The computation of equilibrium assemblage diagrams with Theriak/Domino software; American Mineralogist, v. 95, no. 7, p. 1006–1016.

Diener, J.F.A. and Powell, R. 2012: Revised activity–composition models for clinopyroxene and amphibole; Journal of Metamorphic Geology, v. 30, no. 2, p. 131–142.

Diener, J.F.A., Powell, R., White, R.W. and Holland, T.J.B. 2007: A new thermodynamic model for clino-and orthoamphiboles in the system Na_2O-CaO-FeO-MgO-Al_2O_3-SiO_2-H_2O-O; Journal of Metamorphic Geology, v. 25, no. 6, p. 631–656.

Dubé, B. and Gosselin, P. 2007: Greenstone-hosted quartz-carbonate vein deposits; *in* Mineral deposits of Canada: a synthesis of major deposit-types, district metallogeny, the evolution of geological provinces, and exploration methods, W.D. Goodfellow (ed.), Geological Association of Canada, Mineral Deposits Division, Special Publication no. 5, p. 49–73.

Ferry, J.T. and Spear, F.S. 1978: Experimental calibration of the partitioning of Fe and Mg between biotite and garnet; Contributions to Mineralogy and Petrology, v. 66, no. 2, p. 113–117.

Gagné, S. 2017: Sub-Phanerozoic geology of the Reed Lake area, Flin Flon belt, west-central Manitoba (parts of NTS 63K7, 8, 9, 10); Manitoba Growth, Enterprise and Trade, Manitoba Geological Survey, Preliminary Map PMAP2017-2, scale 1:30 000.

Gagné, S., Syme, E.C., Anderson, S.D. and Bailes, A.H. 2017: Geology of the exposed basement in the Reed Lake area, Flin Flon belt, west-central Manitoba (parts of NTS 63K9, 10, 15, 16); Manitoba Growth, Enterprise and Trade, Manitoba Geological Survey, Preliminary Map PMAP2017-1, scale 1:30 000.

Galley, A.G., Hannington, M.D. and Jonasson, I.R., 2007: Volcanogenic massive sulphide deposits; *in* Mineral deposits of Canada: a synthesis of major deposit-types, district metallogeny, the evolution of geological provinces, and exploration methods, W.D. Goodfellow (ed.), Geological Association of Canada, Mineral Deposits Division, Special Publication no. 5, p. 141–161.

Green, E., Holland, T. and Powell, R. 2007: An order-disorder model for omphacitic pyroxenes in the system jadeite-diopside-hedenbergite-acmite, with applications to eclogitic rocks; American Mineralogist, v. 92, no. 7, p. 1181–1189.

Hodges, K.V. and Spear, F.S. 1982: Geothermometry, geobarometry and the Al_2SiO_5 triple point at Mt. Moosilauke, New Hampshire; American Mineralogist, v. 67, p. 1118–1134.

Hoffman, P.F. 1988: United plates of America, the birth of a craton: Paleoproterozoic assembly and growth of proto-Laurentia; Annual Review of Earth and Planetary Sciences, v. 16, p. 543–603.

Holland, T., Baker, J. and Powell, R. 1998: Mixing properties and activity composition and relationships of chlorites in the system MgO-FeO-Al_2O_3-SiO_2-H_2O; European Journal of Mineralogy, v. 10, no. 3, p. 395–406.

Holland, T. and Blundy, J. 1994: Non-ideal interactions in calcic amphiboles and their bearing on amphibole-plagioclase thermometry; Contributions to Mineralogy and Petrology, v. 116, no. 4, p. 433–447.

Holland, T.J.B. and Powell, R. 1998: An internally consistent thermodynamic data set for phases of petrological interest; Journal of Metamorphic Geology, v. 16, no. 3, p. 309–343.

Holland, T. and Powell, R. 2003: Activity-composition relations for phases in petrological calculations: an asymmetric multicomponent formulation; Contributions to Mineralogy and Petrology, v. 145, no. 4, p. 492–501.

Holland, T.J.B. and Powell, R. 2006. Mineral activity–composition relations and petrological calculations involving cation equipartition in multisite minerals: a logical inconsistency; Journal of Metamorphic Geology, v. 24, no. 9, p. 851–861.

Lazzarotto, M., Gagné, S. and Pattison, D.R.M. 2016: Tectono-metamorphic investigations in the Athapapuskow Lake area, west-central Manitoba (part of NTS 63K12); *in* Report of Activities 2016, Manitoba Growth, Enterprise and Trade, Manitoba Geological Survey, p. 87–98.

Lazzarotto, M., Pattison, D.R.M. and Gagné, S. 2017: Prehnite-pumpellyite– to amphibolite-facies metamorphism in the Athapapuskow Lake area, west-central Manitoba (parts of NTS 63K12, 13); *in* Report of Activities 2017, Manitoba Growth, Enterprise and Trade, Manitoba Geological Survey, p. 104–116.

Lucas, S.B., Stern, R.A., Syme, E.C., Reilly, B.A. and Thomas, D.J. 1996: Intraoceanic tectonics and the development of continental crust: 1.92–1.84 Ga evolution of the Flin Flon Belt, Canada; Geological Society of America Bulletin, v. 108, no. 5, p. 602–629.

NATMAP Shield Margin Project Working Group 1998: Geology, NATMAP Shield Margin Project area, Flin Flon belt, Manitoba/Saskatchewan; Geological Survey of Canada, Map 1968A, scale 1:100 000.

Norquay, L.I. 1997: Structural and metamorphic evolution of the North Star Lake area, Manitoba; M.Sc. thesis, University of Manitoba, 244 p.

Phillips, G.N. and Powell, R. 1993: Link between gold provinces; Economic Geology, v. 88, no. 5, p. 1084–1098.

Stern, R.A., Syme, E.C., Bailes, A.H. and Lucas, S.B. 1995a: Paleoproterozoic (1.90–1.86 Ga) arc volcanism in the Flin Flon Belt, Trans-Hudson Orogen, Canada; Contributions to Mineralogy and Petrology, v. 119, no. 2–3, p. 117–141.

Stern, R.A., Syme, E.C. and Lucas, S.B. 1995b: Geochemistry of 1.9 Ga MORB- and OIB-like basalts from the Amisk collage, Flin Flon Belt, Canada: evidence for an intra-oceanic origin; Geochimica et Cosmochimica Acta, v. 59, no. 15, p. 3131–3154.

Syme, E.C. 2015: Geology of the Athapapuskow Lake area, western Flin Flon belt, Manitoba (part of NTS 63K12); Manitoba Mineral Resources, Manitoba Geological Survey, Geoscientific Report GR2014-1, 209 p.

Syme, E.C. and Bailes, A.H. 1993: Stratigraphic and tectonic setting of early Proterozoic volcanogenic massive sulfide deposits, Flin Flon, Manitoba; Economic Geology, v. 88, no. 3, p. 566–589.

Syme, E.C., Bailes, A.H. and Lucas, S.B. 1995a: Reed Lake, N.T.S. parts of 63K/9, 63K/10; Manitoba Energy and Mines, Geological Services, Preliminary Map 1995F-1, scale 1:50 000.

Syme, E.C., Bailes, A.H. and Lucas, S.B. 1995b: Geology of the Reed Lake area (parts of NTS 63K/9 and 10); *in* Report of Activities 1995, Manitoba Energy and Mines, Geological Services, p. 42–60.

Syme, E.C., Lucas, S.B., Bailes, A.H. and Stern, R.A. 1999: Contrasting arc and MORB-like assemblages in the Paleoproterozoic Flin Flon Belt, Manitoba, and the role of intra-arc extension in localizing volcanic-hosted massive sulphide deposits; Canadian Journal of Earth Sciences, v. 36, p. 1767–1788.

Whalen, J.B., Perhsson, S. and Rayner, N.M. 2016: Significance of pre–1860 Ma granitoid magmatism for crustal evolution and exploration targeting in the Flin Flon assemblage, Trans-Hudson Orogen, Canada; Economic Geology, v. 111, no. 4, p. 1021–1039, doi:10.2113/econgeo.111.4.1021

White, R.W., Powell, R., Holland, T.J.B. and Worley, B.A. 2000: The effect of TiO_2 and Fe_2O_3 on metapelitic assemblages at greenschist and amphibolite facies conditions: mineral equilibria calculations in the system K_2O-FeO-MgO-Al_2O_3-SiO_2-H_2O-TiO_2-Fe_2O_3; Journal of Metamorphic Geology, v. 18, no. 5, p. 497–512.

White, R.W., Powell, R. and Clarke, G.L. 2002: The interpretation of reaction textures in Fe-rich metapelitic granulites of the Musgrave block, central Australia: constraints from mineral equilibria calculations in the system K_2O-FeO-MgO-Al_2O_3-SiO_2-H_2O-TiO_2-Fe_2O_3; Journal of Metamorphic Geology, v. 20, no. 1, p. 41–55.

White, R.W., Powell, R. and Holland, T.J.B. 2007: Progress relating to calculation of partial melting equilibria for metapelites; Journal of Metamorphic Geology, v. 25, no. 5, p. 511–527.

Zenk, M. and Schulz, B. 2004: Zoned Ca-amphiboles and related PT evolution in metabasites from the classical Barrovian metamorphic zones in Scotland; Mineralogical Magazine, v. 68, no. 5, p. 769–786.

Zwanzig, H.V. and Bailes, A.H. 2010: Geology and geochemical evolution of the northern Flin Flon and southern Kisseynew domains, Kississing–File lakes area, Manitoba (parts of NTS 63K, N); Manitoba Innovation, Energy and Mines, Manitoba Geological Survey, Geoscientific Report GR2010-1, 135 p.

GS2018-7

Geology and bedrock mapping of the Wekusko Lake pegmatite field (northeastern block), central Manitoba (part of NTS 63J13)

by D. Benn[1], R.L. Linnen[1] and T. Martins

In Brief:

- Defining zonation and mineralogy of Li bearing pegmatite dikes aids identification of high concentrations of spodumene
- Detailed geological mapping provides a better understanding of morphology, regional deformation and rheology context of pegmatite emplacement
- Future studies will include measuring Li content of micas and geochronology of columbite group minerals

Citation:
Benn, D., Linnen, R.L. and Martins, T. 2018: Geology and bedrock mapping of the Wekusko Lake pegmatite field (northeastern block), central Manitoba (part of NTS 63J13); *in* Report of Activities 2018, Manitoba Growth, Enterprise and Trade, Manitoba Geological Survey, p. 79–88.

Summary

Pegmatite dikes from the Green Bay group of the Wekusko Lake pegmatite field were examined in summer 2018 through geological mapping and relogging drillcore from several diamond drill holes. The pegmatite dikes exhibit five zones: the border zone, the wall zone, the intermediate zone, the central zone and the core zone. The dikes vary in size and not all zones are present in all dikes. The zones vary in mineralogy and crystal size. An abundance of alkali feldspars is characteristic of the wall zone and the intermediate zone, whereas the abundances of albite and spodumene are key for identifying the central zone. The central zone also hosts rare-metal–bearing minerals such as those found in the columbite group. Field mapping reveals that the pegmatites are folded and that the width of the pegmatite affects the degree to which it was folded during regional deformation. Future work will involve mineralogical studies (particularly of muscovite) as vectors for exploration. Uranium-Pb geochronological studies of the columbite-group minerals will also be carried out.

Introduction

With the rise of interest in renewable energy and electric cars, batteries have become significantly more important. Many new battery technologies use Li as a main component. For this reason, Li has become a widely sought-after element. Lithium is typically obtained either through mining pegmatites, where spodumene is the most common Li ore mineral (e.g., Greenbushes, Australia), or extraction from brines (e.g., Salar de Atacama, Chile).

In Manitoba, Li is predominantly associated with Li-Cs-Ta (LCT) pegmatites, the best-known example being the world-class Archean Tanco deposit in southeast Manitoba (Černý, 2005). Trans-Hudson–aged LCT pegmatites are present in the Wekusko Lake pegmatite field (Černý et al., 1981; Martins et al., 2017), approximately 25 km east of Snow Lake in central Manitoba. This pegmatite field is currently the target of exploration work focusing on the Li mineralization of the pegmatite dikes (e.g., FAR Resources Ltd., 2018).

Bedrock mapping at a scale of 1:4 000 (Benn et al., 2018) was undertaken to investigate and document the zoning, morphology and structural controls of the emplacement of the pegmatite dikes. In addition, drillcore from several diamond drill holes was relogged and sampled to provide a better understanding of the mineralogy and zonation of the pegmatite dikes. Mineral studies, particularly focusing on using muscovite as a vector for mineralization, will be one of the next steps of this project. Columbite-group minerals were also sampled for U-Pb geochronology studies to help determine the timing of deformation and emplacement of the pegmatite dikes.

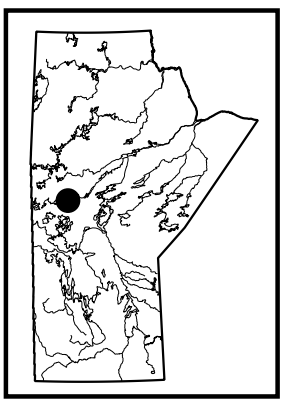

Regional geology

The Wekusko Lake pegmatite field (Černý et al., 1981) is located within the ca. 1.91–1.83 Ga Flin Flon–Glennie complex (Connors et al., 2002) of the Paleoproterozoic Trans-Hudson orogen (Figure GS2018-7-1; modified from the NATMAP Shield Margin Working Group, 1998; Bailes and Galley, 1999), an easterly trending belt approximately 140 km wide and 240 km long. Peak thermal metamorphism is interpreted to have occurred at

[1] Department of Earth Sciences, Western University, London, ON N6A 5B7

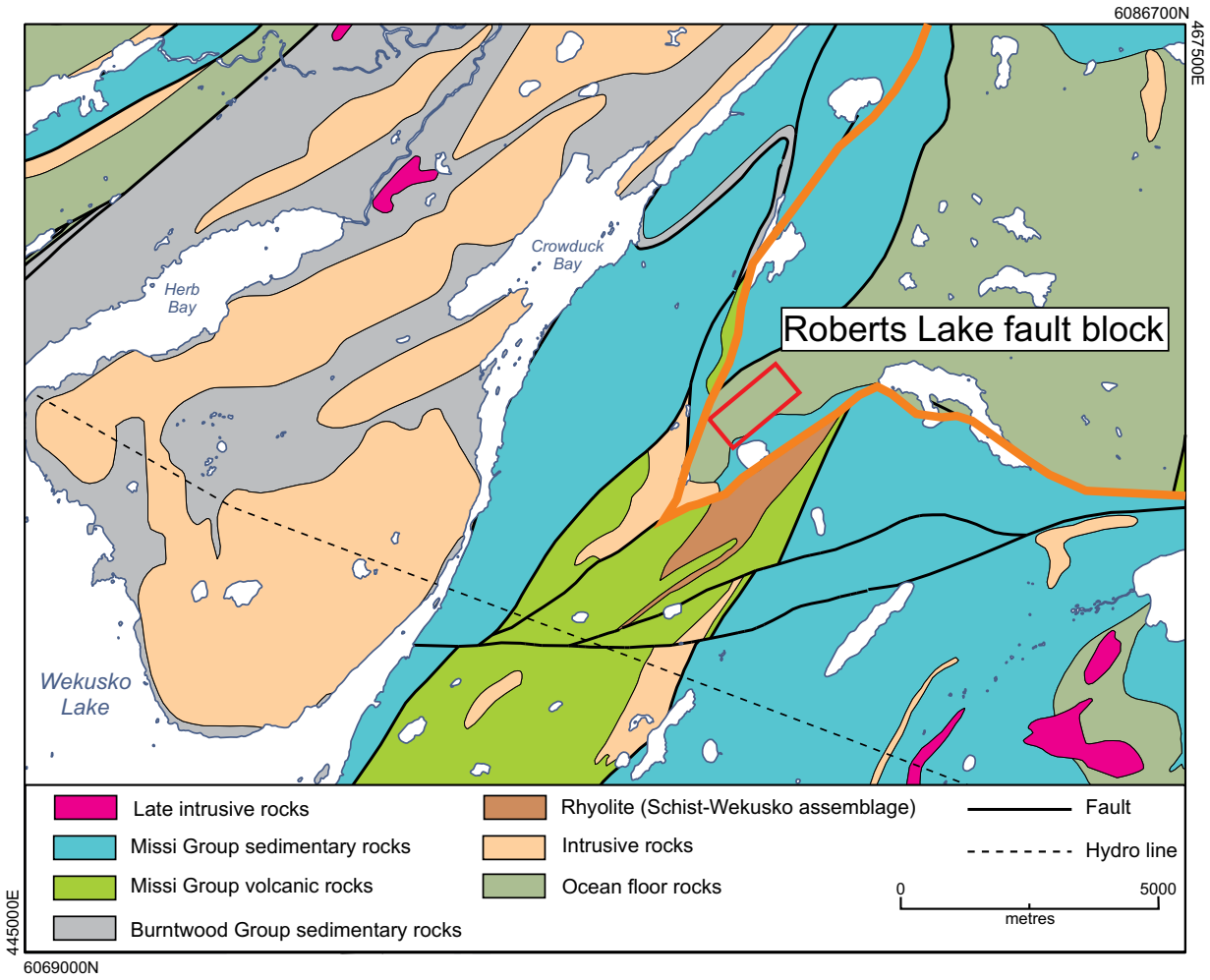

Figure GS2018-7-1: *Regional geology of the east side of Wekusko Lake, central Manitoba. The red square outlines the Green Bay group pegmatite mapping area, and the orange line outlines the Roberts Lake fault block (modified and simplified from NATMAP Shield Margin Working Group, 1998).*

ca. 1.81 Ga, and a sillimanite+garnet-in isograd is mapped in the vicinity of the Wekusko Lake pegmatite field (Connors et al., 2002). The region has undergone five deformation and folding events (D_1 to D_5; Kraus and Williams, 1999; Connors et al., 2002). The first three are linked to the thrusting of the Kisseynew basin over the Flin Flon belt (Kraus and Williams, 1999). This resulted in isoclinal folding and low-angle shear zones. Deformation phase D_4 is associated with east-west shortening during the underthrusting of the Superior plate, which resulted in north-northeast folds. Deformation event D_5 is associated with the renewal of the north-south convergence (Kraus and Williams, 1999).

The pegmatites that are the focus of this report are part of the Green Bay group within the Wekusko Lake pegmatite field (Černý et al., 1981). The studied pegmatites are hosted primarily by a mafic volcanic assemblage. The mafic volcanic assemblage is unconformably overlain by Missi group metasedimentary rocks (Connors et al., 1999). These units make up the Roberts Lake fault block (Figure GS2018-7-1; Connors et al., 1999, 2002). This block is bound to the west by a north-northeast-trending fault and to the south by an east-northeast-trending fault. The two faults meet at the southwestern corner of the Roberts Lake fault block.

Multiple mafic and felsic intrusive events, both syn- and late tectonic, occurred in the Flin Flon belt (Černý et al., 1981; Kraus and Williams, 1999). These events ranged from large granite plutons to smaller dikes, sills and stocks. The emplacement of the granitic pegmatites is thought to be the last intrusive event (Černý et al., 1981; Kraus and Williams, 1999), although folding in the pegmatites may indicate that these dikes could have been emplaced prior to some less or undeformed granitoid bodies. The genetic relationship between the various granitic bodies and the pegmatites in the area remains unclear (Černý et al., 1981).

Unit descriptions

Mafic volcanic rocks (unit 1)

Amphibolite, likely derived from mafic volcanic rock, (Figure GS2018-7-2a) is the predominant map unit in the study area. The amphibolite is host to the pegmatite dikes, is fine grained (<1 mm), foliated and folded, and consists mostly of hornblende, lesser plagioclase and local garnet. Fresh surfaces are dark green and weather to dark grey. Quartz veins occur locally and range in width from veinlets that are less than 1 cm wide to veins up to 30 cm wide. Observed folding is consistent with the regional folding events, with both tight and gentle folds. Foliation in the amphibolite is commonly deflected at the boundary with pegmatite dikes. Aphyric pillow basalt was observed at two outcrops (Figure GS2018-7-2b; Benn et al., 2018), suggesting a subaqueous depositional environment. Pillows are slightly flattened with recessive selvages of darker grey colour. Vesicles are visible at the edges of the pillows. Younging directions could not be determined with certainty but limited observations at one outcrop suggested younging to the east.

The major- and trace-element compositions of mafic volcanic rock samples from outcrop and drillcore are given in Table GS2018-7-1. The SiO_2 content of samples ranges from 45.98 to 51.78 wt. %, MgO from 4.61 to 7.93 wt. % and the average Mg# is 43.73. Samples plotted in the basalt and basaltic andesite sections of a total alkali silica diagram (Figure GS2018-7-3a). The chondrite-normalized rare-earth-element (REE) profiles are relatively flat (Figure GS2018-7-3b), typical of normal mid-ocean-ridge basalt (N-MORB). This supports the previous interpretation (NATMAP Shield Margin Working Group, 1998; Syme et al., 1999) that the amphibolite host unit in the Wekusko Lake pegmatite field is similar to modern ocean-floor basalt.

Quartzofeldspathic gneiss

Quartzofeldspathic gneiss is present in the southern and western parts of the map area (Figure GS2018-7-2c; Benn et al., 2018); it is interpreted as part of the Missi group. It is a feldspar-quartz-biotite metasedimentary gneiss with medium grey fresh surfaces and pink weathered surfaces. It is fine grained (1–2 mm) and strongly foliated. The foliation is dipping greater than 50° and strikes to both the northeast and southwest. Dike 1 intruded into this unit at the southernmost end of the dike, where it quickly thins from 2 m to 30 cm. Quartzofeldspathic gneiss may act as a rheologic control on the pegmatite dikes. Very few pegmatite dikes, other than Dike 1, are hosted by the quartzofeldspathic gneiss unit. These dikes are typically less than 10 cm wide and are barren of Li mineralization.

Garnet-biotite gneiss

Garnet-biotite gneiss, only locally present in the southwestern corner of the map area, is interpreted as part of the Burntwood Group. It is fine grained, mainly composed of feldspar, biotite and garnet with dark grey fresh surfaces. Locally, fine-grained (<2 mm) pink feldspar augens are present and weather to a brown colour. No pegmatite dikes were found intruding this unit.

Granitic pegmatite

Most pegmatite dikes in the map area consist of quartz, K-feldspar, albite, muscovite, spodumene and tourmaline with accessory beryl, Fe-Mn phosphate minerals, apatite, garnet and columbite-group minerals. The spodumene-bearing dikes can be classified as part of the rare-element (REL) class, REL-Li subclass, complex type, spodumene subtype, as per the classification scheme of Černý and Ercit (2005). The pegmatite dikes range in colour from red to white depending on the K-feldspar to albite ratio, with albite-rich zones being white. The pegmatite dikes are very coarse grained with crystals of up to 30 cm in length. The pegmatite contact with the host mafic volcanic rocks shows no observable chilled margin. Tourmaline and local muscovite formed comb structures that are perpendicular to the contacts and are interpreted as growth from the border zones into the wall zones (Figure GS2018-7-2c). Locally, an aplitic phase is present throughout the pegmatite dikes and ranges in size from 5 to 30 cm. The patches contain a similar mineralogy to the surrounding pegmatite. At the north tip of Dike 1, elongation and stretching of minerals was observed (Figure GS2018-7-2d). Deformation in Dike 1 was previously reported by Martins et al. (2017) in feldspar and muscovite (e.g., kink bands in muscovite), which suggests that pegmatite emplacement was prior to the latest stages of regional deformation.

There are at least eight large (>1 m wide) dikes exposed in the map area, all oriented to the southeast. The dikes are folded and undulating over several metres (Figure GS2018-7-2e). The largest dike known (Dike 1) varies from 1 to 15 m wide and is 300 m long at surface. It is hosted by the mafic volcanic rocks except for at its southern tip, where it thins and disappears over a few metres in quartzofeldspathic gneiss (as described above). The thicker dikes show less folding at the surface. As a result, Dike 1 is relatively planar throughout most of its length and is folded only near its northern tip.

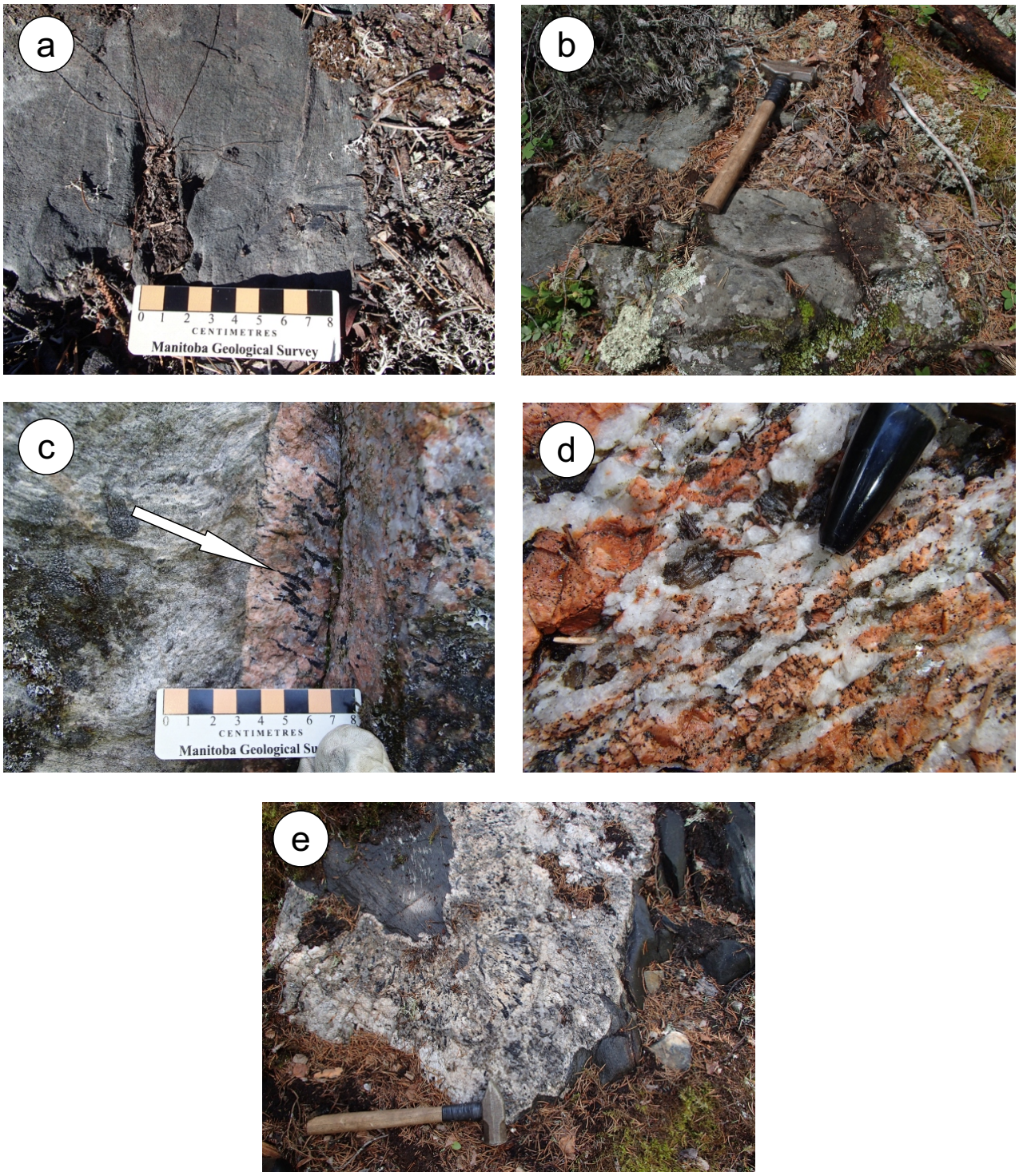

Figure GS2018-7-2: *Outcrop photographs of the map units in the northeastern block of the Wekusko Lake pegmatite field:* ***a)*** *amphibolite, likely derived from massive mafic volcanic rock;* ***b)*** *pillow basalt (hammer for scale, hammer head points north);* ***c)*** *pegmatite dike hosted in quartzofeldspathic gneiss showing tourmaline comb texture perpendicular to the margins of the pegmatite dike (arrow points to tourmaline);* ***d)*** *stretched feldspars from the north edge of Dike 1 (pen tip for scale is 1.5 cm long);* ***e)*** *folded pegmatite dike hosted by amphibolite likely derived from massive mafic volcanic rock (hammer for scale).*

Table GS2018-7-1: Whole-rock geochemical results of the massive and pillow basalt.

Sample	113-18-D007	113-18-16-004-7.5 m	113-18-18-23-325 m	113-18-18-23-33 m	113-18-18-23-182 m	113-18-D088
Rock type	Massive basalt	Massive basalt	Massive basalt	Massive basalt	Massive basalt	Pillow basalt
SiO_2	51.78	45.98	51.14	50.6	48.02	49.01
Al_2O_3	11.84	14.5	14.05	13.5	14.7	13.55
Fe_2O_3	18.95	19.82	13.18	13.44	14.48	13.18
MnO	0.237	0.185	0.184	0.188	0.204	0.199
MgO	4.61	7.44	7.29	7.45	7.93	7.03
CaO	7.84	7.68	10.24	10.33	10.67	9.65
Na_2O	2.79	2.38	2.51	2.54	2.36	2.66
K_2O	0.27	0.13	0.23	0.17	0.19	0.53
TiO_2	2.174	1.729	1.058	1.141	1.141	1.184
P_2O_5	0.15	0.12	0.08	0.08	0.09	0.09
LOI	0.17	0.53	0.76	0.66	0.78	3.44
Total	100.8	100.5	100.7	100.1	100.6	100.5
Sc	47	41	44	46	48	45
Be	<1	<1	<1	<1	<1	<1
V	601	476	345	362	377	365
Cr	<20	50	180	170	190	230
Co	51	75	44	46	50	44
Ni	30	200	90	80	110	100
Cu	170	100	150	140	210	60
Zn	150	130	90	90	100	80
Ga	20	19	17	14	18	17
Ge	1.2	1.4	1.4	1.3	1.4	1.2
As	<5	6	10	<5	25	18
Rb	<1	<1	<1	<1	<1	1
Sr	114	108	137	131	162	161
Y	40.8	29.4	21.5	22.2	23	23.6
Zr	135	95	61	63	67	68
Nb	5.3	4.6	2.2	2.6	1.8	2.3
Mo	<2	<2	<2	<2	<2	<2
Ag	<0.5	<0.5	<0.5	<0.5	<0.5	<0.5
In	0.1	<0.1	<0.1	<0.1	<0.1	<0.1
Sn	<1	<1	<1	<1	<1	<1
Sb	0.2	0.3	0.6	0.4	0.9	0.4
Cs	<0.1	<0.1	0.1	<0.1	<0.1	<0.1
Ba	30	16	35	44	22	63
La	9.3	2.57	3.48	2.92	2.6	3.36
Ce	24.9	8.37	9.6	8.28	7.88	9.67
Pr	3.51	1.51	1.42	1.3	1.29	1.48
Nd	16.9	8.08	7.17	6.95	7.03	6.99
Sm	5	3.44	2.13	2.42	2.47	2.69
Eu	1.68	1.29	0.821	0.878	0.76	0.97
Gd	5.76	3.94	2.78	2.76	3.27	3.31
Tb	1.05	0.76	0.53	0.55	0.59	0.6
Dy	6.95	4.87	3.57	3.65	4.05	4.07
Ho	1.46	1.03	0.76	0.77	0.86	0.87

Table GS2018-7-1 (continued): Whole-rock geochemical results of the massive and pillow basalt.

Sample	113-18-D007	113-18-16-004-7.5 m	113-18-18-23-325 m	113-18-18-23-33 m	113-18-18-23-182 m	113-18-D088
Rock type	Massive basalt	Massive basalt	Massive basalt	Massive basalt	Massive basalt	Pillow basalt
Er	4.26	3.03	2.19	2.25	2.44	2.48
Tm	0.641	0.46	0.318	0.332	0.352	0.357
Yb	4.22	3.06	2.11	2.07	2.37	2.35
Lu	0.634	0.468	0.326	0.336	0.37	0.38
Hf	3.1	2.1	1.4	1.4	1.5	1.6
Ta	0.43	0.33	0.2	0.17	0.22	0.24
W	1.9	1.6	2.5	1.4	1.7	2.7
Tl	<0.05	<0.05	<0.05	<0.05	<0.05	<0.05
Pb	<5	<5	<5	<5	<5	<5
Bi	<0.1	<0.1	<0.1	<0.1	<0.1	<0.1
Th	0.58	0.39	0.27	0.22	0.19	0.23
U	0.17	0.13	0.14	0.1	0.07	0.09

Samples were submitted to Actlabs (Ancaster, ON) for major- and trace-element analyses using research-grade lithogeochemistry package (4Litho-research)

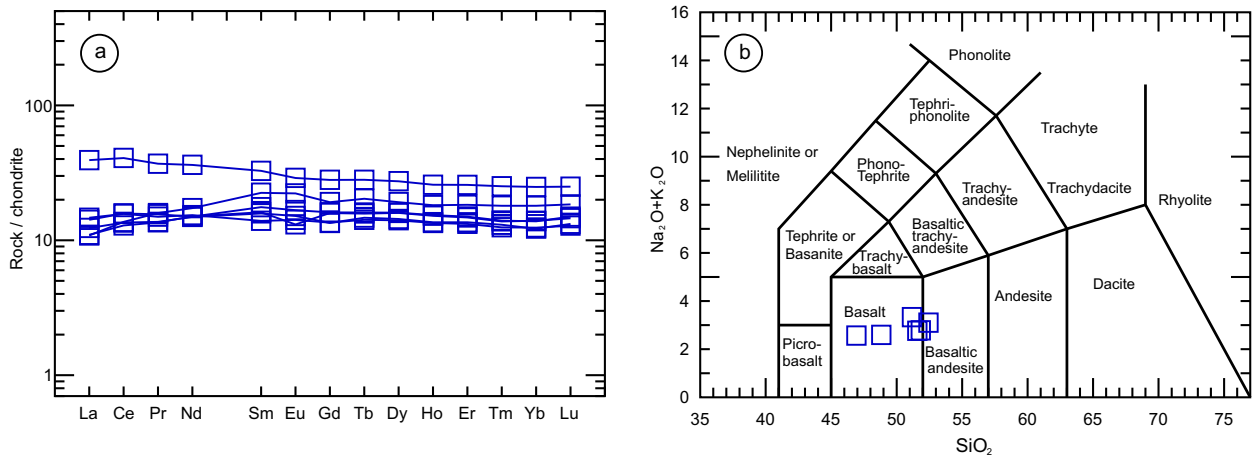

Figure GS2018-7-3: *Major- and trace-element diagrams for mafic volcanic rocks (unit 1):* ***a)*** *total alkalis versus silica (TAS) diagram (after Le Maître et al., 2002);* ***b)*** *chondrite-normalized rare-earth-element spider profile. Normalizing values for chondrite are from Sun and McDonough (1989).*

Other dikes such as Dike 7 and 8, which are 5–10 m thick, show much more folding and undulation. Dike thicknesses change locally as they pinch and swell. Thin, granitic dikes (<30 cm) and dikelets (<1 cm) are also present in the study area. Pegmatites locally exhibit tight folding, and at some locations the pegmatite has folded over on itself causing ballooning (Figure GS2018-7-4). No known Li mineralization is associated with the thin dikes and dikelets.

Mineralogy of the Li-bearing pegmatites

Spodumene is present in three phases in pegmatites at the Wekusko Lake pegmatite field (Martins et al., 2017). The first and most common phase (Figure GS2018-7-5) is euhedral to subhedral and very coarse grained (crystals up to 30 cm in diameter occurring locally). The spodumene is a pale green colour, likely due to Fe impurities (London, 2017). The second phase is fine grained (<2 mm), has a grey-green colour and is intergrown with quartz. The third phase is interstitial spodumene. It is very fine grained and forms small masses between larger, well-developed crystals, suggesting a late crystallization.

There are at least two phases of muscovite as observed by Martins et al. (2017). The first is coarse-grained (<5 cm) subhedral books that are interpreted as primary. Muscovite is present locally as comb structures in the wall zone where it is intergrown with tourmaline, which suggests that these two minerals crystalized at the same time. The second phase of muscovite is secondary

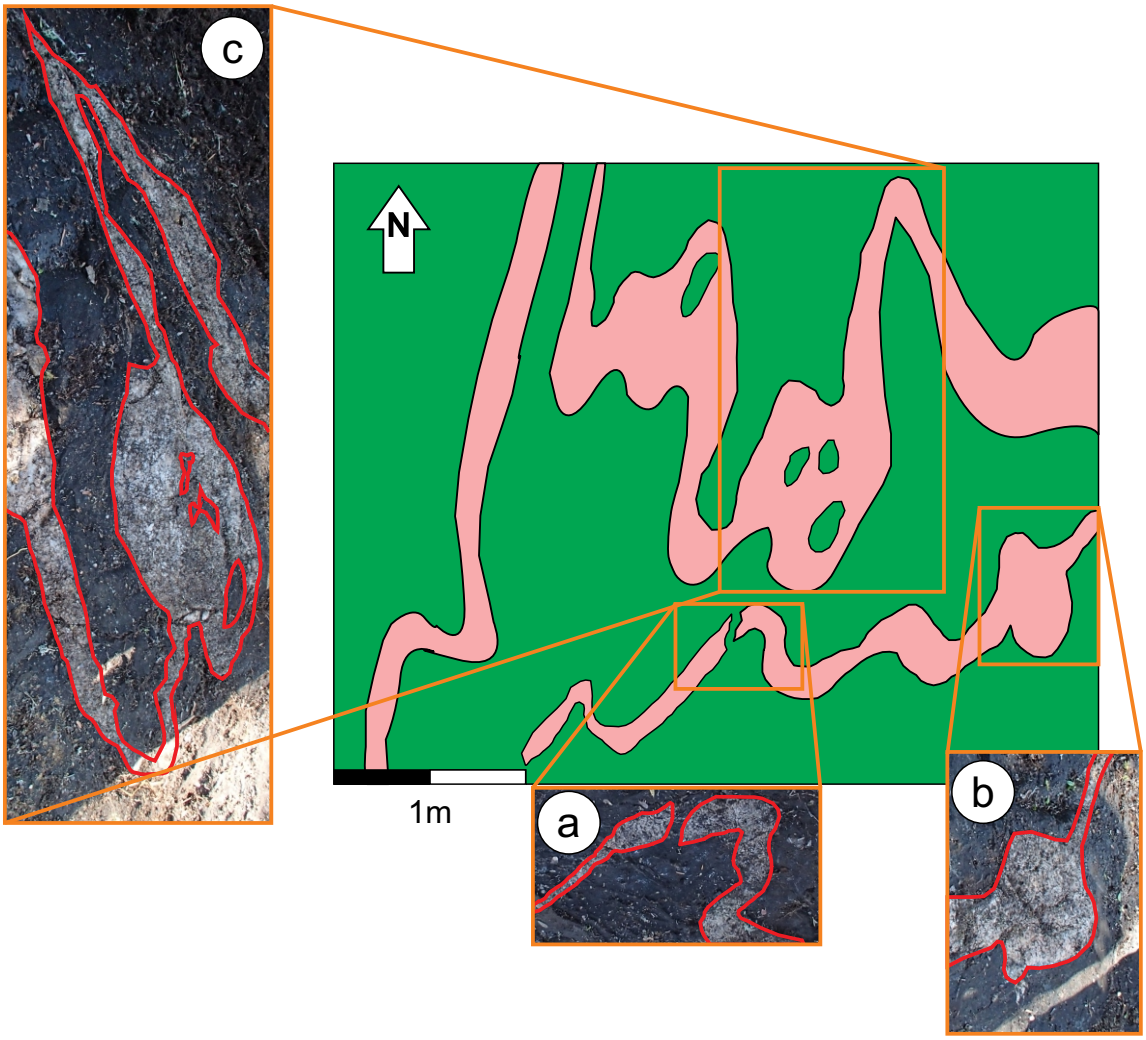

Figure GS2018-7-4: *Sketch and outcrop photos showing folding in pegmatite near Dike 7:* ***a)*** *break in folded pegmatite;* ***b)*** *ballooning in pegmatite;* ***c)*** *ballooning in pegmatite with mafic volcanic xenoliths.*

and is present as fine-grained masses. The secondary muscovite is most commonly found in the wall zone and decreases in abundance toward the centre of the dike.

At least two varieties of feldspar are present. The first occurs as creamy white, very coarse grained crystals (<20 cm) that are likely albite, although perthitic and graphic textures indicate that at least some of the white crystals are K-feldspar. The second is a brick red K-feldspar that occurs as interstitial masses.

Trace amounts of apatite, Fe-Mn phosphate minerals, columbite-group minerals and beryl are present. The apatite is fine grained (<1 mm), has a dark blue colour and is present primarily in the central zone. The phosphate minerals are dark red to brown, medium grained (<1 cm) and present in the central zone of the pegmatite. These phosphates are thought to be part of the triphylite (Fe^{2+}) to lithiophilite (Mn^{2+}) series. Columbite-group minerals are present as black, fine-grained needles (<1 mm) and likely explain the elevated Ta and Nb assay values; identification of the Nb-Ta phases will be undertaken by future petrography. Dikes 1, 5 and 8 all have Ta assay values above 100 ppm (FAR Resources Ltd., 2017, 2018). Columbite-group minerals most commonly occur in the central zone. Beryl forms stubby, white, opaque, euhedral to subhedral, medium-grained (<2 cm) crystals. Beryl potentially explains the Cs anomalies in the pegmatites (Černý and Simpson, 1977), although Cs also substitutes into K-feldspar and mica. Beryl occurs in all zones within the pegmatite, but it is most commonly observed in the wall zone. It is difficult, however, to identify in the central zone because it is easily confused for albite.

Zoning of the Li-bearing pegmatites

Based on observations from drillcore from 29 drillholes, 5 zones for the Li-bearing pegmatite dikes were recognized: the border zone, the wall zone, the inter-

Figure GS2018-7-5: *Primary, phase one spodumene crystal from halved drillcore; coin for scale (arrow points to the spodumene crystal).*

mediate zone, the central zone and the core zone. This builds on the work of Martins et al. (2017), although the border zone was not identified in that study. These zones are not apparent in all eight dikes or at all depths within the dikes. Thin dikes, in particular, tend to lack the central or core zones, and the width of the different zones greatly varies between the dikes. The zones vary in grain size and mineralogy, but grain sizes generally increase toward the centre of the dike. There is a colour variation from red to salmon pink to white from the wall zone to the intermediate zone to the central zone. This may be due to variations in the contents of K-feldspar and albite although the red colour (due to hematization) may also be the result of greater external fluid interaction near pegmatite contacts (Gysi et al., 2016). Detailed feldspar mineralogy will be investigated in the future using petrography and Raman spectroscopy.

Border zone

The border zone is the outermost, smallest zone and is not always present. It is up to 1 cm wide along the outer edge of the pegmatite. The border zone is composed primarily of quartz, muscovite, feldspar and tourmaline. Grain sizes are between 0.5 and 2 mm.

Wall zone

The wall zone (Figure GS2018-7-6a) is composed of K-feldspar, quartz, muscovite, albite and tourmaline with accessory beryl, spodumene and apatite and has a brick red colour. Muscovite is present as both primary and secondary phases. Tourmaline commonly forms comb structures perpendicular to the pegmatite contact. Grain sizes are typically between 0.25 and 2 cm; however, it is not uncommon for larger crystals to be present in the wall zone.

Intermediate zone

The intermediate zone (Figure GS2018-7-6b, c) is composed of albite, K-feldspar, quartz, muscovite and spodumene (5%). Grain sizes range from 0.5 to 5 cm with rare crystals up to 10 cm in length. All three phases of spodumene can be present in this zone. The albite to K-feldspar ratio is approximately 1:1, which gives the zone a salmon pink colour. The K-feldspar forms fine-grained (<0.5 cm) masses, whereas albite occurs as larger subhedral crystals (3–5 cm).

Central zone

The central zone (Figure GS2018-7-6d) is composed of albite, spodumene, quartz and muscovite with accessory apatite, columbite-group minerals and Fe-Mn phosphate minerals, but the central zone is not always present. The central zone contains the highest concentrations of spodumene varying from 10 to 30 modal percent and locally up to 50 modal percent. The average grain size ranges from 3 to 10 cm, with some crystals up to 15 cm long. The central zone has a greyish white colour due to the presence of albite and quartz. Spodumene is mostly seen as euhedral to subhedral crystals between 3 and 6 cm long. Muscovite is present in euhedral to subhedral coarse-grained books.

Core zone

The core zone is the innermost zone of the dike and is composed predominantly of quartz and albite, with minor spodumene (<5%). The grain sizes range from 3 to 10 cm, locally with crystals up to 20 cm long. Spodumene is typically present as large euhedral to subhedral crystals up to 15 cm long. The core zone replaced the central zone in some thinner sections of the dike, but this zone is not always present.

Future work

During this study, samples were collected from all zones and pegmatites at varying depths. Sampling focused on obtaining both primary and secondary muscovite crystals to determine their Li content and to evaluate whether muscovite chemistry is related to the proximity of spodumene or the spodumene grade of a pegmatite zone. Samples of drillcore with high Nb and Ta values were also targeted for geochronology studies.

Lithium substitutions mostly occur in the octahedrally coordinated sites and minor Li^{+}–K^{+} substitution may also occur in the interlayer (Brigatti et al., 2001); therefore, the Li content of the muscovite may reflect the Li content in the melt. Thus, muscovite has the potential

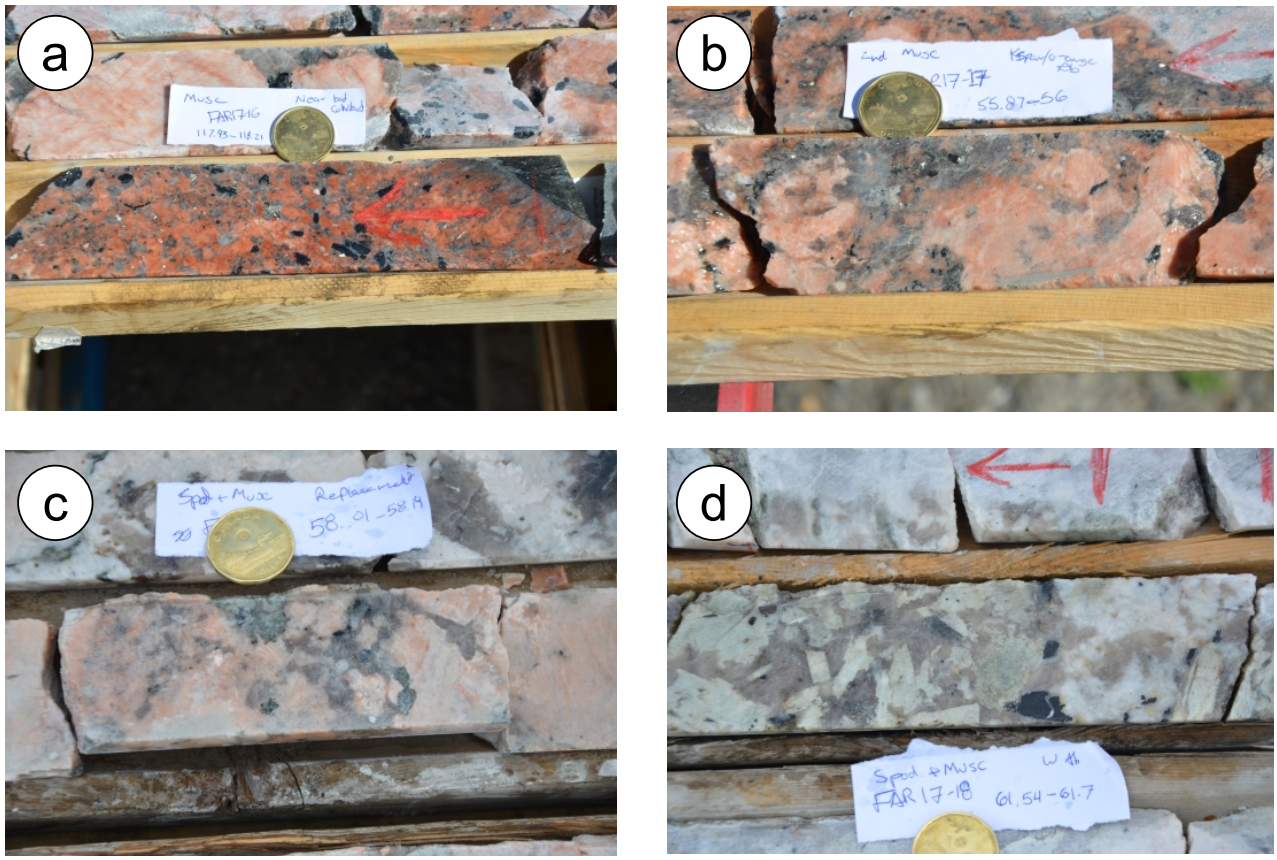

***Figure GS2018-7-6**: Drillcore displaying the transition from **a)** the brick red wall zone to **b)**, **c)** the salmon pink intermediate zone to **d)** the white central zone. Coins for scale.*

to be an indicator mineral for Li exploration in pegmatites; i.e. the Li content of muscovite could indicate the potential for Li mineralization where spodumene is not present in a sample. Lithium content will be determined by laser-ablation inductively coupled plasma–mass spectroscopy (LA-ICP-MS). Peak shifts related to the muscovite molecular structure (muscovite to polylithionite) will be measured by portable Raman spectroscopy and calibrated by LA-ICP-MS to evaluate the utility of portable Raman spectroscopy in Li pegmatite exploration. The portable Raman spectrometer will also be used to determine feldspar compositions (albite versus K-feldspar) and this instrument will be evaluated as a more general tool for use in pegmatite exploration.

Geochronology studies on columbite-group minerals will help determine the timing of the pegmatite emplacement in relation to the peak metamorphism and deformation history of the region.

Economic considerations

Manitoba is highly prospective for Li pegmatites. This includes the Green Bay group of the Wekusko Lake pegmatite field, which contains at least eight large Li-bearing pegmatite dikes. Of those, two contain central zones with more than 2 wt. % Li_2O (FAR Resources Ltd., 2017; FAR Resources Ltd., 2018 lists additional assay results). The Li content within mica grains will be tested to identify the proximity to high spodumene concentrations and to identify the central zone (where spodumene is most abundant) within pegmatite. It is anticipated that variations of Li between mica grains within pegmatite can act as a vector to identify the central zone.

The largest dikes in the Green Bay group of the Wekusko Lake pegmatite field contain central zones with increased abundances of Ta and Nb, hosted by columbite-group minerals. The white colour and stubby crystal habit of the beryl is thought to be related to high Cs values within the mineral structure. The origin of these concentrations is currently under investigation.

Acknowledgments

The authors thank A. Hutchins from the University of Manitoba for providing enthusiastic field assistance. FAR Resources Ltd. is thanked for access to drillcore, field and helicopter support. This project would have not happened without the support of the late K. Anderson,

who is missed. Strider Resources Ltd. is acknowledged for access to light detection and ranging (LiDAR) imagery. Field and logistical support from the Manitoba Geological Survey are also gratefully acknowledged. Discussions with M. Fedikow, J. Singh, D. Ziehlke and J. Ziehlke greatly benefited this project. This study is supported by a Targeted Geoscience Initiative Phase 5 Program grant to R. Linnen from Natural Resources Canada. Critical reviews from K. Reid and C. Böhm are truly appreciated.

References

Bailes, A.H. and Galley, A.G. 1999: Evolution of the Paleoproterozoic Snow lake arc assemblage and geodynamic setting for associated volcanic-hosted massive sulphide deposits, Flin Flon belt, Manitoba, Canada; Canadian Journal of Earth Sciences, v. 36, no. 11, p. 1789–1805.

Benn, D., Martins, T., Linnen, R.L., Ziehlke, J. and Singh, J. 2018: Bedrock geology of the Wekusko Lake pegmatite field (northeastern block), central Manitoba (part of NTS 63J13); Manitoba Growth Enterprise and Trade, Preliminary Map PMAP2018-2, scale 1:4000.

Brigatti, M.F., Kile, D.E. and Poppi, M. 2001: Crystal structure and crystal chemistry of lithium-bearing muscovite-2m1; The Canadian Mineralogist, v. 39, no. 4, p. 1171–1180.

Černý, P. 2005: The Tanco rare element pegmatite deposit, Manitoba: regional context, internal anatomy and global comparisons; *in* Rare element geochemistry and ore deposits, R.L. Linnen and I.M. Samson (ed.), Geological Association of Canada, Short Course Notes, v. 17, p. 127–158.

Černý, P. and Ercit, T.S. 2005: The classification of granitic pegmatites revisited; The Canadian Mineralogist, v. 43, no. 6, p. 2005–2026.

Černý, P. and Simpson, F.M. 1977: The Tanco pegmatite at Bernic Lake, Manitoba: IX, Beryl; The Canadian Mineralogist, v. 15, no. 4, p. 489–499.

Černý, P., Trueman, D.L., Zeihlke, D.V., Goad, B.E. and Paul, B.J. 1981: The Cat Lake–Winnipeg River and the Wekusko Lake pegmatite fields, Manitoba; Manitoba, Department of Energy and Mines, Mineral Resources Division, Economic Geology Report ER80-1, 216 p. plus 5 maps.

Connors, K.A., Ansdell, K.M. and Lucas, S.B. 1999: Coeval sedimentation, magmatism, and fold-thrust development in the Trans-Hudson Orogen: propagation of deformation into an active continental arc setting, Wekusko Lake area, Manitoba; Canadian Journal of Earth Sciences, v. 36, no. 2, p. 275–291.

Connors, K., Ansdell, K. and Lucas, S. 2002: Development of a transverse to orogen parallel extension lineation in a complex collisional setting, Trans-Hudson Orogen, Manitoba, Canada; Journal of Structural Geology, v. 24, no. 1, p. 89–106.

Gysi, A.P., Williams-Jones, A.E. and Collins, P. 2016: Lithogeochemical vectors for hydrothermal processes in the Strange Lake peralkaline granitic REE-Zr-Nb deposit; Economic Geology, v. 111, no. 5, p. 1241–1276.

FAR Resources Ltd. 2017: Phase 3 drilling; FAR Resources Ltd., URL <https://www.farresources.com/phase-3-drilling/> [August 2018].

FAR Resources Ltd. 2018: Phase 4 drilling; FAR Resources Ltd., URL <https://www.farresources.com/phase-4-drilling/> [August 2018].

Kraus, J. and Williams, P.F. 1999: Structural development of the Snow Lake allochthon and its role in the evolution of the southeastern Trans-Hudson Orogen in Manitoba, central Canada; Canadian Journal of Earth Sciences, v. 36, no. 11, p. 1881–1899.

Le Maître, R.W., Streckeisen, A., Zanettin, B., Le Bas, M.J., Bonin, B. and Bateman, P., ed. 2002: Igneous Rocks: A Classification and Glossary of Terms: Recommendations of the International Union of Geological Sciences Subcommission on the Systematics of Igneous Rocks (2nd ed.); Cambridge University Press, 256 p.

London, D. 2017: Reading pegmatites: part 3—what lithium minerals say; Rocks & Minerals, v. 92, no. 2, p. 144–157.

Martins, T., Linnen, R.L., Fedikow, M.A.F. and Singh, J. 2017: Whole-rock and mineral geochemistry as exploration tools for rare-element pegmatite in Manitoba: examples from the Cat Lake–Winnipeg River and Wekusko Lake pegmatite fields (parts of NTS 52L6, 63J13); *in* Report of Activities 2017, Manitoba Growth, Enterprise and Trade, Manitoba Geological Survey, p. 42–51.

NATMAP Shield Margin Project Working Group 1998: Geology, NATMAP shield margin project area (Flin Flon Belt), Manitoba/Saskatchewan; Geological Survey of Canada, Map 1968A, scale 1:100 000.

Sun, S. and McDonough, W.F. 1989: Chemical and isotopic systematics of oceanic basalts: implications for mantle composition and processes; Geological Society of London, Special Publication, v. 42, p. 313–345.

Syme, E. C., Lucas, S. B., Bailes, A. H. and Stern, R. A. 1999: Contrasting arc and MORB-like assemblages in the Paleoproterozoic Flin Flon belt, Manitoba, and the role of intra-arc extension in localizing volcanic-hosted massive sulphide deposits; Canadian Journal of Earth Sciences, v. 36, no. 11, p. 1767–1788.

GS2018-8

Tectonic setting of the Gordon gold deposit, Lynn Lake greenstone belt, northwestern Manitoba (parts of NTS 64C16): evidence from lithogeochemistry, Nd isotopes and U-Pb geochronology

by X.M. Yang and C.J.M. Lawley[1]

In Brief:

- Supracrustal rocks in the Farley Lake area formed in an island-arc to back-arc setting with depleted-mantle sourced volcanism
- Tectonic evolution is reflected by granitoid intrusions ranging from arc, I-type; intra-arc, extension-related, A-type; to late adakite-like
- The latter are ca. 1854 Ma and provide important structural-chemical controls for localization of auriferous vein systems

Citation:
Yang, X.M. and Lawley, C.J.M. 2018: Tectonic setting of the Gordon gold deposit, Lynn Lake greenstone belt, northwestern Manitoba (parts of NTS 64C16): evidence from lithogeochemistry, Nd isotopes and U-Pb geochronology; *in* Report of Activities 2018, Manitoba Growth, Enterprise and Trade, Manitoba Geological Survey, p. 89–109.

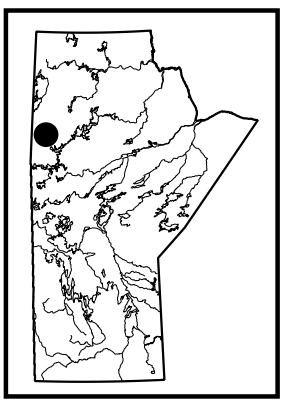

Summary

This report combines new lithogeochemical and Nd isotopic data with previously reported U-Pb zircon geochronological data for supracrustal and intrusive rocks at the Gordon Au deposit in the Farley Lake area, northern part of the Paleoproterozoic Lynn Lake greenstone belt, northwestern Manitoba. Auriferous veins are hosted primarily in unit 4 banded iron formation, which represents part of an interflow sedimentary succession that is coeval with volcanic and volcaniclastic rocks and was intruded by a series of distinct granitoid suites. The volcanic and volcaniclastic rocks (units 1 to 3) share geochemical similarities with modern island-arc volcanic rocks, whereas marine sedimentary rocks intercalated with lesser volcaniclastic rocks (unit 4) were likely deposited in a back-arc setting.

Recent, sensitive high-resolution ion microprobe (SHRIMP) U-Pb zircon ages, together with new lithogeochemical results, establish the following sequence of granitoid magmatism: 1) ca. 1879 Ma, pre–Sickle group, arc, I-type granodiorite-monzogranite (unit 6); 2) ca. 1872 Ma, A-type, alkali-feldspar granite to syenogranite (unit 7) with intra-arc extensional affinity; and 3) ca. 1854 Ma, syn– to post–Sickle group, quartz diorite to monzodiorite (unit 8) formed in a syn- to late-accretionary environment. Quartz diorite samples yielded compositional characteristics that resemble adakites and/or sanukitoids, suggesting derivation from partial melting of previously metasomatized, sub-arc lithospheric mantle. Quartz diorite is coeval with the ca. 1.85 Ga Wathaman-Chipewyan batholith, which marks the terminal, accretionary collision of the Lynn Lake greenstone belt and the Hearne craton to the north. Auriferous veins hosted by pre– to syn–peak metamorphic D_2 faults and related splays, as well as favourable hostrocks (i.e., unit 4 banded iron formation, and units 2 and 3 iron-rich, tholeiitic volcanic and volcaniclastic rocks) that destabilized Au-S complexes within hydrothermal fluids, represent the two dominant ore-system controls.

Adakite-like intermediate intrusions at 1854 Ma significantly predate metamorphic ages and auriferous veins in the Lynn Lake greenstone belt (ca. 1810–1780 Ma). The cospatial relationship between Au deposits and the ca. 1.85 Ga suite, however, suggests that the structural architecture that was later reactivated by auriferous veins was established prior to the continent-continent collision between the composite Hearne and Superior cratons at ca. 1.80 Ga. A similar spatial association between the ca. 1.85 Ga magmatic suite and structures is also documented at the MacLellan Au-Ag deposit (i.e., the 1857 Ma Burge Lake pluton), suggesting that intrusions of this suite may demarcate favourable lithological assemblages and/or structural architecture as main controls for Au deposits.

Introduction

In 2018, the Manitoba Geological Survey (MGS) continued its multiyear bedrock mapping project in the Paleoproterozoic Lynn Lake greenstone belt (LLGB) of northwestern Manitoba (Figure GS2018-8-1). So far, three preliminary maps at 1:20 000 scale have been published by the MGS to cover type areas around the MacLellan Au-Ag, Gordon Au (formerly known as the Farley Lake mine) and Burnt Timber Au mines (Yang and

[1] Natural Resources Canada, Geological Survey of Canada, 601 Booth Street, Ottawa, ON K1A OE8

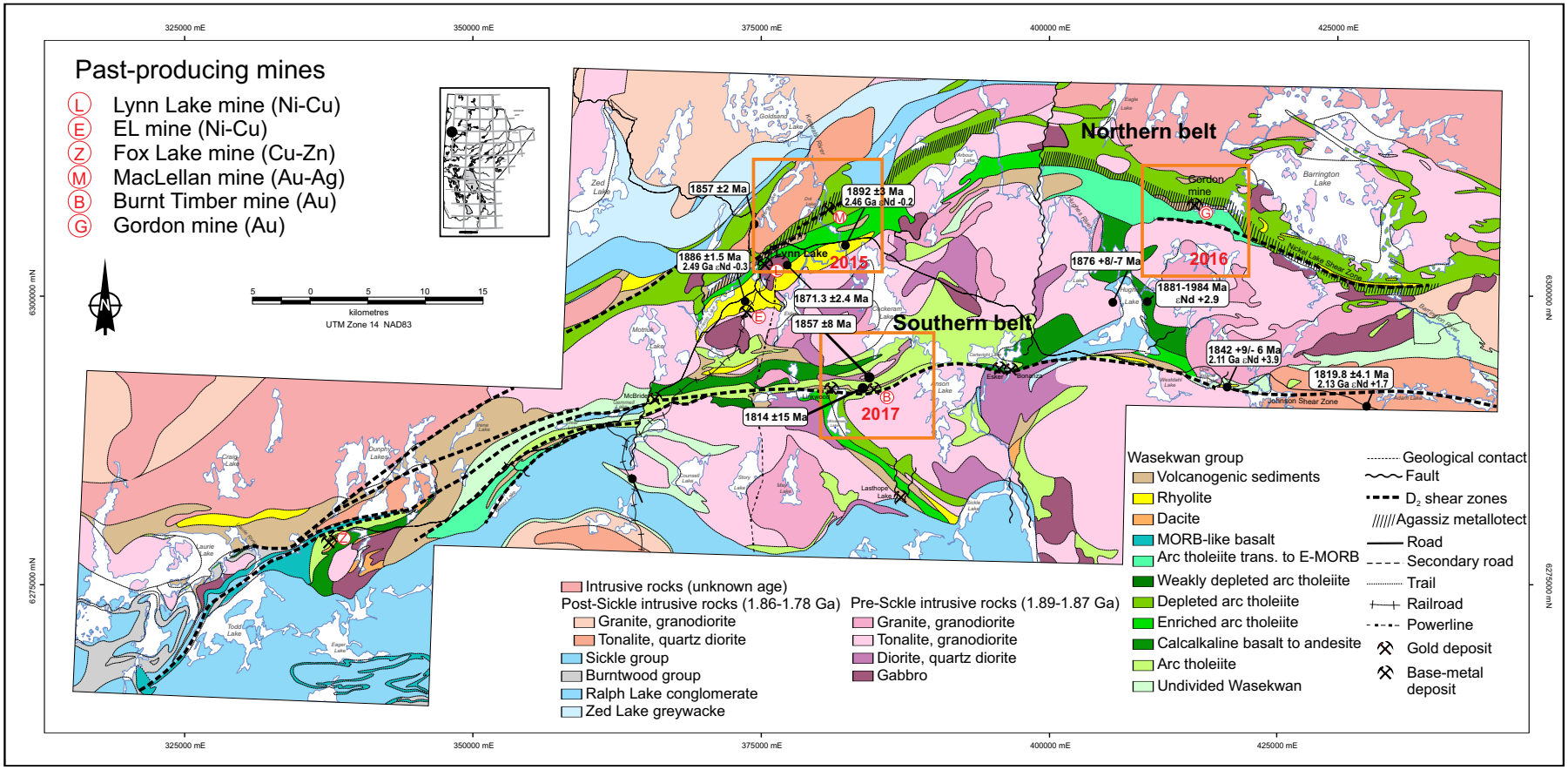

Figure GS2018-8-1: *Regional geology of the Lynn Lake greenstone belt, with U-Pb zircon ages and Nd isotopic compositions (modified and compiled from Gilbert et al., 1980; Manitoba Energy and Mines, 1986; Gilbert, 1993; Zwanzig et al., 1999; Turek et al., 2000; Beaumont-Smith and Böhm, 2002, 2003, 2004; Beaumont-Smith et al., 2006; Beaumont-Smith, unpublished data, 2006; Beaumont-Smith, 2008). Updated, detailed mapping areas at 1:20 000 scale are indicated by the orange boxes, including that surrounding the Gordon Au deposit (labelled 'G'). Abbreviations: MORB, mid-ocean–ridge basalt; E-MORB, enriched MORB; Trans., transitional.*

Beaumont-Smith, 2015, 2016a, 2017). These studies have identified favourable supracrustal rock successions, multiple suites of granitoid intrusions and structural-chemical controls important for localizing Au mineralization. The study of Au mineralization and its relationship with granitoid intrusions, regional metamorphism and structures is ongoing via collaborative research between the MGS and the Geological Survey of Canada (GSC) under Phase 5 of their Targeted Geoscience Initiative program (TGI-5). This report focuses on the timing and composition of magmatic and supracrustal rocks, tectonic implications for magmatism and their genetic relationship to Au mineralization.

This study combines new lithogeochemistry (n = 59 samples) and Nd-isotope (n = 6) datasets with previously published sensitive high-resolution ion microprobe (SHRIMP) U-Pb zircon ages (n = 3; Lawley et al., 2018) for the rock units of the Gordon Au deposit in the Farley Lake area. Together, the data provide geochemical and geochronological constraints to distinguish multiple magmatic suites, unravel the petrogenetic history of supracrustal and intrusive rocks, provide tectonic implications and explore the relationship between magmatism and Au metallogeny.

This report assigns diorite, quartz diorite and minor gabbroic rocks, defined by Yang and Beaumont-Smith (2016a, 2016b) as unit 6b, to a new unit 8 on the basis of SHRIMP U-Pb zircon age data (Lawley et al., 2018), and identifies the presence of arc I-type granitoids; intra-arc, extension-related, A-type granites; and late-orogenic, adakite-like quartz diorites. These intrusive rocks are interpreted to represent diverse tectonic settings, which would provide new insights into the tectonic evolution and Au metallogeny of the Farley Lake area.

General geology

The LLGB (Bateman, 1945) is a major tectonic element of the internal Reindeer zone of the Trans-Hudson orogen (Stauffer, 1984; Lewry and Collerson, 1990), which is the largest Paleoproterozoic orogenic belt of Laurentia (Hoffman, 1988; Corrigan et al., 2007, 2009). The LLGB is bounded to the north by the Southern Indian domain, composed of variably migmatitic metasedimentary rocks, various granitoids and minor metavolcanic rocks (Kremer et al., 2009). Synorogenic basins, including the Kisseynew metasedimentary domain, represent the southern limit of the LLGB (Gilbert et al., 1980; Fedikow and Gale, 1982; Syme, 1985; Zwanzig et al., 1999; Beaumont-Smith and Böhm, 2004; Zwanzig and Bailes, 2010). Paleoproterozoic greenstone belts with ages and lithological assemblages similar to the LLGB occur to the east (Rusty Lake belt), to the west (La Ronge belt) and to the far south (Flin Flon belt; e.g., Ansdell et al., 1999; Park et al., 2002; Ansdell, 2005; Corrigan et al., 2007, 2009; Glendenning et al., 2015; Hastie et al., 2018).

The LLGB consists of two east-trending, steeply dipping belts that contain various supracrustal rocks, known locally as the Wasekwan group (Bateman, 1945; Gilbert et al., 1980), along with younger molasse-type sedimentary rocks that constitute the Sickle group (Figure GS2018-8-1; Norman, 1933). The southern and northern belts are separated by granitoid plutons of the 1.89–1.87 Ga Pool Lake intrusive suite (Figure GS2018-8-1; Gilbert et al., 1980; Baldwin et al., 1987). In the central and southern parts of the LLGB, the Sickle group overlies the Wasekwan group and felsic–mafic plutonic rocks of the Pool Lake intrusive suite along an angular unconformity. The Sickle group correlates well with the 1850–1840 Ma MacLennan group in the La Ronge greenstone belt in Saskatchewan in terms of composition, stratigraphic position and contact relationships (Ansdell et al., 1999; Ansdell, 2005). Cutting the entire LLGB are the much younger Mackenzie dikes (ca. 1267 Ma; Baragar et al., 1996), as indicated by regional aeromagnetic data, that appear to truncate volcanic and plutonic rocks folded during peak metamorphism at 1.81–1.80 Ga.

Significant differences in the geology and geochemistry of the northern and southern belts in the LLGB may reflect regional differences in tectonic settings that are obscured by structural transposition and imbrication during multiple stages of deformation (Gilbert et al., 1980; Syme, 1985; Zwanzig et al., 1999). This complexity leads to the suggestion that the term 'Wasekwan group' should be abandoned because it contains disparate volcanic assemblages that were later structurally juxtaposed during the evolution of the LLGB (Zwanzig et al., 1999), and thus may represent a tectonic collage similar to that described in the Flin Flon greenstone belt (e.g., Stern et al., 1995). However, this report retains the term 'Wasekwan group' to maintain consistency with previous LLGB-related literature.

The Farley Lake area, including the Gordon Au deposit, is situated in the northern belt of the LLGB (Figure GS2018-8-1) and consists mostly of Wasekwan group supracrustal rocks intruded by plutons of the Pool Lake intrusive suite and late intrusive suite (Gilbert et al., 1980; Yang and Beaumont-Smith, 2016a, 2016b; Figure GS2018-8-2). Following the convention of previous workers (e.g., Milligan, 1960; Beaumont-Smith and Böhm, 2004), the intrusions cutting the Wasekwan group (i.e., the Pool Lake intrusive suite of Gilbert et al., 1980) and

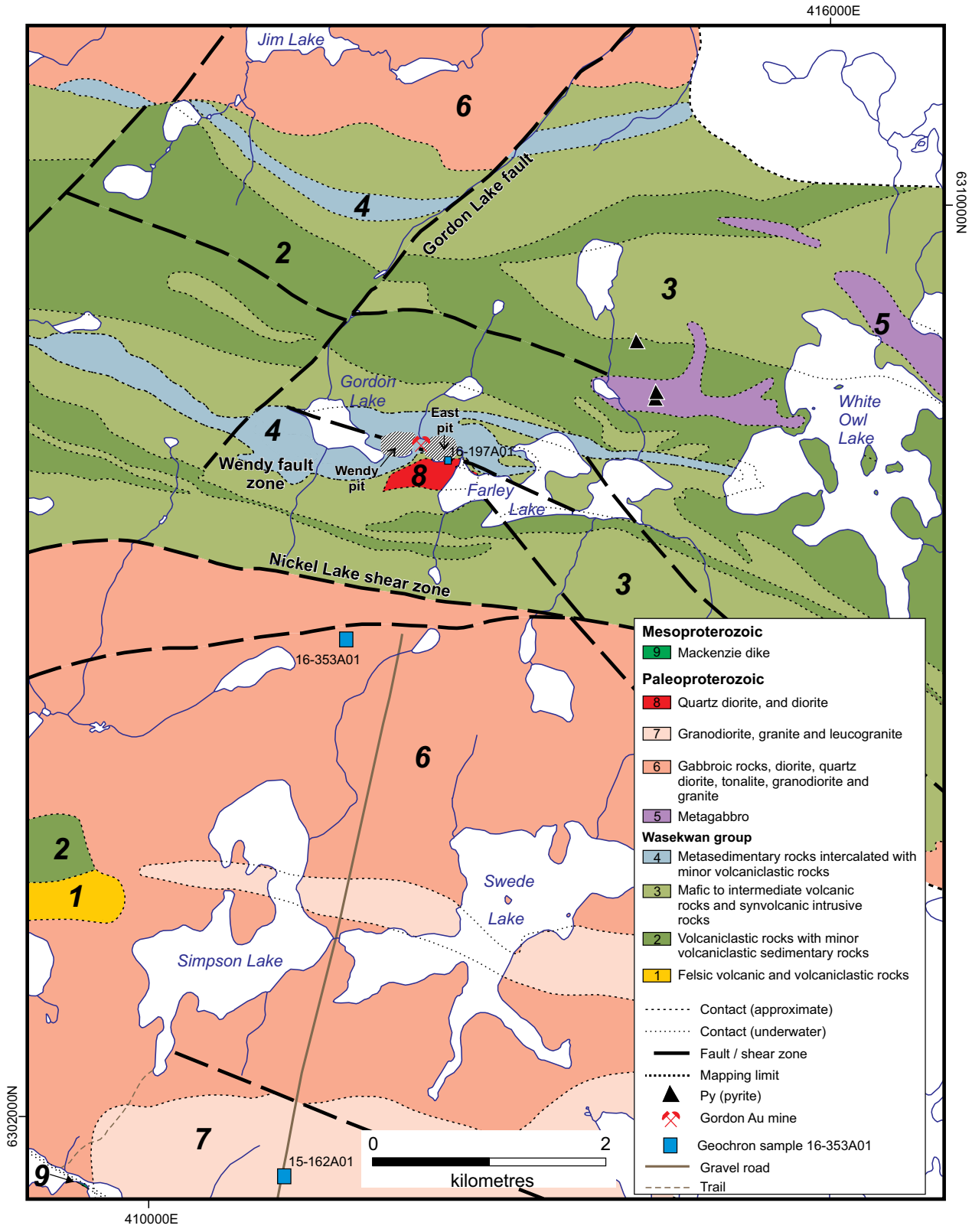

***Figure GS2018-8-2**: Simplified geology of the Farley Lake area, Lynn Lake greenstone belt, northwestern Manitoba (modified from Yang and Beaumont-Smith, 2016a, b). Note: prefix '111' of geochronology sample number is omitted to fit the available space.*

those cutting the Sickle group are called, respectively, the pre-Sickle and post-Sickle suites. Both igneous suites are cut by a late intrusive suite (Yang and Beaumont-Smith, 2015, 2016a, b, 2017) that has an uncertain relationship to the youngest Paleoproterozoic magmatic phase of small pegmatitic and tonalitic intrusions at 1.8–1.78 Ga. A diabase dike interpreted as part of the Mackenzie swarm (ca. 1267 Ma; Baragar et al., 1996) cuts across the southwest corner of the Farley Lake area, as indicated by regional aeromagnetic data. This Mackenzie dike is not further discussed in this report because it is Mesoproterozoic in age and not related to Au metallogeny in the LLGB.

Bedrock mapping in the Farley Lake area in 2016 defined eight map units, including 17 subunits (see Yang and Beaumont-Smith, 2016a, b). Recent SHRIMP U-Pb zircon age data (Lawley et al., 2018) and data presented in this study (see below) suggest that the unit 6b (diorite, quartz diorite and minor gabbroic rocks) defined and described by Yang and Beaumont-Smith (2016a, b) should be changed to a new map unit 8 (Table GS2018-8-1; Figure GS2018-8-2).

It is noted that the supracrustal rocks in the Farley Lake map area, similar to others in the LLGB, were metamorphosed to greenschist to amphibolite facies (Gilbert et al., 1980; Beaumont-Smith and Böhm, 2004; Yang and Beaumont-Smith, 2015, 2016a, 2017); however, for brevity, the prefix 'meta' is omitted in this report. In the following section, the geochemical characteristics of major rock types from different map units are described to determine their magmatic affinities.

Lithogeochemistry

This report compiles geochemical data on 59 whole-rock samples from the Farley Lake area, including 46 samples from this study [note: analyses were carried out using the 4Litho package at Activation Laboratories Ltd. in Ancaster, Ontario; detailed analytical procedures and methods were described in Anderson (2013)], seven from Zwanzig et al. (1999), five from D. Peck (unpublished data, 1999) and one from Beaumont-Smith (2008). Based on the sample locations and/or lithologies, these samples are attributed to the map units defined by Yang and Beaumont-Smith (2016a, b). The major geochemical characteristics are summarized and discussed below for supracrustal (units 1 to 4) and intrusive rocks (units 5 to 8), respectively. Detailed rock descriptions of the different units can be found in Yang and Beaumont-Smith (2016a).

Supracrustal rocks (units 1 to 4)

Classification

Based on the total alkalis versus silica diagram (TAS; Le Bas et al., 1986), seven samples collected from unit 1 felsic to intermediate volcanic and volcaniclastic rocks (Table GS2018-8-1) plot within the fields of andesite, dacite and rhyolite (Figure GS2018-8-3a). Nine samples taken from unit 2 volcaniclastic rocks largely fall into the fields of basalt and basaltic andesite. Nineteen samples from unit 3 mafic to intermediate volcanic rocks plot in the basalt, basaltic andesite and andesite fields. These volcanic and volcaniclastic rocks are dominantly subalkaline (Figure GS2018-8-3a), consistent with the commonly seen volcanic-arc array comprising basalt, andesite and dacite to rhyolite (BADR; Yang and Beaumont-Smith, 2015, 2016a). Based on the calculation of the Rittmann Serial Index σ (= $[Na_2O+K_2O]^2/[SiO_2–43]$, values in wt.%; see Rittmann, 1973), these subalkaline rocks have σ values ranging from 0.39 to 3.06, which can further subdivide them into calcic (tholeiitic) to calcalkaline series (see Yang, 2007), consistent with the studies of Syme (1985) and Zwanzig et al. (1999).

As a comparison, six samples taken from unit 4 sedimentary rocks are also plotted on the TAS diagram (Figure GS2018-8-3a), with two argillite samples (unit 4a) falling into the fields of basaltic andesite and dacite, and four banded iron formation (BIF; unit 4b) samples characterized by very low alkalis (Na_2O+K_2O <0.45 wt.%) and a large range in silica content.

The use of high-field-strength element (HFSE) ratios, such as Zr/TiO_2 and Nb/Y, to classify volcanic and volcaniclastic rocks from units 1 to 3 (Figure GS2018-8-3b) yielded a result similar to the TAS diagram. The HFSEs are commonly considered immobile during hydrothermal alteration and metamorphism up to upper amphibolite facies (Syme, 1985; Rollinson, 1993; Pearce, 1996; Glendenning et al., 2015), thus potentially reflecting the primary compositional characteristics of the supracrustal rocks. All samples have low Nb/Y ratios (<0.7), typical of subalkaline rocks, and low to moderate Zr/TiO_2 ratios, consistent with predominantly mafic to intermediate bulk compositions (Figure GS2018-8-3b; Pearce, 1996).

Rare-earth element patterns

Chondrite-normalized rare-earth element (REE) patterns of units 1 to 4 supracrustal rocks are presented in Figure GS2018-8-4. Unit 1 andesitic to rhyolitic samples display slight light-REE (LREE) enrichment patterns, which are subdivided into felsic and intermediate volcanic rocks, respectively. The former have higher REE

Table GS2018-8-1: Lithostratigraphic units of the Farley Lake area, Lynn Lake greenstone belt, northwestern Manitoba (modified from Yang and Beaumont-Smith, 2016a, b).

Unit	Rock type	Affiliation
9	Diabase of Mackenzie dike (ca. 1267 Ma[1])	Mackenzie dike
	Intrusive contact	
8	Diorite, quartz diorite (1854.4 ±2.4 Ma[2]) and minor gabbroic rocks	Post-Sickle intrusive suite
	Intrusive contact	
7	Granodiorite, granite and leucogranite	Pre-Sickle intrusive suite
7a	Granite and leucogranite (1872.6 ±2.5 Ma[2])	
7b	Granodiorite	
6	Gabbroic rocks, diorite, quartz diorite, tonalite, granodiorite and granite (1879.4 ±4.3 Ma[2]), and associated pegmatic and aplitic dikes	
6a	Tonalite, granodiorite and granite, and associated pegmatic and aplitic dikes	
5	Gabbro and minor diorite	
	Intrusive contact	
4	Sedimentary rocks intercalated with minor volcaniclastic rocks	Wasekwan group
4a	Argillite, metasiltstone and metagreywacke	
4b	Banded iron formation	
4c	Volcaniclastic mudstone, volcaniclastic siltstone and volcaniclastic sandstone	
	Structural contact	
3	Mafic to intermediate volcanic rocks and synvolcanic intrusive rocks	
3a	Diabase and leucogabbroic dikes	
3b	Porphyritic basaltic andesite	
3c	Plagioclase-phyric basalt and aphyric basalt	
3d	Mafic autobreccia	
	Structural contact	
2	Volcaniclastic rocks with minor volcaniclastic sedimentary rocks	
2a	Felsic lapilli tuff and tuff	
2b	Intermediate lapillistone, lapilli tuff and tuff	
2c	Mafic lapillistone, mafic lapilli tuff, tuff and minor mafic mudstone	
2d	Mafic tuff breccia and breccia	
	Structural contact	
1	Felsic volcanic and volcaniclastic rocks: rhyolite, dacite and felsic to intermediate volcaniclastic rocks	
1a	Rhyolite, and dacite (1884 to 1881 Ma[3])	
1b	Felsic to intermediate volcaniclastic rocks	
	Basement?	

[1] Baragar et al. (1996)
[2] Lawley et al. (2018) - summarized in this study
[3] Beaumont-Smith (unpublished data, 2006)

abundance with notable negative Eu anomalies, whereas the latter have lower REE concentrations with a slightly positive Eu anomaly (Figure GS2018-8-4a). Unit 2 basaltic to andesitic volcaniclastic rocks are similarly subdivided into basaltic and andesitic volcaniclastic rocks, respectively. The basaltic group exhibits a flat REE pattern, low REE contents and slightly positive Eu anomalies. The andesitic group, in comparison, has slightly enriched REE patterns, higher REE abundances and no or slightly negative Eu anomalies (Figure GS2018-8-4b).

Unit 3 basalt to andesite samples display varied REE patterns: mafic samples have flat REE profiles with notable positive Eu anomalies, whereas intermediate samples are variably LREE enriched with flat to slightly negative Eu anomalies (Figure GS2018-8-4c). Rare-earth element patterns for unit 3 samples are typical of basaltic to andesitic

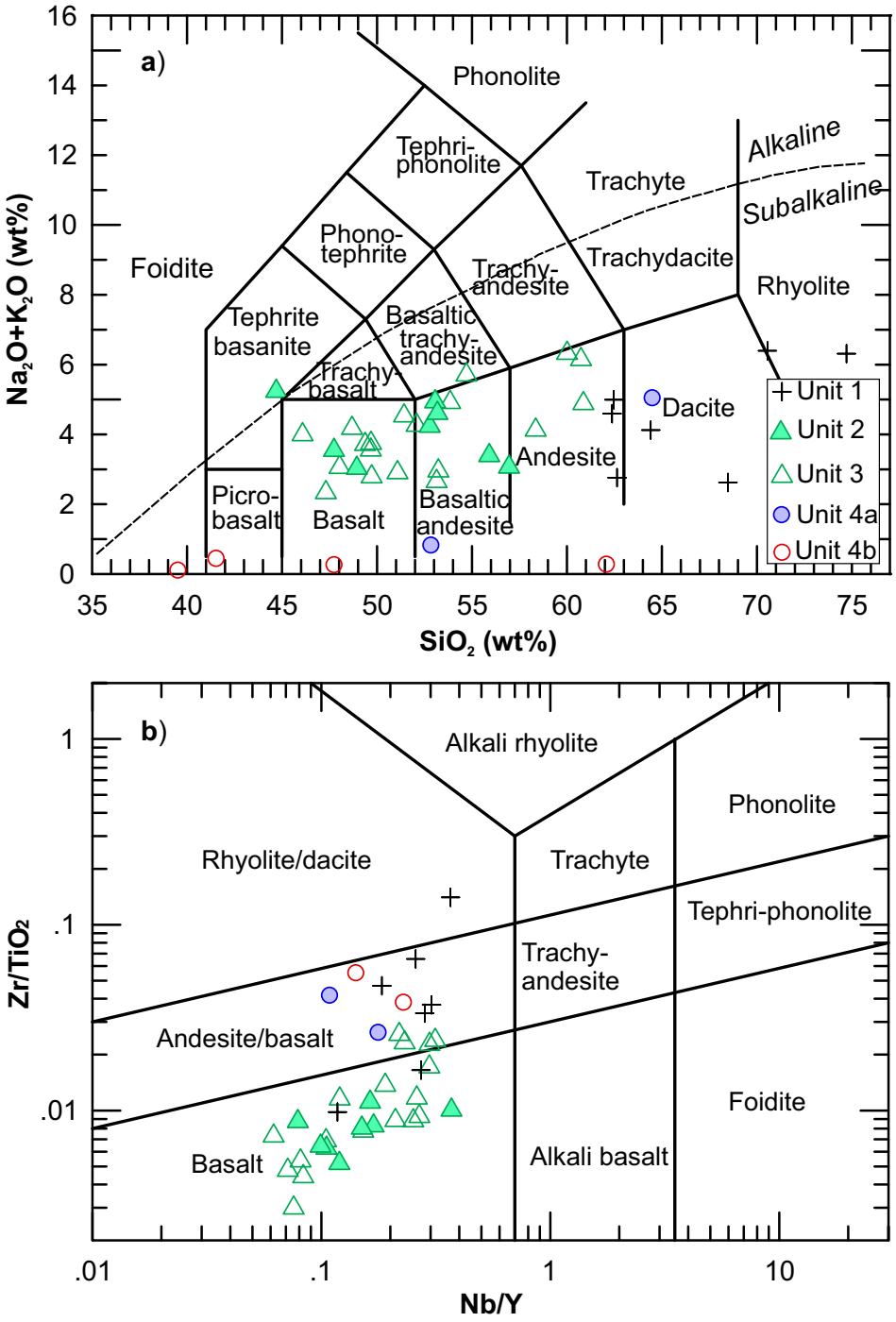

Figure GS2018-8-3: *Geochemical classification of supracrustal rocks from the Farley Lake area:* ***a)*** *total alkalis (Na_2O+K_2O; wt.%) versus SiO_2 (wt.%) diagram (TAS; after Le Bas et al., 1986); dashed line is the boundary between the subalkaline and alkaline series (after Irvine and Baragar, 1971);* ***b)*** *Zr/TiO_2 versus Nb/Y (after Pearce, 1996).*

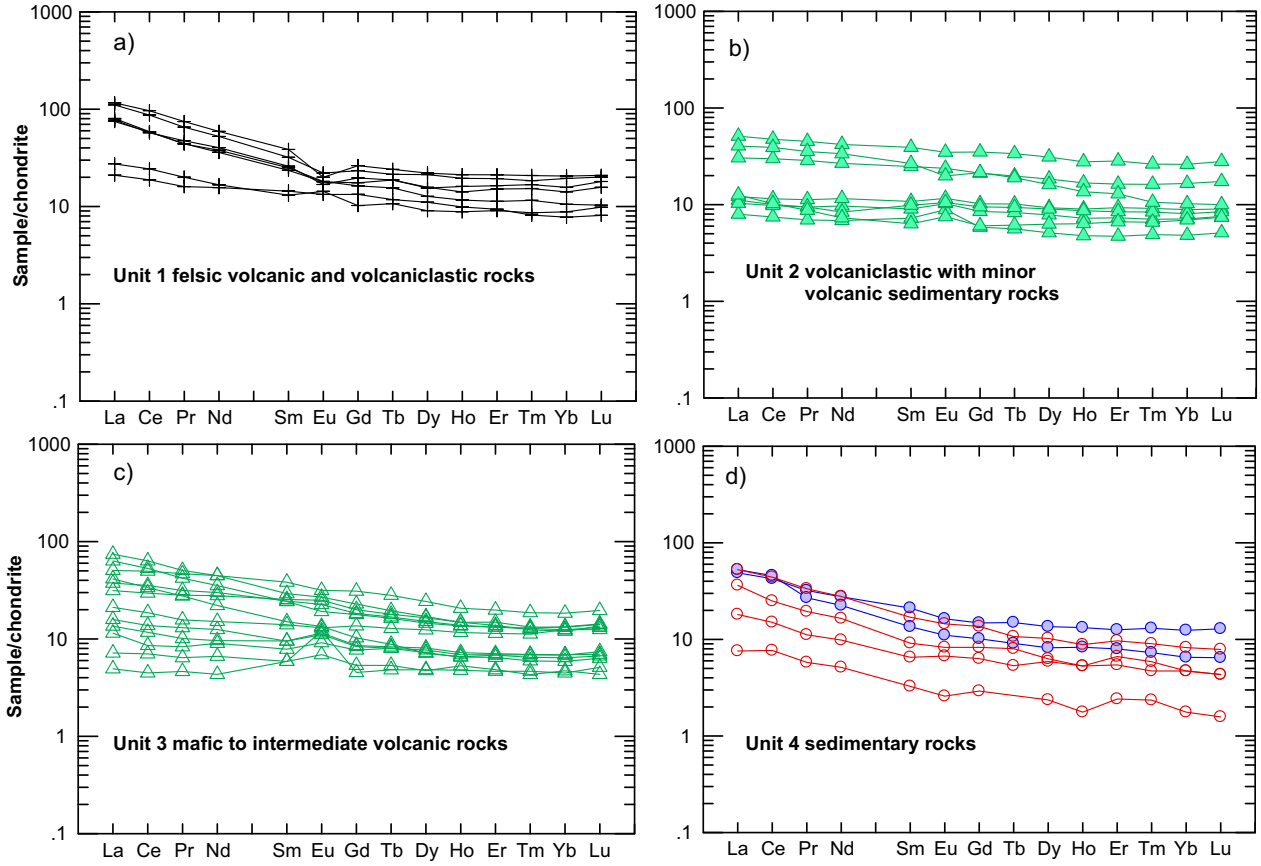

Figure GS2018-8-4: *Chondrite-normalized rare-earth element (REE) patterns of units 1 to 4 supracrustal rocks from the Farley Lake area. Normalizing values from Sun and McDonough (1989). Symbols as in Figure GS2018-8-3. Argillite samples in blue.*

volcanic rocks formed in volcanic-arc settings, consistent with the results of tectonic discrimination diagrams using HFSE systematics (e.g., Zr-Th-Nb [Wood, 1980] and Nb-Zr-Y [Meschede, 1986] ternary plots, not shown).

Unit 4 sedimentary samples display LREE-enriched distribution patterns with no or very subtle Eu anomalies, similar to units 2 and 3 volcanic and volcaniclastic samples. Argillite samples (in blue) have slightly higher REE abundances than the BIF samples (Figure GS2018-8-4d). Interestingly, unit 4 sedimentary samples have a volcanic-arc signature using the Zr-Th-Nb-Y systematics (Wood, 1980; Meschede, 1986). This suggests that unit 4 sedimentary rocks may have been derived, at least in part, from volcanic-arc or island-arc rocks (e.g., Frisch et al., 2011).

Extended trace-element patterns

On primitive-mantle–normalized, extended trace-element plots, unit 1 andesitic to rhyolitic samples can be subdivided into two groups, both of which display pronounced negative Nb, Ta and Ti anomalies (Figure GS2018-8-5a). Andesitic samples have lower trace-element concentrations (i.e., <10 times normalizing values) compared to the dacite to rhyolite samples. The negative Nb anomalies exhibited by unit 1 volcanic rocks are typical of volcanic-arc environments that sequester some HFSE within high-pressure rutile during subduction (cf. Pearce and Peate, 1995; Pearce, 2008).

Unit 2 basaltic to andesitic volcaniclastic rocks exhibit fairly flat extended trace-element profiles (Figure GS2018-8-5b), with subtle negative Nb, Ta and Ti anomalies relative to unit 1. A few samples lack such anomalies, which may be due to the presence of magnetite porphyroblasts (Yang and Beaumont-Smith, 2016a) that are commonly enriched in Nb, Ta, and Ti (cf. Rollinson, 1993) and/or, in the case of volcaniclastic rocks, less contamination from felsic detritus.

Unit 3 basalt and basaltic andesite to andesite samples have varied trace-element abundances, ranging from <1 to ~20 times normalizing values (Figure GS2018-8-5c). These volcanic rocks show a typical arc-like signature, manifested by the presence of negative Nb, Ta, and Ti anomalies, although a few magnetite-bearing samples do not have such pronounced anomalies. It was noticed that Ta contents in seven samples from Zwanzig et al.

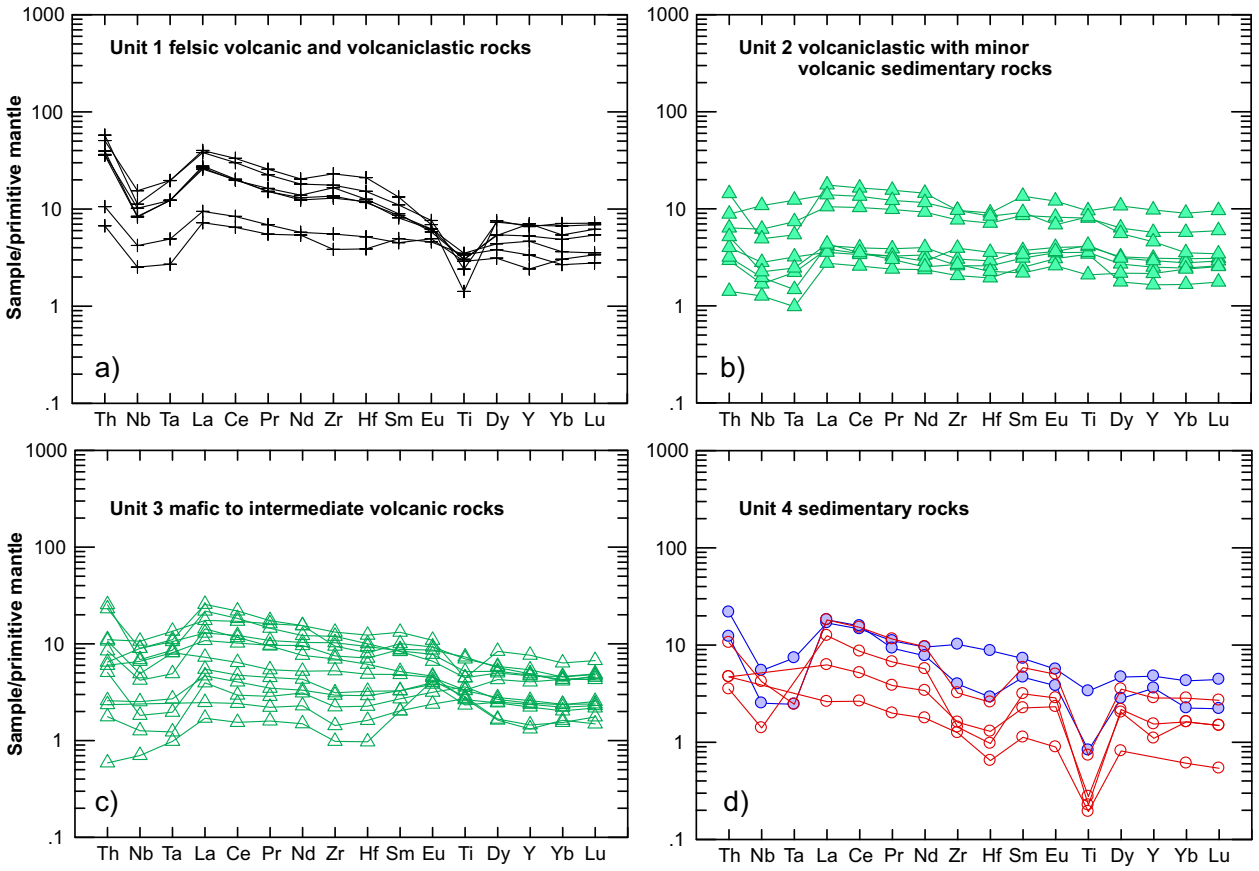

Figure GS2018-8-5: *Primitive-mantle–normalized spider diagram for units 1 to 4 supracrustal rocks. Normalizing values from Sun and McDonough (1989). Symbols as in Figure GS2018-8-3.*

(1999) are anomalously high; these samples were prepared using a tungsten carbide mill, leading to artificially elevated Ta and W contents, whereas other elements were not affected (S. Gagné, pers. comm., 2018). Thus, these seven samples were not plotted in Figure GS2018-8-5c.

Unit 4 sedimentary rocks show a very strong arc signature with pronounced negative Nb, Ta and Ti anomalies (Figure GS2018-8-5d), suggesting that they may have been sourced from arc rocks. Also, most of the sedimentary samples display negative Zr and Hf anomalies (Figure GS2018-8-5d), likely reflecting a provenance lacking in zircon.

Intrusive rocks (units 5 to 8)

Classification

Four samples of unit 5 medium-grained gabbro plot in the quartz gabbro and diorite fields of the CIPW normative Q' versus ANOR classification by Streckeisen and Le Maitre (1979) in Figure GS2018-8-6.

Geochemically, unit 5 gabbroic rocks evolved from magnesian to ferroan affinity, and belong to the calcic to calc-alkali series (Figure GS2018-8-7a, b). The Fe-rich affinity of unit 5 samples is consistent with their σ values ranging from 1.25 to 2.42, which is typical of calcalkaline volcanic-arc rocks (Yang, 2007). Unit 5 samples have aluminum saturation index (ACNK = molar ratio Al/(Ca+Na+K); see Maniar and Piccoli, 1989) values of 0.67 to 0.84, indicating that they are metaluminous.

Unit 6 granitoids occur widely in the Farley Lake area (Figure GS2018-8-2), with a large range of lithologies (Table GS2018-8-1; see Yang and Beaumont-Smith, 2016a for detailed descriptions). Seven whole-rock samples collected from unit 6 vary from quartz diorite, tonalite and granodiorite to monzogranite (Figure GS2018-8-6). The Unit 6 samples are magnesian to ferroan, calcic to calcalkaline and predominantly peraluminous (Figure GS2018-8-7a–c). These granitoid rocks display σ values of 0.99 to 1.32, evolving along the trend of calcic to calcalkalic (Figure GS2018-8-6) that is typical of volcanic-arc–like, calcalkaline granitoid rocks (Yang, 2007; Whalen and Frost, 2013).

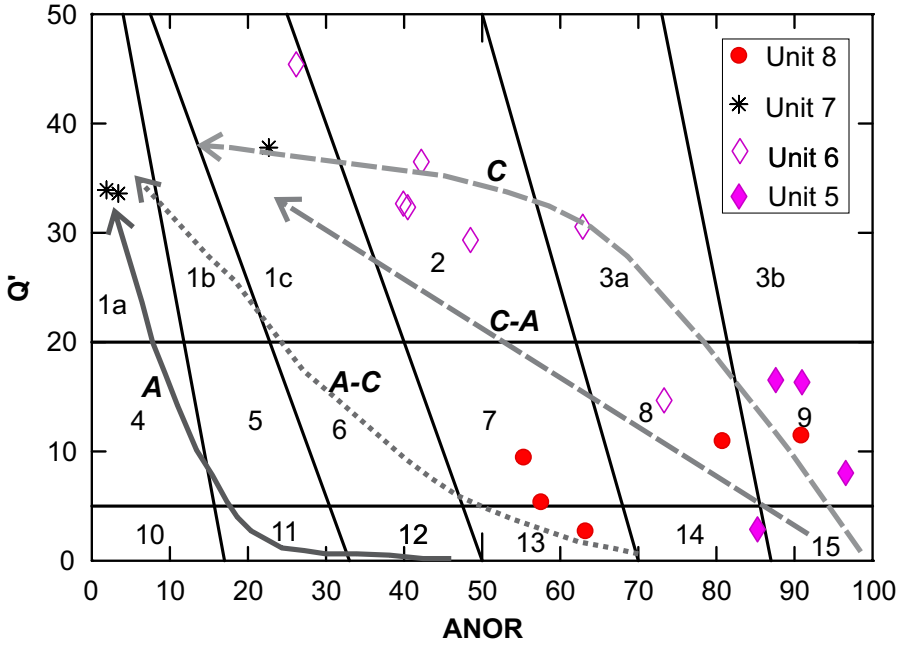

Figure GS2018-8-6: *Classification of units 5 to 8 intrusive rocks from the Farley Lake area, based on the CIPW normative Q' vs. ANOR diagram of Streckeisen and Le Maitre (1979). Q' = CIPW normative 100*qz/(qz+or+ab+an); ANOR = CIPW normative 100*an/(an+or). Rock units: 1a, alkali-feldspar granite; 1b, syenogranite; 1c, monzogranite; 2, granodiorite; 3a, tonalite; 3b, calc tonalite; 4, alkali-feldspar quartz syenite; 5, quartz syenite; 6, quartz monzonite; 7, quartz monzodiorite; 8, quartz diorite; 9, quartz gabbro; 10, alkali-feldspar syenite; 11, syenite; 12, monzonite; 13, monzogabbro; 14, diorite; 15, gabbro. Coarse dashed and solid lines with arrows indicate interpreted differentiation trends of different magmatic suites (after Whalen and Frost, 2013): C, calcic; C-A, calcalkali; A-C, alkali-calcic; A, alkali. Abbreviations: ab, albite; an, anorthite; or, orthoclase; qz, quartz.*

Voluminous bodies of unit 6 granitoids are I-type, based on their mineral assemblage (amphibole, biotite, magnetite), and were likely emplaced in a juvenile to mature island-arc setting (e.g., Rudnick and Gao, 2003; Arndt, 2013).

Unit 7 granite samples are highly evolved in chemical composition, with silica contents of 75.33 to 77.86 wt.% and Mg# [molar 100×MgO/(MgO+FeO^{tot})] of 2 to 37. Three unit 7 granite samples plot in the fields of alkali-feldspar granite and monzogranite (Figure GS2018-8-6) but are compositionally diverse (Figure GS2018-8-7a–c). The chemical variability of unit 7 may reflect grouping of at least two disparate rock types and/or magmatic differentiation of A-type granites (e.g., Eby, 1990) emplaced in an intra-arc extensional setting (see below).

Unit 8 granitoid samples, as defined in this study by SHRIMP U-Pb zircon age determination, occur as a small stock at the south edge of the Gordon Au deposit (Figure GS2018-8-2) that was previously mapped as part of unit 6b in Yang and Beaumont-Smith (2016a, b). Five unit 8 granitoid samples display a compositional range from quartz monzodiorite and quartz diorite to quartz gabbro and monzogabbro in the CIPW normative Q' versus ANOR classification diagram (Figure GS2018-8-6). These rocks have a relatively narrow range and moderate silica contents of 51.46 to 58.62 wt.%, high Al_2O_3 of 15.37 to 16.99 wt.% and moderate to high Mg# of 52 to 60. The mafic to intermediate rocks included within unit 8 are exclusively magnesian, alkali-calcic (except for one calcic sample) and metaluminous. They have σ values ranging from 2.44 to 3.58, attributed mostly to the calcalkaline to alkaline series, albeit one sample (σ = 0.95) is calcic (tholeiitic).

REE patterns

Chondrite-normalized REE patterns of units 5 to 8 intrusive rocks are presented in Figure GS2018-8-8. Unit 5 gabbros have relatively low REE concentrations, approximately 3 to 10.5 times chondrite values. They show flat, undifferentiated REE patterns (low La/Yb ratios of 1.9 to 2.7) with small positive Eu anomalies (Eu*/Eu values of 1.15 to 1.23; Figures GS2018-8-7d and 8a) that may suggest the presence of cumulus plagioclase grains (cf. Rollinson, 1993).

Unit 6 granitoids exhibit enriched REE patterns (La/Yb ratios are 7.3 to 19.9) with marked negative Eu anomalies (Eu*/Eu values of 0.61 to 0.88), except for one sample with a steeply dipping REE profile (La/Yb ratio of 25.1) and a positive Eu anomaly (Eu*/Eu value of 2.16; Figures GS2018-8-7d and -8b), suggesting that plagioclase fractionation prior to emplacement may be a petrogenetic

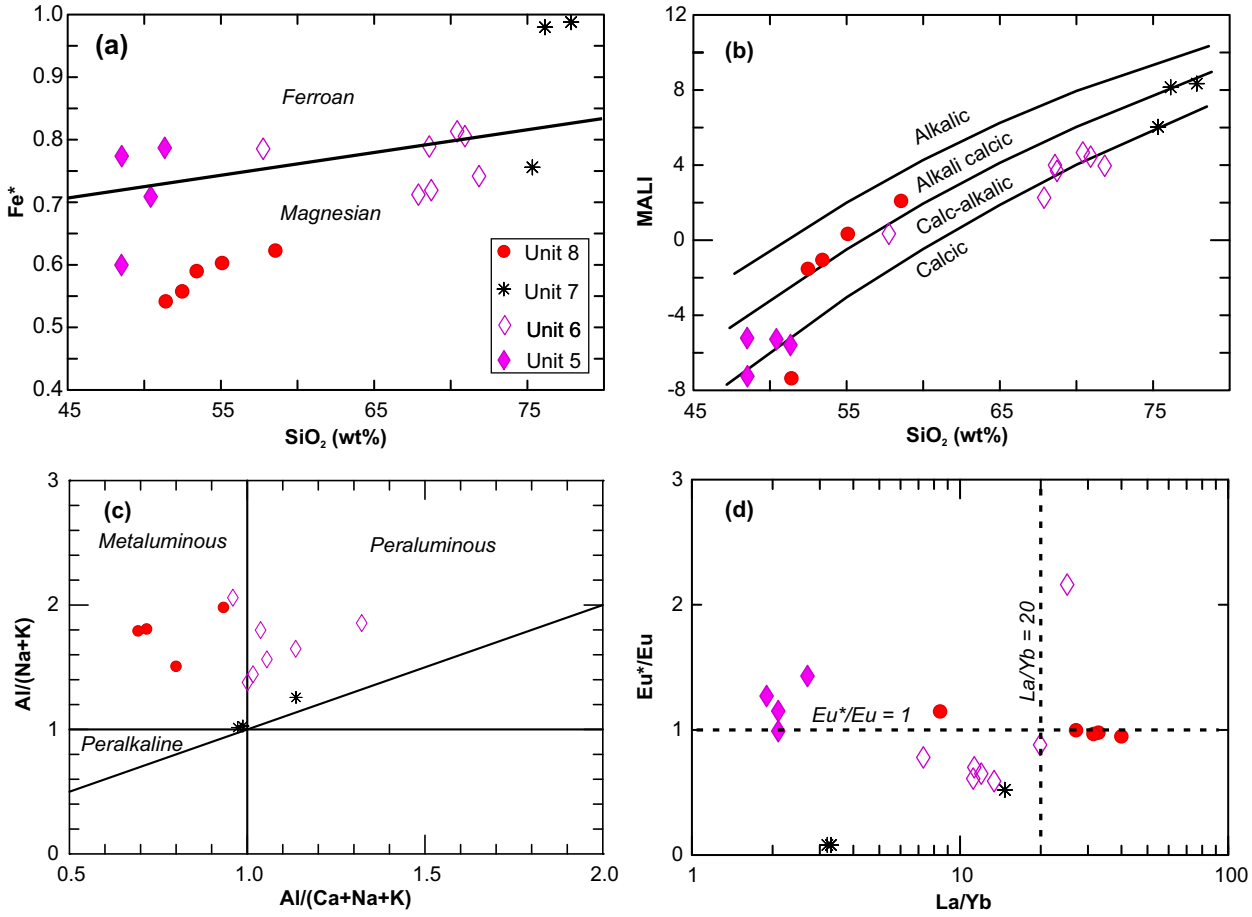

Figure GS2018-8-7: *Geochemical discrimination diagrams for units 5 to 8 intrusive rocks from the Farley Lake area:* ***a)*** *classification of ferroan vs. magnesian granitoids (with fields from Frost et al., 2001); Fe* = $FeO^{tot}/(FeO^{tot}+MgO)$;* ***b)*** *MALI vs. SiO_2 (wt.%); MALI = $Na_2O+K_2O–CaO$ in wt.% (after Frost et al., 2001);* ***c)*** *Shand index (fields from Maniar and Piccoli, 1989); ACNK = $Al_2O_3/(CaO+Na_2O+K_2O)$, A/NK = $Al_2O_3/(Na_2O+K_2O)$, in moles;* ***d)*** *Eu*/Eu vs. La/Yb.*

feature of some unit 6 granitoid plutons (cf. Rollinson, 1993).

Two unit 7 granite samples display flat to slightly enriched REE patterns with pronounced negative Eu anomalies (Figure GS2018-8-8c). These highly evolved granites have La/Yb ratios of 3.2 to 14.7 and Eu*/Eu values of 0.08 to 0.52 (Figure GS2018-8-7d), suggesting that plagioclase may have been involved, either as an early fractionating phase and/or as a residue of its source rocks (e.g., Rollinson, 1993). The third unit 7 sample yielded an REE profile and peraluminous affinity more similar to unit 6 granitoids.

Most quartz diorite and quartz monzodiorite to quartz gabbro samples from unit 8 display strongly LREE-enriched and HREE-depleted patterns without notable Eu anomalies, although one sample yielded relatively lower REE concentrations with a slightly positive Eu anomaly (Figure GS2018-8-8d). These dioritic rocks have high La/Yb ratios of 27.3 to 40.30, and Sr/Y ratios of 45.9 to 55.1, similar to those of adakites or sanukitoids (e.g., Shirey and Hanson, 1984; Stern et al., 1989; Martin et al., 2005; Richards and Kerrich, 2007). One diorite sample (111-16-291A01; see Figure GS2018-8-8d), however, has a La/Yb ratio of 8.5 and Sr/Y ratio of 36.3, atypical of adakites (Richards and Kerrich, 2007).

Extended trace-element patterns

Figure GS2018-8-9 shows primitive-mantle–normalized, extended trace-element profiles for units 5 to 8 intrusive rocks. Unit 5 gabbroic rocks have low HFSE contents, ranging from <1 to 10 times primitive-mantle–normalized values. They display flat trace-element profiles with negative Nb, Ta, Zr and Hf anomalies and slightly positive Ti anomalies (Figure GS2018-8-9a). These HFSE systematics represent a typical arc signature with cumulative phases (e.g., Ti-bearing magnetite), indicative of relatively oxidized magmas. The REE patterns also indicate

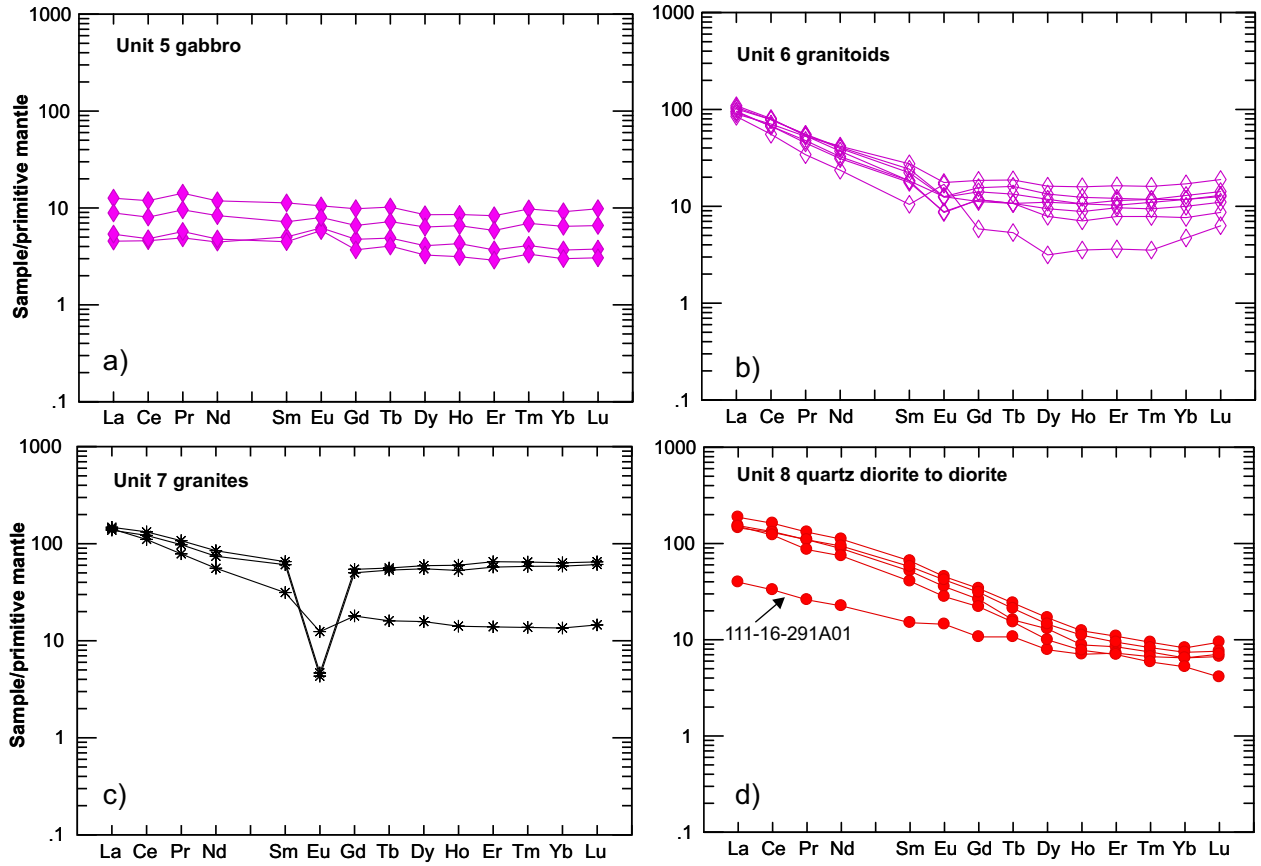

Figure GS2018-8-8: *Chondrite-normalized rare-earth element (REE) patterns of units 5 to 8 intrusive rocks. Normalizing values from Sun and McDonough (1989). Symbols as in Figure GS2018-8-6.*

the presence of cumulate plagioclase in some of the gabbroic rocks of unit 5 (Figure GS2018-8-8c).

Unit 6 granitoid samples display enriched trace-element patterns with negative slopes and pronounced negative Nb, Ta, and Ti anomalies (Figure GS2018-8-9b), suggesting that they may have been emplaced in a magmatic-arc setting. One quartz diorite sample (111-16-292A01) is characterized by positive Ti, Zr, Hf and Eu anomalies suggestive of cumulative phases such as Ti-bearing magnetite, zircon and plagioclase.

Unit 7 granite samples are Th-rich relative to other HFSEs, with pronounced negative Nb and Ti anomalies (Figure GS2018-8-9c). Two alkali-feldspar granite samples are relatively Ta rich, distinct from continental-arc magmatism, and yielded positive Hf anomalies, more typical of an intra-arc extensional environment.

Quartz diorite to quartz monzogabbroic rocks of unit 8 are relatively Th rich and yielded pronounced negative Nb, Ta, Zr, Hf, and Ti anomalies (Figure GS2018-8-9d). The major (MgO rich, moderate SiO_2, Al_2O_3 rich) and trace-element (Y and HREE poor; Sr rich) characteristics of unit 8 samples are similar to those of adakite-sanukitoid rocks, which are interpreted to have been derived from prior metasomatized lithospheric mantle beneath a magmatic arc and/or direct melting of a subducting slab (e.g., Shirey and Hanson, 1984; Stern et al., 1989; Martin et al., 2005).

Tectonic settings

Geochemical characteristics of the supracrustal rocks (units 1 to 4) and intrusive rocks (units 5 to 8) described above document a heterogeneous suite of calcalkaline to tholeiitic, magnesian to ferroan, and metaluminous to moderately peraluminous rocks based on their variable trace-element profiles (Figures GS2018-8-4 to -9). Most of these rocks yielded pronounced negative Nb, Ta and Ti anomalies typical of rocks that formed in an arc-like setting, as was suggested elsewhere in the LLGB (Syme, 1985; Zwanzig et al., 1999). Analyzed rocks from the Farley Lake area, however, are dissimilar to some of the relatively Th-poor and Nb-rich mafic volcanic rocks hosting the MacLellan deposit (Glendenning et al., 2015), except for unit 8 intrusive rocks that yielded a distinct trace-element signature.

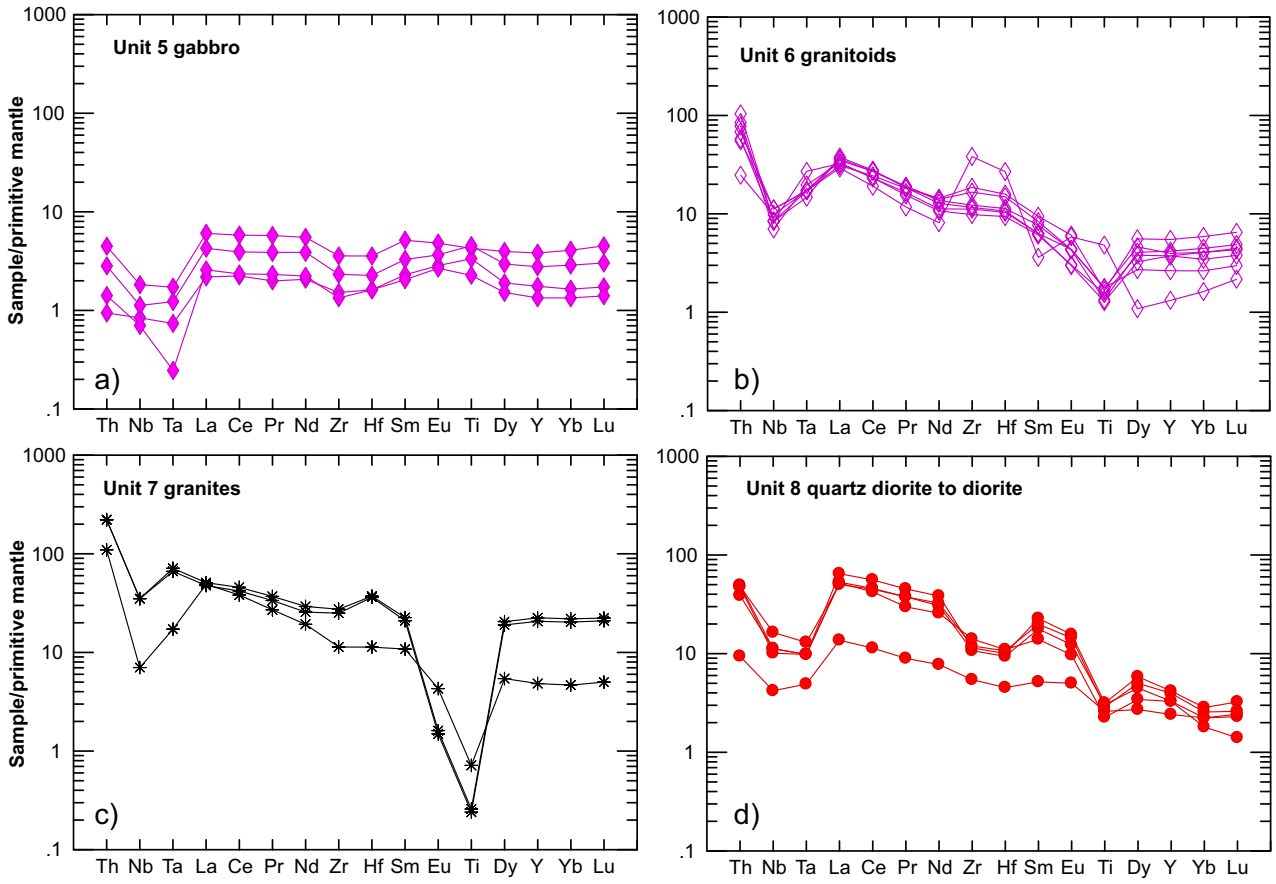

Figure GS2018-8-9: *Primitive-mantle–normalized, extended trace-element patterns of units 5 to 8 intrusive rocks. Normalizing values from Sun and McDonough (1989). Symbols as in Figure GS2018-8-6.*

As a comparison, unit 5 gabbroic rocks are plotted together with units 6 to 8 granitoid rocks in tectonomagmatic discrimination diagrams (Figure GS2018-8-10a, b) to further characterize their tectonic affinity. Samples from units 5, 6 and 8 plot exclusively in the volcanic-arc granitoid field defined by Pearce et al. (1984). Units 5, 6 and 8 rocks are also comparable to arc I-type granitoids, following the approach of Christiansen and Keith (1996). Two unit 7 granite samples, however, fall into the field of within-plate or A-type granites (Figure GS2018-8-10a). Similar results are obtained by using the Zr (ppm) versus 10^4Ga/Al discrimination diagram (not shown) of Whalen et al. (1987). On the Hf–Rb/30–Ta*3 ternary discrimination diagram (Figure GS2018-8-10b; Harris et al., 1986), unit 7 granites are located in the field of within-plate granites, whereas units 5, 6 and 8 samples plot mostly in the volcanic-arc and within-plate granite fields. Magmatic suites, therefore, seem to represent a complex assemblage of granitoid rock types, with each geochemical composition reflecting the complex interplay between magmatic processes, source compositions and tectonic settings.

Sm-Nd geochemical and isotopic systematics

In order to obtain isotope geochemical information on the nature and evolution of volcanic rocks in the Farley Lake area, six volcanic samples from map units 1a, 3b, and 3c (Table GS2018-8-1) were selected for Sm-Nd isotopic analysis at the University of Alberta. Detailed analytical procedures followed the approach described in Böhm et al. (2007) and Anderson (2013). The analytical results are listed in Table GS2018-8-2.

The Sm/Nd ratios range from 0.21 to 0.29 (average 0.26) and tend to decrease with increasing silica content (i.e., 0.28 to 0.29 in unit 3c basalt, 0.22 to 0.29 in unit 3b andesite and 0.21 in unit 1a rhyolite; Table GS2018-8-2). The systematic variation of Sm/Nd ratios with rock type is consistent with magmatic differentiation. We note that the Sm/Nd ratios of the Farley Lake volcanic samples are higher than the upper continental crust (0.19; see Goldstein et al., 1984) and average continental crust (0.195; Rudnick and Gao, 2003) but lower than the primitive mantle (0.33) and N-type MORB (0.36; Sun and McDonough, 1989). Basaltic Sm/Nd ratios from unit 3c

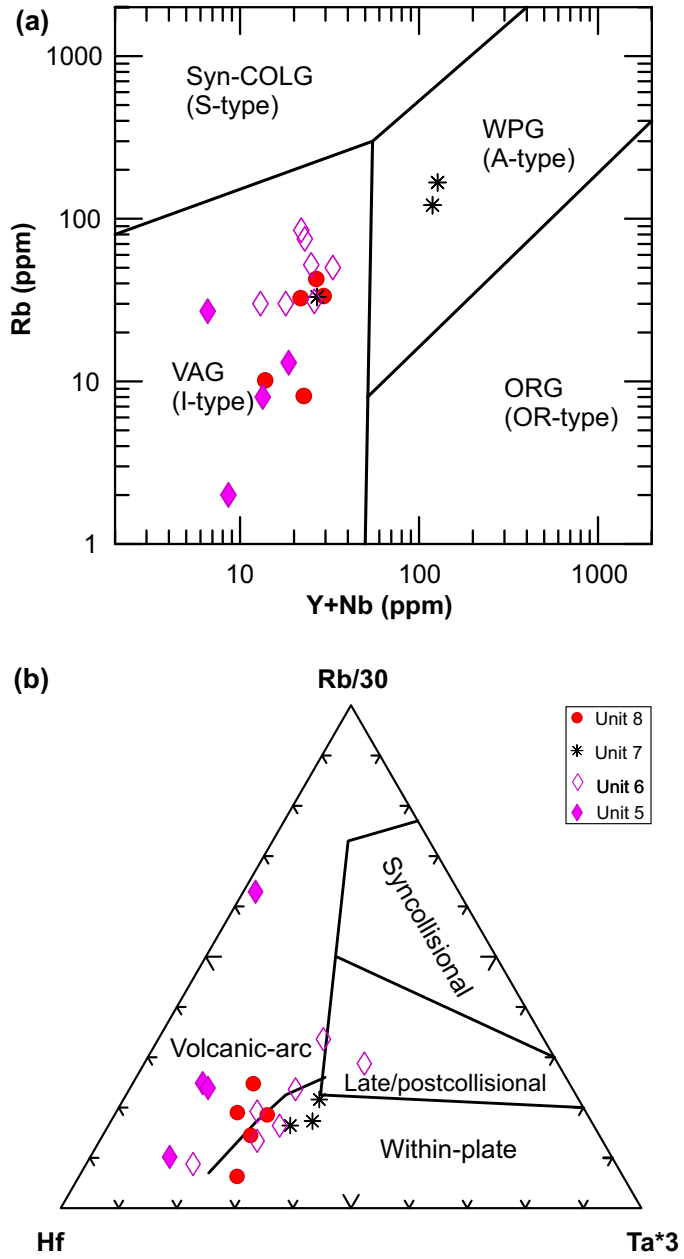

Figure GS2018-8-10: *Tectonomagmatic discrimination diagrams for units 5 to 8 intrusive rocks from the Farley Lake area:* ***a)*** *Rb (ppm) vs. (Y+Yb; ppm); the fields of ORG (ocean-ridge granitoids), syn-COLG (syncollision granitoids), VAG (volcanic-arc granitoids) and WPG (within-plate granitoids) are from Pearce et al. (1984) and correspond to the fields of OR-type, I-type, S-type and A-type granitoids, respectively, proposed by Christiansen and Keith (1996);* ***b)*** *Hf–Rb/30–Ta*3 ternary diagram (after Harris et al., 1986).*

resemble E-type MORB (0.29), whereas andesitic Sm/Nd ratios from unit 3b are similar to OIB (0.26; Sun and McDonough, 1989). These Sm/Nd ratios are consistent with the primitive-mantle–normalized, extended trace-element profiles (Figure GS2018-8-9), which suggest a volcanic-arc affinity (cf. Goldstein et al., 1984; Rollinson, 1993).

Similarly, $^{147}Sm/^{144}Nd$ isotopic ratios of the volcanic rocks in the Farley Lake area range from 0.1257 to 0.1761, and tend to increase with decreasing silica content (Table GS2018-8-2). The $^{143}Nd/^{144}Nd$ ratios range from 0.511960 to 0.512598. On a plot of $^{147}Sm/^{144}Nd$ versus $^{143}Nd/^{144}Nd$ ratios (Figure GS2018-8-11), the volcanic rock samples define a linear array that corresponds to an age of 1877 ±180 Ma with an initial $^{143}Nd/^{144}Nd$ ratio of 0.51039 ±0.00019 (ε_{Nd} = 3.6; Ludwig, 2008). The relatively large analytical uncertainty and MSWD of this regression are due largely to excess data-point scatter. Nevertheless, the Sm-Nd errorchron age is comparable to the TIMS U-Pb zircon age of 1884 Ma obtained for a unit 1a rhyo-

Table GS2018-8-2: Sm-Nd isotope composition of volcanic rocks from the Farley Lake area, Lynn Lake greenstone belt.

Sample	Easting[1]	Northing[1]	Rock type	Map unit[2]	Sm (ppm)	Nd (ppm)	Sm/ Nd	$^{147}Sm/^{144}Nd$	$^{143}Nd/^{144}Nd$	Uncert.*	εNd_0	T_{DM} (Ga)	T (Ma)	εNd_T
111-16-210A01	409596	6303716	Rhyolite	1	5.52	26.55	0.21	0.1257	0.511960	0.000007	-13.2	2.08	1884	4.0
111-16-220B01	411975	6309079	Aphyric andesite	3b	2.13	7.38	0.29	0.1743	0.512533	0.000006	-2.0	N/A	1884	3.4
111-16-318A01	409573	6297103	Amphibole-porphyroblastic andesite	3b	3.88	17.48	0.22	0.1344	0.512040	0.000007	-11.7	2.15	1884	3.4
111-16-203A01	413972	6306969	Plagioclase-phyric basalt	3c	3.60	12.95	0.28	0.1682	0.512460	0.000006	-3.5	N/A	1884	3.4
111-16-207A01	413710	6306883	Plagioclase-phyric andesite	3c	5.67	21.19	0.27	0.1617	0.512378	0.000007	-5.1	N/A	1884	3.4
111-16-215A01	412813	6309586	Plagioclase-phyric basalt	3c	1.35	4.63	0.29	0.1761	0.512598	0.000010	-0.8	N/A	1884	4.2

Notes:
[1] UTM Zone14N, NAD83
[2] Map units in Yang and Beaumont-Smith (2016b)
T_{DM} not calculated for samples with $^{147}Sm/^{144}Nd > 0.14$
All samples relative to La Jolla $^{143}Nd/^{144}Nd = 0.511850$
* Uncertainty is 2 σ abolute errors on $^{143}Nd/^{144}Nd$; estimated error of $^{147}Sm/^{144}Nd$ is better than 0.2%
T_{DM} uses the linear model of Goldstein et al. (1984)

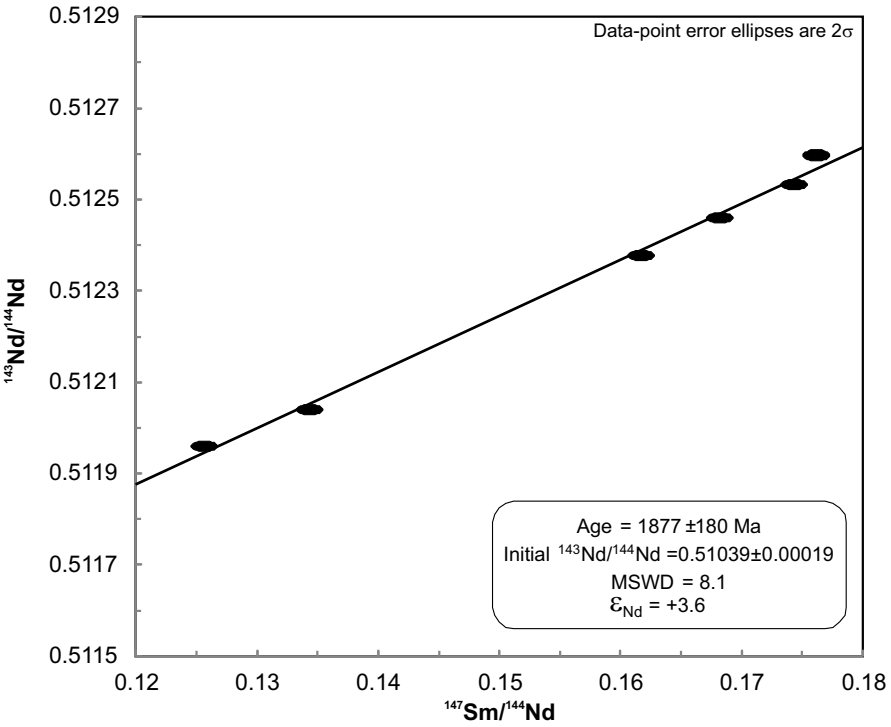

Figure GS2018-8-11: *Errorchron plot of $^{147}Sm/^{144}Nd$ vs. $^{143}Nd/^{144}Nd$ ratios for the Farley Lake volcanic rocks, Lynn Lake greenstone belt.*

lite sample (Beaumont-Smith, unpublished data, 2006; Yang and Beaumont-Smith, 2016a).

Figure GS2018-8-12 presents a time (t) versus ε_{Nd} evolution diagram for the 1884 Ma Farley Lake volcanic rocks. The evolution line of depleted mantle is based on Goldstein et al. (1984). Six samples of volcanic rocks from the Farley Lake area yielded ε_{Nd} values ranging from +3.4 to +4.2 at an age of 1884 Ma, suggesting that they are derived from a depleted mantle source and that crustal contamination was limited. The two dashed lines show the trend of ε_{Nd} values of the magmas since their separation from the depleted-mantle source at approximately 2.2 to 2.1 Ga (T_{DM}; Table GS2018-8-2). The juvenile Nd isotopic compositions, combined with their trace-element characteristics (e.g., slightly enriched, notable Nb, Ta and Ti anomalies), suggest that the Farley Lake volcanic rocks were emplaced into an island-arc environment (see the insets in Figure GS2018-8-12).

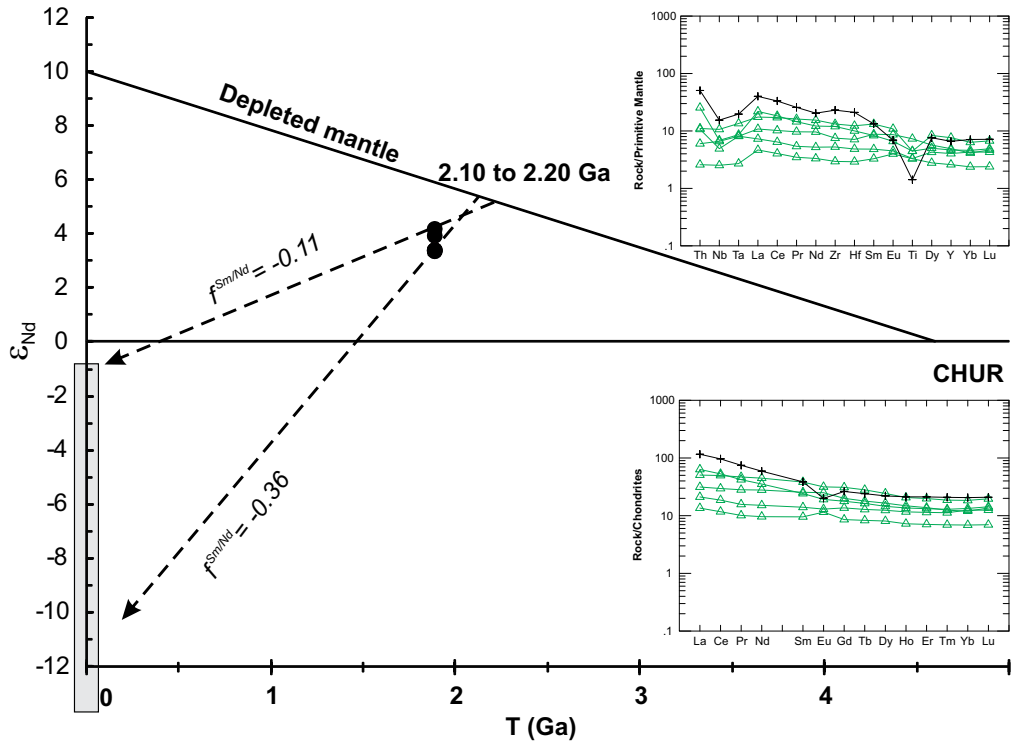

Figure GS2018-8-12: *Time (t) vs. ε_{Nd} evolution diagram for the 1.884 Ga Farley Lake volcanic rocks. Insets show the REE patterns and extended trace-element profiles of these six volcanic samples analyzed for Sm-Nd isotopes (Table GS2018-8-2). $f^{Sm/Nd}$ denotes fractionation factor (see Rollinson, 1993).*

SHRIMP U-Pb zircon dating

In order to establish timing of the various granitoid magmatism events in the Farley Lake area, three granitoid samples with distinctively different compositions were selected on the basis of field relationships for U-Pb zircon age determination using the sensitive high-resolution ion microprobe (SHRIMP) at the Geological Survey of Canada, Ottawa. Details about the method and data may be found in Lawley et al. (2018). Concordia diagrams for these samples are presented in Figure GS2018-8-13.

Sample 111-16-353A01 is a medium-grained granodiorite collected from a unit 6 granitoid pluton (Yang and Beaumont-Smith, 2016a) that intruded the volcanic and volcaniclastic rocks intercalated with metasedimentary rocks and BIF (Figure GS2018-8-2). Zircon grains recovered from this sample are prismatic to stubby and display oscillatory zoning. Concordant zircon grains yielded a weighted average $^{207}Pb/^{206}Pb$ age of 1879.4 ±4.3 Ma (Figure GS2018-8-13a). This age falls into the range for the 1890 to 1876 Ma Pool Lake plutonic suite (Baldwin et al., 1987; Beaumont-Smith and Böhm, 2002, 2003, 2004), implying that the granodiorite is part of the pre-Sickle intrusive suite (Yang and Beaumont-Smith, 2016a).

Sample 111-15-162A01 is a foliated, medium- to coarse-grained alkali-feldspar granite collected from a unit 7 granite intrusion that cuts unit 6 granitoid rocks (Yang and Beaumont-Smith, 2016a, b; Figure GS2018-8-2). Zircon grains retrieved from this sample display complex growth zoning, some with metasomatic domains. Concordant zircon grains yielded a weighted average $^{207}Pb/^{206}Pb$ age of 1872.6 ±2.5 Ma (Figure GS2018-8-13b), attributed to the pre-Sickle intrusive suite.

Sample 111-15-162A01 is a moderately foliated, medium-grained quartz diorite taken from a small stock that cuts mafic volcanic rocks and intercalated BIF at the south edge of the Gordon open pit (Figure GS2018-8-2). Zircon grains recovered from this sample are prismatic with typically oscillatory zonation. Concordant zircon grains yielded a weighted average $^{207}Pb/^{206}Pb$ age of 1854.4 ±2.4 Ma (Figure GS2018-8-13c). The age of the quartz diorite suggests that it could belong to the ca. 1865–1850 Ma Wathaman-Chipewyan plutonic suite (Corrigan et al., 2009).

Conclusions and economic considerations

Bedrock geological mapping, petrographic observations, lithogeochemical characterization and Sm-Nd

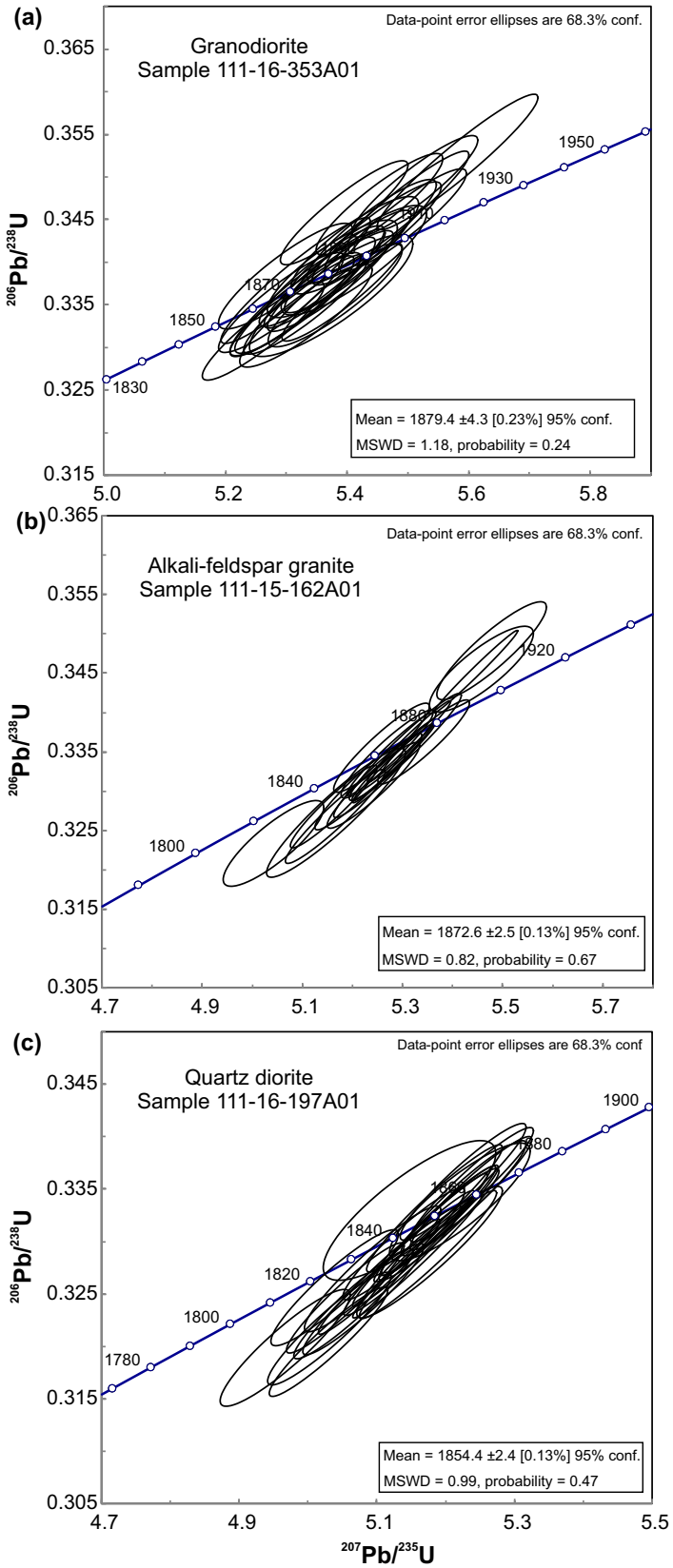

Figure GS2018-8-13: *Concordia diagram of sensitive high-resolution ion microprobe (SHRIMP) U-Pb zircon age data for granitoid samples from the Farley Lake area, Lynn Lake greenstone belt:* ***a)*** *unit 6 granodiorite, sample 111-16-353A01, UTM 412105E, 6306254N (Zone 14, NAD83);* ***b)*** *unit 7 alkali-feldspar granite, sample 111-15-162A01, UTM 411172E, 6301517N; and* ***c)*** *unit 8 quartz diorite, sample 111-16-197A01, UTM 412573E, 6307761N).*

isotopic results for volcanic rocks in the Farley Lake area provide clues to the origin and tectonic setting of the LLGB. Mafic to felsic volcanic rock samples yielded Sm/Nd ratios <1; enriched REE patterns; and extended trace-element profiles with notable, negative Nb, Ta and Ti anomalies. They follow a BADR compositional trend, suggesting that the volcanic (and sedimentary) rocks hosting the Gordon Au deposit in the Farley Lake area may have been deposited in an island-arc to back-arc tectonic setting.

Fine-grained interflow sediments, including BIF, argillite and lesser turbidite successions, are interpreted to be coeval with mafic to felsic volcanic rocks and likely mark volcanic hiatuses in a marine environment marginal to the active arc. An initial ε_{Nd} ratio of +3.6 for a suite of six, presumably cogenetic samples that yielded an errorchron age of 1877 ±180 Ma further suggests that a depleted mantle was the primary source of volcanism, which is in contrast to enriched, plume-like sources inferred for mafic volcanic rocks hosting the MacLellan Au-Ag deposit and elsewhere in the LLGB (Glendenning et al., 2015). The juvenile character of the Farley Lake volcanic rocks suggests that crustal contamination was limited, which is consistent with their interpreted island-arc setting and magma sourcing from a depleted mantle. Felsic to mafic volcanic rocks of the LLGB are also coeval with the subduction of the Manikewan ocean plate and may have been situated on the upper plate above a subduction zone (i.e., polarity to southeast) prior to the terminal stage of accretionary orogenesis with the Archean Hearn craton to the northwest (Hoffmann, 1988; Corrigan et al., 2007, 2009; Zwanzig and Bailes, 2010).

The SHRIMP U-Pb zircon ages, together with field relationships (Yang and Beaumont-Smith, 2016a, b), of granitoid rocks at Farley Lake indicate that supracrustal rocks were intruded by a successive suite of granitoid intrusions with distinct geochemistry. Pre-Sickle, volcanic-arc, I-type granodiorite likely intruded an immature to mature arc at ca. 1879 Ma, whereas the composition of ca. 1872 Ma granitic rocks (A-type) is more typical of an intra-arc extensional environment. These granitoids with different geochemical affinities suggest that intrusive rocks were structurally juxtaposed after emplacement, possibly during regional, main deformation at 1.81–1.80 Ga (see Beaumont-Smith and Böhm, 2002, 2003, 2004), and/or that disparate source regions were tapped at the same time within an evolving arc.

Younger (ca. 1854 Ma) adakite-like quartz diorite to monzodiorite are temporally and geochemically distinct from other granitoid rocks at Farley Lake. The composition of intermediate granitoids may be indicative of direct partial melting of the subducting slab and/or partial melting of prior metasomatized sub-arc lithospheric mantle due to instability within the mantle wedge after accretionary orogenesis but prior to ca. 1.83–1.80 Ga continent-continent collision between the Superior and Hearne cratons (Corrigan et al., 2009). Adakite-like intrusions, which are not related to older arc-type granitoid rocks, are known elsewhere as important hostrocks for some orogenic Au, intrusion-related Au, Fe oxide–Cu–Au and Carlin-type Au deposits (Groves et al., 2016). Intra-arc extensional settings represent favourable geological environments for Au concentration as late to postorogenic magmatism heated the crust and drove hydrothermal fluids.

Mapping reported here and previously, however, documents a pre-existing to synchronous deformation and metamorphic timing for an early generation of auriferous veins at the Gordon Au deposit. Peak metamorphism likely occurred at 1.81–1.80 Ga and continued until ca. 1.78 Ga, based on metamorphic zircon and/or monazite ages for the LLGB (Beaumont-Smith and Böhm, 2002, 2003, 2004; Lawley et al., 2018). Postdeformational veins were also reported from vein studies prior to flooding of the open pit at the Gordon Au deposit. The late timing of these veins and whether they contain Au are important questions that remain to be resolved. Nevertheless, the ca. 1854 Ma adakite-like intrusions predate the inferred timing of the earliest generation of auriferous veins by tens of millions of years. Adakite-like intrusions, therefore, represent an unlikely source for Au in the LLGB.

The spatial relationship between adakite-like intrusions and Au deposits in the LLGB, however, may still have economic significance. Adakite-like intrusions sampled within the open pit at the Gordon Au deposit, coupled with the distribution of other ca. 1.85 Ga plutons along the main Au-rich trend in the northern LLGB, suggest that auriferous fluids were focused along faults that reactivated the same structural architecture exploited by adakite-like intrusions. The most favourable faults for Au mineralization in the LLGB may therefore represent some of the earliest structures that juxtaposed the disparate volcanic and magmatic suites. Whether the distinct ca. 1.85 Ga magmatic event represents a favourable marker for Au in the LLGB and/or elsewhere in the Trans-Hudson orogeny, however, requires further study. In contrast, faults and favourable lithological assemblages that destabilize Au-S complexes within circulating hydrothermal fluids are clearly important and represent dominant ore-system controls at the Gordon Au deposit. The timing and source of auriferous fluids are the subject of ongoing

collaborative research between the MGS and the GSC via the TGI-5 program.

Acknowledgments

The authors thank C. Kovachik, J. Watts and E. Amyotte for providing enthusiastic and capable field assistance; E. Anderson and N. Brandson for thorough logistical support; and C. Epp for cataloguing, processing and preparing the samples. We thank T. Martins and C.O. Böhm for constructive reviews of the manuscript and R.F. Davie for technical editing of the report. Alamos Gold Inc. generously allowed access to its properties and drillcore facilities.

References

Anderson, S.D. 2013: Geology of the Garner–Gem lakes area, Rice Lake greenstone belt, southeastern Manitoba (parts of NTS 52L11, 14); Manitoba Mineral Resources, Manitoba Geological Survey, Geoscientific Report GR2013-1, 135 p.

Arndt, N.T. 2013: The formation and evolution of the continental crust; Geochemical Perspectives, v. 2, p. 405–533.

Ansdell, K.M. 2005: Tectonic evolution of the Manitoba-Saskatchewan segment of the Paleoproterozoic Trans-Hudson Orogen, Canada; Canadian Journal of Earth Sciences, v. 42, p. 741–759.

Ansdell, K.M., Corrigan, D., Stern, R. and Maxeiner, R. 1999: SHRIMP U-Pb geochronology of complex zircons from Reindeer Lake, Saskatchewan: implications for timing of sedimentation and metamorphism in the northwestern Trans-Hudson Orogen; Geological Association of Canada–Mineralogical Association of Canada, Joint Annual Meeting, Program with Abstracts, v. 24, p. 3.

Baldwin, D.A., Syme, E.C., Zwanzig, H.V., Gordon, T.M., Hunt, P.A. and Stevens, R.P. 1987: U-Pb zircon ages from the Lynn Lake and Rusty Lake metavolcanic belts, Manitoba: two ages of Proterozoic magmatism; Canadian Journal of Earth Sciences, v. 24, p. 1053–1063.

Baragar, W.R.A., Ernst, R.E., Hulbert, L. and Peterson, T. 1996: Longitudinal petrochemical variation in the Mackenzie dyke swarm, northwestern Canadian Shield; Journal of Petrology, v. 37, p. 317–359.

Bateman, J.D. 1945: McVeigh Lake area, Manitoba; Geological Survey of Canada, Paper 45-14, 34 p.

Beaumont-Smith, C.J. 2008: Geochemistry data for the Lynn Lake greenstone belt, Manitoba (NTS 64C11-16); Manitoba Science, Technology, Energy and Mines, Manitoba Geological Survey, Open File OF2007-1, 5 p.

Beaumont-Smith, C.J. and Böhm, C.O. 2002: Structural analysis and geochronological studies in the Lynn Lake greenstone belt and its gold-bearing shear zones (NTS 64C10, 11, 12, 14, 15 and 16), Manitoba; *in* Report of Activities 2002, Manitoba Industry, Trade and Mines, Manitoba Geological Survey, p. 159–170.

Beaumont-Smith, C.J. and Böhm, C.O. 2003: Tectonic evolution and gold metallogeny of the Lynn Lake greenstone belt, Manitoba (NTS 64C10, 11, 12, 14, 15 and 16), Manitoba; *in* Report of Activities 2003, Manitoba Industry, Economic Development and Mines, Manitoba Geological Survey, p. 39–49.

Beaumont-Smith, C.J. and Böhm, C.O. 2004: Structural analysis of the Lynn Lake greenstone belt, Manitoba (NTS 64C10, 11, 12, 14, 15 and 16); *in* Report of Activities 2004, Manitoba Industry, Economic Development and Mines, Manitoba Geological Survey, p. 55–68.

Beaumont-Smith, C.J., Machado, N. and Peck, D.C. 2006: New uranium-lead geochronology results from the Lynn Lake greenstone belt, Manitoba (NTS 64C11-16); Manitoba Science, Technology, Energy and Mines, Manitoba Geological Survey, Geoscientific Paper GP2006-1, 11 p.

Böhm, C.O., Zwanzig, H.V. and Creaser, R.A. 2007: Sm-Nd isotope technique as an exploration tool: delineating the northern extension of the Thompson Nickle Belt, Manitoba, Canada; Economic Geology, v. 102, p. 1217–1231.

Christiansen, E.H. and Keith, J.D. 1996: Trace-element systematics in silicic magmas: a metallogenic perspective; *in* Trace element geochemistry of volcanic rocks: applications for massive sulfide exploration, D.A. Wyman (ed.), Geological Association of Canada, Short Course Notes, no. 12, p. 115–151.

Chauvel, C., Arndt, N.T., Kielinzcuk, S. and Thom, A. 1987: Formation of Canadian 1.9 Ga old continental crust. I: Nd isotopic data; Canadian Journal of Earth Sciences, v. 26, p. 396–406.

Corrigan, D., Galley, A.G. and Pehrsson, S. 2007: Tectonic evolution and metallogeny of the southwestern Trans-Hudson Orogen; *in* Mineral Deposits of Canada: A Synthesis of Major Deposit-Types, District Metallogeny, the Evolution of Geological Provinces, and Exploration Methods, W.D. Goodfellow (ed.), Geological Association of Canada, Mineral Deposits Division, Special Publication 5, p. 881–902.

Corrigan, D., Pehrsson, S., Wodicka, N. and de Kemp, E. 2009: The Palaeoproterozoic Trans-Hudson Orogen: a prototype of modern accretionary processes; *in* Ancient Orogens and Modern Analogues, J.B. Murphy, J.D. Keppie, and A.J. Hynes (ed.), Geological Society of London, Special Publications, v. 327, p. 457–479.

Eby, G.N. 1990: The A-type granitoids: a review of their occurrence and chemical characteristics, and speculations on their petrogenesis; Lithos, v. 26, p. 115–134.

Fedikow, M.A.F. and Gale, G.H. 1982: Mineral deposit studies in the Lynn Lake area; *in* Report of Field Activities 1982, Manitoba Department of Energy and Mines, Mineral Resources Division, p. 44–54.

Frisch, W., Meschede, M. and Blakey, R. 2011: Plate tectonics: continental drift and mountain building. Springer, Heidelberg, 212 p.

Frost, B.R., Barnes, C.G., Collins, W.J., Arculus, R.J., Ellis, D.J. and Frost, C.D. 2001: A geochemical classification for granitic rocks; Journal of Petrology, v. 42, p. 2033–2048.

Gilbert, H.P. 1993: Geology of the Barrington Lake–Melvin Lake–Fraser Lake area; Manitoba Energy and Mines, Geological Services, Geological Report GR87-3, 97 p.

Gilbert, H.P., Syme, E.C. and Zwanzig, H.V. 1980: Geology of the metavolcanic and volcaniclastic metasedimentary rocks in the Lynn Lake area; Manitoba Energy and Mines, Mineral Resources Division, Geological Paper GP80-1, 118 p.

Glendenning, M.W.P., Gagnon, J.E. and Polat, A. 2015: Geochemistry of the metavolcanic rocks in the vicinity of the MacLellan Au-Ag deposit and an evaluation of the tectonic setting of the Lynn Lake greenstone belt, Canada: evidence for a Paleoproterozoic-aged rifted continental margin; Lithos, v. 233, p. 46–68.

Goldstein, S.L., O'Nions, R.K. and Hamilton, P.J. 1984: A Sm-Nd study of atmospheric dusts and particulates from major river systems; Earth and Planetary Science Letters, v. 70, p. 221–236.

Groves, D.I., Goldfarb, R.J. and Santosh, M. 2016: The conjunction of factors that led to formation of giant gold provinces and deposits in non-arc settings; Geoscience Frontiers, v. 7, p. 303–314.

Hoffman, P.H. 1988: United plates of America, the birth of a craton: Early Proterozoic assembly and growth of Laurentia; Annual Reviews of Earth and Planetary Sciences, v. 16, p. 543–603.

Harris, N.B.W., Pearce, J.A. and Tindle, A.G. 1986: Geochemical characteristics of collision-zone magmatism; *in* Collision Tectonics, M.P. Coward and A.C. Reis (ed.), Geological Society of London, Special Publications, v. 19, p. 67–81.

Hastie, E.C.G., Gagnon, J.E. and Samson, I.M. 2018: The Paleoproterozoic MacLellan deposit and related Au-Ag occurrences, Lynn Lake greenstone belt, Manitoba: an emerging, structurally controlled gold camp; Ore Geology Reviews, v. 94, p. 24–45.

Irvine, T.N. and Baragar, W.R.A. 1971: A guide to the chemical classification of the common volcanic rocks; Canadian Journal of Earth Sciences, v. 8, p. 523–548.

Kremer, P. D., Rayner, N. and Corkery, M.T. 2009: New results from geological mapping in the west-central and northeastern portions of Southern Indian Lake, Manitoba (parts of NTS 64G1, 2, 8, 64H4, 5); *in* Report of Activities 2009, Manitoba Science, Innovation, Energy and Mines, Manitoba Geological Survey, p. 94–107.

Lawley, C.J.M., Schneider, D., Yang, E., Davis, W.J., Jackson, S.E., Yang, Z., Zhang, S. and Selby, D. 2018: Age relationships and preliminary U-Pb zircon geochronology results from the Lynn Lake greenstone belt; *in* Targeted Geoscience Initiative: 2017 report of activities, volume 1, N. Rogers (ed.), Geological Survey of Canada, Open File 8358, p. 133–137.

Le Bas, M.J., Le Maitre, R.W., Streckeisen, A. and Zanettin, B. 1986: A chemical classification of volcanic rocks based on the total alkali silica diagram; Journal of Petrology, v. 27, p. 745–750.

Lewry, J.F. and Collerson, K.D. 1990: The Trans-Hudson Orogen: extent, subdivisions and problems; *in* The Early Proterozoic Trans-Hudson Orogen of North America, J.F. Lewry and M.R. Stauffer (ed.), Geological Association of Canada, Special Paper 37, p. 1–14.

Ludwig, K.R. 2008: User's manual for Isoplot 3.70: a geochronological toolkit for Microsoft Excel; Berkeley Geochronology Center, Special Publication 4, 76 p.

Maniar, P.D. and Piccoli, P.M. 1989: Tectonic discrimination of granitoids; Geological Society of America Bulletin, v. 101, p. 635–643.

Manitoba Energy and Mines 1986: Granville Lake, NTS 64C; Manitoba Energy and Mines, Minerals Division, Bedrock Geology Compilation Map Series, Map 64C, scale 1:250 000.

Martin, H., Smithies, R.H., Rapp, R., Moyen, J.-F. and Champion, D., 2005: An overview of adakite, tonalite-trondhjemite-granodiorite (TTG), and sanukitoid: relationships and some implications for crustal evolution; Lithos, v. 79, p. 1–24.

Meschede, M. 1986: A method of discriminating between different types of mid-ocean basalts and continental tholeiites with the Nb-Zr-Y diagram; Chemical Geology, v. 56, p. 207–218.

Milligan, G.C. 1960: Geology of the Lynn Lake district; Manitoba Department of Mines and Natural Resources, Mines Branch, Publication 57-1, 317 p.

Norman, G.W.H. 1933: Granville Lake district, northern Manitoba; Geological Survey of Canada, Summary Report, Part C, p. 23–41.

Moyen, J.-F. and Martin, H. 2012: Forty years of TTG research; Lithos, v. 148, p. 312–336.

Park, A.F., Beaumont-Smith, C.J. and Lentz, D.R. 2002: Structure and stratigraphy in the Agassiz Metallotect, Lynn Lake greenstone belt (NTS 64C/14 and /15), Manitoba; *in* Report of Activities 2002, Manitoba Industry, Trade and Mines, Manitoba Geological Survey, p. 171–186.

Pearce, J.A. 1996: A user's guide to basalt discrimination diagrams; *in* Trace Element Geochemistry of Volcanic Rocks: Applications for Massive Sulphide Exploration, D.A. Wyman (ed.), Geological Association of Canada, Short Course Notes, no. 12, p. 79–113.

Pearce, J.A. 2008: Geochemical fingerprinting of oceanic basalts with applications to ophiolite classification and the search for Archean oceanic crust; Lithos, v. 100, p. 14–48.

Pearce, J.A., Harris, N.B.W. and Tindle, A.G. 1984: Trace element discrimination diagrams for the tectonic interpretation of granitic rocks; Journal of Petrology, v. 25, p. 956–983.

Pearce, J.A. and Peate, D.W. 1995: Tectonic implications of the composition of volcanic arc magmas; Annual Review of Earth and Planetary Sciences, v. 23, p. 251–285.

Richards, J.P. and Kerrich, R. 2007: Special paper: dakite-like rocks: their diverse origins and questionable role in metallogenesis; Economic Geology, v. 102, p. 537–576, URL <https://doi.org/10.2113/gsecongeo.102.4.537> [November 2018].

Rittmann, A. 1973: Stable mineral assemblages of igneous rocks; Springer-Verlag, Berlin, 262 p.

Rollinson, H.R. 1993: Using geochemical data: evaluation, presentation, interpretation; Routledge, Taylor & Francis Group, London and New York, 352 p.

Rudnick, R.L. and Gao, S. 2003: Composition of the continental crust; Treatise on Geochemistry, v. 3, p. 1–64.

Shirey, S.B. and Hanson, G.N. 1984: Mantle-derived Archaean monozodiorites and trachyandesites; Nature, v. 310, p. 222–224.

Stauffer, M.R. 1984: Manikewan: an Early Proterozoic ocean in central Canada, its igneous history and orogenic closure; Precambrian Research, v. 25, p. 257–281.

Stern, R., Hanson, G.N. and Shirey, S.B. 1989: Petrogenesis of mantle derived LILE-enriched Archaean monzodiorite, trachyandesites (sanukitoids) in southern Superior Province; Canadian Journal of Earth Sciences, v. 26, p. 1688–1712.

Stern, R.A., Syme, E.C. and Lucas, S.B. 1995: Geochemistry of 1.9 Ga MORB- and OIB-like basalts from the Amisk collage, Flin Flon Belt, Canada: evidence for an intra-oceanic origin; Geochimica et Cosmochimica Acta, v. 59, p. 3131–3154.

Streckeisen, A.L. and LeMaitre, R.W. 1979: A chemical approximation to modal QAPF classification of the igneous rocks; Neues Jahrbuch für Mineralogie, v. 136, p. 169–206.

Sun, S.-s. and McDonough, W.F. 1989: Chemical and isotopic systematics of oceanic basalts: implications for mantle composition and processes; *in* Magmatism in the Ocean Basins, A.D. Saunders and M.J. Norry (ed.), Geological Society of London, Special Publications, v. 42, p. 313–345.

Syme, E.C. 1985: Geochemistry of metavolcanic rocks in the Lynn Lake Belt; Manitoba Energy and Mines, Geological Services, Geological Report GR84-1, 84 p. plus 1 map at 1:100 000 scale.

Turek, A., Woodhead, J. and Zwanzig H.V. 2000: U-Pb age of the gabbro and other plutons at Lynn Lake (part of NTS 64C); *in* Report of Activities 2000, Manitoba Industry, Trade and Mines, Manitoba Geological Survey, p. 97–104.

Whalen, J.B., Currie, K.L. and Chappell, B.W. 1987: A-type granites: geochemical characteristics, discrimination and petrogenesis; Contributions to Mineralogy and Petrology, v. 95, p. 407–419.

Whalen, J.B. and Frost, C.D. 2013: The Q-ANOR diagram: a tool for the petro-genetic and tectonomagmatic characterization of granitic suites; URL <https://www.researchgate.net/publication/290161821> [September 2018].

Wood, D.A. 1980: The application of a Th-Hf-Ta diagram to problems of tectonomagmatic classification and to establishing the nature of crustal contamination of basaltic lavas of the British Tertiary volcanic province; Earth and Planetary Science Letters, v. 50, p. 11–30.

Yang, X.M. 2007: Using the Rittmann Serial Index to define the alkalinity of igneous rocks; Neues Jahrbuch für Mineralogie, v. 184, p. 95–103.

Yang, X.M. and Beaumont-Smith, C.J. 2015: Geological investigations of the Keewatin River area, Lynn Lake greenstone belt, northwestern Manitoba (parts of NTS 64C14, 15); *in* Report of Activities 2015, Manitoba Mineral Resources, Manitoba Geological Survey, p. 52–67.

Yang, X.M. and Beaumont-Smith, C.J. 2016a: Geological investigations in the Farley Lake area, Lynn Lake greenstone belt, northwestern Manitoba (part of NTS 64C16); *in* Report of Activities 2016, Manitoba Growth, Enterprise and Trade, Manitoba Geological Survey, p. 99–114.

Yang, X.M. and Beaumont-Smith, C.J. 2016b: Bedrock geology of the Farley Lake area, Lynn Lake greenstone belt, northwestern Manitoba (part of NTS 64C16); Manitoba Growth, Enterprise and Trade, Manitoba Geological Survey, Preliminary Map PMAP2016-5, scale 1:20 000.

Yang, X.M. and Beaumont-Smith, C.J. 2017: Geological investigations of the Wasekwan Lake area, Lynn Lake greenstone belt, northwestern Manitoba (parts of NTS 64C10, 15); *in* Report of Activities 2017, Manitoba Growth, Enterprise and Trade, Manitoba Geological Survey, p. 117–132.

Zwanzig, H.V., Syme, E.C. and Gilbert, H.P. 1999: Updated trace element geochemistry of ca. 1.9 Ga metavolcanic rocks in the Paleoproterozoic Lynn Lake belt; Manitoba Industry, Trade and Mines, Geological Services, Open File Report OF99-13, 46 p.

Zwanzig, H.V. and Bailes, A.H. 2010: Geology and geochemical evolution of the northern Flin Flon and southern Kisseynew domains, Kississing–File lakes area, Manitoba (parts of NTS 63K, N); Manitoba Innovation, Energy and Mines, Manitoba Geological Survey, Geoscientific Report GR2010-1, 135 p.

GS2018-9

Summary of helium occurrences in southwestern Manitoba

by M.P.B. Nicolas

In Brief:

- 80% of the oil and gas wells tested in Manitoba have helium gas
- Six wells have economic helium concentration between 0.30 to 2.00 mol %
- Deadwood, Winnipeg, Bakken and Torquay formations have good potential as helium reservoirs

Citation:
Nicolas, M.P.B. 2018: Summary of helium occurrences in southwestern Manitoba; *in* Report of Activities 2016, Manitoba Growth, Enterprise and Trade, Manitoba Geological Survey, p. 110–118.

Summary

Southwestern Manitoba is geologically well positioned for economic helium deposits within its sedimentary strata. A search of oil and gas technical well files identified 69 wells with recorded helium occurrences. Of those occurrences, six wells had helium values above the economic cut-off of 0.30 mol % He with ranges from 0.30 to 2.00 mol % He. The best helium values came from the sandstone of the lower Winnipeg Formation to the weathered Precambrian regolith interval, the Middle Bakken Member to Torquay Formation interval and the Mission Canyon Formation. The source of this helium is thought to be the basement Precambrian rocks and radioactive (high gamma ray or 'hot') shales of the Upper Bakken Member. The best prospects for economic helium deposits are within the Deadwood to Winnipeg formations interval overlying Precambrian rocks where basement structural features may have created trapping conditions; and within the Middle Bakken Member to Torquay Formation interval where the Middle Bakken Member sandstone is thick and the Upper Bakken Member shale has a strong gamma-ray ('hot') signature.

Introduction

The second element on the periodic table after hydrogen, helium is a nontoxic, chemically inert, light element with a low density, low boiling point and high thermal conductivity. These properties make it the ideal element for a multitude of uses, including in cryogenic applications, as a coolant for superconductors such as the magnets used in magnetic resonance imaging (MRI) machines and particle colliders (e.g., the Large Hadron Collider), in fibre optics and silicon wafer manufacturing, in the space industry, in air tanks for scuba diving, as a shielding gas in arc welding, as a tracer gas for detecting leaks in an industrial high vacuum, in high pressure systems and in balloons, the most commonly known use.

The United States is the world's largest producer of helium (accounting for 80% of the worldwide helium production), followed by Algeria, Qatar, Russia and Canada (United States Geological Survey, 2018). Increased demand and a decreased US supply have resulted in an increase in the price of helium, sparking a renewed interest to explore for helium in politically stable countries like Canada, and specifically in provinces such as Saskatchewan (Yurkowski, 2016).

Helium is formed primarily by the radioactive decay of uranium- and thorium-bearing minerals in crystalline Precambrian basement rocks and in detrital sedimentary rocks such as shale. In the subsurface, this element can diffuse through solid rock into porewater, where its transmissivity is strongly controlled by the chemistry of the migrating fluids in which it resides. Unless trapped underground, this small and light element will reach the Earth's surface, where it easily escapes the atmosphere into space. Less than 5 ppm He resides in the Earth's atmosphere.

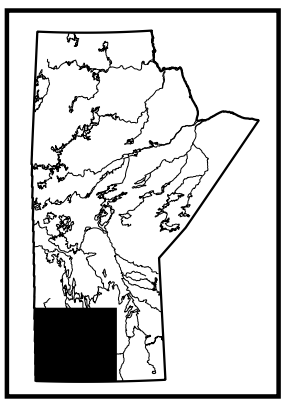

Helium can occur in the subsurface in concentrations of up to 8% (National Academy of Sciences, 2000), in association with natural gases such as nitrogen, carbon dioxide, methane and minute amounts of other noble gases. Economic concentrations of helium can be produced as a byproduct of oil and gas production operations and is referred to as crude helium. It is estimated that at concentrations greater than 0.3% by volume (or 0.3 mol % assuming ideal gas conditions), helium can be economically separated from natural gas during the removal of nitrogen, a process used to improve the heating value of natural gas (National Academy of Sciences, 2000).

In Manitoba, exploration for helium was conducted near the community of Lundar, on the east side of Lake Manitoba. In 1962, Hemisphere Helium Corporation drilled two wells at L.S. 14, Sec. 17, Twp. 20, Rge. 5, W 1st Mer. (abbreviated 14-17-20-05W1) and 16-15-20-06W1, where they collected four fluid samples that returned helium concentrations of 0.2–2.0 mol % from the lower sandstone member of the Winnipeg Formation (Hemisphere Helium Corporation Ltd., 1962a, b). Both wells had drill stem tests (DSTs) run, testing the Red River Formation and the lowermost sandstone beds of the Winnipeg Formation to the uppermost interval of the weathered Precambrian rocks. All DST results show strong initial gas flows, followed by a decrease in gas and increase in water flows over the course of the tests (Hemisphere Helium Corporation Ltd., 1962a, b).

Before 1950, documented helium occurrences were identified in 2-22-2-9W1, 8-26-2-9W1, 3-9-12-7W1, 8-23-20-6W1 and NE-35-12-7W1. Concentrations measured were between 0.08 and 5.44% helium by volume. Sparse information is available on these occurrences and the stratigraphic intervals from which these gas analyses were collected is uncertain. These occurrences are shown in Figure GS2018-9-1 and listed Table GS2018-9-1; however, although these occurrences are worth mentioning, they will not be discussed further herein due to the uncertainty of the information available.

No known active helium exploration has occurred in the province since 1962, but recent increases in demand has resulted in more inquiries on occurrences in Manitoba. The purpose of this paper is to summarize the known helium occurrences in southwestern Manitoba and provide some geological context to those occurrences.

Helium occurrences

Helium occurrences have been documented during oil and gas operations in Manitoba because gas analyses

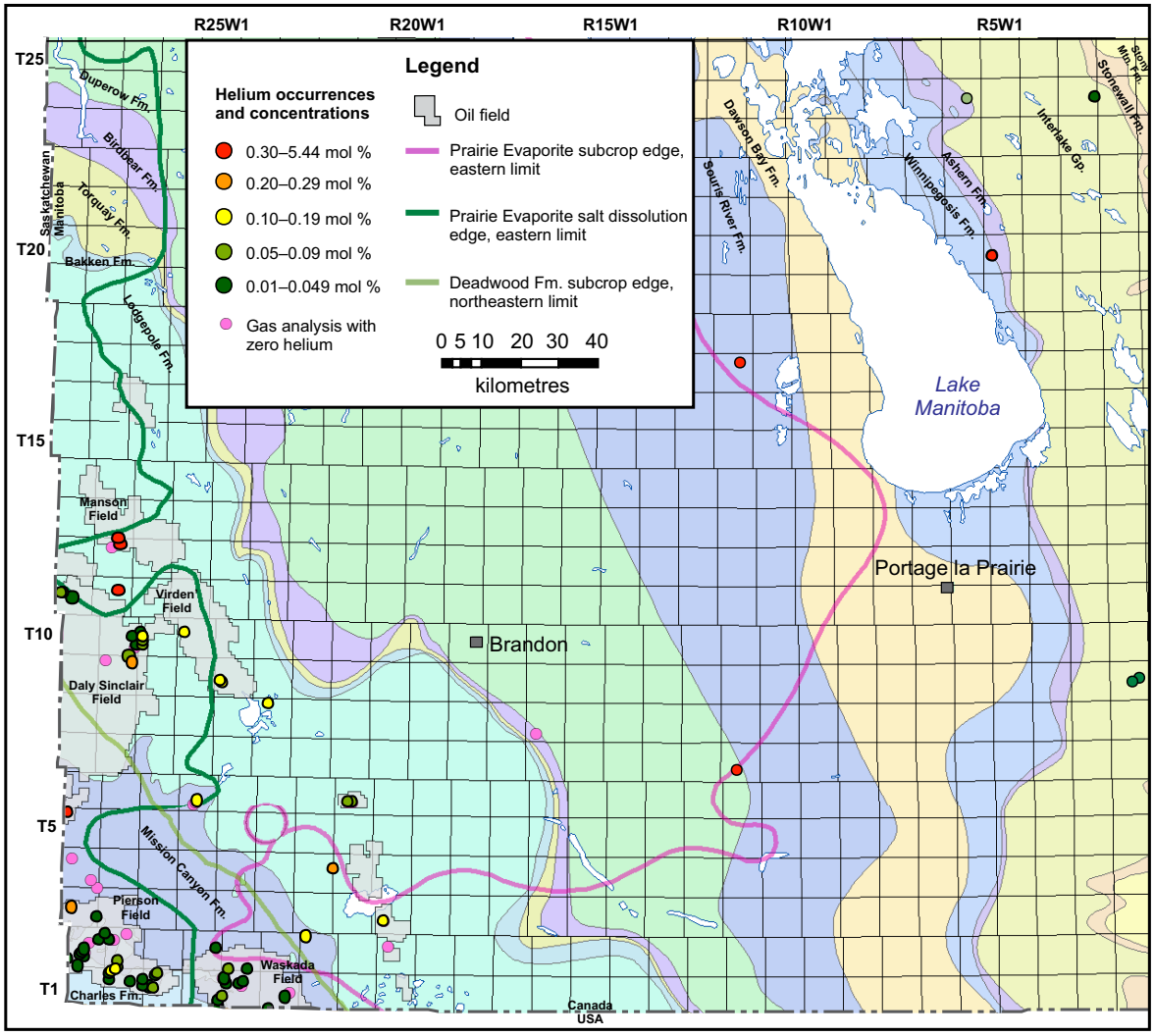

Figure GS2018-9-1: *Paleozoic stratigraphic map showing the distribution of gas analyses and helium occurrences in southwestern Manitoba. Select oil fields are labelled. Abbreviations: Fm., Formation; Gp., Group; Mtn., Mountain.*

Table GS2018-9-1: Helium concentrations reported in gas analyses for southwestern Manitoba. He air free is the concentration of the gas with the air removed and directly measured, and He acid free is the concentration of the gas with the acidic components (H_2S and CO_2) removed. Abbreviations: Fm., Formation; Mb., Member; TVD, true vertical depth.

UWI/location	Licence	Easting	Northing	Depth interval tested (m)	He air free (mol %)	He acid free (mol %)	N_2 air free (mol %)	N_2 acid free (mol %)	CO_2 air free (mol %)	H_2S air free (mol %)	CH_4 air free (mol %)	CH_4 acid free (mol %)	Stratigraphic unit
100/03-05-001-24W1/00	2755	378536.60	5428839.40	913.0–917.0	0.02	0.02	16.67	16.82	0.89	0.00	47.01	47.43	MC-2 Mb.
1C0/16-10-001-24W1/00	5273	382615.89	5431864.69	915.8–918.8	0.02	0.02	5.55	5.57	0.35	0.07	45.83	46.02	Lower Amaranth Mb.
100/13-07-001-25W1/00	2758	366852.68	5432076.42	930.0–948.0	0.06	0.06	19.38	19.38	0.02	0.00	67.24	67.25	MC-3b Mb.
100/16-19-001-25W1/00	7780	368212.17	5435406.94	906.8–908.5 (TVD)**	0.01	0.01	3.61	3.66	1.12	0.19	24.66	24.99	Lower Amaranth Mb.
100/15-21-001-25W1/00	4245	370991.07	5435255.84	898.0–908.0	0.02	0.02	7.84	7.88	0.36	0.09	49.31	49.53	Lower Amaranth Mb.
100/03-27-001-25W1/00	5127	372244.36	5435672.60	897.0–900.0	0.03	0.04	6.84	8.30	17.56	0.00	74.80	90.73	Lower Amaranth Mb.
100/11-30-001-25W1/00	2194	367359.30	5436589.05	920.5–930.2	0.03	0.03	11.04	11.12	0.60	0.13	49.56	49.92	MC-3b Mb.
102/11-30-001-25W1/00	3647	367414.70	5436642.28	924.0–926.0	0.03	0.03	9.07	9.12	0.45	0.06	47.57	47.81	MC-3b Mb.
100/10-01-001-26W1/00	2869	365969.08	5430064.82	912.0–928.0	0.02	0.02	12.14	12.18	0.30	0.00	62.14	62.33	Lower Amaranth Mb.
100/02-12-001-26W1/00	3094	365940.66	5430847.89	935.5–937.5	0.01	0.01	0.00	0.00	0.17	0.00	43.81	43.88	MC-3a Mb.
102/02-12-001-26W1/00	3914	365965.51	5430850.80	933.0–936.3	0.01	0.01	0.00	0.00	0.17	0.00	73.81	56.85	MC-3a Mb.
100/14-17-001-27W1/00	7420	349338.57	5434285.60	963.1–965.2 (TVD)	0.09	0.09	13.93	13.94	0.04	0.00	69.10	69.13	Lower Amaranth Mb.
100/01-19-001-27W1/00	8193	348535.87	5434529.74	959.8–964.2 (TVD)	0.04	0.04	14.34	14.47	0.82	0.10	67.08	67.70	Lower Amaranth Mb.
100/01-20-001-27W1/00	7473	350157.50	5434573.80	963.0–966.0	0.01	0.01	3.23	3.23	0.08	0.00	41.31	41.34	Lower Amaranth Mb.
100/16-29-001-27W1/00	7490	350251.12	5437515.49	949.9–950.0 (TVD)	0.02	0.02	12.28	12.29	0.07	0.00	63.84	63.88	Lower Amaranth Mb.
100/04-33-001-27W1/00	7505	350485.05	5437811.97	940.7–943.6 (TVD)	0.08	0.08	16.37	16.38	0.07	0.00	51.12	51.16	Lower Amaranth Mb.
100/16-22-001-28W1/00	7489	343680.96	5436063.48	986.2–990.8 (TVD)	0.01	0.01	5.39	5.40	0.11	0.00	68.27	68.35	Lower Amaranth Mb.
100/01-24-001-28W1/00	7434	346914.75	5434578.76	968.2–971.3 (TVD)	0.02	0.02	8.38	8.39	0.13	0.00	62.61	62.69	Lower Amaranth Mb.
100/01-25-001-28W1/00	8086	346976.17	5436222.99	967.7–973.1 (TVD)	0.05	0.05	17.57	17.70	0.74	0.00	63.32	63.79	Lower Amaranth Mb.
100/02-30-001-28W1/00	7485	338189.61	5436474.64	1006.0–1007.9 (TVD)	0.03	0.03	12.18	12.18	0.03	0.00	52.53	52.55	Lower Amaranth Mb.
100/15-30-001-28W1/00	7486	338217.13	5437846.77	1002.6–1006.6 (TVD)	0.01	0.01	7.62	7.63	0.11	0.00	44.13	44.18	Lower Amaranth Mb.
100/05-32-001-28W1/00	7487	339060.77	5438654.69	1001.3–1005.1 (TVD)	0.11	0.11	42.77	42.78	0.03	0.00	48.86	48.87	Lower Amaranth Mb.
100/10-32-001-28W1/00	7579	339888.82	5438874.10	979.6–985.6 (TVD)	0.14	0.14	54.54	54.64	0.18	0.00	27.73	27.78	Lower Amaranth Mb.
100/15-32-001-29W1/02	7447	330283.70	5439771.87	1031.2–1033.0 (TVD)	0.01	0.01	2.68	2.68	0.12	0.00	57.32	57.39	Lower Amaranth Mb.
02-22-002-09W1*					0.04		12.23		0.20		87.53		cannot be determined
08-26-002-09W1*					~0.04?								cannot be determined
100/08-31-002-23W1/00	2706	388023.33	5447265.80	812.0–932.0	0.17	0.18	62.59	64.94	2.49	1.13	11.71	12.15	MC-1 Mb.
100/01-03-002-25W1/00	5056	373093.00	5438927.00	877.0–880.0	0.03	0.03	6.58	7.57	13.11	0.00	79.76	91.79	Lower Amaranth Mb.
102/04-05-002-25W1/00	8078	368644.51	5439134.72	898.5–899.8	0.06	0.06	8.97	8.97	0.02	0.00	90.69	90.71	Lower Amaranth Mb.
100/05-24-002-26W1/00	2766	365454.00	5444482.91	893.0–909.0	0.03	0.03	79.02	79.04	0.02	0.00	7.74	7.74	MC-2 and MC-1 Mb.
100/04-04-002-28W1/00	7581	340722.27	5439683.12	878.0–982.0 (TVD)	0.06	0.06	21.83	21.85	0.08	0.00	39.22	39.25	Lower Amaranth Mb.
100/01-08-002-28W1/00	7225	340335.87	5441339.85	988.0–988.8 (TVD)	0.07	0.07	26.58	26.92	1.21	0.07	53.81	54.51	Lower Amaranth Mb.

Table GS2018-9-1 (continued): Helium concentrations reported in gas analyses for southwestern Manitoba. He air free is the concentration of the gas with the air removed and directly measured, and He acid free is the concentration of the gas with the acidic components (H_2S and CO_2) removed. Abbreviations: Fm., Formation; Mb., Member; TVD, true vertical depth.

UWI/location	Licence	Easting	Northing	Depth interval tested (m)	He air free (mol %)	He acid free (mol %)	N_2 air free (mol %)	N_2 acid free (mol %)	CO_2 air free (mol %)	H_2S air free (mol %)	CH_4 air free (mol %)	CH_4 acid free (mol %)	Stratigraphic unit
102/02-30-002-28W1/00	7503	338448.71	5446288.16	971.4–976.8 (TVD)	0.02	0.02	16.15	16.30	0.74	0.18	52.44	52.93	Lower Amaranth Mb.
100/13-06-002-29W1/00	7521	327721.58	5441502.68	1032.3–1032.8 (TVD)	0.04	0.04	9.93	9.99	0.54	0.08	50.60	50.92	Lower Amaranth Mb.
100/08-09-002-29W1/00	3906	332250.20	5442137.57	1020.5–1035.0	0.02	0.02	8.65	8.79	1.10	0.50	40.01	40.66	Lower Amaranth and MC-3b mb.
100/12-09-002-29W1/00	4045	331086.47	5442547.08	1022.5–1025.5	0.05	0.05	8.23	8.23	0.01	0.00	64.34	64.35	Lower Amaranth Mb.
100/03-16-002-29W1/00	4373	331577.71	5443346.81	1033.5–1036.5	0.02	0.02	13.36	13.39	0.22	0.00	61.61	61.75	MC-3b mb.
100/10-16-002-29W1/00	4303	331865.89	5444078.98	1007–1026.5	0.01	0.01	8.86	8.88	0.23	0.00	47.64	47.75	Lower Amaranth Mb.
100/01-26-002-29W1/00	7541	335779.51	5446388.02	981.3–985.2	0.05	0.05	21.94	22.01	0.33	0.00	56.43	56.62	Lower Amaranth Mb.
100/01-36-002-29W1/00	6625	337427.23	5448004.93	1002.5–1004.0	0.01	0.01	0.24	0.24	0.71	0.00	82.94	83.53	MC-3b mb.
100/16-08-003-21W1/00	4869	407907.32	5451204.80	783–787	0.15	0.16	46.21	50.51	8.52	0.00	12.03	13.15	upper Whitewater Lake Mb.
100/10-12-003-29W1/00	3277	335003.63	5452388.94	991.5–995.5	0.02	0.02	12.19	12.19	0.04	0.00	22.57	22.58	MC-3 Mb.
100/16-17-003-29W1/00	3446	328909.49	5454650.89	1003–1014	0.30	0.30	20.90	20.90	0.00	0.00	47.31	47.31	MC-3 Mb.
102/13-19-004-22W1/00	5063	395261.00	5464534.00	772.5–777.5	0.22	0.22	79.23	80.06	1.04	0.00	1.08	1.09	upper Whitewater Lake Mb.
102/09-31-005-29W1/00	2647	327906.14	5478887.96	946.5–948.5	0.68	0.83	42.98	52.73	13.43	5.06	8.01	9.83	MC-1 Mb.
100/02-16-006-22W1/00	1883	399704.84	5481225.54	650.0–655.0	0.10	0.12	55.13	65.95	16.41	0.00	1.36	1.63	upper Virden Mb.
100/04-16-006-22W1/00	1884	398892.74	5481241.88	662.9–662.9	0.07	0.08	39.22	44.42	11.70	0.01	1.22	1.38	lower Virden Mb.
100/15-09-006-26W1/00	4669	360508.55	5481644.00	759–764.5	0.17	0.18	29.38	30.53	3.11	0.65	8.32	8.65	MC-1 Mb.
100/03-33-008-24W1/00	5193	378575.73	5506293.78	579.1–582.0	0.19	0.21	69.68	78.42	11.15	0.00	1.03	1.16	Lower Amaranth Mb.–Lodgepole Fm.
100/04-17-009-25W1/00	4137	366952.98	5511582.09	645.0–652.0	0.17	0.17	9.70	9.78	0.85	0.00	4.42	4.46	lower Virden Mb.
100/09-18-009-25W1/00	4122	366603.64	5512238.15	639.0–647.0	0.20	0.22	13.51	14.75	8.39	0.00	7.66	8.36	Whitewater Lake Mb.
100/13-25-009-28W1/00	3281	344171.50	5516582.56	715.5–746.0	0.21	0.21	66.35	66.35	0.00	0.00	17.11	17.11	Lodgepole Fm.
100/15-35-009-28W1/00	3293	343425.14	5518211.66	730.0–738.5	0.09	0.09	49.80	49.92	0.25	0.00	27.06	27.13	Lodgepole Fm.
100/13-20-010-26W1/00	3820	357458.49	5524431.71	649.0–655.5	0.16	0.19	14.80	17.32	9.07	5.48	5.86	6.86	Virden Mb.
100/10-07-010-27W1/00	2572	346720.95	5521068.75	705.3–718.7	0.08	0.08	99.57	99.57	0.00	0.00	0.34	0.34	Lodgepole Fm.
100/07-18-010-27W1/00	2562	346749.20	5522286.52	1071.4–1079.0	0.04	0.04	99.29	99.38	0.09	0.00	0.56	0.56	Souris River Fm.
100/07-18-010-27W1/03	4385	346749.69	5522243.31	1071.1–1079.0	0.07	0.07	98.48	98.48	0.00	0.00	0.61	0.61	Lodgepole Fm.
100/15-18-010-27W1/00	15	346766.10	5523092.01	915.9–919.9	0.20	0.20	94.30	92.42	0.00	0.00	6.10	6.00	Duperow Fm.
100/15-18-010-27W1/00	15	346766.10	5523092.01	1066.5–1070.2	0.10	0.10	96.69	96.60	0.00	0.00	0.55	0.00	Souris River Fm.
102/15-18-010-27W1/00	2294	346763.88	5523076.46	870–1071.4	0.16	0.16	97.24	97.25	0.01	0.00	2.45	2.45	Duperow or Souris River Fm.
100/11-19-010-27W1/00	2564	346491.10	5524366.90	1080.5–1082	0.04	0.04	99.60	99.60	0.00	0.00	0.35	0.35	Souris River Fm.

Table GS2018-9-1 (continued): Helium concentrations reported in gas analyses for southwestern Manitoba. He air free is the concentration of the gas with the air removed and directly measured, and He acid free is the concentration of the gas with the acidic components (H_2S and CO_2) removed. Abbreviations: Fm., Formation; Mb., Member; TVD, true vertical depth.

UWI/location	Licence	Easting	Northing	Depth interval tested (m)	He air free (mol %)	He acid free (mol %)	N_2 air free (mol %)	N_2 acid free (mol %)	CO_2 air free (mol %)	H_2S air free (mol %)	CH_4 air free (mol %)	CH_4 acid free (mol %)	Stratigraphic unit
100/10-12-010-28W1/00	167	345084.10	5521073.82	699.5–721.5	0.01	0.01	99.10	99.10	0.00	0.00	0.69	0.69	Lodgepole Fm.
102/10-12-010-28W1/00	2571	345180.01	5521129.08	1076.6–1078.1	0.01	0.01	99.10	99.10	0.00	0.00	0.69	0.69	Souris River Fm.
100/13-13-010-28W1/00	635	344359.31	5523135.73	733.0–736.4	0.05	0.05	38.55	39.94	3.37	0.00	10.59	10.97	Lodgepole Fm.
100/16-22-011-28W1/00	9009	340748.16	5534927.33	822.7–830.9 (TVD)	1.28	1.30	78.05	79.37	1.66	0.00	11.61	11.81	Middle Bakken Mb.–Torquay Fm.
100/09-16-011-29W1/00	6997	329117.10	5532976.60	844.5–845.5	0.02	0.02	0.30	0.31	2.99	0.05	89.53	92.34	Middle Bakken Mb.–Torquay Fm.
100/05-20-011-29W1/00	10496	326360.71	5534451.02	853.4–863.0 (TVD)	0.08	0.08	22.97	22.97	0.01	0.00	7.42	7.42	Middle Bakken Mb.
102/06-20-011-29W1/00	10497	326563.95	5534446.16	849.9–862.3 (TVD)	0.01	0.01	39.76	39.79	0.07	0.00	2.82	2.82	Middle Bakken Mb.
03-09-012-07W1*					3.38—5.44		93.17						cannot be determined
NE-35-12-17W1*					1.19		97.37		0.20				cannot be determined
100/13-26-012-28W1/00	9575	341320.26	5546302.11	688.7–692.1 (TVD)	0.53	0.56	81.89	86.98	5.85	0.00	1.12	1.19	Middle Bakken Mb.
100/02-03-013-28W1/00	9197	340742.71	5548222.23	668.3–680.4 (TVD)	0.43	0.45	75.80	79.35	4.47	0.00	6.79	7.11	Middle Bakken Mb.
100/14-17-020-05W1/00	1846	561704.00	5619715.80	304.8–326.7	2.00	2.00	89.49	91.51	2.21	0.00	8.09	8.27	lower Winnipeg mb.
08-23-020-06W1*					0.08		99.92		0.00				cannot be determined
100/01-24-024-03W1/00	2171	587719.61	5659942.96	187.1–194.8	0.04	0.05	79.42	95.20	0.00	0.00	0.00	0.00	Red River Fm.

* Historical gas analysis on wells drilled prior to 1950. Results may be questionable.
** (TVD) denotes horizontal wells with measured depths converted to true vertical depths (TVD).

are required to be submitted under Manitoba's *Oil and Gas Act*. This has resulted in a concentration of documented helium occurrences in oil-producing areas that may be representative of the larger helium potential in the Williston Basin in Manitoba.

A search of the Manitoba Growth, Enterprise and Trade, Petroleum Technical Well files (https://www.gov.mb.ca/iem/petroleum/gis/technical.html) resulted in a total of 120 gas analyses from 86 wells. Of those wells, 69 (or 80%) of them reported helium concentrations. Table GS2018-9-1 lists those helium concentrations broken down as He air free and He acid free, where the former is the concentration of the gas with the air removed and the latter is the concentration of the gas with the acidic components (H_2S and CO_2) removed; concentrations of other selected gas components are listed in Table GS2018-9-1 for context. These helium occurrences are widely distributed, both geographically and stratigraphically, throughout Manitoba (Figures GS2018-9-1, -2). The youngest tested interval is the Triassic–Jurassic Amaranth Formation interval, and the oldest is the lower Winnipeg Formation sandstone to weathered Precambrian regolith interval. The most gas tests have occurred within those intervals with an affinity to produce natural gas, such as the Amaranth and Mission Canyon formations in the Pierson and Waskada oil fields (Figure GS2018-9-1). In the last five years, gas analyses have been conducted on the Middle Bakken Member to Torquay Formation interval in the Daly-Sinclair and Manson oil fields, where potentially economical helium concentrations of 0.45–1.3 mol % occur between townships 11 and 13, range 28W1.

This study identified six wells that have helium concentrations at or above the economic cut off for crude helium at 0.3 mol %. The highest results come from the Hemisphere Helium et al Lauder Prov. 14-17-20-05W1 well (one of the original Hemisphere Helium Corporation exploration wells) at 2.00 mol % from the lower Winnipeg Formation sandstone to the weathered Precambrian regolith interval, and from the Middle Bakken Member to Torquay Formation interval in the CPEC Elkhorn Hzntl 16-22-11-28W1 well with 1.30 mol %. High helium values have also been found within the MC-1 and MC-3 members of the Mission Canyon Formation. Figure GS2018-9-2 summarizes the helium occurrences based on their stratigraphic location.

Helium exploration

The exploration for helium requires the same approach (source, migration, trap) and data as conventional oil and gas exploration, but with some differences. Brown (2010) states that the best places to explore for helium include in old sediments with stagnant porewater (>100 Ma; Early Cretaceous or older); in areas with saline and cool shallow traps because helium degasses from fluids at low pressures (preferably between 0.5 to 2.5 km depth); at the end of long migration pathways, which maximize gas exposure to helium-bearing water; and away from supercharged and thermally mature hydrocarbon systems to avoid dilution in natural gas–rich reservoirs.

The best sources for these accumulations are old siliciclastic sediments, fractured shales, arkoses, granite wash and shallow fractured basement rocks (Brown, 2010). The best traps are capped by especially impervious rocks, such as halite, anhydrite and some very tight highly organic shales (Broadhead, 2005).

When considering all these factors, southwestern Manitoba is favourable for helium exploration because

- southwestern Manitoba is located on the northeastern rim of the Williston Basin, hundreds of kilometres away from the supercharged, thermally mature basin centre located in North Dakota.
- there is long-range migration of basinal fluid flow updip as the strata shallows toward the northeast.
- basinal fluid and gas are trapped by a multitude of northwest-trending subcrop and outcrop stratigraphic edges.
- Paleozoic–Jurassic groundwater in southwestern Manitoba is saline (Palombi and Rostron, 2013) and does not occur over any major heat anomalies.
- the maximum depth to the Precambrian surface in Manitoba is approximately 2.3 km (TGI Williston Working Group, 2008), placing all the Manitoba strata within the preferred depths to maximize helium degassing conditions.

Using these criteria, the oldest sedimentary rocks in Manitoba, the basal sandstones of the Deadwood and Winnipeg formations, may be the best candidates for helium exploration. These potential helium reservoir rocks directly overlie fractured Precambrian basement helium source rocks and together underlie a good portion of the Phanerozoic rocks in Manitoba, Saskatchewan, Alberta, Montana and North Dakota, resulting in a large catchment area and long-range migration opportunities for helium. The limited subsurface distribution of the Deadwood Formation in Manitoba is shown in Figure GS2018-9-1 but the Winnipeg Formation is present throughout southwestern Manitoba, underlying the entire map area.

In the extreme southwestern corner of Manitoba, these formations are excellent candidates to have old,

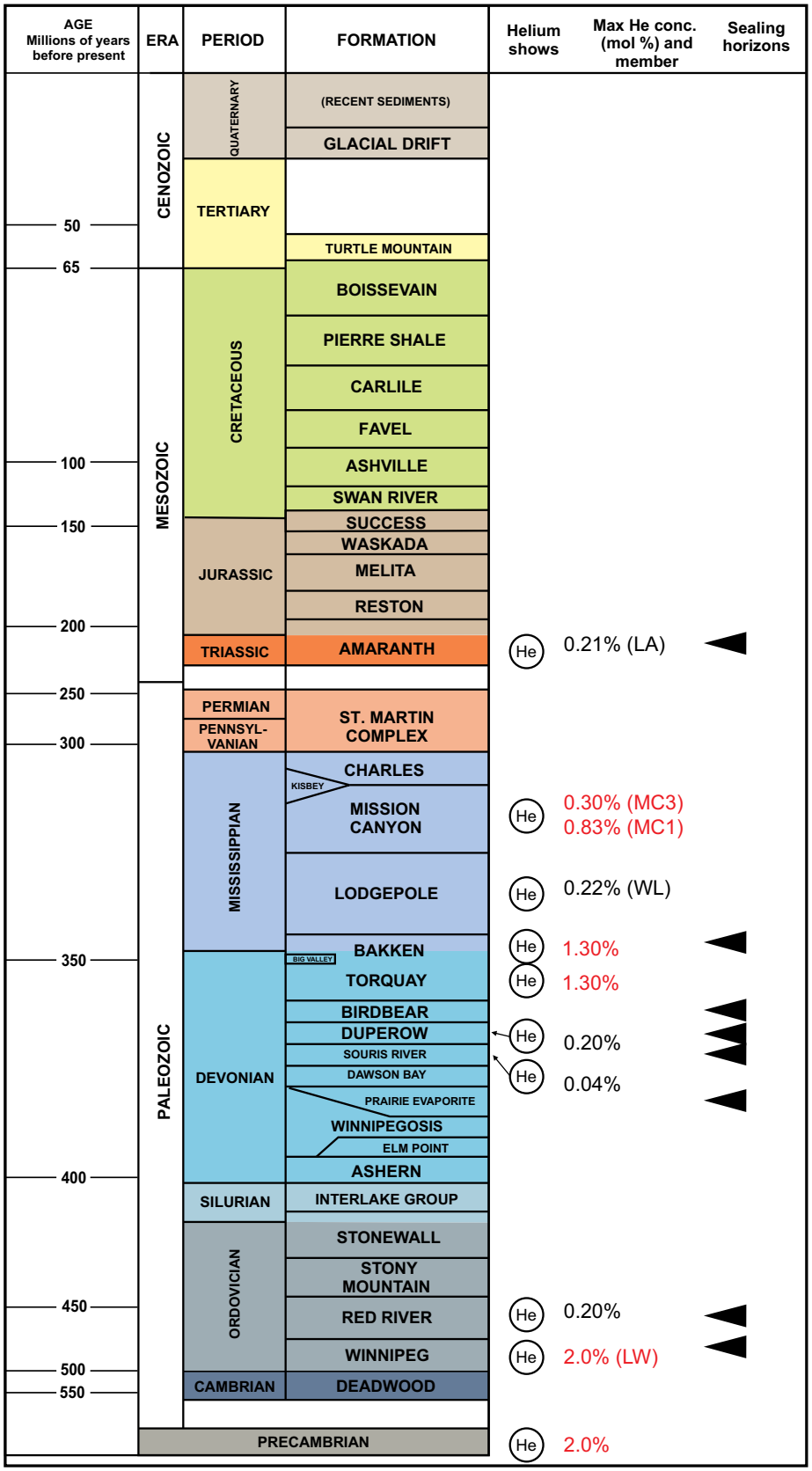

Figure GS2018-9-2: *Stratigraphic column of southwestern Manitoba showing helium occurrences: maximum helium concentrations reported for that interval; the abbreviation in parentheses indicates the member in which the occurrence was measured, if known; and known potential sealing horizons. Red text indicates values equal to or above 0.30 mol % He. Abbreviations: LA, lower Amaranth Formation; LW, lower Winnipeg Formation; MC1, MC-1 member; MC3, MC-3 member; WL, Whitewater Lake Member.*

saline, cool and locally stagnant porewater, creating the right conditions for the accumulation of helium for hundreds of millions of years if a proper cap is present. Halite and anhydrite are the only sedimentary rocks that can block the upward migration of helium; however, siliceous or kerogen-rich shales have also been known to serve as a cap (Broadhead, 2005). The upper shale member of the Winnipeg Formation has been known to be cemented (Yurkowski, 2016) and highly organic in places (Seibel and Bend, 2001), and the lower sandstone member is silicified in places (McCabe, 1978) and may therefore serve as a cap, but due to limited drillhole data in this region this is difficult to ascertain. Basement structural features can provide the right conditions for entrapment, such as that seen in the west. In Saskatchewan, at the site of the original producing wells, in township 17, range 14W3, the Deadwood Formation drapes a Precambrian structural high known as the Wilhelm structure, and is capped with a silicified siltstone. The Wilhelm structure has the some of the highest recorded helium concentrations (2%) in Saskatchewan (Yurkowski, 2016), and produced helium for 14 years in the late 1960s and early 1970s. In contrast, the high helium concentration in the Winnipeg Formation at 14-17-20-05W1 is 2.0 mol %, occurs at shallow depths between 256.0 and 326.8 m, and is associated with fresh groundwater, suggesting that there can be a wide range of conditions in which elevated levels of helium can potentially occur.

The Middle Bakken Member to Torquay Formation interval is capped with the regionally continuous, tight organic-rich shale of the Upper Bakken Member. This shale can have a very strong gamma-ray ('hot') signature and is a good candidate as a direct source for the high helium values measured in the Bakken–Torquay formations oil reservoir; however, the high helium occurrences in the Bakken–Torquay formations interval and the helium occurrences further south in township 10, range 27W1 in the Lodgepole, Duperow and Souris River formations all follow a north-south linear trend, suggesting a possible structural influence on the helium source and trapping mechanism. This region also falls within the boundaries of the Superior boundary zone (a deep crustal suture), the Birdtail-Waskada Zone (a post–Prairie Evaporite zone of structural disturbance) and within an embayment where the Prairie Evaporite salt is fully dissolved (Figure GS2018-9-1). All of these features can enhance localized fluid flow, result in localized thickening of potential reservoir units as is seen in the Middle Bakken Member sandstone (Nicolas, 2012) and may be related to basement faults. In the Daly-Sinclair region the horizons with helium occurrences all follow the eastern edge of a structural high that may also be related to a basement fault (Nicolas, 2012). These basement faults may serve as effective conduits to move helium-enriched fluids upward, permeating and trapping the fluids in several horizons. In addition, the Souris River and Duperow formations have multiple shale beds that may also serve locally as helium sources. Overall, the source of the helium is uncertain and may be a product of multiple combined sources but the helium appears to be preferentially trapped under shales with strong gamma-ray signatures where there are structurally controlled traps.

The sealing horizons on top of helium-charged reservoirs must be effective at preventing the small helium atom from escaping. A minimum of eight such seals exist in southwestern Manitoba and are identified in Figure GS2018-9-2. These include, from oldest to youngest, the upper Winnipeg Formation shales (when silicified or high in kerogen), the Lake Alma Member anhydrite in the Red River Formation, the Prairie Evaporite, the multiple anhydrite beds of the Souris River and Duperow formations, the upper member anhydrite beds of the Birdbear Formation, the Upper Bakken Member organic-rich shale and the Upper Amaranth Member of the Amaranth Formation. The Mississippian Charles Formation and the Dando Evaporite are not considered effective seals in Manitoba due to their irregular and limited distribution.

The most effective seal regionally is the Prairie Evaporite salt beds. This has been demonstrated in Saskatchewan where it serves as a good seal over the underlying Winnipegosis Formation, where high helium values have been identified from several wells in the southeastern corner of the province (M. Yurkowski, pers. comm., 2018). These helium occurrences occur dominantly where the Prairie Evaporite salt beds are not dissolved. Limited helium analyses in Manitoba make testing this theory difficult, but extrapolation from Saskatchewan studies suggests it may be worth investigating. Figure GS2018-9-1 shows the Prairie Evaporite salt dissolution edge relative to the documented helium occurrences.

Conclusions

Southwestern Manitoba has the right geological conditions for economic helium deposits. The best targets are the Bakken–Torquay formations interval, which benefits from the overlying 'hot' shales, and the Deadwood–lower Winnipeg formations interval, which sits directly over the Precambrian rocks. The areas with high solution gas may dilute the helium content too much for proper economic evaluation, suggesting the Amaranth, Mission Canyon and Lodgepole formations are the less likely targets, although that is not to say that they may not have local accumulations. Other Paleozoic formations are

generally poorly explored and have too few analyses to suggest if and where there may be any helium deposits.

Economic considerations

A rise in helium demand globally has sparked a worldwide exploration rush for the commodity. Helium can be produced with oil and gas using infrastructure already in place and provided by the petroleum industry. The helium potential within the oil and gas produced may serve as a good economic opportunity for operators to improve profits from these wells and may help to extend the life of marginal oil wells.

Acknowledgments

The author thanks M. Yurkowski from the Saskatchewan Geological Survey for her motivation, good discussions and technical review of this paper. P. Fulton-Regula from the Manitoba Petroleum Branch is acknowledged for the critical review of this paper.

References

Broadhead, R. 2005: Helium in New Mexico—geologic distribution, resource demand, and exploration possibilities; New Mexico Geology, v. 27, p. 9.

Brown, A. 2010: Formation of high helium gases: a guide for explorationists; American Association of Petroleum Geologists, AAPG Convention, April 11–14, 2010, New Orleans, Louisiana, poster.

Hemisphere Helium Corporation Ltd. 1962a: Petroleum technical well file for licence 1845; Manitoba Growth, Enterprise and Trade, Petroleum Branch, p. 55, URL <http://content.gov.mb.ca/iem/petroleum/documents/technical/001845.pdf> [November 2018].

Hemisphere Helium Corporation Ltd. 1962b: Petroleum technical well file for licence 1846; Manitoba Growth, Enterprise and Trade, Petroleum Branch, p. 75, URL <http://content.gov.mb.ca/iem/petroleum/documents/technical/001846.pdf> [November 2018].

McCabe, H.R. 1978: Reservoir potential of the Deadwood and Winnipeg Formations, southwestern Manitoba; Manitoba Department of Mines, Resources and Environmental Management, Mineral Resources Division, 54 p.

National Academy of Sciences 2000: The impact of selling the federal helium reserve; National Academy Press, Washington, D.C., 99 p.

Nicolas, M.P.B. 2012: Stratigraphy and regional geology of the Late Devonian–Early Mississippian Three Forks Group, southwestern Manitoba (NTS 62F, part of 62G, K); Manitoba Innovation, Energy and Mines, Manitoba Geological Survey, Geoscientific Report GR2012-3, 92 p.

Palombi, D. and Rostron, B.J. 2013: Regional hydrogeological characterization of the northeastern margin of the Williston Basin; Manitoba Mineral Resources, Manitoba Geological Survey, Open File OF2011-3, set of 55 1:3 000 000 scale maps.

Seibel, C. and Bend, S. 2001: Organofacies and source potential of the Middle Ordovician Winnipeg Formation within southern Saskatchewan; *in* Canadian Society of Petroleum Geologists Annual Convention Program with Abstracts, June 18–22, 2001, Canadian Society of Petroleum Geologists, p. 4, URL <http://www.cspg.org/documents/Conventions/Archives/Annual/2001/14-082.pdf> [September 2018].

TGI Williston Working Group 2008: Precambrian erosional surface: structure contour; Manitoba Science, Technology, Energy and Mines, Manitoba Geological Survey, Stratigraphic Map SM2008-PC-S, digital web release, scale 1:1 000 000, URL <http://www.gov.mb.ca/iem/geo/williston tgi/mapfiles/pdfs/057_prec_precambrian_eros_surf_str.pdf>.

United States Geological Survey 2018: Helium; United States Geological Survey, Mineral Commodity Summaries, January 2018, URL <https://minerals.usgs.gov/minerals/pubs/commodity/helium/mcs-2018-heliu.pdf> [November 2018].

Yurkowski, M. 2016: Helium in southwestern Saskatchewan: accumulation and geological setting; Saskatchewan Ministry of the Economy, Saskatchewan Geological Survey, Open File Report 2016-1, 20 p.

GS2018-10

Lithium concentrations in brine springs near Lake Winnipegosis, west-central Manitoba (parts of NTS 63C, 62N16, 62O12, 13)

by M.P.B. Nicolas and S.E. Grasby[1]

In Brief:

- Brine springs along Lake Winnipegosis contain low levels of lithium, averaging 1263 ppb
- Goundwater mixing has diluted the lithium concentration coming out from the springs
- Deep subsurface Winnipeg Formation brines have good potential as a lithium source

Citation:
Nicolas, M.P.B. and Grasby, S.E. 2018: Lithium concentrations in brine springs near Lake Winnipegosis, west-central Manitoba (parts of NTS 63C, 62N16, 62O12, 13); *in* Report of Activities 2018, Manitoba Growth, Enterprise and Trade, Manitoba Geological Survey, p. 119–124.

Summary

The most common and cost-effective source of lithium within the brine deposits are deep brines in continental sedimentary basins. Southern Manitoba has a complex groundwater aquifer system, with salinities ranging from brines in the deeper aquifers and brine springs to freshwater in the shallower and eastern aquifers. The brine springs occur along and near the shores of Lake Winnipegosis on large salt flats and have chemical signatures indicative of mixed halite dissolution brine and freshwater. Lithium concentrations in these brines range from 150 to 6300 ppb, with an average of 1263 ppb.

Introduction

Saline groundwater in continental sedimentary basins are generated from evaporitic concentration and/or halite dissolution, where the former is a primary process and the latter is a secondary (diagenetic) process (Clayton et al., 1966; Walter et al., 1990). Both these mechanisms provide opportunities for trace elements to accumulate, potentially reaching economic concentrations. In Manitoba, the mineral potential of brines remains largely under-explored and little understood, as exemplified by the current level of knowledge about lithium concentrations in these saline groundwater systems. Active exploration for this element in deep saline waters found in continental sedimentary basins is presently occurring in the Province, and the lithium values it reveals may prove these waters to be a cost-effective source of this element.

Southern Manitoba has a complex groundwater aquifer system, with salinities ranging from brines in the deeper western aquifers to freshwater in the shallower eastern aquifers (Grasby and Betcher, 2002; Grasby and Chen, 2005; Nicolas, 2017). Oil and gas operations in Manitoba produce large quantities of these brines, which contain a wide range of trace elements. Although few in number, preliminary results indicate that the lithium concentrations in Manitoba's brines are low. However, extrapolation of better, more comprehensive results from Saskatchewan suggests that there is potential for lithium concentrations to be higher than currently recorded in Manitoba and that more work needs to be done to evaluate the deeper aquifers (Nicolas, 2017). In addition, little is known about the potential of brine springs, which occur in west-central Manitoba.

Nicolas (2017) reported on the known lithium concentrations in the deep brines, as well as shallow freshwater aquifers, and this paper focuses on the lithium content of brine springs that are located near and along the shores of Lake Winnipegosis in west-central Manitoba.

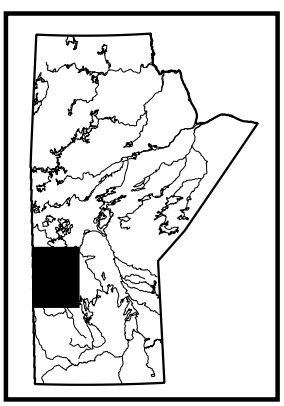

Southern Manitoba hydrogeology

Grasby et al. (2000) and Grasby and Chen (2005) described the complex history of the hydrodynamics of the Western Canada Sedimentary Basin (WCSB) over the last 50 m.y.; their findings are summarized here. The deep basin waters represent original evaporated sea waters that have remained as interstitial brines since near the time they were deposited. During the Laramide orogeny (50–84 Ma ago), uplift of the western portion of the WCSB allowed influx of freshwater from the topographic highs in the northwestern United States at the western edge of the basin. Travelling through the porous sediments, these

[1] Geological Survey of Canada, 3303-33rd Street, N.W., Calgary, AB T2L 2A7

freshwaters dissolved portions of the Prairie Evaporite in southwestern Saskatchewan, and the resulting hydraulic pressures pushed existing deep saline groundwater to partially migrate northward and eastward. To this day, these deep brines display chemical signatures indicative of evaporated seawater affected by rock–water interactions and have never been mixed with freshwater. On the eastern side of the basin, flow of groundwater in southwestern Manitoba during the Laramide orogeny followed regional topographical gradients, similar to modern day, with a northeastern flow direction. As the uppermost sediments of the WCSB eroded, the gradient decreased, but with little change in groundwater flow direction. During the last ice age, thick glacial ice over Manitoba resulted in a reversal of the topographic gradient and groundwater flow. Of great importance was the fact that the basal meltwater of the glacier significantly increased hydraulic pressures, forcing large volumes of freshwater into the porous Devonian carbonate rocks present at the basal-ice surface. This freshwater influx penetrated deeply into the carbonate succession toward the southwest, resulting in partial dissolution of the Prairie Evaporite. Upon glacial retreat, and the subsequent glacial rebound, the groundwater again reversed its flow path, back to the current northeastern direction. The brine springs near and along the shores of Lake Winnipegosis are the surface seeps of this saline groundwater. Grasby and Chen (2005) identified the hydrochemistry of these brine springs as bearing the signatures of mixed halite dissolution brine and freshwater.

In southern Manitoba, a hydrological divide separates two regional groundwater-flow systems (Figure GS2018-10-1). West of the divide, the groundwater matches the saline water system described above and hosts the brine springs, whereas east of the divide the groundwater is freshwater (Grasby and Betcher, 2002). The eastern flow system is the carbonate-rock aquifer and consists of gently west-dipping, carbonate-dominated strata from the Ordovician Red River Formation up to the Souris River Formation (Grasby and Betcher, 2002).

Hydro- and lithostratigraphy

The brine springs are located within Devonian-aged carbonate rock outcrops of the Winnipegosis, Dawson Bay and Souris River formations (Figure GS2018-10-1). These formations fall within the Winnipegosis aquifer and Devonian aquifer (Dawson Bay and Souris River combined) of Bachu and Hitchon (1996), or equally the Winnipegosis aquifer and Manitoba aquifer (Dawson Bay and Souris River combined) of Palombi (2008), and are separated by the Prairie aquiclude in the deep subsurface. Once past the Prairie Evaporite formation edge to the north and east, these aquifers combine into one open aquifer system, which is exposed at the land surface and which discharges brine waters as springs.

Nearby outcrops of the McArdle salt flat (also referred to as the Red Deer River salt spring; Figure GS2018-10-2a) suggest that Winnipegosis Formation reefs may underlie most, if not all, brine springs (Bezys and McCabe, 1996; Bezys et al., 1997). These reefs are known for having high water drives in the subsurface, essentially concentrating fluid flow upward. They are often associated with collapse structures overtop due to the localized rapid dissolution of the Prairie Evaporite, which results in overlying formations draping overtop of these structures, creating zones of enhanced permeability. In those areas where the Prairie Evaporite was not present, and which were therefore not affected by dissolution, draping of the overlying carbonate rocks on the reefs would have the same effect on permeability due to natural compaction of the rocks over time.

Salt-flat and brine-spring morphology

The morphology of the salt flats varies in size from small sites to large flat-lying, uniform, treeless, iron-stained to whitish grey expanses (Figure GS2018-10-2b). Brine pools, which are clear with a light blue substrate (Figure GS2018-10-2c), and brine boils (shallower ponds with percolating gas bubbles; Figure GS2018-10-2d) occur at the discharge sites and are commonly surrounded by red to green algae, algal mats, and brine-loving vegetation and bacteria (Bezys et al., 1997; Grasby and Londry, 2007). The sites are often littered with glacially transported boulders and erratics, and are often extensively corroded (Bezys et al., 1997).

Brine spring sampling

Over the course of three years (1998–2000) a total of 46 samples were collected from brine springs near Lake Winnipegosis, and major element and isotope values were originally reported in Grasby and Chen (2005). Lithium concentrations were recorded but not reported at the time of publication; sampling methods are described in Appendix 1 of Grasby and Chen (2005).

Lithium concentrations

The hydrochemistry of the saline groundwater in the basin is variable and is dependent on location within the basin, which is itself related to the generative mechanism that characterizes these brines, be it evaporitic concentration (of seawater) or halite dissolution (of existing salt deposits). Nicolas (2017) summarized the variable lithium concentrations in Manitoba's groundwater, with

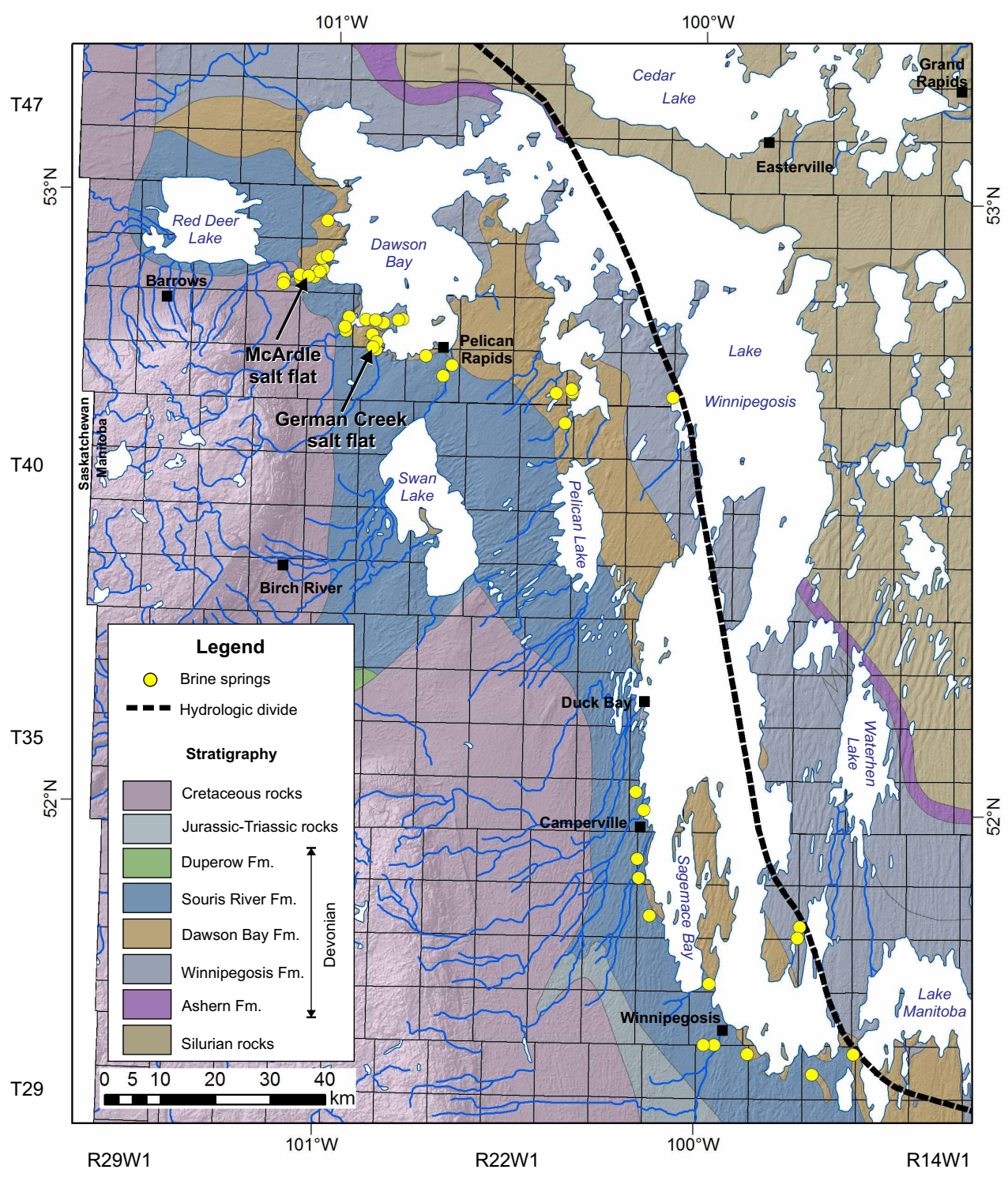

Figure GS2018-10-1: *Regional geology of the study area in west-central Manitoba with digital elevation model (United States Geological Survey, 2002), showing the hydrological divide (which follows the 2000 mg/L dissolved-solids contour) and the location of the brine springs samples.*

Figure GS2018-10-2: *Field photographs of* ***a)*** *the McArdle salt flat, in west-central Manitoba, also referred to as the Red Deer River salt spring, and collection location of sample M983075;* ***b)*** *the German Creek salt flat, in west-central Manitoba, showing large salt-flat and discharge-site morphology;* ***c)*** *a close up of a brine pool;* ***d)*** *brine boils (scale card shows size in centimetres). Sample M993016 was collected at this salt flat.*

values from brines in the oil wells ranging from 0.258 to 7.32 ppm, values from freshwater to brackish water wells ranging from 0.01 ppb to 0.3 ppm, and values from shallow saline waters to brines in monitoring wells ranging from 0.488 to 3.84 ppm. Despite the small number of analytical results from deep brines, lithium concentrations in Manitoba's groundwater are low, with overall higher concentrations in the deep Jurassic and Paleozoic brines of southwestern Manitoba's oil region. Shallower brines and saline waters measured from the groundwater monitoring wells have lower lithium concentrations compared with the brines derived from deep oil wells. Freshwater-dominated Cambro-Ordovician aquifers along the eastern erosional edge of the Williston Basin, and located east of the hydrological divide, have extremely low lithium concentrations.

The lithium concentrations for the 46 brine springs that occur near and along the shores of Lake Winnipegosis are listed in Table GS2018-10-1. The lithium concentrations range from 150 to 6300 ppb, with an average of 1263 ppb. These values are comparable to or slightly higher than those reported in Nicolas (2017) from groundwater east of the hydrological divide within the Cambro-Ordovician aquifer (carbonate-rock aquifer).

Discussion and conclusions

The lithium values from the brine springs are extremely low, falling far below economic limits for economic extraction from brines, which is estimated to be approximately 100 ppm (Munk et al., 2016). All but three of the reported values are above the mean lithium concentrations of seawater of 183 ppb (Riley and Tongudai, 1964), indicating some degree of lithium enrichment into the system. Since the brine springs consist of mixed brine waters from halite dissolution (likely dominated by the dissolution of the Prairie Evaporite, with minor influence from thinner evaporite beds in other Devonian formations) and freshwater, the source of this lithium enrichment is uncertain. The enrichment could come from a combination of lithium-bearing salt minerals and impurities within the Prairie Evaporite, and/or from freshwater enriched with lithium from the numerous lithium-bearing pegmatite occurrences in the Precambrian in Manitoba.

Table GS2018-10-1: Lithium concentrations from brine springs.

Sample Number	Sec	Twp	Rge (W1)	Latitude	Longitude	Li (ppb)
M983073		24	20	51.92644	-100.156393	770
M983074	17	35	19	52.00679	-100.141327	860
M983075		45	25	52.86719	-101.054513	1500
M983076		45	25	52.87543	-101.039318	1200
M983077		45	25	52.90154	-101.018757	980
M983078B		44	24	52.79866	-100.885302	1300
M983079	13	44	25	52.78675	-100.967345	830
M993008	24	44	25	52.80285	-100.956783	1500
M993009		44	24	52.79950	-100.911783	1600
M993010		45	25	52.88052	-101.030283	1300
M993011		45	25	52.87672	-101.048100	1400
M993012		45	25	52.89797	-101.033833	180
M993013		44	24	52.80175	-100.812500	1600
M993014		44	24	52.79505	-100.863617	1400
M993015		44	24	52.77542	-100.892683	150
M993016		44	24	52.75143	-100.882100	1400
M993017	12	44	25	52.78003	-100.964200	610
M993019		45	26	52.86253	-101.136100	1500
M993020		45	26	52.85482	-101.135983	1400
M993021		43	23	52.72865	-100.676367	530
M993022		43	24	52.71053	-100.699300	560
M993024		43	23	52.74282	-100.747700	170
M993025		44	24	52.76343	-100.880750	6300
M993026		45	25	52.86305	-101.089867	1400
M993027		45	20	52.68765	-100.349800	1300
M993028		45	20	52.69268	-100.352933	1300
M993029		45	21	52.63725	-100.368667	1400
M993030		45	21	52.68613	-100.393467	2700
M993031		43	19	52.68155	-100.079967	1400
M993032	6	34	19	51.89552	-100.151133	500
M993033	17	33	19	51.83398	-100.121750	550
M993034	4	32	18	51.72317	-99.961533	1100
M993035	4	31	18	51.62373	-99.946283	1400
M993036	36	30	18	51.60950	-99.859033	1200
M993037	5	31	18	51.62382	-99.974533	1300
M993038	4	31	18	51.81832	-99.724883	1200
M993039	1	33	17	51.80000	-99.729867	750
M993040	36	30	16	51.60998	-99.580883	3200
M993041	30	25	19	52.03652	-100.162567	420
M003001	17	30	16	51.57663	-99.688408	470
M003002		45	26	52.86985	-101.092713	1300
M003003		45	25	52.86839	-101.069483	1500
M003004		45	24	52.75444	-100.890475	970
M003005		44	24	52.79962	-100.823825	1600
M003006		44	24	52.79866	-100.885302	1400
M003007		46	25	52.95979	-101.021657	690

Although these are lower than optimal concentration values often considered as targets for exploration, brines in this region may present less challenges for lithium extraction due to their relatively low calcium concentrations (when compared to deep-basin brines to the west). High calcium in brines can be problematic, causing a common ion effect that inhibits extraction of lithium carbonate, such that sodium-rich brines are a preferable exploration target. In a similar sense, other sodium-rich brines, which are known to occur in the Winnipeg Formation, may prove a better exploration target given their known lower calcium contents (Ferguson et al., 2005).

Economic considerations

Lithium has been identified as a critical element (United States Geological Survey, 2018) since its demand has grown substantially over the last few years, mainly because of its use in rechargeable batteries, and is currently experiencing an exploration boom.

Extraction of lithium from brines using emerging technologies continues to push the boundaries and lower the minimum concentration required for deposits to be economic. Although lithium concentrations in Manitoba's deep brines are low, the water chemistry of the brine springs, as well as of the deeper brines of the Winnipeg Formation, marks these as favourable for lithium extraction.

Acknowledgments

The authors would like to thank T. Martins from the Manitoba Geological Survey for her support and guidance on this project, and critical review of this paper.

Natural Resources Sector, Lands and Minerals Sector contribution 20180188.

References

Bachu, S. and Hitchon, B. 1996: Regional-scale flow of formation waters in the Williston Basin; America Association of Petroleum Geologist Bulletin, v. 80, p. 248–264.

Bezys, R.K. and McCabe, H.R. 1996: Lower to middle Paleozoic stratigraphy of southwestern Manitoba; Geological Association of Canada–Mineralogical Association of Canada, Joint Annual Meeting, Winnipeg, Manitoba, May 27–29, 1996, Field Trip Guidebook B4, p. 92.

Bezys, R.K., Ducharme, E.B., Bamburak, J.D. and Fedikow, M.A.F. 1997: A geochemical study of saline brine sediments as a guide to prairie-type micro-disseminated mineralization and other precious metals in west central Manitoba (NTS 63C); *in* Report of Activities 1997, Manitoba Energy and Mines, Geological Services, p. 118–122.

Clayton, R.N., Friedman, I., Graf, D.L., Mayeda, T.K., Meents, W.F. and Shrimp, N.F. 1966: The origin of saline formation waters: 1. Isotopic composition; Journal of Geophysical Research, v. 71, p. 3869–3882.

Ferguson, G., Betcher, R.N. and Grasby, S.E. 2005: Water chemistry of the Winnipeg Formation in Manitoba; Geological Survey of Canada, Open File 4933, 37 p.

Grasby, S.E. and Betcher, R.N. 2002: Regional hydrogeochemistry of the carbonate rock aquifer, southern Manitoba; Canadian Journal of Earth Sciences, v. 39, p. 1053–1063.

Grasby, S.E. and Chen, Z. 2005: Subglacial recharge into the Western Canada Sedimentary Basin — impact of Pleistocene glaciation on basin hydrodynamics; Geological Society of America Bulletin, v. 117, p. 500–514.

Grasby, S.E. and Londry, K.L. 2007: Biogeochemistry of hypersaline springs supporting a mid-continent marine ecosystem: an analogue for Martian springs?; Astrobiology, v. 7, p. 662–683.

Grasby, S.E., Betcher, R., Osadetz, K.G. and Render, F. 2000: Reversal of the regional flow system of the Williston Basin in response to Pleistocene glaciation; Geology, v. 28, p. 635–638.

Munk, L.A., Hynek, S.A., Bradley, D.C., Boutt, D., Labay, K. and Jochens, H. 2016: Lithium brines: a global perspective; Review in Economic Geology, v. 18, p. 339–365.

Nicolas, M.P.B. 2017: Preliminary investigation of the potential for lithium in groundwater in sedimentary rocks in southwestern Manitoba; *in* Report of Activities 2017, Manitoba Growth, Enterprise and Trade, Manitoba Geological Survey, p. 183–190.

Palombi, D.D. 2008: Regional hydrogeological characterization of the northeastern margin in the Williston Basin; M.Sc. thesis, University of Alberta, Edmonton, Alberta, 196 p.

Riley, J.P. and Tongudai, M. 1964: The lithium content of sea water; Deep Sea Research and Oceanographic Abstracts, v. 11, p. 563–568.

United States Geological Survey 2002: Shuttle Radar Topography Mission, digital topographic data, Manitoba; United States Geological Survey, URL <ftp://edcsgs9.cr.usgs.gov/pub/data/srtm/>, portions of files N48W88W.hgt.zip through N60W102.hgt.zip, 1.5 Mb (variable), 90 m cell, zipped hgt format [March 2003].

United States Geological Survey 2018: Draft critical minerals list—summary of methodology and background information—United States Geological Survey technical input document in response to Secretarial Order No. 3359; United States Department of the Interior, United States Geological Survey; Open-file Report 2018-1021, 26 p.

Walter, L.M., Stueber, A.M. and Huston, T.J. 1990: Br-Cl-Na systematics in Illinois basin fluids: constraints on fluid origin and evolution; Geology, v. 18, p. 315–318.

GS2018-11

Stratigraphy, lithology and petroleum potential of the Upper Devonian Duperow Formation in the Manitoba Potash Corporation core at 3-29-20-29W1, southwestern Manitoba (part of NTS 65K1)

by M.P.B. Nicolas and N. Chow[1]

In Brief:

- The continuous 153.36 m core showed stratigraphic basin continuity of the Saskatoon, Wymark and Seward members
- The cyclical carbonate-evaporite sequence recorded subtidal, intertidal and supratidal lithofacies
- Oil shows have been documented, supporting conventional reservoir models
- Organic-rich mudstone beds indicate good source rock generative potential, supporting unconventional reservoir models through self-sourcing

Citation:
Nicolas, M.P.B. and Chow, N. 2018: Stratigraphy, lithology and petroleum potential of the Upper Devonian Duperow Formation in the Manitoba Potash Corporation core at 3-29-20-29W1, southwestern Manitoba (part of NTS 65K1); *in* Report of Activities 2018, Manitoba Growth, Enterprise and Trade, Manitoba Geological Survey, p. 125–135.

Summary

The Upper Devonian Duperow Formation is a cyclical carbonate-evaporite sequence within the Elk Point Basin. The Manitoba Potash Corporation (MPC) core from L.S. 3, Sec. 29, Twp. 20, Rge. 29, W 1st Mer. has a full section of the Duperow Formation, which is 153.36 m thick (502.90–656.26 m true vertical depth) with 99% of core recovered during drilling. The members preserved in this core are the Saskatoon, Wymark and Seward members, from bottom to top. Preliminary lithofacies analysis indicates that the subtidal, intertidal and supratidal lithofacies associations recognized in other studies of the Duperow Formation in Manitoba are also present in the MPC core.

Drill-stem tests of the Duperow Formation in the MPC well have returned muddy water, but oil shows have been documented throughout this formation in this core, which is supportive of a conventional reservoir model. Rock-Eval 6 analyses of thin, organic-rich lime mudstone beds indicate fair to very good source rock generative potential, supportive of an unconventional reservoir model through self-sourcing.

Introduction

The Upper Devonian (Frasnian) Duperow Formation is a cyclical carbonate-evaporite sequence that is present in the eastern side of the Elk Point Basin. In Manitoba, the Duperow Formation has a maximum thickness of 220 m in the extreme southwestern corner, where it occurs at maximum depths greater than 1500 m (Bates et al., 2016). It gradually shallows and thins to an erosional edge in the northeastern direction (TGI Williston Basin Working Group, 2008a, b). As the Duperow Formation has only been observed in the subsurface, core and downhole geophysical logs must be used for detailed study of this formation.

During the early mineral and oil exploration years in Manitoba, Duperow Formation cores were occasionally recovered (Figure GS2018-11-1), but all were short intervals and telescopic in nature. In 1986, Canamax Resources Inc. drilled a potash testhole as a pilot hole for the construction of a mine shaft for an underground potash mine in L.S. 3, Sec. 29, Twp. 20, Rge. 29, W 1st Mer. (abbreviated 3-29-20-29W1) located at UTM Zone 14, 325102.38W, 5624312.3N (NAD84). A continuous core was acquired at this location, from 14.0 to 900.0 m true vertical depth (TVD). With a total core recovery average of 96%, this core represents the first continuous look at the subsurface units in southwestern Manitoba, from the uppermost Cretaceous units to the base of the Devonian Winnipegosis Formation. This stratigraphic core was previously owned by Manitoba Potash Corporation (MPC). In 2014, the Manitoba Geological Survey (MGS) acquired this core from MPC and has stored it at the MGS Midland Sample and Core Library in Winnipeg (Nicolas, 2016). To maintain the integrity of this valuable core and provide MGS geologists the opportunity to fully and properly catalogue the core, access to it is currently limited.

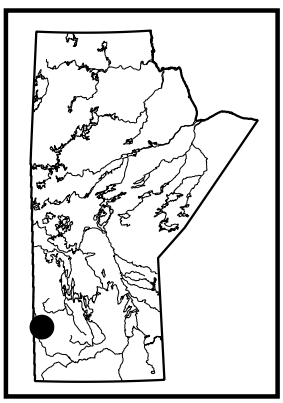

In this core, the Devonian Duperow Formation is preserved from 502.90 to 656.26 m TVD, and has a total thickness of 153.36 m and 99% core recovery. The formation is covered from core 106, box 368 to core 129, box 487. This is the only core in Manitoba currently in archival storage that fully preserves the Duperow Formation, providing a

[1] Department of Geological Sciences, University of Manitoba, 125 Dysart Road, Winnipeg, MB R3T 2N2

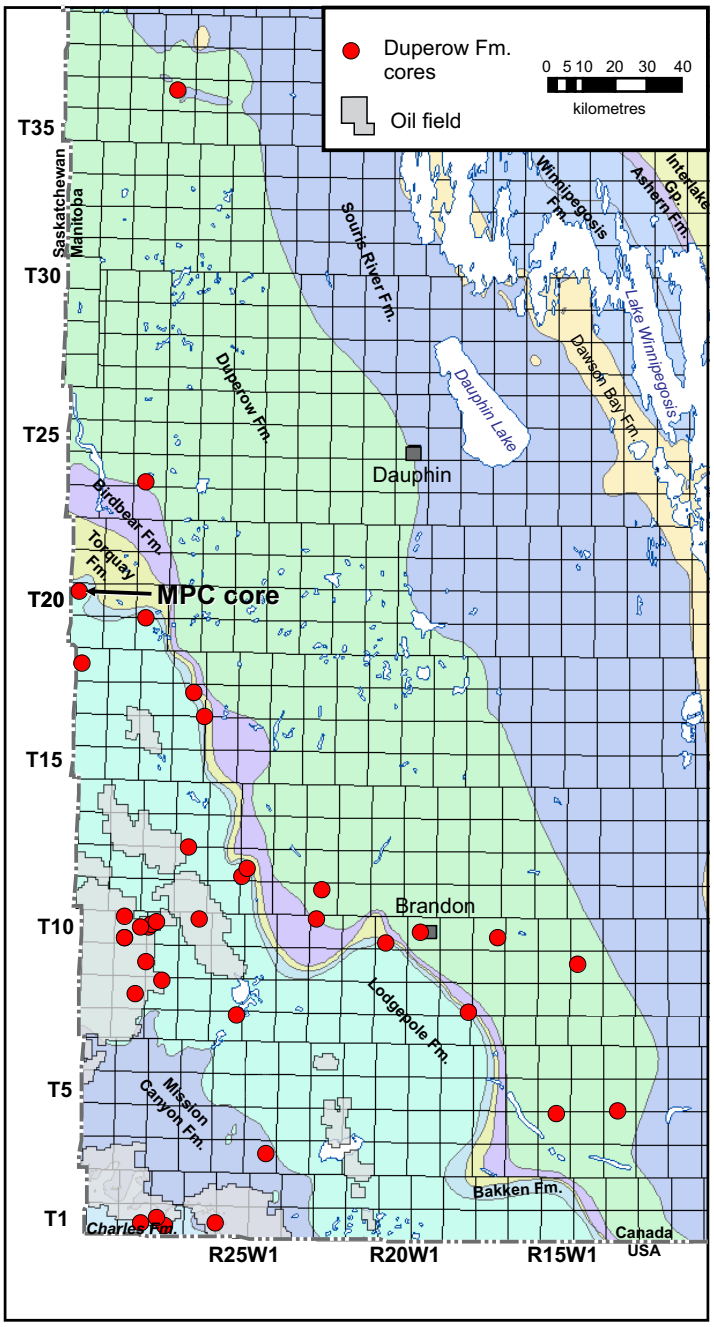

Figure GS2018-11-1: *Geological map of southwestern Manitoba showing the location of the Manitoba Potash Corporation (MPC) core and other Duperow Formation cores. Stratigraphic information is from Nicolas et al. (2010). Abbreviations: Fm., Formation; Gp., Group.*

complete and rare glimpse into the lithology and stratigraphy of the formation.

Previous work

The Duperow Formation was identified by the MGS as a formation that was poorly documented and understood in southwestern Manitoba, in comparison to other parts of the Elk Point Basin (e.g.,Wilson, 1967; Wilson and Pilatzke, 1987; Cen and Salad Hersi, 2006a, b). Through a regional cross-border study between Saskatchewan and Manitoba during the Targeted Geoscience Initiative II, Nicolas and Barchyn (2008) suggested that the stratigraphy for the Duperow Formation, including the Saskatoon, Elstow, Wymark and Seward members, in southeastern Saskatchewan is directly correlative with that in southwestern Manitoba. This was based on long-range correlations using geophysical wireline logs. For Manitoba to formally adopt the stratigraphic framework for this

formation, further study, which included core logging, would be required. From this need, a collaborative study of the Duperow Formation in Manitoba was initiated in 2011 between the MGS and the University of Manitoba. At the University of Manitoba, a B.Sc. thesis on the middle unit of the Wymark Member was completed by L. Eggie in 2012 (Eggie, 2012; Eggie et al., 2012). As an outgrowth of this work, a collaborative research and development agreement was set up between the University of Manitoba, ARC Resources Ltd. (Calgary), Natural Sciences and Engineering Research Council, and the MGS to support an M.Sc. thesis on the entire formation, which was completed by K. Bates in 2016 (Bates, 2016; Bates et al., 2016). The purpose of the project was to better understand the stratigraphy, lithofacies, diagenesis and petroleum potential of the formation throughout southwestern Manitoba. Through detailed core logging and subsurface correlations, Bates (2016) concluded that the Elstow Member could not be differentiated from the Saskatoon Member in Manitoba, hence only the Saskatoon, Wymark and Seward members are present, supporting previous studies by Kent (1983) and Cen and Salad Hersi (2006a). These earlier studies did not include the MPC core due to the confidentiality and inaccessibility of the core at that time.

Stratigraphy

The Duperow Formation is part of the Saskatchewan Group, which occurs throughout the Elk Point Basin. In Manitoba and in the MPC core, the Duperow Formation consists of, from oldest to youngest, the Saskatoon, Wymark and Seward members. Figure GS2018-11-2 shows the stratigraphic column and core log for the MPC core; the stratigraphic picks are provided in Table GS2018-11-1. The formation conformably overlies the Souris River Formation and conformably underlies the Birdbear Formation (Figure GS2018-11-4).

Saskatoon Member

The Saskatoon Member in the MPC core is 15.26 m thick and conformably overlies the Hatfield Member of the Souris River Formation. The lower contact is a hardground surface developed on mottled-nodular fossiliferous wackestone that is overlain by burrow-mottled lime mudstone (Figure GS2018-11-4).

The Saskatoon Member consists of fossiliferous wackestone-packstone to floatstone-framestone, commonly with large stromatoporoid fragments and articulated brachiopods; burrow-mottled dolomudstone, with recognizable *Planolites* and *Thalassinoides* burrows; and laminated, anhydritic argillaceous dolomudstone.

Wymark Member

The Wymark Member in the MPC core is 97.78 m thick and conformably overlies the Saskatoon Member. The lower contact is at the base of a nodular argillaceous lime mudstone identified as the C2 marker bed (cf. Wilson, 1967; Figure GS2018-11-5a). This member can be subdivided informally into three distinct conformable units:

1) the lower unit is 20.98 m thick and has an upper contact defined by the C1 marker bed;
2) the middle unit is 46.75 m thick with an upper contact defined by the B marker bed; and
3) the upper unit is 30.05 m thick with an upper contact at the A marker bed.

The marker beds can be correlated basin-wide (Wilson, 1967) and are characterized by high gamma-ray spikes that correspond to argillaceous beds (Figure GS2018-11-2).

The lower unit consists of alternating thick intervals of 1) mottled fossiliferous packstone, locally grading to fossiliferous floatstone-rudstone and framestone, with large stromatoporoids, corals, crinoid ossicles and articulated brachiopods, and argillaceous laminae throughout; and 2) nodular to burrow-mottled, slightly argillaceous, lime mudstone to dolomudstone and fossiliferous wackestone, with *Planolites* and rare stromatoporoid fragments and disarticulated brachiopods. The C1 marker bed appears to be massive to mottled, silty dolostone to siltstone (Figure GS2018-11-5b).

The middle unit is composed of thick intervals of 1) mottled fossiliferous packstone to floatstone with fragments of stromatoporoids, corals, crinoid ossicles and brachiopods; 2) wavy-laminated argillaceous lime mudstone to dominantly fossiliferous wackestone, with *Chondrites*, *Planolites* and rare *Skolithos* burrows, and scattered crinoid ossicles; and 3) planar-laminated argillaceous dolomudstone to lime mudstone with local dolopackstone interbeds and nodular anhydrite. Brecciated beds and convolute lamination occur locally. Two intermediate marker beds, P1 and P2, as well as the B marker bed, are well developed on the gamma-ray log, and consist of in situ brecciated, lime mudstone clasts within a shale to argillaceous lime mudstone matrix (Figure GS2018-11-5c).

The upper unit is composed of thick intervals of 1) fossiliferous floatstone, grading to packstone in places, with stromatoporoids, articulated brachiopods and corals; 2) wavy-laminated argillaceous lime mudstone to fossiliferous wackestone; and 3) shale and argillaceous dolomudstone/mudstone, with minor anhydrite nodules.

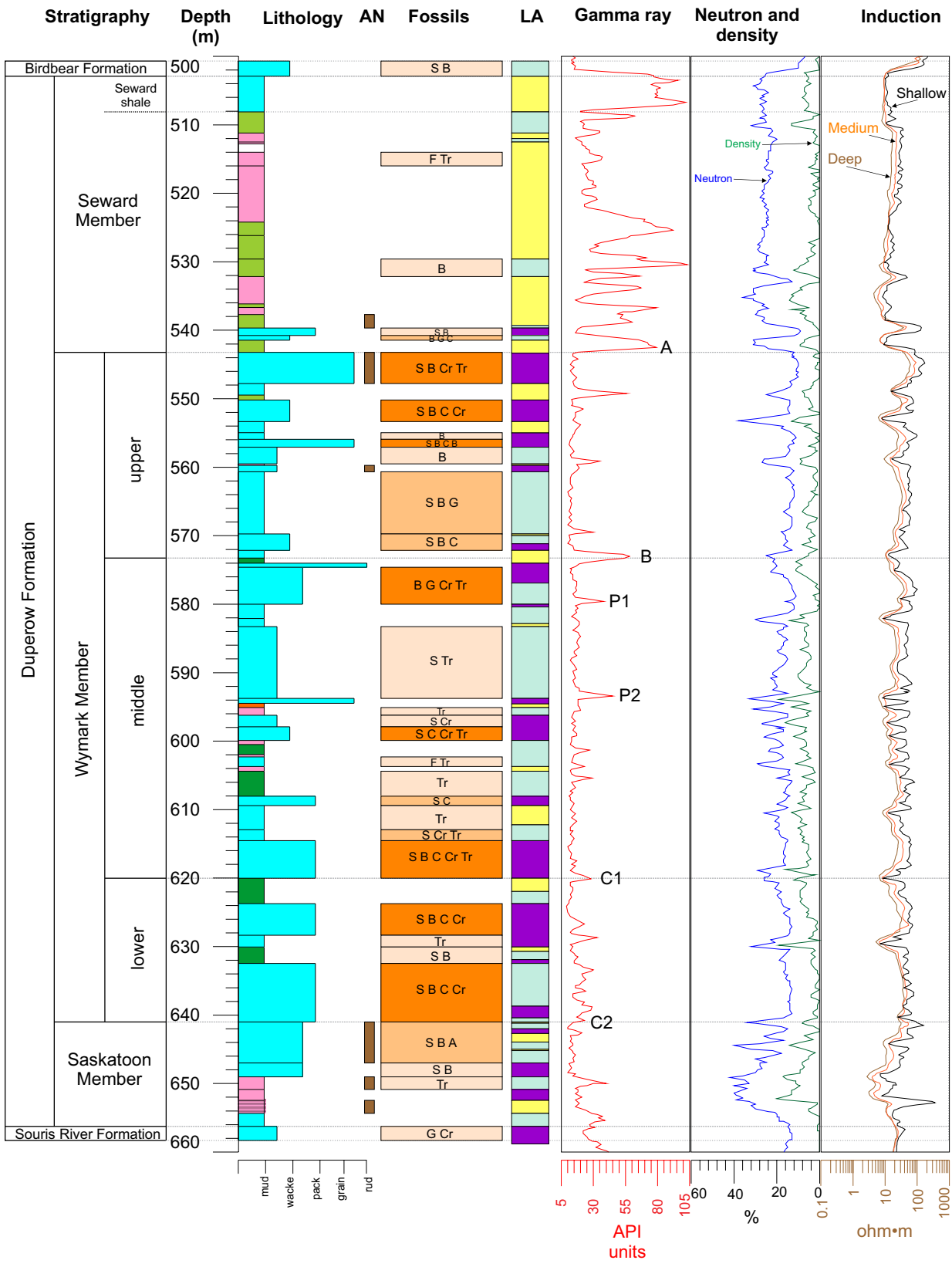

Figure GS2018-11-2: *Core log for the Duperow Formation in the Manitoba Potash Corporation (MPC) core at 3-29-20-29W1 with tracks for the stratigraphy, lithology, anhydrite occurrence (AN), fossils, lithofacies associations (LA), and gamma-ray, density and neutron, and induction downhole wireline geophysical logs. Prominent marker beds are labelled on the gamma-ray track. The core log legend is provided in Figure GS2018-11-3. Abbreviations: grain, grainstone; mud, mudstone; pack, packstone; rud, rudstone; wacke, wackestone.*

Table GS2018-11-1: Stratigraphic tops and thicknesses of the Duperow Formation and its members in the Manitoba Potash Corporation (MPC) core at 3-29-20-29W1.

Stratigraphic unit	Core depth (m)	Thickness (m)
Duperow Formation	502.90	153.36
Seward Member	502.90	40.32
Seward shale	502.90	5.22
base of Seward shale	508.12	-
Wymark Member	543.22	97.78
upper	543.22	30.05
middle	573.27	46.75
lower	620.02	20.98
Saskatoon Member	641.00	15.26
Souris River Formation	656.26	-

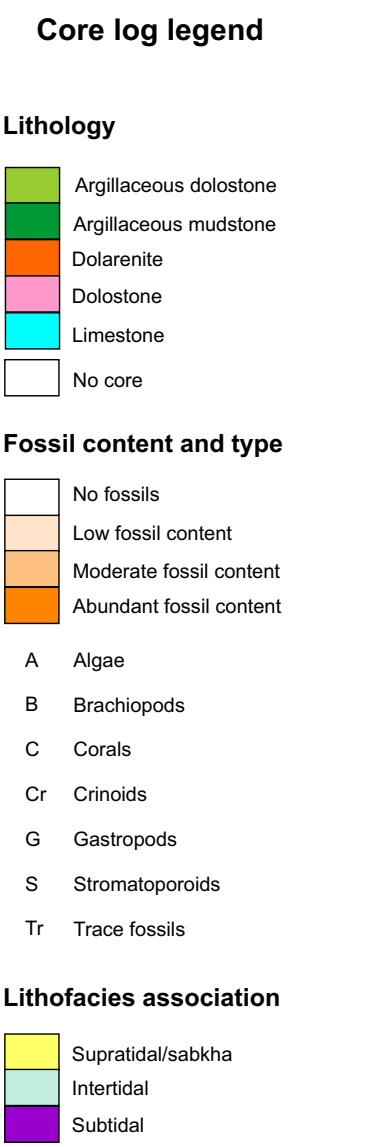

Figure GS2018-11-3: *Core log legend for Figure GS2018-11-2.*

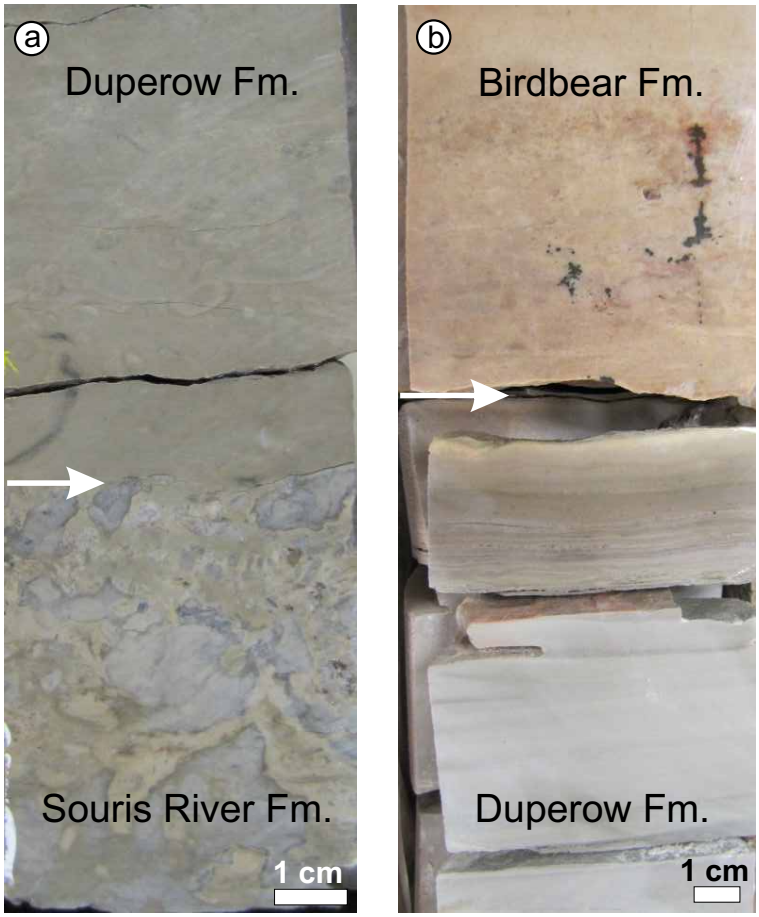

Figure GS2018-11-4: *Core photograph of lower and upper contacts of the Duperow Formation:* ***a)*** *at a depth of 656.26 m between the Souris River and Duperow formations, and* ***b)*** *at a depth of 502.90 m between the Birdbear and the Duperow formations, in the Manitoba Potash Corporation (MPC) core at 3-29-20-29W1; arrows mark contacts. Abbreviation: Fm., Formation.*

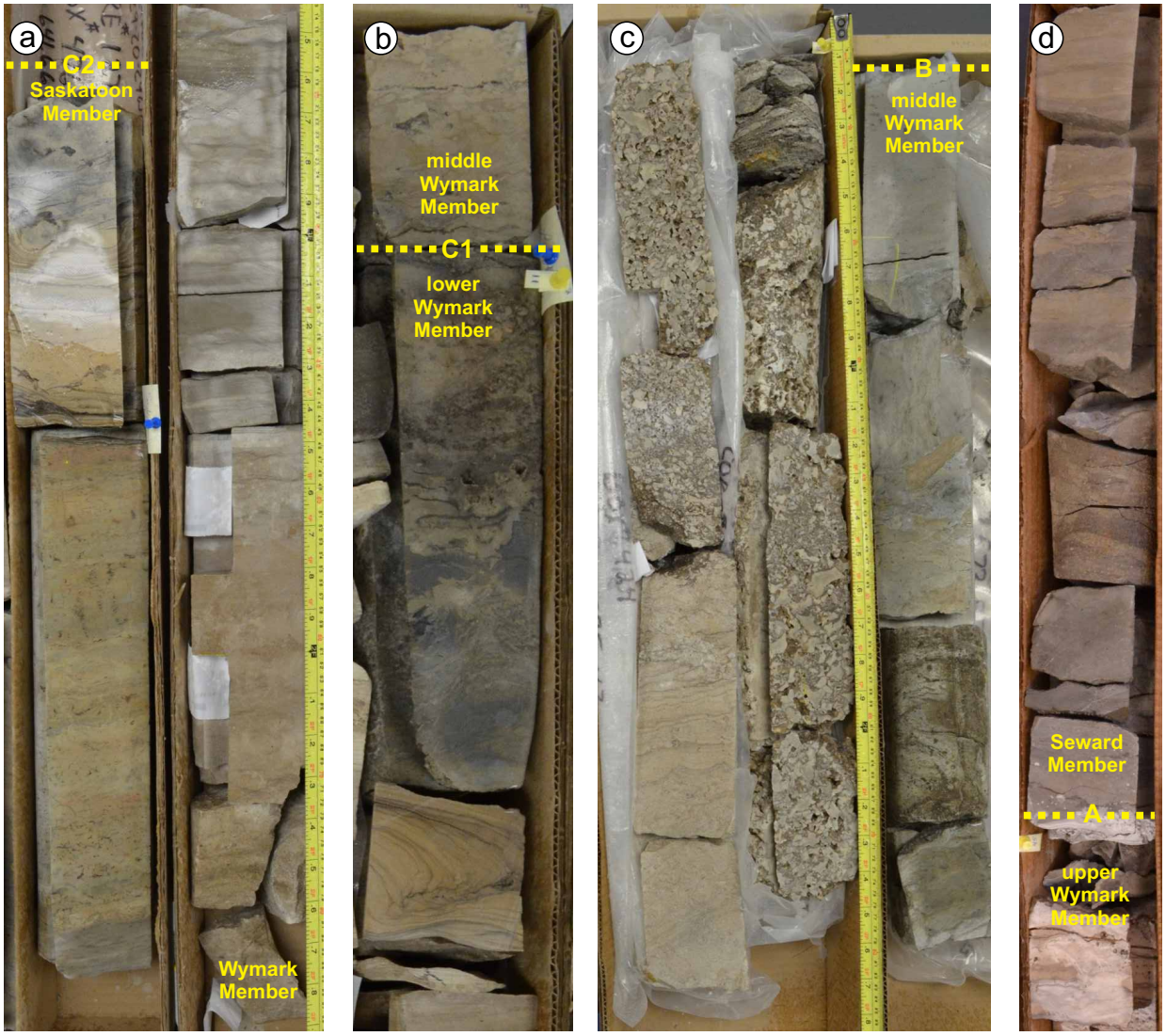

Figure GS2018-11-5: *Core photographs of key marker beds and contacts within the Manitoba Potash Corporation (MPC) core at 3-29-20-29W1:* ***a)*** *contact between Saskatoon and Wymark members, the C2 marker bed is within the lower Wymark Member;* ***b)*** *contact between lower and middle units of the Wymark Member, C1 marker bed is within the lower unit;* ***c)*** *B marker bed marking the top of the middle Wymark Member;* ***d)*** *contact between the Wymark and Seward members, A marker bed is at the base of the Seward Member. Core is 8 cm wide.*

The A marker bed is shale to argillaceous lime mudstone to dolomudstone (Figure GS2018-11-5d).

Seward Member

In the MPC core, the Seward Member is 40.32 m thick, with a lower contact at the base of the A marker bed and a conformable upper contact with limestones of the lower member of the Birdbear Formation. The Flat Lake Evaporite is not present in this core. The Seward Member is dominated by alternating intervals of 1) burrow-mottled to wavy-laminated, argillaceous lime mudstone to fossiliferous wackestone, with fragments of brachiopods, gastropods and corals; and 2) red-brown to green-grey, laminated to mottled, argillaceous dolomudstone to shale, which is locally brecciated. Fossiliferous floatstone, oncoid rudstone-floatstone and microbial laminite occur in the lower 2 m of the member. The upper 5.22 m is the Seward shale, a red-brown argillaceous dolomudstone with a characteristic high gamma-ray log signature (Figure GS2018-11-2).

Lithofacies associations

Previous sedimentological studies of the Duperow Formation in southwestern Manitoba have recognized a variety of carbonate and evaporite lithofacies that are interpreted to have been deposited in peritidal environments in an arid, interior platform (Eggie, 2012; Eggie et al., 2012; Bates, 2016; Bates et al., 2016). These litho-

facies are grouped into 1) subtidal, 2) intertidal and 3) supratidal/sabkha lithofacies associations. They form metre- to decametre-scale, shallowing-upward cycles.

Preliminary lithofacies analysis of the Duperow Formation in the MPC core indicates that the lithofacies framework developed by previous studies can also be applied to this core (Figure GS2018-11-2). The subtidal lithofacies association in the MPC core is dominated by fossiliferous wackestone-packstone to floatstone-framestone, with abundant stromatoporoids and corals and nodular packstone (Figure GS2018-11-6a–c). The intertidal lithofacies association consists mainly of wavy-laminated to burrow-mottled lime mudstone-dolomudstone to wackestone (Figure GS2018-11-6d). The supratidal/sabkha lithofacies association is composed mainly of planar-laminated dolomudstone and shale (Figure GS2018-11-6e, f). Anhydrite laminae and beds are rare, which is in contrast to the supratidal/sabkha lithofacies association present in other Duperow Formation cores, as described by Eggie (2012) and Bates (2016). Metre-scale, shallowing-upward cycles are recognized in all members of the Duperow Formation. Full cycles have the basal, subtidal lithofacies association that is overlain by the intertidal lithofacies association and the supratidal/sabkha lithofacies association, but many cycles are incomplete.

Oil shows

The Duperow Formation, which is stratigraphically equivalent to the prolific oil-producing Leduc Formation in Alberta, has oil production throughout the Elk Point Basin, including Saskatchewan, North Dakota and Montana. Live oil staining was observed in all three members of the Duperow Formation in Manitoba, as documented in Bates (2016). In the MPC core, the best oil shows occur in the upper beds of the lower Wymark Member and throughout the middle Wymark Member, and minor oil shows were observed in the upper Wymark Member and the lowermost beds of the Seward Member (Figure GS2018-11-7). While no oil staining was observed in the Saskatoon Member, the medium brown colouration of the rocks may have masked the staining, and no ultraviolet (UV) fluorescent tests were conducted on this member. The oil shows in the other members in the MPC core vary from brown spotty staining that fluoresces under UV light; to bituminous blebs and fracture coatings that produce a streaming white cut when dissolved in acetone and viewed under UV light; to mudstone laminae that commonly produce a streaming milky white cut in acetone under UV light.

Much of the core, particularly the limestone intervals, glow light yellow when viewed under UV light, which made identification of distinct oil staining challenging. It is uncertain if this UV fluorescence is due to mineralogy or petroleum, given the extent and consistency of UV fluorescence commonly observed on the core, particularly in the Wymark Member. Fresh samples were taken for UV testing in order to mitigate possible drilling mud contamination. Drilling records indicate no petroleum-based drilling muds were used during the drilling of the upper 700 m of this well (which includes the Duperow Formation); diesel was added to the drilling mud only below 700 m in anticipation of the salt sections expected at deeper depths.

Rock-Eval 6 results

Laminae and thin beds of dark brown, argillaceous lime mudstone are present throughout the Duperow Formation in the MPC core. Select samples from the Saskatoon and Wymark members (depths between 587.18 and 647.05 m) were collected for Rock-Eval 6 analysis to help characterize the organic matter and source rock potential of these laminae and beds; the results are listed in Table GS2018-11-2. Most of the samples have total organic carbon (TOC) values between 0.5 and 1.0 wt. %, which indicate good source rock generative potential. However, one sample (106-16-3884-587.18) from the middle Wymark Member has a TOC of 4.23 wt. %, indicating excellent source rock potential. The maximum temperature (Tmax) values for all the samples fall just below the oil window threshold of 435°C, indicating the rocks are slightly thermally immature. Kerogen type was determined by comparing the hydrogen index (HI) and oxygen index (OI) values, with most samples falling between type 2 (oil prone) and type 3 (gas prone) kerogens. However, two samples (106-16-3384-587.18 and 106-16-3384-608.09), both from the middle Wymark Member, have low OI and high HI values typical of type 2 kerogens (Peters, 1986).

Despite the thermal immaturity of the samples, some of these organic-rich beds have a halo of oil staining in the adjacent fossiliferous wackestone-packstone. This suggests localized hydrocarbon migration out of the argillaceous lime mudstones and the potential for an unconventional resource, where the source and the reservoir beds occur together.

Fractures and fluid flow

Fractures were common and prominent through the MPC core. The Wymark and Seward members have abundant long vertical fractures (Figure GS2018-11-7), which are commonly open and rarely completely or partially sealed with calcite or a bituminous residue. In addition,

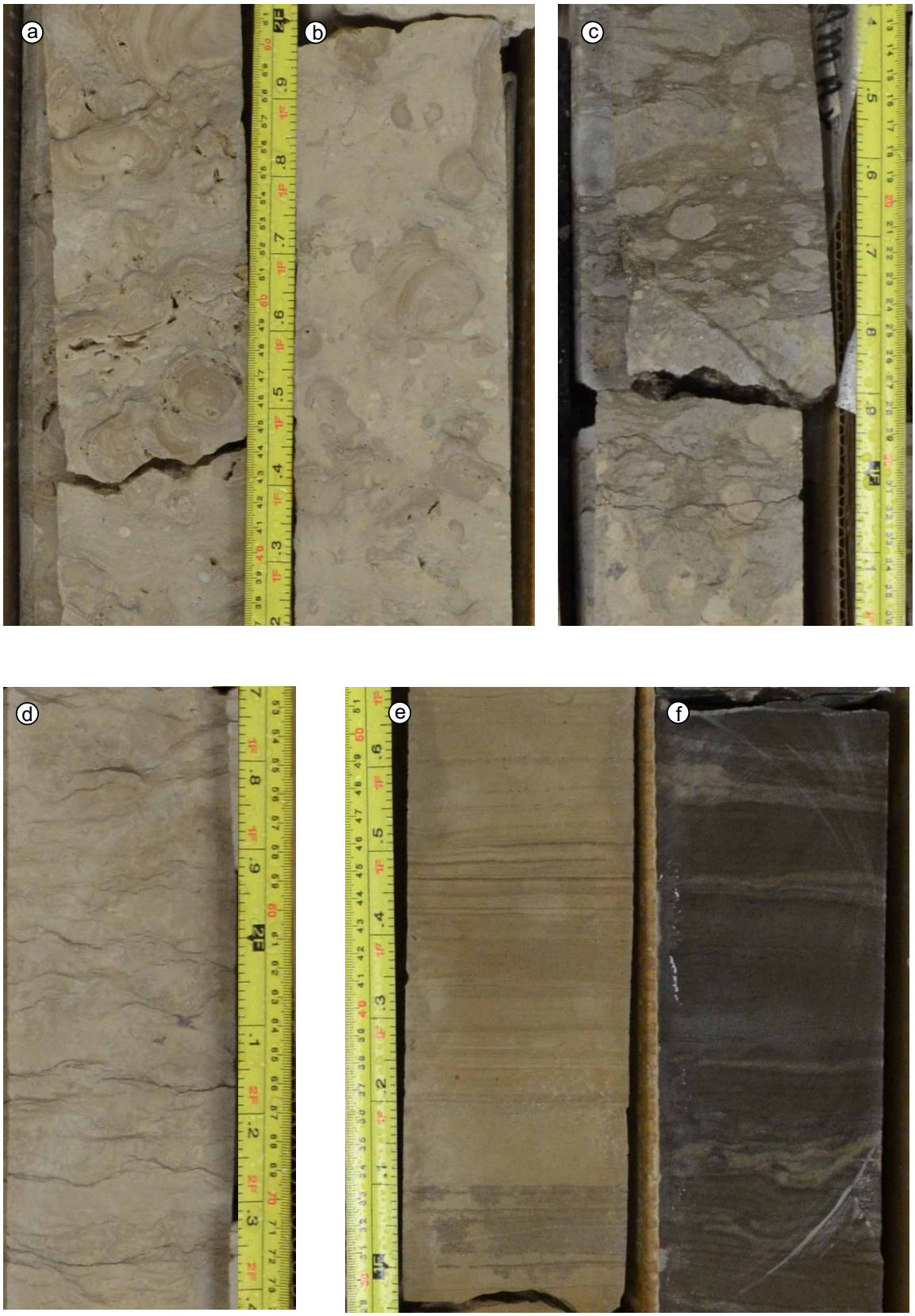

Figure GS2018-11-6: *Core photographs from the Manitoba Potash Corporation (MPC) core at 3-29-20-29W1 showing examples of the most dominant lithofacies within each lithofacies association:* ***a, b)*** *subtidal stromatoporoid floatstone at 624.79 and 624.09 m, respectively;* ***c)*** *subtidal nodular packstone at 635.40 m;* ***d)*** *intertidal, wavy-laminated to burrow-mottled mudstone to wackestone at 583.97 m;* ***e)*** *supratidal/sabkha planar-laminated dolomudstone at 652.94 m; and* ***f)*** *supratidal/sabkha interbedded dolomudstone and anhydrite at 653.64 m.*

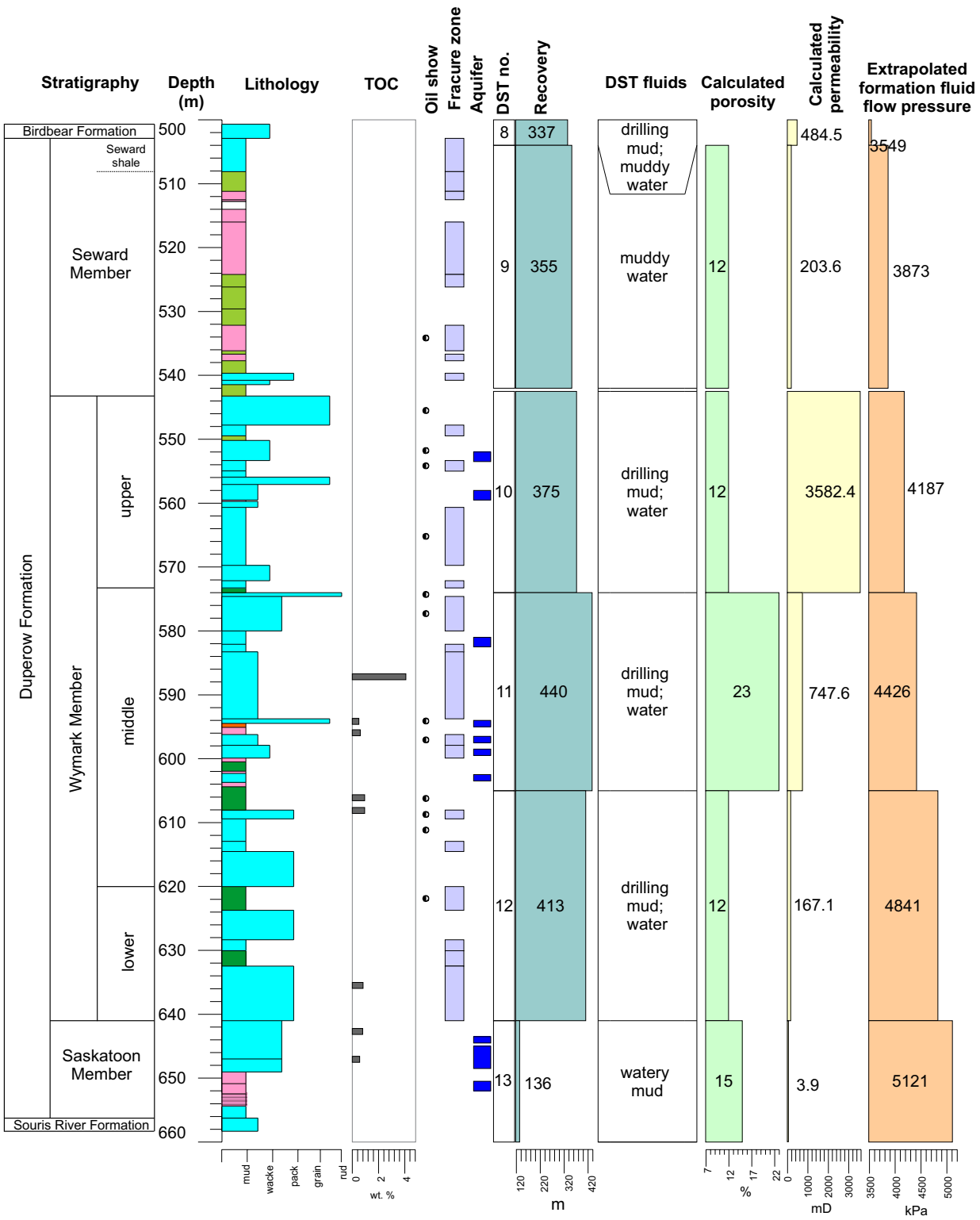

Figure GS2018-11-7: *Core log for the Duperow Formation in the Manitoba Potash Corporation (MPC) core at 3-29-20-29W1 with tracks for the stratigraphy, lithology, total organic carbon, oil shows, fracture zones, aquifer zones and drill-stem test (DST) results, including DST number, recovery, fluids, calculated porosity, calculated permeability and extrapolated formation fluid flow pressure. See Figure GS2018-11-3 for lithology legend. Abbreviations: grain, grainstone; kPa, kilopascal; mD, millidarcy; mud, mudstone; pack, packstone; rud, rudstone; TOC, total organic carbon; wacke, wackestone.*

Table GS2018-11-2: Rock-Eval 6 results for samples from the Manitoba Potash Corporation (MPC) core at 3-29-20-29W1. Abbreviations: HI, hydrogen index (mg hydrocarbons/g C_{org}; ratio of S2/TOC); MinC, mineral carbon; OI, oxygen index (mg CO_2/g C_{org}; ratio of S3/TOC); PC, pyrolyzed carbon; PI, production index (S1/(S1+S2); RC, residual carbon; S1, hydrocarbons thermally distilled from 1 g of rock; S2, hydrocarbons generated by pyrolytic degradation of kerogen from 1 g of rock; S3, milligrams of CO_2 generated from organic source in 1 g of rock; S3CO, milligrams of CO generated from organic source from 1 g of rock; Tmax, maximum temperature; TOC, total organic carbon.

Sample number	Depth (m)	TOC (wt. %)	Tmax (°C)	S1 (mg/g)	S2 (mg/g)	S3 (mg/g)	S3CO (mg/g)	MinC (wt. %)	PC (wt. %)	RC (wt. %)	HI	OI	PI
106-16-3884-587.18	587.18	4.23	422	0.22	9.54	1.38	0.30	7.6	0.89	3.34	226	33	0.02
106-16-3884-594.15	594.15	0.52	414	0.01	0.38	0.35	0.05	7.3	0.05	0.47	73	67	0.04
106-16-3884-595.94	595.94	0.63	418	0.03	2.09	0.38	0.07	8.1	0.20	0.43	332	60	0.01
106-16-3884-606.12	606.12	0.98	428	0.04	1.74	0.62	0.11	1.4	0.18	0.80	178	63	0.02
106-16-3884-608.09	608.09	0.97	422	0.06	4.07	0.34	0.03	10.8	0.37	0.60	420	35	0.02
106-16-3884-635.50	635.50	0.84	426	0.04	1.38	0.66	0.11	8.7	0.15	0.69	164	79	0.03
106-16-3884-642.70	642.70	0.82	431	0.07	1.13	0.81	0.05	7.3	0.13	0.69	138	99	0.06
106-16-3884-647.05	647.05	0.58	431	0.05	1.47	0.44	0.09	10.3	0.15	0.43	253	76	0.03

zones of rubbly core are common and suggestive of intervals with extreme fracturing. No fractures were observed in the Saskatoon Member.

Six drill-stem tests (DSTs) were conducted in the Duperow Formation in this well. The DSTs had very good fluid recovery, although it consisted mostly of muddy water, indicating that this formation has very high fluid flows, as well as moderate to good porosity and variable permeability, and as expected, increased formation fluid flow pressure with depth (Figure GS2018-11-7). During drilling, there were 10 separate aquifers with large and steady fluid flows encountered, occurring mainly in vuggy and fractured packstone to floatstone beds, and locally in porous wackestone beds. In the Saskatoon Member, aquifer zones occurred in limestones between anhydrite-rich beds. The highest fluid recovery was in the middle Wymark Member, which has five high flow aquifers, whereas the lowest was in the Saskatoon Member despite it having three high flow aquifer zones. The DST results in the Saskatoon Member indicate moderate to good porosity but low permeability, suggesting that high formation pressure is likely the driver for higher fluid flow. Given the occurrence of three aquifers in this member, it is possible that the member contains fractures and that the MPC core simply did not intersect the fractures.

Conclusions

The Duperow Formation members preserved in this core, from bottom to top, are the Saskatoon, Wymark and Seward members. Preliminary lithofacies analysis indicates that the subtidal, intertidal and supratidal/sabkha lithofacies associations recognized in other studies of the Duperow Formation in Manitoba are also present in the MPC core.

The preliminary findings of this study indicate that oil has migrated through the formation (conventional reservoir model), but also supports the potential for a self-sourcing capacity (unconventional reservoir model). High fluid flows measured throughout the formation provide the hydrokinetic energy required for fluid migration and trapping. The Rock-Eval results for samples of organic-rich lime mudstones indicate good oil generative potential but fall just below the oil generation window. These results are in agreement with those of Bates et al. (2016) and support the idea that the Duperow Formation may be within the oil window in southwestern Manitoba, closer to the Pierson and Waskada oil fields, and could be both a source and reservoir rock.

Future work

Future work is expected to address stratigraphic correlation of the Duperow Formation in the MPC core with other cores in the Elk Point Basin. Detailed petrographic and geochemical studies are ongoing at the University of Manitoba.

Economic considerations

The Duperow Formation is an oil-producing horizon in Saskatchewan, North Dakota and Montana, and recent studies suggest there is moderate potential in southwestern Manitoba as well. The ability to view the entire Duperow Formation in the continuous MPC core provides much needed clarity on its stratigraphy, lithofacies architecture and oil potential. Preliminary findings from this study support that the Duperow Formation in Manitoba does have oil potential, both as a conventional and unconventional oil target.

Acknowledgments

The authors would like to thank G. Dakoru for collecting the Rock-Eval samples. The authors would like to acknowledge C. Epp and the summer students of the MGS Midland Core and Sample Library for their care and attention to detail during preparation of the core for viewing.

References

Bates, K. 2016: Stratigraphy, sedimentology and petroleum potential of the Upper Devonian Duperow Formation, southwest Manitoba; M.Sc. thesis, University of Manitoba, Winnipeg, Manitoba, 228 p.

Bates, K., Chow, N. and Nicolas, M.P.B. 2016: Preliminary results from sedimentological investigations and petroleum evaluation of the Upper Devonian Duperow Formation, southwestern Manitoba; *in* Report of Activities 2016, Manitoba Growth, Enterprise and Trade, Manitoba Geological Survey, p. 157–167.

Cen, X.C. and Salad Hersi, O. 2006a: A revised lithostratigraphic framework and characteristics of the Upper Devonian Duperow Formation, southeastern Saskatchewan; *in* Summary of Investigations 2006, Volume 1, Saskatchewan Industry Resources, Saskatchewan Geological Survey, Miscellaneous Report 2006-4.1, Paper A-9, 17 p.

Cen, X.C. and Salad Hersi, O. 2006b: Sedimentology, microfacies analysis, and depositional setting of the Late Devonian Duperow Formation, southeastern Saskatchewan; *in* Summary of Investigations 2006, Volume 1, Saskatchewan Industry Resources, Saskatchewan Geological Survey, Miscellaneous Report 2006-4.1, Paper A-10, 18 p.

Eggie, L. 2012: Sedimentology and petroleum reservoir potential of the middle unit of the Wymark Member in the Upper Devonian Duperow Formation, southwestern Manitoba; B.Sc. thesis, University of Manitoba, Winnipeg, Manitoba, 145 p.

Eggie, L., Chow, N. and Nicolas, M.P.B. 2012: Sedimentology of the Wymark Member (middle unit) of the Upper Devonian Duperow Formation, southwestern Manitoba (NTS 62F14, 15, 16); *in* Report of Activities 2012, Manitoba Innovation, Energy and Mines, Manitoba Geological Survey, p. 160–171.

Kent, D.M. 1983: Carbonate and associated rocks of the Williston Basin: their origin, diagenesis, and economic potential; *in* Patterns of sedimentation, diagenesis and hydrocarbon accumulation in Cretaceous rocks of the Rocky Mountains, D.D. Rice and D.L. Gauthier (ed.), Society of Economic Paleontologists and Mineralogists, Short Course Notes No. 11. p. 72–87.

Nicolas, M.P.B. 2016: Preliminary investigation from the Cretaceous section of the Manitoba Potash Corporation core at 3-29-20-29W1, southwestern Manitoba (NTS 65K1); *in* Report of Activities 2016, Manitoba Growth, Enterprise and Trade, Manitoba Geological Survey, p. 150–156.

Nicolas, M.P.B. and Barchyn, D. 2008: Williston Basin Project (Targeted Geoscience Initiative II): summary report on Paleozoic stratigraphy, mapping and hydrocarbon assessment, southwestern Manitoba; Manitoba Science, Technology, Energy and Mines, Manitoba Geological Survey, Geoscientific Paper GP2008-2, 21 p.

Nicolas, M.P.B., Matile, G.L.D., Keller, G.R. and Bamburak, J.D. 2010: Phanerozoic geology of southern Manitoba; Manitoba Innovation, Energy and Mines, Manitoba Geological Survey, Stratigraphic Map Series, Map 2010-1, Sheet A: Paleozoic, Sheet B: Phanerozoic, scale 1:600 000.

Peters, K.E. 1986: Guidelines for evaluating petroleum source rock using programmed pyrolysis; American Association of Petroleum Geologist Bulletin, v. 70, no. 3, p. 318–329.

TGI Williston Basin Working Group 2008a: Devonian Duperow Formation: isopach; Manitoba Science, Technology, Energy and Mines, Manitoba Geological Survey, Stratigraphic Map Series SM2008-DD-I, scale 1:1 000 000, URL <http://www.manitoba.ca/iem/geo/willistontgi/mapfiles/pdfs/036_dev_duperow_fm_iso.pdf> [October 2018].

TGI Williston Basin Working Group 2008b: Devonian Duperow Formation: structure contour; Manitoba Science, Technology, Energy and Mines, Manitoba Geological Survey, Stratigraphic Map Series SM2008-DD-S, scale 1:1 000 000, URL <http://www.manitoba.ca/iem/geo/willistontgi/mapfiles/pdfs/036_dev_duperow_fm_str.pdf> [October 2018].

Wilson, J.L. 1967: Carbonate-evaporite cycles in lower Duperow Formation of Williston Basin; Bulletin of Canadian Petroleum Geology, v. 15, p. 230–312.

Wilson, J.L. and Pilatzke, R.H. 1987: Carbonate-evaporite cycles in the lower Duperow Formation of the Williston Basin; *in* Willison Basin: anatomy of a cratonic oil province, M.W. Longman (ed.), Rocky Mountain Association of Geologists, p. 119–146.

GS2018-12

Lithostratigraphy of the Neepawa DDH No. 1 Prov. core at 15-29-14-14W1, southwestern Manitoba (part of NTS 62J3)

by K. Lapenskie and M.P.B. Nicolas

In Brief:

- Examination of nearly 500 m of Paleozoic strata from drillcore Neepawa DDH allowed for positive correlations from the deep subsurface to outcrop belt, and indicates that additional studies may lead to the resolution of the stratigraphic framework of Manitoba
- Refining and resolving Paleozoic stratigraphy of Manitoba has positive implications for petroleum and industrial mineral industries, and carbonate-hosted lead-zinc mineralization exploration

Citation:
Lapenskie, K. and Nicolas, M.P.B. 2018: Lithostratigraphy of the Neepawa DDH No. 1 Prov. core at 15-29-14-14W1, southwestern Manitoba (part of NTS 62J3); *in* Report of Activities 2018, Manitoba Growth, Enterprise and Trade, Manitoba Geological Survey, p. 136–149.

Summary

Drillcore Neepawa DDH No. 1 Prov. 15-29-14-14W1, drilled in the vicinity of the town of Neepawa, provides a rare view of the entire lower Paleozoic section in the subsurface of southwestern Manitoba. Terminating in Precambrian iron formation, this core consists of 491.10 m of continuous core from the Ordovician Winnipeg Formation to the Devonian Souris River Formation. Correlations of established outcrop-based lithostratigraphic units were extrapolated to the subsurface in Manitoba and, where established, mostly Manitoba-derived lithostratigraphic units and nomenclature are used. Several correlation issues were resolved within this core and inconsistencies were identified, which indicates that through additional study of drillcore and outcrop these issues may be resolved Manitoba-wide. Refining the stratigraphic framework of the Williston Basin has positive implications for the petroleum and industrial mineral industries and for Mississippi Valley–type deposit exploration.

Introduction

In 1978, Neepawa Mines Ltd. completed an exploration drillhole at L.S. 15, Sec. 29, Twp. 14, Rge. 14, W 1st Mer. (abbreviated 15-29-14-14W1), near the town of Neepawa, as part of a project investigating base metal potential in Precambrian basement (Figure GS2018-12-1). A total of 937.87 m of core was acquired and the uppermost 763.35 m of core, composed of Paleozoic, Mesozoic and Quaternary strata, was retained by the Manitoba Geological Survey (MGS). This drillcore is officially known as Neepawa DDH No. 1 Prov. 15-29-14-14W1 (oil and gas well licence 2472, Manitoba Growth, Enterprise and Trade, Winnipeg; Assessment File 91210, Manitoba Growth, Enterprise and Trade, Winnipeg) and referred to herein as Neepawa DDH.

Most of the lower Paleozoic stratigraphy in Manitoba has been characterized by outcrop mapping in combination with examination of shallow stratigraphic drillcores. The Neepawa DDH core offers a unique opportunity to observe the entire lower Paleozoic stratigraphy in the subsurface of the Williston Basin in southwestern Manitoba. In addition, downhole wireline geophysical spontaneous potential and resistivity logs are available and provide a critical correlation tool to link lithostratigraphy and geophysical log signatures in the subsurface.

The lower Paleozoic stratigraphic framework of southwestern Manitoba contains many inconsistencies (Lammers, 1988; Bezys and Conley, 1998; Nicolas and Barchyn, 2008; Lapenskie and Nicolas, 2017). Lateral variations in lithology, facies changes and stratigraphic boundaries, coupled with few core available in this transitional area, have made correlating units across the basin challenging. In particular, parts of the Ordovician Red River Formation, the Silurian Interlake Group, and parts of the Devonian Dawson Bay and Souris River formations are not consistently correlated between outcrop and the subsurface. Neepawa DDH provides an opportunity to address these issues by identifying which units can be correlated and which require more work to refine the correlations.

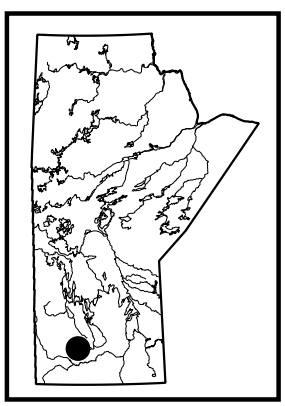

Regional geology

Southwestern Manitoba is covered by a thick succession of gently southwest-dipping sedimentary rocks deposited on the northeastern edge of the Williston Basin during the Phanerozoic (Figure GS2018-12-1). Deposition spanned the Cambrian to Mississippian, Triassic to Cretaceous, early Paleogene and Quaternary periods. Significant periods of

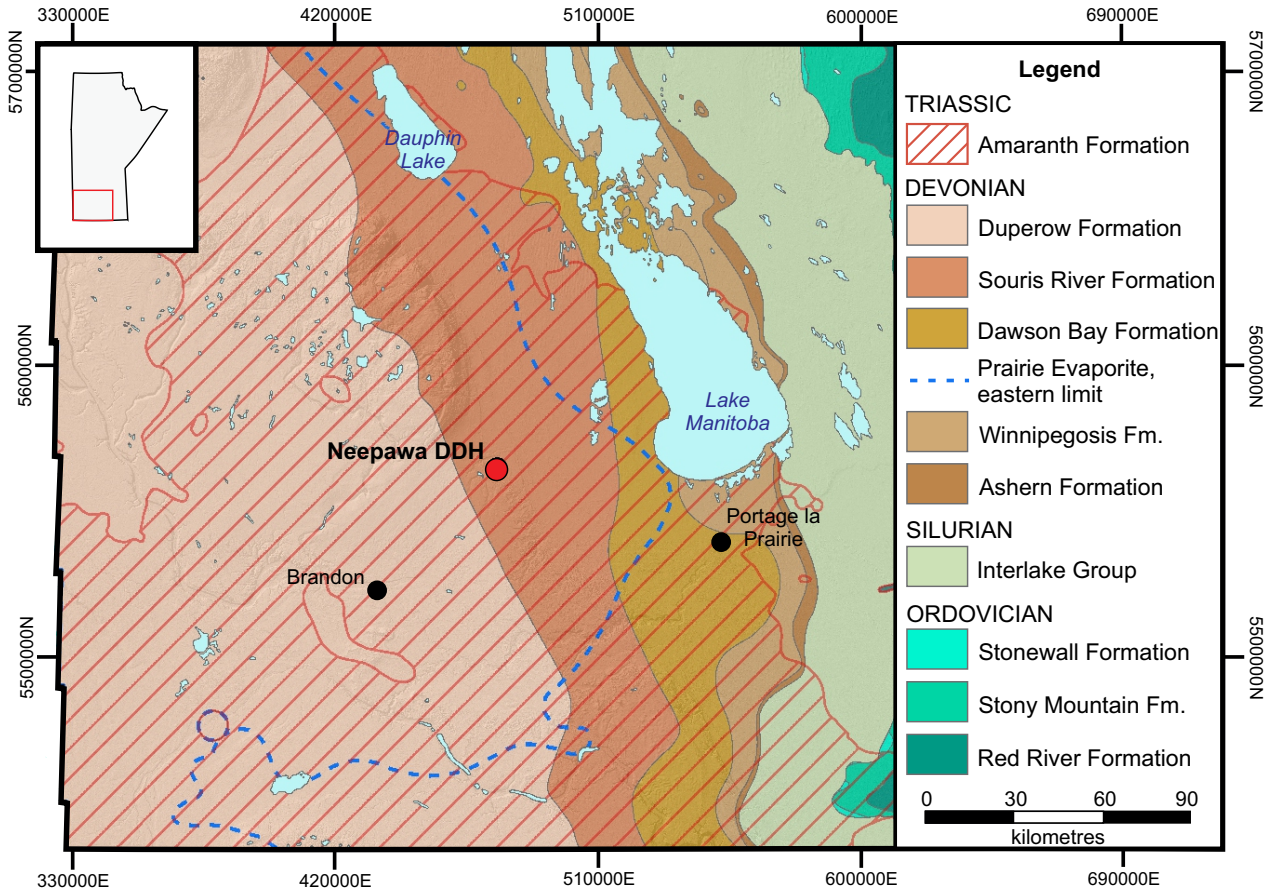

Figure GS2018-12-1: *Regional bedrock geology of southwestern Manitoba (after Nicolas et al., 2010); formations younger than the Duperow Formation (excluding the Triassic Amaranth Formation) are not shown. The area is underlain by Precambrian igneous and metamorphic rocks (not exposed in map area). Location of drillhole Neepawa DDH No. 1 Prov. 15-29-14-14W1 (Neepawa DDH) is shown.*

nondeposition and/or erosion occurred at the boundary between the Cambrian and Ordovician, at the boundary between the Silurian and Devonian, within most of the Paleogene, and during lesser hiatus periods within the Jurassic and Cretaceous. The Paleozoic rocks of the Williston Basin are predominantly composed of marine platform carbonate rocks, interbedded with minor successions of siliciclastic rocks and evaporites, and overlie basement Precambrian igneous and metamorphic rocks.

Stratigraphy

Neepawa DDH provides a nearly complete core of the lower Paleozoic from the basal Ordovician Winnipeg Formation to the middle Devonian Souris River Formation (Figure GS2018-12-2). The section is mostly composed of dolostone and limestone, with subordinate sandstone, shale and evaporitic units. A detailed description of the lithostratigraphy of Neepawa DDH is provided in Table GS2018-12-1 and a core log with the lithostratigraphy and geophysical signatures is provided in Figure GS2018-12-3. Neepawa DDH was drilled to a true vertical depth of 937.87 m, with the upper 763.35 m composed of Paleozoic, Mesozoic and Quaternary strata and the lower 174.52 m composed of Precambrian rocks. Assessment File 91210 provides a brief description of the Precambrian section. Mesozoic and Quaternary strata were not examined for this study.

Ordovician

The Ordovician section of Neepawa DDH is composed of the siliciclastic Winnipeg Formation, and a thick succession of lime mudstone, lime wackestone, dolomudstone, dolowackestone and dolobindstone of the Red River, Stony Mountain and Stonewall formations. The Cambrian Deadwood Formation is absent in this core. The upper Stonewall Formation is Silurian in age, with the Ordovician–Silurian boundary present in the vicinity of the t-marker bed (Norford et al., 1998; Kleffner et al., 2005; Desrochers et al., 2010; Demski et al., 2010a, b, 2011a, b).

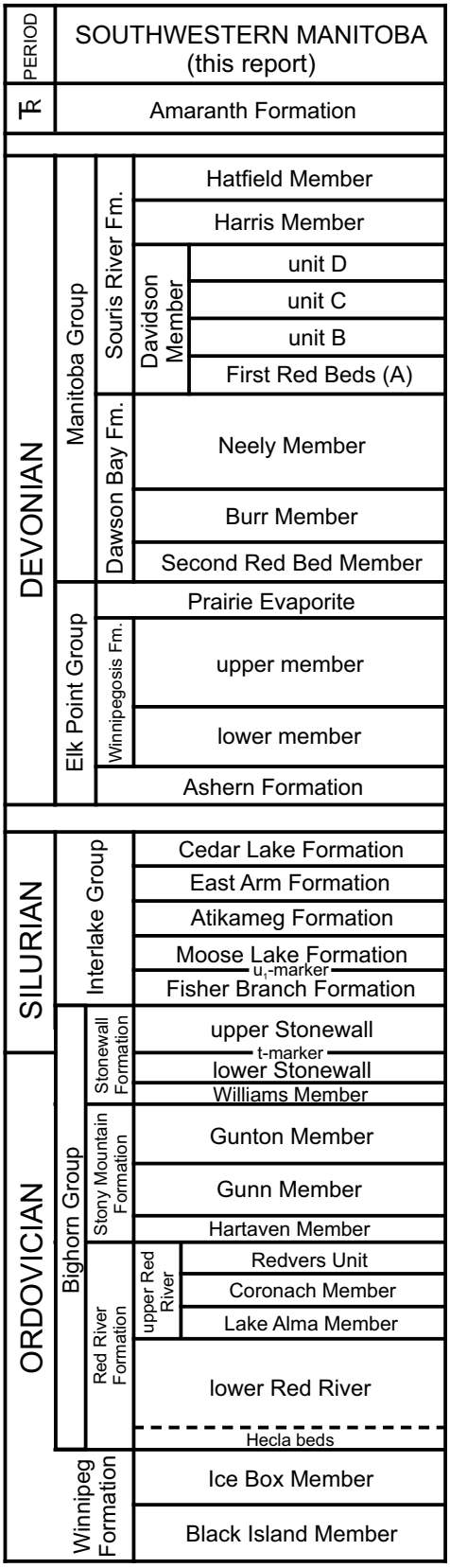

Figure GS2018-12-2: *Stratigraphic column of Neepawa DDH No. 1 Prov. 5-29-14-14W1 core. Abbreviations: Fm., Formation; TR, Triassic.*

Table GS2018-12-1: Lithostratigraphy and generalized lithology of drillcore Neepawa DDH No. 1 Prov. 15-29-14-14W1; refer to Assessment File 91210 (Manitoba Growth, Enterprise and Trade, Winnipeg) for a description of the Precambrian section. Asterisks indicate estimated depths (core boxes were missing at these depths).

Total vertical depth (m)	Thickness (m)	Description
n/a–272.25	n/a	**Amaranth Formation**
		Lower Amaranth Member
		Pinkish-red feldspathic to lithic wacke
272.25–388.60	116.35	**Manitoba Group**
272.25–323.15	50.90	**Souris River Formation**
272.25–273.88	1.63	**Hatfield Member**
		Pinkish-buff dolomudstone; laminated to bedded; argillaceous; evaporitic, gypsum-anhydrite nodules and beds; pyritic; intercrystalline porosity, 10%; upper contact sharp
273.88–301.85	27.97	**Harris Member**
		Reddish-, greyish- to bluish-buff cyclical dolomudstone to gypsum-anhydrite; laminated to bedded; dolomudstone sequences laminated to bedded, argillaceous, stromatolitic, uncommonly brecciated, bituminous, intercrystalline porosity, 15%, passing sharply upward to evaporite; gypsum-anhydrite sequences laminated to massively bedded, nodular, impermeable, passing sharply to carbonate rocks; upper contact sharp
301.85–323.15	21.30	**Davidson Member**
301.85–305.80	3.95	**unit D**
		Blue-grey to purplish-buff interbedded dolomudstone and gypsum-anhydrite; laminated to massively bedded, nodular; argillaceous; intercrystalline porosity, 2%; pyritic; upper contact sharp
305.80–309.30	3.50	**unit C**
		Pinkish- to bluish-buff interbedded shale, dolomudstone and gypsum-anhydrite; laminated to massively bedded, nodular; intercrystalline porosity, 5%; upper contact sharp
309.30–321.50	12.20	**unit B**
		Pinkish-yellowish–buff calcareous dolomudstone; laminated to bedded to massive, porcelaneous, wispy argillaceous laminations, stylolitic, mottled; biostromal; evaporitic, gypsum-anhydrite nodules; intercrystalline to vuggy porosity, 10%; upper contact sharp
321.50–323.15	1.65	**First Red Beds (unit A)**
		Purple to red-brown interbedded dolomudstone, shale and gypsum-anhydrite; laminated to bedded, burrowed, nodular; intercrystalline porosity, 10%; upper contact sharp
323.15–388.60*	65.45	**Dawson Bay Formation**
323.15–351.90	28.75	**Neely Member**
		Tan-buff (pinkish-yellowish) lime mudstone-wackestone to calcareous dolomudstone-wackestone; coarsely crystalline; laminated to massively bedded, wispy argillaceous laminations, bituminous beds, brecciated beds, probably crossbeds, burrowing; argillaceous to shaly; evaporitic, gypsum-anhydrite nodules, laminations and beds; fossiliferous, tabulate corals, rugose corals, stromatoporoids; becomes increasingly evaporitic upward; upper contact gradational
351.90–382.55	30.65	**Burr Member**
		Tan-buff (purplish-yellowish) lime mudstone to lime wackestone; laminated to massively bedded to massive, mottled; argillaceous; fossiliferous (brachiopods, crinoids); evaporitic, gypsum-anhydrite infilling horizontal and vertical fractures; intercrystalline porosity, 10%; upper contact sharp? core is very rubbly, lithology changes significantly
382.55–388.60*	6.05	**Second Red Bed Member**
		Red-brown to mottled grey dolomudstone to shale; massive; very argillaceous; uncommon gypsum laminations; pyritic; intercrystalline porosity, 10%; upper contact sharp
388.60*–448.37	59.77	**Elk Point Group**
388.60*–403.90*	15.30	**Prairie Evaporite**
		Pink, grey, buff and red-brown shale to dolomudstone interbedded with blue-grey gypsum-anhydrite; laminated to bedded; argillaceous; upper contact not observed

Table GS2018-12-1 (continued): Lithostratigraphy and generalized lithology of drillcore Neepawa DDH No. 1 Prov. 15-29-14-14W1; refer to Assessment File 91210 (Manitoba Growth, Enterprise and Trade, Winnipeg) for a description of the Precambrian section. Asterisks indicate estimated depths (core boxes were missing at these depths).

Total vertical depth (m)	Thickness (m)	Description
403.90*–437.30	33.40	**Winnipegosis Formation**
403.90*–406.20	2.30	**upper member**
		Light tan-buff, calcareous dolofloatstone to doloboundstone; reefal facies; massively bedded; fossiliferous, stromatoporoidal; evaporitic, gypsum-anhydrite nodules and infilling vugs; vuggy and intercrystalline porosity, 10%; upper contact not observed
406.20–437.30	31.10	**lower member**
		Tan-buff (yellowish-pinkish to brownish) dolomitic lime wackestone to calcareous dolowackestone; massively bedded, mottled; coarsely crystalline; fossiliferous; evaporitic, gypsum-anhydrite infilling porosity; pyritic; vuggy, mouldic, intercrystalline and fracture porosity, 15%; upper contact sharp, associated with a very argillaceous interval with bituminous laminations
437.30–448.37	11.07	**Ashern Formation**
		Reddish-brown to reddish- or purplish-grey dolomudstone; mottled; very argillaceous; evaporitic, gypsum-anhydrite nodules and laminations; pyritic; intercrystalline porosity, 5%; upper contact sharp
448.37–529.75	81.38	**Interlake Group**
448.37–476.90	28.53	**Cedar Lake Formation**
		Tan-buff (greyish, greenish to reddish) interbedded dolomudstone, dolowackestone, dolobindstone-doloboundstone; laminated to massively bedded, mottled, intraclastic beds, porcelaneous beds; 'raindrop' texture; fossiliferous, stromatoporoids, crinoids; argillaceous, reddish- and greenish-grey clay; intercrystalline, vuggy and fracture porosity, 15%; upper contact sharp, disconformable
476.90–504.15	27.25	**East Arm Formation**
		Tan-buff (greenish, pinkish and reddish) interbedded dolomudstone, dolowackestone-dolofloatstone and dolobindstone-doloboundstone; laminated to massively bedded, porcelaneous beds, intraformational clasts, stromatolitic, stromatoporoidal; variably fossiliferous; argillaceous, greenish-grey clay; intercrystalline and vuggy porosity, 10%; upper contact gradational
504.15–508.25	4.10	**Atikameg Formation**
		Tan-buff dolomudstone; laminated to bedded, compact interbeds, stromatolitic; mouldic and vuggy porosity, 20%; upper contact gradational
508.25–511.25	3.00	**Moose Lake Formation**
		Tan-buff dolomudstone to dolowackestone to dolobindstone; laminated, stromatolitic; fossiliferous; intercrystalline, mouldic and vuggy porosity, 15%; upper contact gradational
511.05–511.25	0.20	**u_1-marker bed**
		Pinkish–tan-buff dolomudstone; burrowed; argillaceous; upper contact gradational
511.25–529.75	18.50	**Fisher Branch Formation**
		Pinkish–tan-buff dolomudstone interbedded with yellowish tan-buff dolowackestone to dolofloatstone; laminated to massively bedded, burrowed, mottled, upper beds porcelaneous; basal marker bed reddish-pink argillaceous dolomudstone; fossiliferous, brachiopods (i.e., *Virgiana decussata*), solitary rugose corals (i.e., *Rhegmaphyllum*), tabulate corals (i.e., favositids), stromatoporoids; mouldic, vuggy, fracture porosity, 10%; evaporitic, gypsum-anhydrite infilling vugs, fractures; pyritic; upper contact gradational
529.75–725.00	195.25	**Bighorn Group**
529.75–544.20	14.45	**Stonewall Formation**
529.75–531.85	2.10	**upper Stonewall**
		Pinkish– to greyish–tan-buff dolomudstone; laminated to massively bedded; intercrystalline and fracture porosity, 2%; upper contact sharp
531.85–533.55	1.70	**t-marker bed**
		Tan to red to grey quartz wacke to dolomudstone; laminated to bedded, burrowed; argillaceous and arenaceous, coarse- to medium-grained quartz sand, frosted, intraformational clasts; intercrystalline and vuggy porosity, 2%; upper contact sharp

Table GS2018-12-1 (continued): Lithostratigraphy and generalized lithology of drillcore Neepawa DDH No. 1 Prov. 15-29-14-14W1; refer to Assessment File 91210 (Manitoba Growth, Enterprise and Trade, Winnipeg) for a description of the Precambrian section. Asterisks indicate estimated depths (core boxes were missing at these depths).

Total vertical depth (m)	Thickness (m)	Description
533.55–537.50	3.95	**lower Stonewall**
		Tan-buff dolomudstone to dolobindstone; laminated, biostromal; argillaceous to arenaceous; intercrystalline, vuggy and fracture porosity, 5%; upper contact gradational
537.50–544.20	6.70	**Williams Member**
		Reddish-brown to pinkish–tan-buff dolomudstone; laminated to bedded, mottled, burrowed; argillaceous and arenaceous, medium-grained quartz sand, frosted, well rounded; vuggy porosity, 10%; upper contact sharp
544.20–586.40	42.20	**Stony Mountain Formation**
544.20–563.45	19.25	**Gunton Member**
		Light tan-buff (yellowish to reddish) dolomudstone; laminated to bedded to massive, wispy argillaceous laminations, mottled; argillaceous; rarely fossiliferous; pyritic; intercrystalline to fracture porosity, 5%; upper contact sharp
563.45–571.50	8.05	**Gunn Member**
		Light to medium grey slightly calcareous dolomudstone; laminated to massively bedded, burrowed; argillaceous, uncommon beds of shale; intercrystalline porosity, 5%; upper contact gradational
571.50–586.40	14.90	**Hartaven Member**
		Medium grey variably dolomitic lime wackestone interbedded with minor shale beds; laminated to bedded, mottled, burrowed; very fossiliferous, brachiopods, solitary corals, skeletal fragments; argillaceous; pyritic; intercrystalline and vuggy porosity, 10%; upper contact gradational
586.40–725.00	138.60	**Red River Formation**
586.40–615.95	29.55	**upper Red River**
586.40–592.75	6.35	**Redvers Unit**
		Tan- to grey-buff dolomudstone and lime mudstone; laminated to bedded, wispy argillaceous laminations, some mottled and burrowed beds; some chert nodules; uncommon anhydrite nodules; pyritic; intercrystalline porosity, 10%; upper contact sharp
592.75–601.50	8.75	**Coronach Unit**
		Tan-buff to blue-grey dolomudstone; arenaceous bed above contact, coarse-grained quartz sand, frosted, well rounded; laminated to bedded, mottled, brecciated beds; wispy argillaceous laminations; argillaceous; some gypsum-anhydrite nodules; pyritic; intercrystalline porosity, 5%; upper contact sharp and irregular
601.50–615.95	14.45	**Lake Alma Member**
		Tan-buff to blue-grey dolomudstone; laminated to bedded to massive, mottled and burrowed, wispy argillaceous laminations; gypsum-anhydrite common; intercrystalline and vuggy porosity, 5%; upper contact sharp
615.95–724.70	108.75	**lower Red River**
		Grey-buff lime mudstone to lime wackestone interbedded with dolomudstone to dolowackestone; massive to massively bedded, wispy argillaceous laminations, mottled and burrowed; fossiliferous; rare nodular gypsum-anhydrite, rare chert nodules; intercrystalline and vuggy porosity, 5%; rare irregular fractures; upper contact gradational
724.70–725.00	0.30	**Hecla beds**
		Dark grey lime wackestone; argillaceous and arenaceous, abundant frosted quartz grains; upper contact sharp
725.00–763.35	38.35	**Winnipeg Formation**
725.00–757.05	32.05	**Ice Box Member**
		Medium to dark olive-grey shale; laminated, fissile, burrowed intervals, slickenslides; fossiliferous; intercrystalline porosity, 5%; hematitic; pyritic; tertiary gypsum; upper contact sharp
757.05–763.35	6.30	**Black Island Member**
		Reddish–dark grey slightly calcareous quartz wacke; bedded, flaser bedding in places; burrowed; hematitic; pyritic; intercrystalline porosity, 5%; upper contact gradational
763.35–937.87	n/a	**Precambrian**
		Iron formation; iron oxide, mostly magnetite, but also includes maghemite and hematite; iron formation is fine grained and finely laminated, interbedded with green siltstone and greywacke

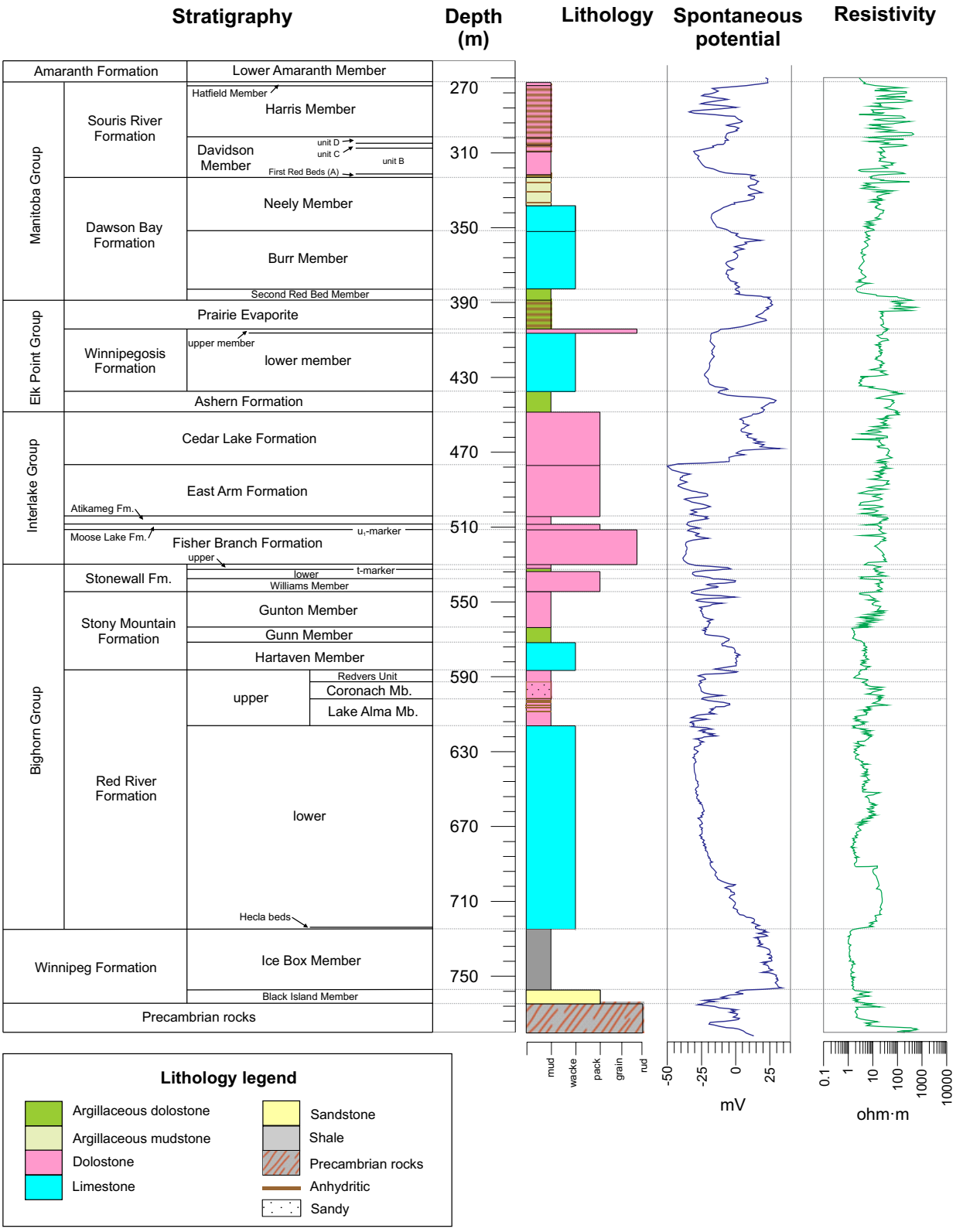

Figure GS2018-12-3: *Core log for the Neepawa DDH No. 1 Prov. 5-2914-14W1 core, showing tracks for lithology and geophysical logs. Geophysical logs have been depth corrected relative to the lithology log. Abbreviations: Fm., Formation; grain, grainstone; Mb., Member; mud, mudstone; mV, millivolt; pack, packstone; rud, rudstone; wacke, wackestone.*

Winnipeg Formation

The Winnipeg Formation disconformably overlies Precambrian iron formation. The formation is 38.35 m thick, with the basal Black Island Member composing 6.30 m of the formation and the remainder of the section composed of the Ice Box Member. The Black Island Member is a fairly well consolidated quartz wacke. Compared to the outcrop belt of southern Manitoba, this sandstone is less well sorted and much more friable (Lapenskie, 2016). The Black Island Member gradationally transitions into arenaceous shale of the overlying Ice Box Member. The Winnipeg Formation is disconformably overlain by the Red River Formation.

Red River Formation

The Red River Formation is composed of variably argillaceous carbonate rocks, with a basal 0.30 m thick argillaceous and arenaceous lime wackestone transitional unit referred to as the Hecla beds. The remainder of the lower Red River Formation is composed of argillaceous carbonate rocks. The lower Red River Formation is not completely dolomitized, and consists of interbedded calcareous and dolomitic mudstone and wackestone. The boundary between the upper and lower Red River Formation is conformable.

The upper Red River Formation in the subsurface in Saskatchewan is subdivided into the Lake Alma Member, Coronach Member and Redvers Unit. Nicolas and Barchyn (2008) noted that these units could be successfully correlated eastward into Manitoba using geophysical logs, and that formal adoption should be considered. The Lake Alma Member, Coronach Member and Redvers Unit were identified in Neepawa DDH, demonstrating that these units can be successfully correlated eastward into Manitoba. However, previous attempts at picking these units have been inconsistent, and detailed stratigraphic work is needed to fully address this issue.

The Lake Alma Member conformably overlies the lower Red River Formation, and is composed of argillaceous and evaporitic dolomudstone; the Lake Alma anhydrite is absent from this core, as it is limited to the extreme southwestern corner of Manitoba and eastern Saskatchewan. The Coronach Member disconformably overlies the Lake Alma Member and is composed of, in ascending order, a basal arenaceous dolomudstone, laminated to bedded dolomudstone and evaporitic dolomudstone. The Coronach Member is reported as being composed of a cyclical sequence of four units in Saskatchewan: a basal arenaceous dolomudstone, fossiliferous wackestone, laminated microdolomite and upper evaporite (Glass, 1990; Natural Resources Canada, 2018). Three of these four units are present in Neepawa DDH: the basal arenaceous dolomudstone, laminated dolomudstone and evaporitic dolomudstone. The Redvers Unit disconformably overlies the Coronach Member and is composed of bedded to laminated dolomudstone and lime mudstone. The Stony Mountain Formation disconformably overlies the Red River Formation.

Stony Mountain Formation

The Stony Mountain Formation is composed of a variable sequence of lime wackestone and dolomudstone interbedded with subordinate amounts of shale. The formation is subdivided into the Hartaven, Gunn and Gunton members; the Penitentiary Member is not recognized in southwestern Manitoba (Nicolas and Barchyn, 2008). The Hartaven Member is composed of shaly, fossiliferous lime wackestone. The Gunn Member is composed of a burrowed, argillaceous dolomudstone that gradationally transitions into the rarely fossiliferous, argillaceous dolomudstone of the Gunton Member. The upper contact of the Stony Mountain Formation is disconformable and occurs in the vicinity of two significant argillaceous beds. The higher of the two argillaceous beds contains quartz sand grains, which is indicative of the arenaceous Williams Member of the Stonewall Formation, therefore, the base of the upper marker bed was selected as the contact between the Stony Mountain and Stonewall formations.

Stonewall Formation

The Stonewall Formation is composed of a succession of dolostone beds, and is subdivided by the arenaceous t-marker bed. The basal Williams Member is composed of an argillaceous and arenaceous dolomudstone. The lower Stonewall Formation is composed of dolomudstone to dolobindstone and is biostromal in places.

The t-marker bed occurs as a distinctive quartz wacke to arenaceous dolomudstone in the upper portion of the Stonewall Formation. Historically, this marker bed, used in conjunction with the *Aphelognathus–Ozarkodina* conodont turnover boundary, was used to demarcate the Ordovician–Silurian boundary (Norford et al., 1998). Recent chemostratigraphic studies have demonstrated that the Ordovician–Silurian boundary occurs at a positive $\delta^{13}C$ excursion, termed the Hirnantian isotopic carbon excursion (HICE; Kleffner et al., 2005; Desrochers et al., 2010), and that this excursion generally occurs in the vicinity of the t-marker bed and conodont turnover (Demski et al., 2010a, b, 2011a, b; Lapenskie, 2012). Further study of Neepawa DDH is required to confirm the presence of the *Aphelognathus–Ozarkodina* conodont

turnover and HICE to accurately identify the Ordovician–Silurian boundary.

The upper Stonewall Formation is composed of dolomudstone, but is lacking fossils and biostromal development. The upper contact is disconformable.

Silurian

The majority of the Silurian stratigraphy of Neepawa DDH consists of the Interlake Group. In the subsurface of Manitoba, the Interlake Group has been informally subdivided into lower and upper units, divided by a v-marker bed (Bezys and Conley, 1998). In the outcrop belt of Manitoba, the Interlake Group is formally subdivided, in ascending order, into the Fisher Branch, Moose Lake, Atikameg, East Arm and Cedar Lake formations (Stearn, 1956; Glass, 1990; Natural Resources Canada, 2018). Historically, the Inwood Formation was formally recognized between the Fisher Branch and Moose Lake formations but the name has been discarded as further study of northern and southern outcrops in Manitoba's Interlake region demonstrated that the Inwood Formation was being picked inconsistently in relation to the Fisher Branch, Moose Lake and Atikameg formations (Lammers, 1988; Bezys and Conley, 1998). For this study, the Inwood Formation is not formally recognized and Inwood Formation–type lithology is considered to be uppermost Fisher Branch Formation.

A lack of sufficient core of the Interlake Group in southwestern Manitoba and the challenges of using geophysical logs that have never been adequately compared to core lithology, has made correlation efforts of the Interlake Group formations into the deeper subsurface difficult (Bezys and Conley, 1998). This has resulted in numerous correlation inconsistencies between the subsurface and outcrop belt, which is compounded by the subtle and frequent lithological variations that occur throughout the Interlake Group.

Fisher Branch Formation

The lowermost Fisher Branch Formation is composed of interbedded dolomudstone and fossiliferous dolowackestone to dolofloatstone. The early Silurian index fossil *Virgiana decussata* (Norford, 1971), a pentamerid brachiopod, occurs within this unit, as well as diverse and abundant coral and stromatoporoid fauna. The uppermost Fisher Branch Formation is porcelaneous, similar to an Inwood Formation–type lithology. The upper contact of the Fisher Branch Formation is gradational and marked by the u_1-marker bed.

Moose Lake Formation

The basal Moose Lake Formation is defined by the u_1-marker bed, a burrowed and argillaceous dolomudstone. The remainder of the formation is characterized as dolomudstone to dolowackestone to dolobindstone, and is stromatolitic and fossiliferous. The upper contact of the Moose Lake Formation is gradational and was demarcated where porosity became more pervasive.

Atikameg Formation

The Atikameg Formation is composed of dolomudstone interbedded with compact stromatolitic beds. It is less stromatolitic than the Moose Lake Formation and lacks macrofossils. The u_2-marker bed is absent, however, the core is missing and mixed where the u_2-marker bed was expected to occur, between 501.40 and 504.40 m. The upper contact of the Atikameg Formation is gradational.

East Arm Formation

Highly variable interbeds of dolostone comprise the East Arm Formation. The v-marker bed, commonly found within the middle of this formation, is absent in Neepawa DDH. The lithology of the formation varies from dolomitic mudstone, wackestone, floatstone, bindstone to boundstone. Porcelaneous, intraformational clastic, brecciated, and stromatolitic and stromatoporoidal beds are common throughout. The East Arm Formation and Cedar Lake formations are both argillaceous, containing variable amounts of reddish-pink and greenish-grey clay associated with brecciated beds and increased porosity.

Two zones of diagenetic alteration were observed from 496.53 to 496.65 m and 478.80 to 478.82 m (Figure GS2018-12-4). These zones are characterized by greatly increased vuggy porosity and the majority of the original lithology has been replaced by fine- to coarse-crystalline, brown to blue-grey dolomite. These zones superficially resemble hydrothermal dolomite identified in drillcore M-01-07 in southwestern Manitoba (NTS 63C/1; Bamburak, 2007; Rawluk, 2010); thin section and carbon and oxygen isotope work is required to determine the nature of this alteration.

The upper contact of the East Arm Formation was difficult to pick and is uncertain since the contact is best defined when the Cross Lake Member of the overlying Cedar Lake Formation is present and its presence was questionable in Neepawa DDH. In this core the occurrence of the Chemahawin Member of the overlying Cedar Lake Formation was also questionable. However, prominent crinoid-rich and stromatoporoidal beds, similar to the Cross Lake and Chemahawin members, occur

Figure GS2018-12-4: *Diagenetic alteration of the East Arm Formation in drillcore from Neepawa DDH No. 1 Prov. 15-29-14-14W1:* ***a)*** *photograph of dolostone from 495.30 to 498.40 m, zone of alteration outlined in green dashes;* ***b)*** *photograph of diagenetic alteration from 496.53 to 496.65 m, scale bar in centimetres. Arrow indicates up direction in core.*

above the designated contact between the East Arm and Cedar Lake formations in Neepawa DDH. This may indicate that the contact between the formations is significantly higher than placed, as discussed below. The upper contact was designated as gradational.

Cedar Lake Formation

The Cedar Lake Formation is similar to the East Arm Formation in that it also consists of a highly varied sequence of dolostone. In outcrop, the base of this formation is marked by the Chemahawin and Cross Lake members, but their presence in this core is uncertain, since no previous attempts have been made to extrapolate these members this far to the west (Glass, 1990; Natural Resources Canada, 2018). Interestingly, approximately 17.00 m above the lower contact there are two thin, red, argillaceous, crinoid-rich beds between 459.20 and 459.90 m, with the uppermost bed overlain by a stromatoporoidal bed from 458.65 to 459.20 m (Figure GS2018-12-5). These beds are similar to the crinoidal Cross Lake Member and reefal to stromatoporoidal Chemahawin Member. Further work is needed to confirm if these beds are the Cross Lake and Chemahawin members, and confirm if these beds can be correlated from the outcrop to the subsurface.

The remainder of the Cedar Lake Formation is composed of beds of dolomudstone, dolowackestone, and dolobindstone to doloboundstone. Beds are variably porcelaneous, fossiliferous and intraclastic. The distinctive 'raindrop' texture of the Silurian strata of Manitoba occurs within this formation. The upper contact of the Cedar Lake Formation is an angular unconformity and represents a significant period of nondeposition and erosion.

Devonian

The Devonian section of Neepawa DDH consists of interbedded shale, dolostone, limestone and evaporite, which comprise three complete shale-carbonate-evaporite cycles (Ashern Formation–Winnipegosis Formation–Prairie Evaporite; Dawson Bay Formation; and Davidson Member of the Souris River Formation) and the beginning of a fourth incomplete cycle (Harris and Hatfield members of the Souris River Formation; Fedikow et al., 2004).

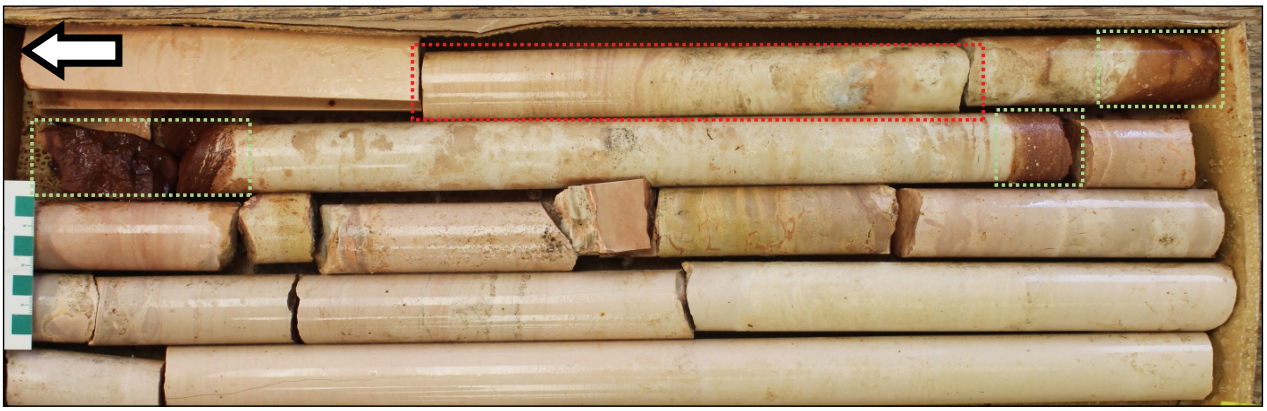

Figure GS2018-12-5: *Photograph of core from drillhole Neepawa DDH No. 1 Prov. 15-29-14-14W1 from 458.70 to 461.80 m. Two red, argillaceous, crinoid-rich beds are outlined in green dashes, and the single stromatoporoidal bed is outlined in red. Arrow indicates up direction in core. Scale bar in centimetres.*

Ashern Formation

The Ashern Formation is composed of reddish- or purplish-grey dolomudstone. The formation is very argillaceous, but not shaly. In places the Ashern Formation is evaporitic, with gypsum-anhydrite nodules and laminations. The upper contact is sharp.

Winnipegosis Formation

The Winnipegosis Formation is informally subdivided into lower and upper members. The lower member is composed of lime wackestone to dolowackestone. The upper contact of the lower member is sharp and occurs at a prominent bituminous marker bed that has been noted elsewhere in Saskatchewan and Manitoba (Jones, 1964, 1965; Norris et al., 1982). This bituminous bed is a local marker bed and cannot be used for basin-wide correlations. This contact occurs within a very argillaceous zone and is characterized by a gradual decrease in argillaceous content up-section into the upper member.

The upper member of the Winnipegosis Formation is composed of reefal facies dolofloatstone to doloboundstone. The member is fossiliferous, with stromatoporoids comprising the main faunal component. The upper contact of the Winnipegosis Formation was not observed, as core was missing from 397.80 to 403.90 m; it is inferred to be sharp.

Prairie Evaporite

The Prairie Evaporite is composed of interbedded shale, evaporitic dolomudstone and gypsum-anhydrite. The basal transition beds are absent, and no salt beds were encountered because the Neepawa DDH was drilled east of the salt dissolution edge of the Prairie Evaporite. The upper contact of the Prairie Evaporite was inferred to be sharp, as the strata immediately above this contact is disturbed. The Prairie Evaporite caps the first shale-carbonate-evaporite sequence in the Devonian strata.

Dawson Bay Formation

The Dawson Bay Formation encompasses the second shale-carbonate-evaporite cycle in the Neepawa DDH. The Second Red Bed, Burr and Neely members comprise the Dawson Bay Formation in the subsurface of Manitoba. The basal Second Red Bed Member is composed of dolomudstone to shale. It is disconformably overlain by lime mudstone to lime wackestone of the Burr Member. This member is fossiliferous, with brachiopods and crinoids as the primary faunal component. The upper contact is inferred as sharp, as the core was in poor condition at this interval.

The uppermost Neely Member is composed of calcareous and dolomitic mudstone and wackestone interbedded with shale and evaporite. The member becomes increasingly evaporitic upward, with gypsum-anhydrite occurring as nodules, laminations and beds. The Hubbard Evaporite is absent in Neepawa DDH. When the Hubbard Evaporite is absent, the contact between the Neely Member and the overlying Souris River Formation is gradational (Glass, 1990; Natural Resources Canada, 2018), therefore picking this boundary in the Neepawa DDH was difficult. The gradational contact was placed where non-evaporitic beds became red, argillaceous dolomudstone to shale.

Souris River Formation

The third and fourth shale-carbonate-evaporite cycles comprise the Souris River Formation. The Davidson Member encompasses the third cycle. The member is subdivided into four units: the First Red Beds (unit A), unit B, unit C and unit D (Figure GS2018-12-2; Lane, 1964;

Glass, 1990; Natural Resources Canada, 2018). The First Red Beds is composed of purple to red-brown evaporitic dolomudstone to shale and is formally recognized in the subsurface and outcrop belt of Manitoba. It is disconformably overlain by unit B, which consists of biostromal to porcelaneous calcareous dolomudstone. Unit B is disconformably overlain by unit C, an interbedded shale, dolomudstone and evaporite. Unit C is disconformably overlain by unit D, which is composed of evaporitic dolomudstone and gypsum-anhydrite. Unit D marks the end of the third complete shale-carbonate-evaporite sequence in Neepawa DDH. The Davidson Member is disconformably overlain by the Harris Member.

The one formal and three informal units of the Davidson Member may be correlative with the four units of the Point Wilkins Member (Norris et al., 1982) of the outcrop belt of Manitoba. Examination of additional drillcore across the Manitoba section of the Williston Basin is required to determine if these members can be correlated.

The Harris Member marks the beginning of the incomplete fourth shale-carbonate-evaporite cycle. The member is composed of at least 14 discrete shale-carbonate-evaporite cycles and a 15th incomplete cycle at the top of the member. Some of the cycles did not have a middle carbonate bed. In the west, the Harris Member is reported as being composed of eight cycles, with two prominent halite zones, informally referred to as the lower and upper Harris halite (Lane, 1964; Glass, 1990; Natural Resources Canada, 2018). The halite zones do not extend to Manitoba, and are therefore absent in this core. The Harris Member is disconformably overlain by the Hatfield Member.

The Hatfield Member is composed of an argillaceous and evaporitic dolomudstone. It is disconformably overlain by feldspathic to lithic wacke of the Triassic Lower Amaranth Member, Amaranth Formation. This contact marks the uppermost limit of the Paleozoic section of Neepawa DDH.

Results

Examination of Neepawa DDH resulted in the resolution of several stratigraphic issues. The lower Paleozoic stratigraphic framework in Manitoba contains correlation inconsistencies from the outcrop belt to deeper subsurface in the southwestern part of the province. In the subsurface of Manitoba, some formations and members are not formally recognized, whereas these intervals have formally recognized units in the outcrop belt of Manitoba and eastern Saskatchewan. Where possible, nomenclature from the outcrop belt, and to a lesser degree from eastern Saskatchewan, were applied to Neepawa DDH. Below is a summary of the correlation issues that were successfully resolved:

- the Lake Alma Member, Coronach Member and Redvers Unit, where defined in the upper Red River Formation; these units are formally recognized in eastern Saskatchewan; and
- the Fisher Branch, Moose Lake, Atikameg, East Arm and Cedar Lake formations, where defined in the Interlake Group; these units are formally recognized in the outcrop belt of Manitoba.

Some correlation issues still remain to be resolved and additional work is required to address these issues:

- investigating the occurrence and reliability of the u_2- and v-marker beds in the Interlake Group;
- formalizing and correlating the informal units of the subsurface Davidson Member to the informal beds of the outcrop-based Point Wilkins Member; and
- resolving the number of discrete shale-carbonate-evaporite cycles present in the Harris Member, Souris River Formation in the subsurface of Manitoba.

Investigations of additional drillcore from the subsurface are essential in resolving the above stratigraphic inconsistencies. Additional core logging will also confirm if the upper Red River Formation and Interlake Group can be successfully subdivided in other parts of the subsurface of Manitoba.

Future work

Future work on this core may include $\delta^{13}C$ and $\delta^{18}O$ stable isotope profiling of the entire core to assist in stratigraphic correlations and resolving stratigraphic inconsistencies. As mentioned, this would be useful for identifying the Ordovician–Silurian boundary, in conjunction with conodont analysis of the core. The diagenetically altered zones from 496.53 to 496.65 m and 478.80 to 478.82 m in the East Arm Formation require thin section work and $\delta^{13}C$ and $\delta^{18}O$ isotopic analysis to determine the nature of diagenesis and whether these zones may be hydrothermal dolomite.

Economic considerations

The Neepawa DDH core provided an important first step to successfully correlating outcrop with the subsurface in Manitoba, but further work is required to resolve issues and formalize stratigraphic relationships. An accurate and well-defined stratigraphic framework in Manitoba's Williston Basin will be beneficial for petroleum exploration, understanding of brines and groundwater, industrial mineral deposit exploration, and Mississippi Valley-type Pb-Zn deposit exploration.

Acknowledgments

The authors thank C. Epp, N. Brandson, E. Anderson and P. Sidhu for assistance with core viewing. P. Sidhu is also thanked for photographing core. T. Hodder is thanked for his thorough review of this report.

References

Bamburak, J.D. 2007: Manitoba Geological Survey's stratigraphic corehole drilling program, 2007 (parts of NTS 62N1, 16, 63C1); *in* Report of Activities 2007, Manitoba Science, Technology, Energy and Mines, Manitoba Geological Survey, p. 166–174.

Bezys, R.K. and Conley, G.G. 1998: Geology of the Silurian Interlake Group in Manitoba; Manitoba Energy and Mines, Stratigraphic Map Series, SI-1, scale 1:2 000 000.

Demski, M.W., Stewart, L.A., Elias, R.J., Young, G.A., Nowlan, G.S. and Dobrzanski, E.P. 2010a: Hirnantian (Latest Ordovician) event in the centre of North America? Colour, carbon isotopic excursion, and conodont turnover; International Palaeontological Association, International Palaeontological Congress, London, England, June 28–July 2, 2010, Program and Abstracts, v. 3, abstract S26.

Demski, M.W., Stewart, L.A., Elias, R.J., Young, G.A., Nowlan, G.S. and Dobrzanski, E.P. 2010b: Hirnantian (latest Ordovician) strata in the heart of the continent? Intriguing results from the Williston Basin, Manitoba; GeoCanada 2010 conference, Calgary, Alberta, May 10–13, 2010, poster abstract, URL <https://www.geoconvention.com/archives/2010/0208_GC2010_Hirnantian_Strata_in_Heart_of_the_Continent.pdf> [September 2018].

Demski, M.W., Wheadon, B., Stewart, L.A., Elias, R.J., Young, G.A., Nowlan, G.S. and Dobrzanski, E.P. 2011a: Latest Ordovician glacio-eustatic fluctuation in the Williston and Hudson Bay basins of Manitoba, Canada: conodont turnover, isotopic carbon excursion, and subaerial exposure; Geological Survey of America, Annual Meeting, Minneapolis, Minnesota, October 9, 2011, Abstracts with Program, v. 43, no. 5, p. 611.

Demski, M.W., Wheadon, B., Stewart, L.A., Elias, R.J., Young, G.A., Nowlan, G.S. and Dobrzanski, E.P. 2011b: Ordovician-Silurian boundary interval in the Williston and Hudson Bay basins, Manitoba: isotopic carbon excursion and conodont turnover; Geological Association of Canada and Mineralogical Association of Canada, Joint Annual Meeting, Ottawa, Ontario, May 25–27, 2011, Abstracts, v. 34, p. 50–51.

Desrochers, A., Farley, C., Achad, A., Asselin, E. and Riva, J.F. 2010: A far-field record of the end of Ordovician glaciation: the Ellis Bay Formation, Anticosti Island, eastern Canada; Paleogeography, Palaeoclimatology, Palaeoecology, v. 296, p. 248–263.

Fedikow, M.A.F., Bezys, R.K., Bamburak, J.D., Hosain, I.T. and Abercrombie, H.J. 2004: Prairie-type microdisseminated mineralization in the Dawson Bay area, west-central Manitoba (NTS 63C14 and 15); Manitoba Industry, Economic Development and Mines, Manitoba Geological Survey, Geoscientific Report GR2004-1, 76 p.

Glass, D.J. (ed.) 1990: Lexicon of Canadian Stratigraphy, volume 4, western Canada; Canadian Society of Petroleum Geologists, Calgary, Alberta, 772 p.

Jones, J.L. 1964: The stratigraphy of the Middle Devonian Winnipegosis Formation in Saskatchewan; Third International Williston Basin Symposium, Regina, Saskatchewan, September 17–19, 1964, Saskatchewan Geological Society, North Dakota Geological Society, Billings Geological Society, p. 73–91.

Jones, J.L. 1965: The Middle Devonian Winnipegosis Formation of Saskatchewan; Saskatchewan Department of Mineral Resources, Report 98, 105 p.

Kleffner, M.A., Bergström, S.M. and Schmitz, B. 2005: Revised chronostratigraphy of the Ordovician/Silurian boundary interval in eastern Iowa and northeastern Illinois based on $\delta^{13}C$ chemostratigraphy; Iowa Geological Survey, Guidebook Series, v. 24, p. 46–49.

Lammers, G.E. 1988: Silurian stratigraphy of the Interlake area; *in* Report of Field Activities 1988, Manitoba Energy and Mines, Minerals Division, p. 43–48.

Lane, D.M. 1964: Souris River Formation in southern Saskatchewan; Saskatchewan Department of Mineral Resources, Report 92, 72 p.

Lapenskie, K. 2012: Depositional and faunal changes in the Upper Ordovician to Lower Silurian of core M-4-03, from near Churchill, Manitoba; B.Sc. thesis, University of Manitoba, Winnipeg, Manitoba, 211 p.

Lapenskie, K. 2016: Preliminary investigations into the high-purity silica sand of the Winnipeg Formation, southern Manitoba; *in* Report of Activities 2016, Manitoba Growth, Enterprise and Trade, Manitoba Geological Survey, p. 176–180.

Lapenskie, K. and Nicolas, M.P.B. 2017: Detailed examination of drillcore RP95-17, west-central Manitoba (NTS 63C7): evidence of potential for Mississippi Valley–type lead-zinc deposits; *in* Report of Activities 2017, Manitoba Growth, Enterprise and Trade, Manitoba Geological Survey, p. 158–172.

Natural Resources Canada 2018: Weblex Canada: lexicon of Canadian geological names on-line; Natural Resources Canada, URL <https://weblex.nrcan.gc.ca/weblexnet4/weblex_e.aspx> [September 2018].

Nicolas, M.P.B. and Barchyn, D. 2008: Williston Basin Project (Targeted Geoscience Initiative II): summary report on Paleozoic stratigraphy, mapping and hydrocarbon assessment, southwestern Manitoba; Manitoba Science, Technology, Energy and Mines, Manitoba Geological Survey, Geoscientific Paper GP2008-2, 21 p.

Nicolas, M.P.B., Matile, G.L.D., Keller, G.R. and Bamburak, J.D. 2010: Phanerozoic geology of southern Manitoba; Manitoba Innovation, Energy and Mines, Manitoba Geological Survey, Stratigraphic Map Series, Map 2010-1, Sheet B: Phanerozoic, scale 1:600 000.

Norford, B.S. 1971: Silurian stratigraphy of northern Manitoba; *in* Geoscience Studies in Manitoba, A.D. Turnock (ed.); Geological Association of Canada, Special Paper 9, p. 199–207.

Norford, B.S., Nowlan, G.S., Haidle, F.M. and Bezys, R.K. 1998: The Ordovician-Silurian boundary interval in Saskatchewan and Manitoba; *in* Eighth International Williston Basin Symposium, J.E. Christopher, C.F. Gilboy, D.F. Paterson and S.L. Bend (ed.), Saskatchewan Geological Society, Special Publication Number 13, p. 653–700.

Norris, A.W., Uyeno, T.T. and McCabe, H.R. 1982: Devonian rocks of the Lake Winnipegosis-Lake Manitoba outcrop belt, Manitoba; Manitoba Department of Energy and Mines, Mines Branch, Publication 77-1, 280 p.

Rawluk, C. 2010: Sedimentology of Silurian Interlake Group dolostones near Duck Bay, west-central Manitoba; B.Sc. thesis, University of Manitoba, Winnipeg, Manitoba, 110 p.

Stearn, C.W. 1956: Stratigraphy and paleontology of the Interlake Group and Stonewall Formation in southern Manitoba; Geological Survey of Canada, Memoir 281, 162 p.

GS2018-13

Kimberlite-indicator minerals and clast-lithology composition of till, Kaskattama highland region, northeastern Manitoba (parts of NTS 53N, O, 54B, C)

by T.J. Hodder and S.E. Kelley[1]

In Brief:

- Till KIM counts are elevated compared to regional data
- The lowest KIM yields are associated with samples indicating a Hudson Bay Basin provenance, while the highest KIM yields are associated with till samples that have a relatively elevated greywacke/greenstone or granitoid provenance signature
- Till composition, ice-flow data and stratigraphy indicate the potential for multiple KIM sources

Citation:
Hodder, T.J. and Kelley, S.E. 2018: Kimberlite-indicator minerals and clast-lithology composition of till, Kaskattama highland region, northeastern Manitoba (parts of NTS 53N, O, 54B, C); *in* Report of Activities 2018, Manitoba Growth, Enterprise and Trade, Manitoba Geological Survey, p. 150–165.

Summary

Quaternary geology fieldwork was conducted at a reconnaissance-scale in the Kaskattama highland area to document the Quaternary stratigraphy and till composition. The diamond potential of this region was investigated using kimberlite-indicator–mineral (KIM) counts from till samples. Indicator mineral results are the focus of this report and are combined with ice-flow and till-clast–lithology data to provide a context to interpret provenance.

Kimberlite-indicator minerals were recovered from glacial sediments (till) in the Kaskattama highland area and KIM counts are elevated relative to data from the surrounding area. The lowest KIM counts were from till with a high Hudson Bay Basin (carbonate-dominated) and low undifferentiated greenstone and greywacke (UGG) provenance signature. The highest KIM counts are associated with till samples that have a relatively elevated UGG or elevated granitoid provenance signature. Till samples with relatively elevated UGG concentration have an interpreted east or southeast provenance, which is supported by ice-flow data and the recovery of distinct east-sourced erratics. Till samples with a relatively elevated granitoid clast concentration have a correlation with the southwest-trending Hayes streamlined-landform flowset. Considering the likely provenance for granitoid clasts is to the northwest, the presence of relatively high concentrations of granitoid clasts in the Hayes flowset could be indicative of a higher inheritance from previous ice-flow events or a palimpsest dispersal pattern. Interpretation of till-composition and ice-flow data has indicated there are likely multiple sources for the KIMs recovered during this study. Detailed work is recommended to clarify local-scale dispersal patterns.

Introduction

The Manitoba Geological Survey (MGS) conducted Quaternary geology fieldwork in the Kaskattama highland region of northeastern Manitoba during the summers of 2016 and 2017 (parts of NTS 53N, O, 54B, C; Hodder and Kelley, 2016; Hodder, 2017). A key aspect of this project is documenting the till composition and Quaternary stratigraphy at a reconnaissance-scale in this remote region of northeastern Manitoba. As part of this project, the diamond potential of the region is being assessed through kimberlite-indicator–mineral (KIM) counts from till samples. The purpose of this study is to publish KIM data collected in 2017, along with previously released 2016 data (Hodder and Kelley, 2017), as a data repository item (Hodder, 2018b) and to provide the mineral exploration industry timely updates on new geological knowledge. This report provides insight into the relationships between KIM recovery and till composition, primarily clast-lithology counts, which when combined with ice-flow–indicator data provide an important context to interpret KIM provenance.

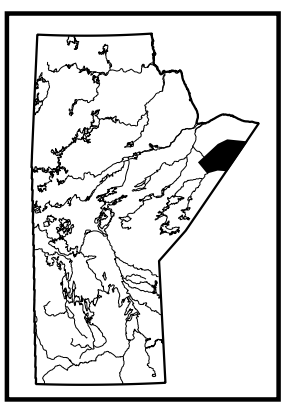

Regional setting

The Kaskattama highland in northeastern Manitoba, a prominent topographic high within the Hudson Bay Basin, rises 130 m above the flat-lying Hudson Bay Lowland terrain, reaching a maximum elevation of 235 m asl. The Gods River is the main drainage channel flowing northwestward toward a confluence with the Hayes River, which drains

[1] Department of Earth and Environmental Sciences, University of Waterloo, 200 University Avenue, Waterloo, ON N2L 3G1

northeastward into Hudson Bay. The Kaskattama River drains northeastward to Hudson Bay with the headwaters situated on the Kaskattama highland. Access to the region is by air-support or by winter road into the First Nation community of Shamattawa.

Geomorphology

Two streamlined-landform flowsets, defined as discrete assemblages of subglacial streamlined landforms based on their similar direction and the degree of internal consistency (Kleman and Borgstrom, 1996; Clark et al., 2000; Greenwood and Clark, 2009), are present in the geomorphic record of the study area (Figure GS2018-13-1). The Hayes flowset is southwest-trending (204–207° in the study area) and is attributed to the large deglacial Hayes lobe (Dredge and Cowan, 1989). On the Kaskattama highland, the landscape is dominated by a curvilinear flowset of northwest-oriented streamlined landforms, referred herein as the Kaskattama flowset. The trend of this flowset is interpreted to be toward the northwest based on the surficial till composition discussed in this report. The boundary between the two flowsets is sharp, distinct and delineated by a northeast-oriented channel.

Bedrock geology

Regionally, the area is underlain by Paleozoic carbonate sedimentary rocks of the Hudson Bay Basin (Nicolas and Armstrong, 2017), with Precambrian crystalline rocks mapped in the southwestern portion of the study area (Manitoba Department of Mines, Natural Resources and Environment, 1979). Bedrock is hidden beneath thick Quaternary sediments throughout the study area. Outcrops of Paleozoic bedrock were only observed along the base of the Gods River, northwest and south of the First Nation community of Shamattawa.

Distinctive erratics

The lithology of clasts within till can assist with the delineation of glacial transport directions and distances (glacial dispersal), as well as potentially identifying buried unmapped bedrock units. Glacial dispersal can be mapped at varying scales from continental (hundreds of kilometres) to regional (tens of kilometres) to local (<10 km). In northern Manitoba, two groups of distinctive erratics are the result of continental-scale glacial dispersal from eastern and northern source areas.

Distinctive erratics of eastern provenance include clasts derived from the Omarolluk Formation and oolitic jasper clasts. The Omarolluk Formation, of the Belcher Group in southeastern Hudson Bay (Figure GS2018-13-2), is a distinctive greywacke with hemispherical calcareous concretions (Prest et al., 2000; Jackson, 2013). These erratics, commonly referred to as Omars (Prest et

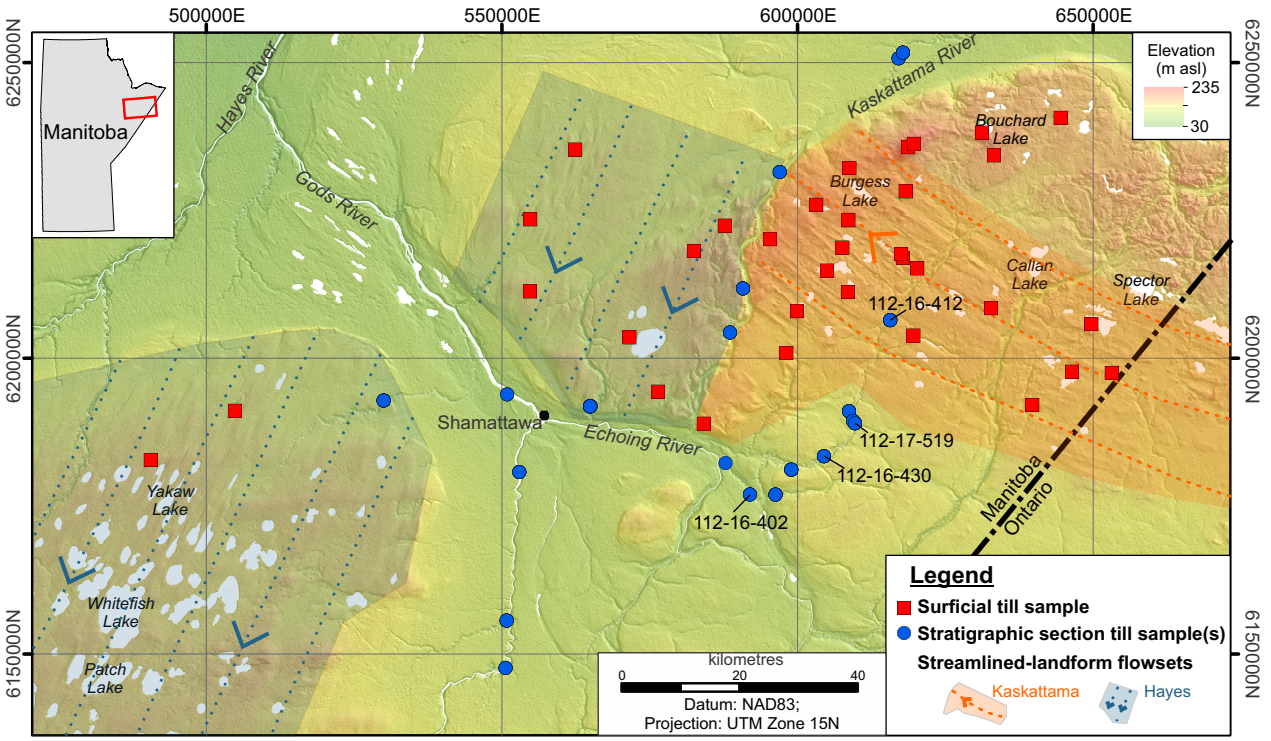

Figure GS2018-13-1: *Till sample sites and streamlined-landform flowsets in the Kaskattama highland region, northeastern Manitoba. Background hillshade image was generated using Canadian Digital Surface Model (Natural Resources Canada, 2015).*

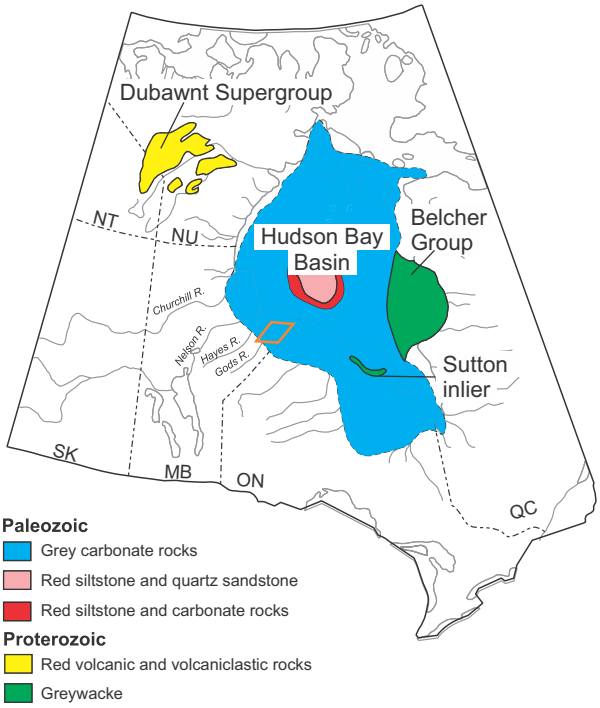

Figure GS2018-13-2: *Bedrock sources of distinctive continental-scale erratics observed in northeastern Manitoba and outline of the Hudson Bay Basin. The location of this study is depicted by the orange polygon. Figure is modified from Kaszycki et al. (2008).*

al., 2000), were transported westward by the Laurentide Ice Sheet (LIS) into the study area, a minimum of 650 km from known outcrops in southeastern Hudson Bay. As such, the presence of Omars within glacial sediments has been used to infer an eastern provenance (Prest et al., 2000; Nielsen and Fedikow, 2002; Trommelen et al., 2013). Omars are easily identified in the large pebble to boulder size-fractions, but in smaller size-fractions these erratics become more difficult to confidently identify. Metavolcanic and metasedimentary rocks that comprise greenstone belts in the Canadian Shield can often resemble the matrix of Omar clasts in small size-fractions. As such, Omar clasts without distinctive concretions and greenstone clasts are indistinguishable during clast-lithology counts. A second distinctive lithology of eastern origin, oolitic jasper, is easily recognized in clast-lithology counts. These clasts are interpreted to be derived from the Kipalu Formation of the Belcher Group (Jackson, 2013) or from iron formation rocks found at the Sutton inlier (Figure GS2018-13-2; Stott et al., 2010).

Distinctive erratics derived from the Dubawnt Supergroup of central mainland Nunavut are also found throughout northern Manitoba (Dredge and McMartin, 2011). These include reddish to pinkish sandstone and conglomerate of the Thelon Formation, and purple to mauve rhyolite with glassy quartz and chalky sanidine phenocrysts and volcaniclastic rocks with phlogopite phenocrysts of the Christopher Island Formation (Rainbird et al., 2003). These erratics were transported into northeastern Manitoba by ice flow(s) with a net glacial dispersal of over 800 km, by either the LIS and/or precursor ice sheets.

Methods

Field data collection

Helicopter-supported fieldwork was undertaken by the MGS during the 2016 and 2017 field seasons. A total of 116 till samples were collected from surficial sites and stratigraphic river section exposures (Figure GS2018-13-1; 34 surficial and 82 stratigraphic samples). At 64 till sample sites, an additional 11.4 L of till was collected for KIM analysis. Surficial till samples were collected from C-horizon material in hand-dug pits or with an auger. Sediments exposed at river sections were first cleared to remove any slump material and till samples were collected every 1–4 m depth depending on the stratigraphy observed at the section. Clast-fabric measurements were completed within till at selected sample sites to assess the paleo-ice flow during deposition and assist till provenance interpretations. Clast-fabric measurements taken included the trend and plunge of 30 clasts with an a:b axis ratio of >1.5. In situ, lodged, cobble- to boulder-sized clasts with parallel striae on their upper surface are considered good indicators of paleo–ice-flow direction (McMartin and Paulen, 2009) and the striae were measured where encountered in sections.

Clast-lithology counts

Clast-lithology counts were conducted for each till sample to aid in the determination of provenance. Clasts larger than 2 mm were initially sieved into 2–4, 4–8 and 8–30 mm size-fractions and counts conducted on each fraction with the assistance of an optical microscope. These size-fractions were then summed and expressed as a count percentage of the 2–30 mm size-fraction. Clasts were separated into 14 rock types during identification and simplified into three provenance classes for the purpose of this report: granitoid, Hudson Bay Basin (HBB) and undifferentiated greenstone and greywacke (UGG). To establish a clast-lithology composition-derived till classification, the three provenance classes were processed by k-means cluster analysis after a centred log ratio transformation. For a thorough review of k-means cluster analysis methods used in this study see Wang (2018). Data presented herein are to support KIM provenance

interpretations, and a more thorough review of clast-lithology count data will be part of a forthcoming report.

Kimberlite-indicator mineral processing and classification

Blind KIM till samples were submitted to the De Beers Group of Companies (De Beers) to be analyzed through in-kind support. The KIM sample locations were withheld from De Beers, to allow equal opportunity for follow-up by all interested parties when the data (with sample locations) are publicly released along with this report. Heavy mineral concentrate from the <0.5 mm size-fraction of the till sample was passed over a 0.3 mm aperture sieve and the <0.3 mm size-fraction was discarded, leaving only the 0.3–0.5 mm size-fraction. Suspected KIM grains were then selected visually, and analyzed by electron microprobe. The KIM grains were initially classified using electron microprobe results, following the methodology outlined by Thorleifson et al. (1994). The Mg-ilmenite grains were confirmed using the compositional field defined by Wyatt et al. (2004; Figure GS2018-13-3a). Diamond-inclusion Cr-spinel grains were identified according to modified discriminate diagrams after Fipke et al. (1995; Figure GS2018-13-3b, c). Although, caution should be exercised when relying on the TiO_2 versus Cr_2O_3 discriminate plot (Figure GS2018-13-3b), as chromite grains from chromite deposits in the McFaulds Lake ('Ring of Fire') area of northern Ontario can plot within this diamond inclusion and intergrowth field (Gao and Crabtree, 2016). The Cr-diopside grains were confirmed using the Cr_20_3 versus Al_2O_3 plot defined by Nimis (2002; Figure GS2018-13-3d). Garnet grains were classified according to the method outlined by Grütter et al. (2004; Figure GS2018-13-3e).

Results

Till-clast–lithology composition

The lithology of clasts within till samples was determined to help identify major directions of glacial dispersal and hence till provenance. The k-means cluster analysis of simplified till-clast–lithology count data identified seven clusters, herein referred to as till types and displayed on a ternary diagram in Figure GS2018-13-4. The spatial distribution of till types separated into surficial and stratigraphic section samples is presented in Figure GS2018-13-5.

Till types 1 and 2 are characterized by elevated concentrations of UGG clasts. Till type 1 is separated from till type 2 based on a higher UGG content and/or lower granitoid content (Figure GS2018-13-4). Till types 3, 4 and 5 are characterized by high concentrations of HBB clasts. Till type 5 is distinguished from till types 3 and 4 based on its lower UGG content and higher granitoid content (Figure GS2018-13-4). Till type 3 is distinguished from till types 4 and 5 based on its higher UGG content (Figure GS2018-13-4). Till type 6 is characterized by average UGG and high granitoid concentrations. Till type 7 is unique and contains high UGG and granitoid concentrations and is only documented at two surficial sites (Figure GS2018-13-5).

Surficial till types

The surficial tills within the Hayes and Kaskattama flowsets are compositionally distinct from each other. The surficial till in the Kaskattama flowset contains till types 1 and 2 whereas the Hayes flowset contains till types 3 and 6 (Figure GS2018-13-5). One sample from each flowset belongs to till type 7, which has elevated UGG and granitoid concentrations, unique to the entire dataset (Figure GS2018-13-5b). The contrast in clast-lithology composition of these flowsets suggests a different till provenance for each flowset, as would be expected as these landscapes contain streamlined landforms suggestive of near perpendicular ice flow.

The Kaskattama flowset is characterized by a higher concentration of UGG clasts in the surficial till. The interpreted source of these clasts is the Belcher Group, with the nearest known exposures a minimum of 650 km to the east in the Belcher Islands, or the Sutton inlier, located 400 km to the southeast. Based on this observation, the Kaskattama flowset has been assigned a northwest trend. This interpretation is further supported by the presence of oolitic jasper clasts in four samples, and higher concentrations of oolitic jasper in till types 1 and 2 (Table GS2018-13-1), the source of which is to the east and/or southeast. Four out of the five surficial till samples that are north of the Kaskattama flowset are classified as till type 2 and two contain oolitic jasper clasts (Figure GS2018-13-6), which would suggest correlation with the same ice-flow event that deposited the surficial till associated with the Kaskattama flowset.

The southwest-trending (204–207°) Hayes flowset has relatively high concentrations (19.7–28.7 ct. %) of granitoid clasts in till type 6 samples. The closest known source of granitoid bedrock is to the southwest or northwest. The presence of Dubawnt erratics in three till samples from the Hayes flowset suggest an initial provenance to the northwest. The transport of these clasts into the study area does not correspond with the trend of the Hayes flowset (southwest) and could represent a palimpsest dispersal pattern or a region with a higher

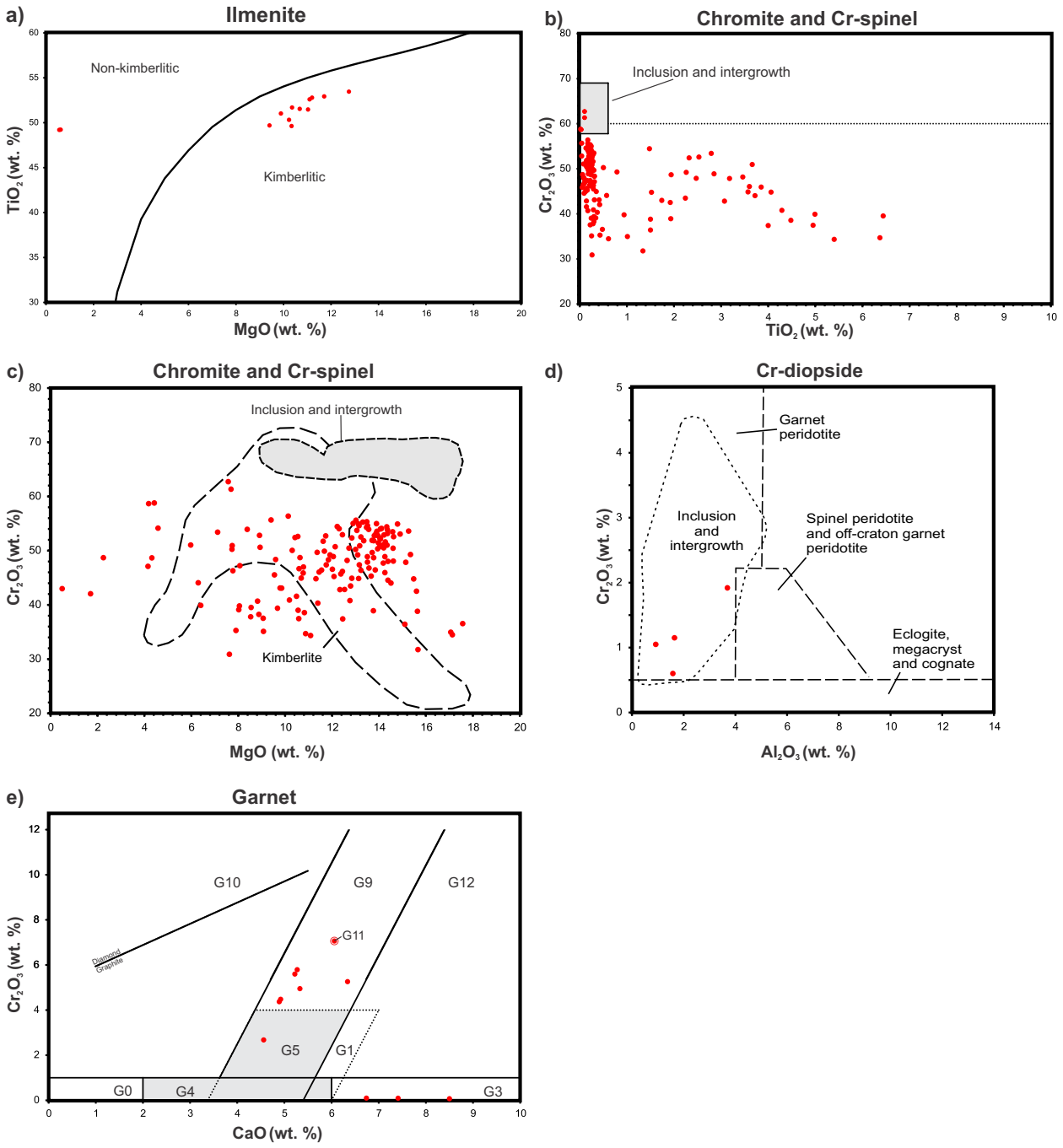

Figure GS2018-13-3: *Bivariate plots of compositional data for kimberlite-indicator minerals:* ***a)*** *TiO_2 versus MgO discriminate for ilmenite grains; compositional field for kimberlite after Wyatt et al. (2004);* ***b)*** *Cr_2O_3 versus TiO_2 for chromite and Cr-spinel grains; diamond inclusion and intergrowth field modified after Fipke et al. (1995); a dashed line representing 60 wt. % Cr_2O_3 is shown for visual reference;* ***c)*** *Cr_2O_3 versus MgO for chromite and Cr-spinel grains; compositional field for diamond inclusion and intergrowth after Fipke et al. (1995); compositional field for kimberlite from Nowicki et al. (2007);* ***d)*** *Cr_2O_3 versus Al_2O_3 for Cr-diopside grains; compositional field for diamond inclusion and intergrowth is from Nimis (2002); other compositional fields are from Ramsay and Tompkins (1994);* ***e)*** *Cr_2O_3 versus CaO for garnet grains; garnet classification fields after Grütter et al. (2004); the G5 and G4 classifications indicated by the light grey fill pattern are distinguished by Mg-number; the stippled G1 group does not overlap G4, G5, G9 or G12 categories as G1 garnet grains are distinguished by a higher TiO_2 content; G11 garnets are also classified based on a higher TiO_2 content and are differentiated from G1 garnets by a higher Cr_2O_3 content; a G11 garnet classified from this study is highlighted.*

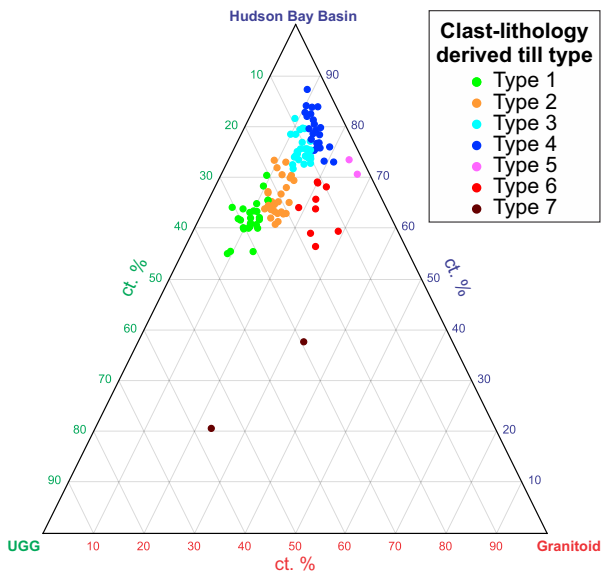

Figure GS2018-13-4: *Till types, derived from k-means cluster analysis, displayed on a ternary diagram. Abbreviation: UGG, undifferentiated greenstone and greywacke.*

compositional inheritance from a previous ice-flow event (e.g., Trommelen et al., 2013). Three till type 3 samples were sampled in the Hayes flowset northeast of Shamattawa and one was sampled near Yakaw Lake (Figure GS2018-13-5), and these samples all have elevated pink carbonate clast concentrations (>95th percentile), which suggests a central Hudson Bay provenance input (Figure GS2018-13-2). This observation would suggest at least some northeast-derived detritus was deposited in the Hayes flowset (by southwest-trending ice flow).

Stratigraphic ice-flow data and till type

Combining ice-flow data and corresponding till composition provides insight into sediment provenance. Clast-fabric data along with paleo–ice-flow directions from in situ, lodged and striated clasts are presented in Figure GS2018-13-7, separated according to the till type assigned to the interval where the ice-flow observation was recorded.

The majority (n=5 of 9) of ice-flow data associated with till types 1 and 2 indicate deposition by northwest-southeast–oriented ice flow. This is in agreement with the surficial till of the Kaskattama flowset (northwest-trending landforms) and suggests an eastern provenance. This interpretation is supported by the provenance of UGG clasts, which is interpreted to be from the Belcher Group located in eastern Hudson Bay or the Sutton inlier in northern Ontario, as discussed above. Particularly strong northwest-trending fabrics were observed within till types 1 and 2 along the Echoing River and its tributaries, east of Shamattawa. Three south- to southwest-trending ice-flow indicators are present in till types 1 and 2, which could be as a result of inheritance of this till type composition after a switch in ice-flow direction. Nearly all (n=8 of 9) of the ice-flow data obtained for till type 3 samples indicates deposition by south- or southwest-trending ice flow. All ice-flow data obtained from till type 4 samples indicate deposition by southwest- or south-trending ice flow, which is in agreement with the composition of this till type, high HBB clast concentrations and low UGG concentrations. Till type 6 ice-flow data yielded two strong indicators of south-trending ice flow and one scattered fabric indicating an east-west trend.

Distinctive erratic trends

Oolitic jasper clasts observed within till samples have a strong correlation to till types 1 and 2. This reinforces an eastern provenance for these till types (Table GS2018-13-1; Figure GS2018-13-6). Outside of the Kaskattama flowset and sections near the Echoing River, only one oolitic jasper clast was observed in a sample from 5 km west of the Hayes–Kaskattama flowsets boundary (Figure GS2018-13-6). Oolitic jasper clasts have been observed as far west as Southern Indian Lake (Hodder, 2018a) and as far south as Morden in Manitoba to date.

Shell fragments observed in till were sourced from marine sediments that were overridden by ice-sheet advances and integrated into the subglacial sediments. The extent of marine sediments deposited by earlier nonglacial seas (e.g., Bell Sea) is likely similar to the current distribution of marine sediments in northeastern Manitoba (Matile and Keller, 2007), the largest source of which was Hudson Bay. Therefore shell fragments in till in the Kaskattama highland area were sourced from the northwest through to the southeast, with the largest source to the northeast (Hudson Bay). Shell fragments observed in till-clast–lithology counts are strongly correlated to till types 3 and 4 (Table GS2018-13-1; Figure GS2018-13-6), which are distinguished by their elevated HBB clast count. This observation reinforces a local to Hudson Bay Basin provenance for these till types.

The distribution of Dubawnt erratics in the study area is more variable and likely a reflection of multiple episodes of deposition and re-entrainment by the LIS and earlier ice sheets. There is a slight correlation of Dubawnt erratics with till types 6 and 7. These types only represent 9.5% of till samples collected but account for three of the nine Dubawnt erratics observed. Till samples from the Hayes flowset recovered three of the nine Dubawnt erratics. The presence of Dubawnt erratics in till samples from the Kaskattama flowset and from sections to the

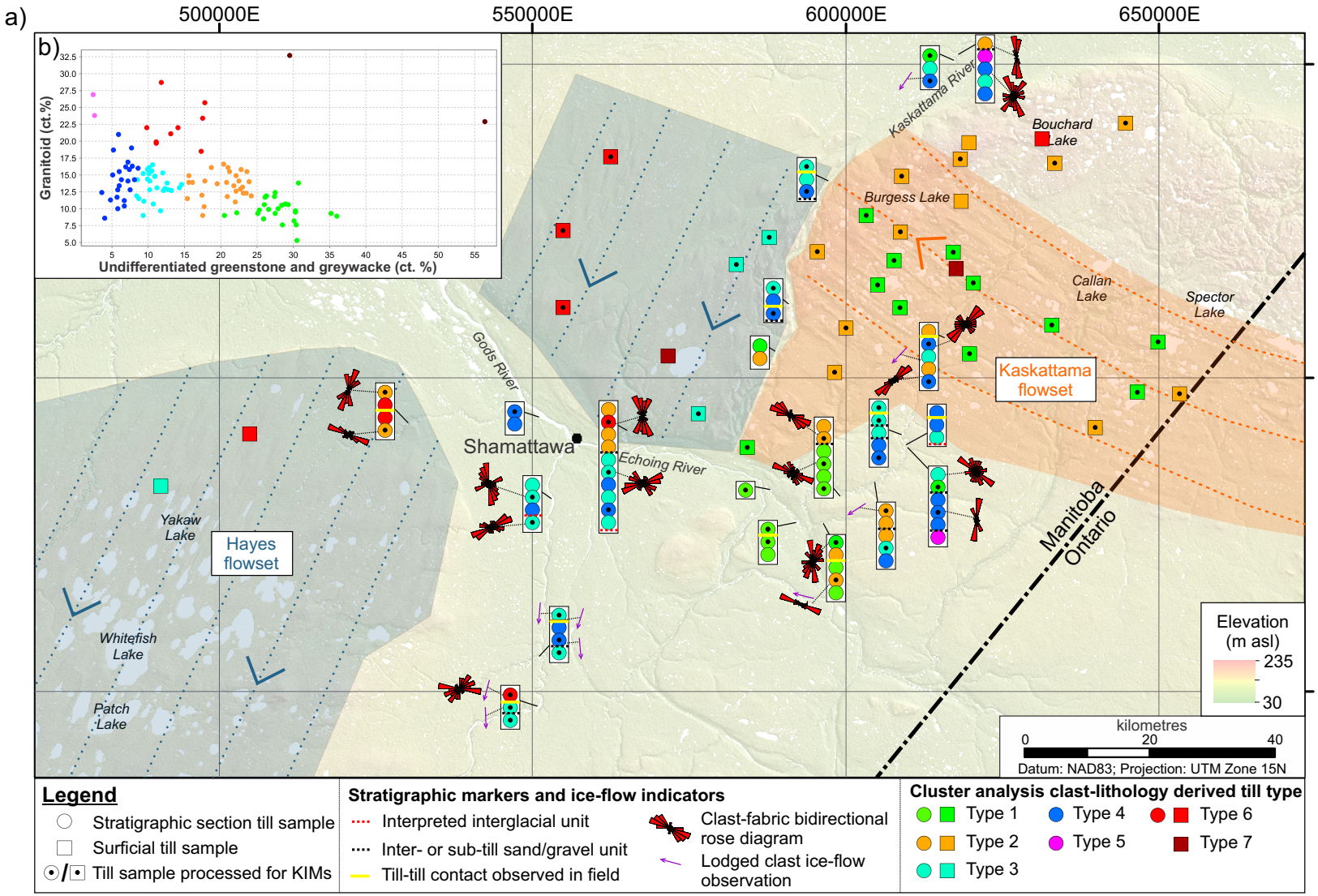

Figure GS2018-13-5: *Till types derived from k-means cluster analysis:* ***a)*** *till samples classified by till type; stratigraphic section till samples are displayed as stacked symbols; ice-flow data obtained at sections is displayed where measured as bidirectional rose diagrams or as the azimuth of the lodged clast; background hillshade image of the Kaskattama highland area was generated using Canadian Digital Surface Model (Natural Resources Canada, 2015);* ***b)*** *bivariate plot of granitoid versus undifferentiated greenstone and greywacke concentrations in till samples, classified according to designated till type. Abbreviation: KIM, kimberlite-indicator mineral.*

Table GS2018-13-1: Count of till samples containing distinct erratics. Samples were assigned to clast-lithology composition-derived till types, Kaskattama highland area.

Till type	Percentage of sample population	Oolitic jasper erratic	Shell fragment	Dubawnt Supergroup erratic
Type 1	21.6	7	2	2
Type 2	24.1	4	1	1
Type 3	23.3	1	9	3
Type 4	19.8	0	10	0
Type 5	1.7	0	0	0
Type 6	7.8	0	0	2
Type 7	1.7	0	0	1
Total		12	22	9

north and south indicate that these clasts have undergone multiple ice-flow transport events.

Omars were observed at the base of every section that was logged at an active rivercut/streamcut (Figure GS2018-13-6). Since the defining characteristics of Omars (greywacke with hemispherical calcareous concretions) are only obvious in the large pebble– to boulder-size range, identification in clast-lithology counts is inhibited by clast size, and thus they are not reported in clast-lithology counts. The pervasive presence of Omars at the described sections suggests a strong influence of the lithology of the source bedrock on the UGG content of till in the study area. Boulder-size Omars observed in the field can reach impressive sizes (Figure GS2018-13-8a, b), considering the nearest mapped source is 650 km to the east of this study area.

Kimberlite-indicator mineral results

A total of 181 KIM grains were recovered during this study. The visual identification, chemistry and total grain counts are presented in Data Repository Item DRI2018001[2] accompanying this report (Hodder, 2018b). The majority of the KIMs recovered are chromite and Cr-spinel grains (86%; n=155). Of these grains 58% (n=90 of 155) are considered Cr-spinel (>45 wt. % Cr_2O_3; >10 wt. % MgO) and 42% (n=65 of 155) are considered chromite (>30 wt. % Cr_2O_3). Chromite and Cr-spinel are collectively grouped as Cr-spinel herein and in DRI2018001, in accordance with the terminology established in the MGS KIM database (Keller et al., 2004). Four of these Cr-spinel grains are considered to fall within the diamond inclusion and intergrowth compositional field based on their elevated Cr_2O_3 (>58 wt. %) and low TiO_2 (<0.4 wt. %) contents. Eleven Mg-ilmenite grains were recovered. Four Cr-diopside grains were recovered, and all four plot within the diamond inclusion and intergrowth field defined by Nimis (2002; Figure GS2018-13-3d). Eleven garnet KIMs were recovered: seven G9-garnets, three G3-garnets and one G11-garnet. The spatial distribution of total KIM counts per sample (Figure GS2018-13-9) does not appear to show a well-defined dispersal pattern, which was not the goal of this reconnaissance-scale survey.

Kimberlite-indicator–mineral provenance trends

The relationship between KIM recovery and clast-lithology composition-derived till types is presented in Table GS2018-13-2. The average KIM recovery per sample in the dataset is 2.8 KIMs. The highest average KIM recovery was from till type 2 at 3.6 KIMs. Till types 1, 3 and 6 have a similar average KIM recovery. Till type 4 stands out because of the relatively low average KIM recovery (1.0 KIMs) associated with this till composition.

Only four samples of till type 6 were sampled for KIM analysis during this survey. These four samples (6.3% of sample population) contained four of the seven G9-garnets recovered, highlighted by three G9-garnets recovered at a surficial till sample site within the Hayes flowset (Figure GS2018-13-10). This is a relatively small dataset to confidently infer associations, but would preliminarily indicate either a correlation between till type 6 or the Hayes flowset with G9-garnet recovery. The three other G9-garnets were all recovered from surficial till samples in the Kaskattama flowset.

The recovery of Cr-diopside is spatially correlated, with three of the four Cr-diopside grains recovered in the southwestern region of the Kaskattama highland (Figure GS2018-13-10). Two of these samples correspond to till type 3, with one sample having a corresponding strong southwest-trending ice flow indicated, and one sample corresponds to till type 2 and is part of the Kaskattama

[2] MGS Data Repository Item DRI2018001 containing the data or other information sources used to compile this report is available online to download free of charge at https://www.gov.mb.ca/iem/info/library/downloads/index.html, or on request from minesinfo@gov.mb.ca, or by contacting the Resource Centre, Manitoba Growth, Enterprise and Trade, 360–1395 Ellice Avenue, Winnipeg, Manitoba R3G 3P2, Canada.

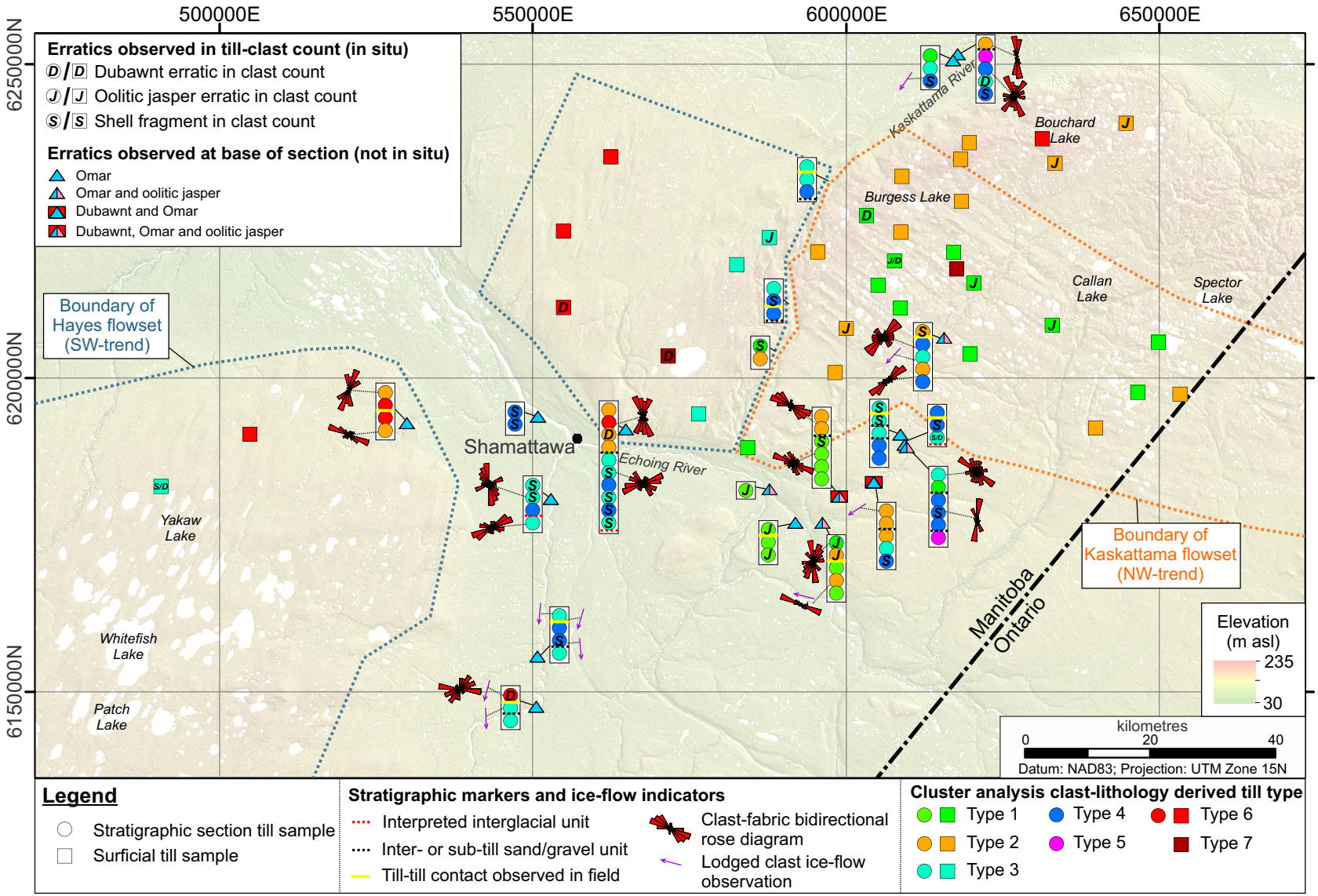

Figure GS2018-13-6: *Locations of exotic erratics observed during clast-lithology counts from till samples and in the field at the base of sections described in the Kaskattama highland area. Background hillshade image was generated using Canadian Digital Surface Model (Natural Resources Canada, 2015). Abbreviations: Dubawnt, Dubawnt Supergroup; NW, northwest; Omar, Omarolluk Formation erratic; SW, southwest.*

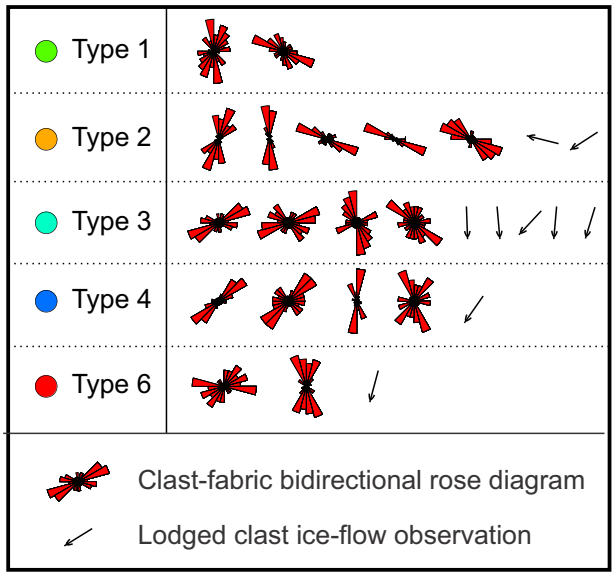

Figure GS2018-13-7: *Summary of ice-flow data associated with stratigraphic section till samples in the Kaskattama highland area. No ice-flow data was obtained for till type 5 or 7 samples.*

flowset (northwest-trending). Therefore, there appears to be a spatial correlation, but not a till composition correlation with Cr-diopside grains recovered in this area (Figure GS2018-13-10).

A cluster of samples located east of the Echoing River recovered the majority (n=6 of 11) of Mg-ilmenite grains during this study (Figure GS2018-13-10). These samples all have similar till composition and ice-flow indicators suggesting that the source of these KIMs is to the southeast and/or east.

Interestingly, KIM recovery from the Kaskattama and Hayes flowsets (Figure GS2018-13-9), and associated till types (Hayes flowset, till types 3 and 6; Kaskattama flowset, till types 1 and 2), have similar average KIM recovery. Given the compositional contrast of till associated with each streamlined-landform flowset, the simplest interpretation is that there are multiple sources for the KIMs recovered from each flowset, which is likely the case for the entire dataset. For example, the highest returns of 15 KIMs (11 km south of Shamattawa on Gods River) and 17 KIMs (15 km south of Spector Lake near the Ontario–Manitoba border) are on opposite sides of the study area, have near perpendicular ice-flow directions indicated and have a different till type. This highlights the prospectivity of the region for diamond exploration but also the need to collect additional data to define dispersal patterns.

Northeastern Manitoba regional KIM distribution

This study expanded on a regional KIM survey conducted in 2001 and 2002 by the MGS that sampled accessible Quaternary sections along the Nelson, Angling, Pennycutaway, Fox, Hayes, Yakaw and Gods rivers (Nielsen and Fedikow, 2002; Hodder et al., 2017), and these datasets are plotted in Figure GS2018-13-11, along with data from the MGS KIM database (Keller et al., 2004). Regionally, till samples from the Kaskattama highland area recovered the highest KIM counts, and also the highest proportion of samples that recovered KIMs.

The junction of the Hayes and Gods rivers has previously been highlighted as a region to conduct follow-up work based on previous work at section 15 (Figure GS2018-13-11; Syme et al., 2004; Hodder et al., 2017). Till sampled (n=7) from 16 to 28 m below ground surface at section 15, below a suspected intertill interglacial unit, had corresponding clast fabrics (n=2) indicating northwest-southeast–oriented ice flow (Hodder et al., 2017). The UGG (16.9–24.5 wt. %) and granitoid contents (7.4–12.4 wt. %) from this till interval would correspond to a till type 1 or 2 classification within this study (cf. Figure GS2018-13-5b). The KIM recovery from this interval ranged from 2 to 11 KIMs. These observations, based on results in this report, would indicate a likely east to southeast provenance for the till interval sampled at section 15. Deposition of this till could be related to one of the northwest-trending ice-flow events observed during this study in the Kaskattama highland or a previous west- to northwest-trending ice-flow event, since this ice-flow direction occurred multiple times in northeastern Manitoba, and has been mapped as far west as Lynn Lake in Manitoba (Gauthier and Hodder, 2017) and into Saskatchewan (Schreiner, 1984).

Conclusion

Kimberlite-indicator minerals were recovered from glacial sediments (till) in the Kaskattama highland area. Till composition, stratigraphic observations and ice-flow data obtained during this study has provided additional insight into KIM provenance to assist further drift exploration efforts in this remote region of Manitoba. Preliminary conclusions regarding till and KIM provenance include

- the sharp contact between the Kaskattama and Hayes flowsets is reflected in the contrasting till composition of each landscape, the Kaskattama flowset is interpreted to be northwest-trending and the Hayes flowset is southwest-trending;
- till type 1 (highest UGG content) is restricted to the Kaskattama highland (including section samples);
- oolitic jasper clast recovery in till is strongly correlated to till type 1 and 2 (elevated UGG content) and supports a southeast to east provenance indicated

Figure GS2018-13-8: *Examples of distinctive erratics observed at the base of stratigraphic sections in the Kaskattama highland area:* ***a)*** *boulder-size Omarolluk Formation erratic (Omar) at section 112-17-519, rock hammer for scale is 43 cm in length;* ***b)*** *boulder-size Omar at section 112-16-402, co-author for scale is 177 cm in height;* ***c)*** *oolitic jasper cobble at section 112-16-412, cobble shown is 19 cm long;* ***d)*** *Dubawnt Supergroup erratic at section 112-16-430, pebble shown is 5 cm in diameter. See Figure GS2018-13-1 for section locations.*

by the Kaskattama flowset and the majority of stratigraphic ice-flow data for these till types;

- samples with a strong Hudson Bay Basin and weak UGG provenance signature have the lowest average KIM recovery; and
- the recovery of KIM grains from different till compositions, flowsets and stratigraphic units indicates the potential for multiple KIM sources in the region.

Economic considerations

The Kaskattama highland region of northeastern Manitoba is a remote and largely unexplored frontier area of northern Manitoba. Till sampled in this region yielded above average KIMs and has elucidated the diamond potential of the region. Till-composition data coupled with ice-flow data has provided insight into potential dispersal patterns in the Kaskattama highland area. Till provenance data indicate that there are likely multiple sources for the recovered KIMs, requiring additional investigations to clarify local-scale dispersal patterns.

Acknowledgments

C. Böhm is thanked for his enthusiastic field assistance and insightful discussions throughout the project.

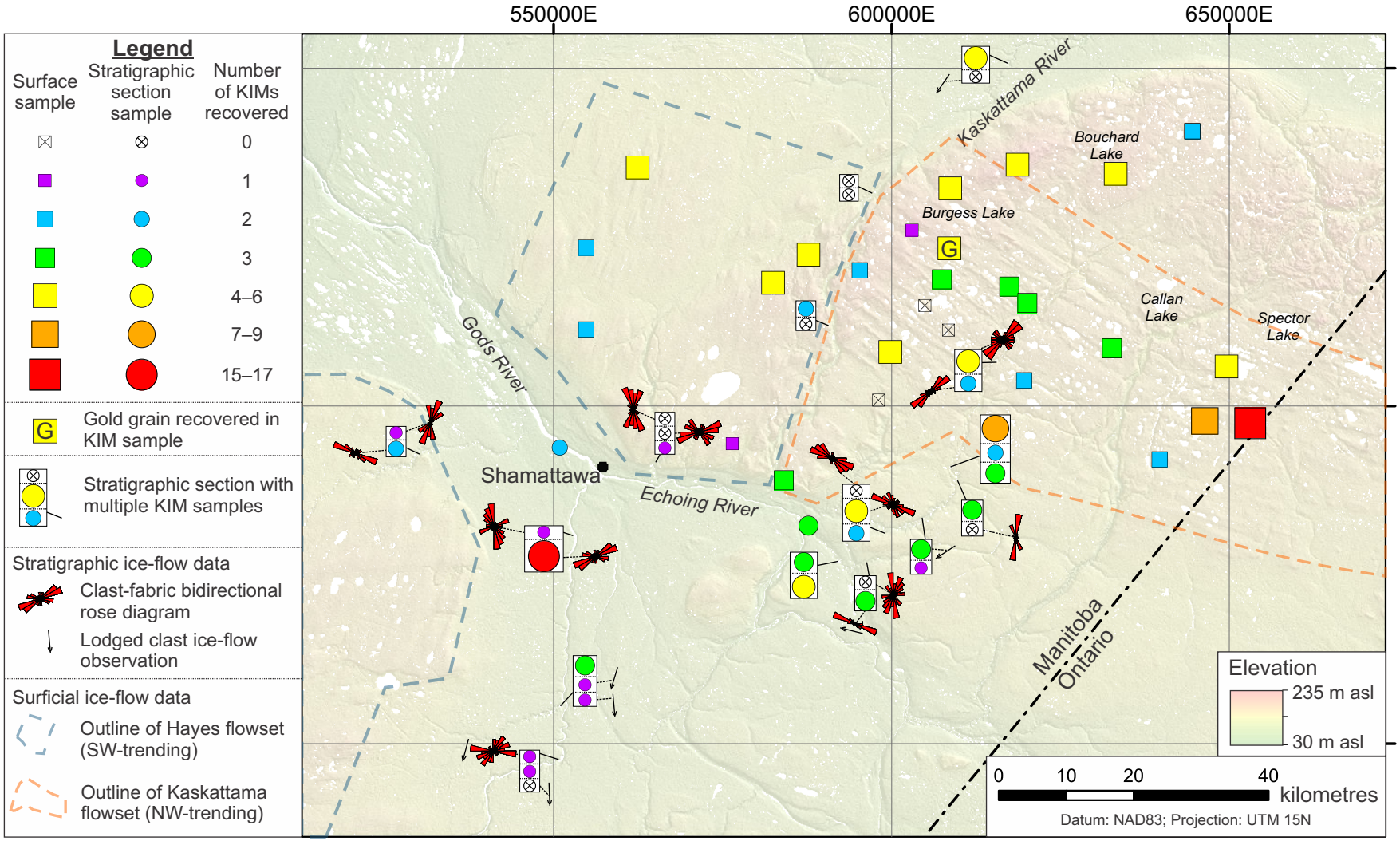

Figure GS2018-13-9: *Kimberlite-indicator mineral (KIM) results displayed as proportional-sized symbols, Kaskattama highland area. Background hillshade image was generated using Canadian Digital Surface Model (Natural Resources Canada, 2015). Abbreviations: NW, northwest; SW, southwest.*

Table GS2018-13-2: Kimberlite-indicator mineral (KIM) recovery according to clast-lithology composition-derived till type, Kaskattama highland area.

Till type	No. of samples	Cr-diopside	Cr-spinel	DI Cr-spinel	Mg-ilmenite	G3-garnet	G9-garnet	G11-garnet	Total KIM	Average KIM recovery
Type 1	19	0	44	1	5	1	2	1	54	2.8
Type 2	16	1	52	1	3	0	1	0	58	3.6
Type 3	16	2	42	2	2	1	0	0	49	3.1
Type 4	9	0	8	0	0	1	0	0	9	1.0
Type 6	4	1	5	0	1	0	4	0	11	2.8
Total	64	4	151	4	11	3	7	1	181	2.8

Abbreviation: DI, diamond inclusion

Prairie Helicopters Inc., and in particular pilot K. Dunthorne, are thanked for providing excellent air support during both field seasons of this project. The De Beers Group of Companies is thanked for their continued analytical support for Quaternary projects at the MGS by providing KIM processing. Thanks also go to N. Brandson, E. Anderson and C. Epp from the MGS for logistical support throughout the project. C. Böhm and M. Nicolas are thanked for their review of this publication.

References

Clark, C.D., Knight, J. and Gray, J.T. 2000: Geomorphological reconstruction of the Labrador Sector of the Laurentide Ice Sheet; Quaternary Science Reviews, v. 19, p. 1343–1366.

Dredge, L.A. and Cowan, W.R. 1989: Quaternary geology of the southwestern Canadian Shield; *in* Quaternary Geology of Canada and Greenland, R.J. Fulton (ed.), Geological Survey of Canada, Geology of Canada Series, no. 1, p. 214–248.

Dredge, L.A. and McMartin, I. 2011: Glacial stratigraphy of northern and central Manitoba; Geological Survey of Canada, Bulletin 600, 27 p.

Fipke, C.E., Gurney, J.J. and Moore, R.O. 1995: Diamond exploration techniques emphasising indicator mineral geochemistry and Canadian examples; Geological Survey of Canada, Bulletin 423, 96 p.

Gao, C. and Crabtree, D.C. 2016: Results of regional till and modern alluvium sampling in the McFaulds Lake ("Ring of Fire") area, northern Ontario; Ontario Geological Survey, Open File Report 6309, 164 p.

Gauthier, M.S. and Hodder, T.J. 2017: Till sampling and ice-flow mapping between Leaf Rapids, Lynn Lake and Kinoosao, northwestern Manitoba (parts of NTS 64B12, 64C9, 11, 12, 14–16, 64F3, 4); *in* Report of Activities 2017, Manitoba Growth, Enterprise and Trade, Manitoba Geological Survey, p. 191–204.

Greenwood, S.L. and Clark, C.D. 2009: Reconstructing the last Irish Ice Sheet 1: changing flow geometries and ice flow dynamics deciphered from the glacial landform record; Quaternary Science Reviews, v. 28, p. 3085–3100.

Grütter, H.S., Gurney, J.J., Menzies, A.H. and Winter, F. 2004: An updated classification scheme for mantle-derived garnet, for use by diamond explorers; Lithos, v. 77, p. 841–857.

Hodder, T.J. 2017: Quaternary stratigraphy and till sampling in the Kaskattama highland region, northeastern Manitoba (parts of NTS 53N, O, 54B, C): year two; *in* Report of Activities 2017, Manitoba Growth, Enterprise and Trade, Manitoba Geological Survey, p. 205–214.

Hodder, T.J. 2018a: Ice-flow history and till composition of the Southern Indian Lake area, north-central Manitoba (parts of NTS 64G1, 2, 7–10, 64B15); Manitoba Growth, Enterprise and Trade, Manitoba Geological Survey, Open File OF2018-1, 21 p.

Hodder, T.J. 2018b: Kimberlite-indicator–mineral data derived from glacial sediments (till) in the Kaskattama highland area of northeastern Manitoba (parts of NTS 53N, O, 54B, C); Manitoba Growth, Enterprise and Trade, Manitoba Geological Survey, Data Repository Item DRI2018001, Microsoft® Excel® file.

Hodder, T.J. and Kelley, S.E. 2016: Quaternary stratigraphy and till sampling in the Kaskattama highland region, northeastern Manitoba (parts of NTS 53N, O, 54B, C); *in* Report of Activities 2016, Manitoba Growth, Enterprise and Trade, Manitoba Geological Survey, p. 187–195.

Hodder, T.J. and Kelley, S.E. 2017: Kimberlite-indicator-mineral results derived from glacial sediments (till) in the Kaskattama highland area of northeast Manitoba (parts of NTS 53N, O, 54B, C); Manitoba Growth, Enterprise and Trade, Manitoba Geological Survey Open File, OF2017-1, 6 p.

Hodder, T.J., Gauthier, M.S. and Nielsen, E. 2017: Quaternary stratigraphy and till composition along the Hayes, Gods, Nelson, Fox, Stupart, Yakaw, Angling and Pennycutaway rivers, northeast Manitoba (parts of NTS 53N, 54C, 54D, 54F); Manitoba Growth, Enterprise and Trade, Manitoba Geological Survey, Open File OF2017-4, 20 p.

Jackson, G.D. 2013: Geology, Belcher Islands, Nunavut; Geological Survey of Canada, Open File 4923, 149 p.

Kaszycki, C.A., Dredge, L.A. and Groom, H. 2008: Surficial geology and glacial history, Lynn Lake - Leaf Rapids area, Manitoba; Geological Survey of Canada, Open File 5873, 105 p.

Keller, G.R., Bogdan, D.J. and Matile, G.L.D. 2004: Manitoba Kimberlite Indicator Mineral Database (Version 3.0); Manitoba Industry, Economic Development and Mines, Manitoba Geological Survey, Open File Report OF2004-25, zipped Microsoft Access® 2000 database.

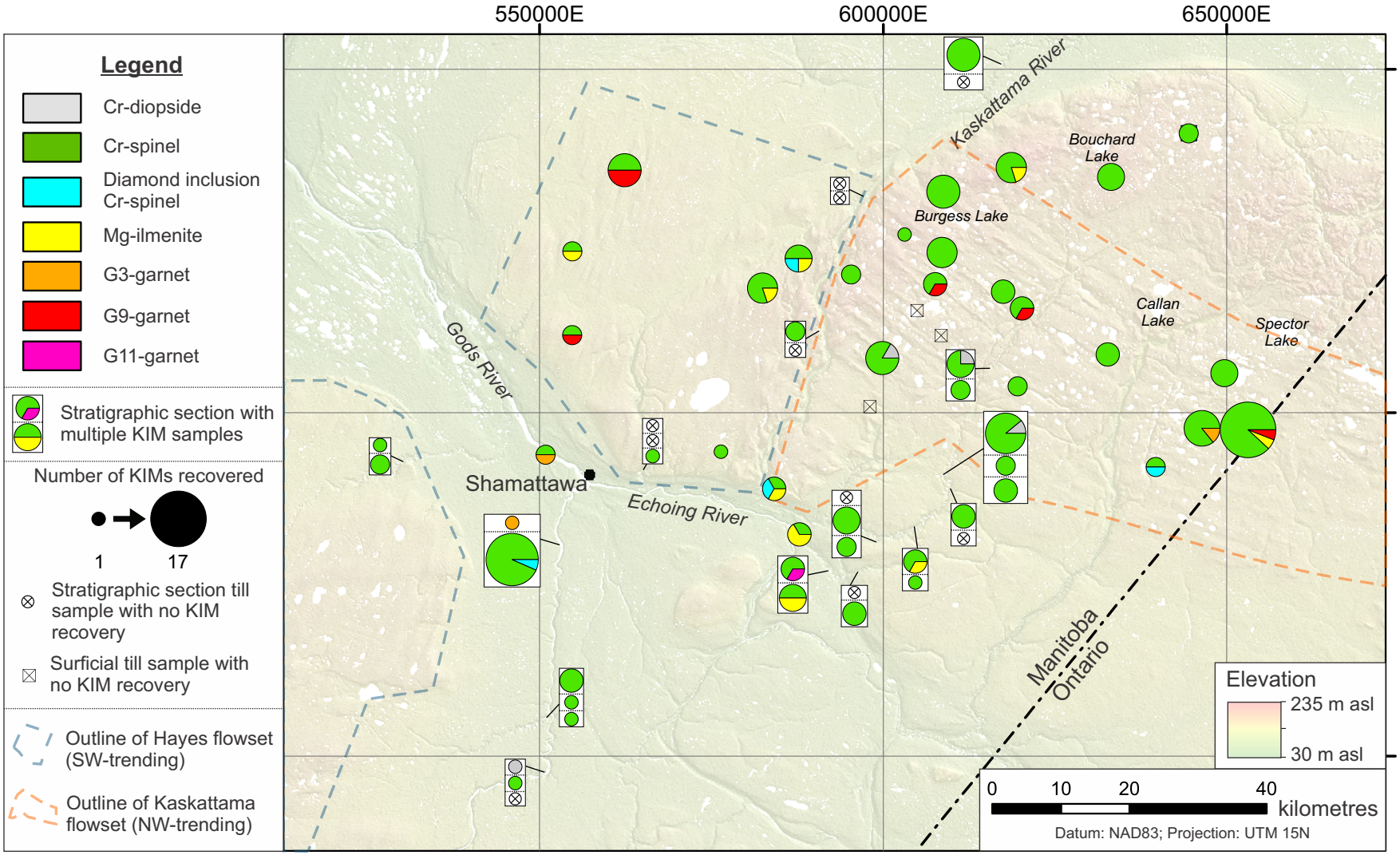

Figure GS2018-13-10: *Kimberlite-indicator mineral (KIM) results displayed as proportional-sized compositional pie charts, Kaskattama highland area. Background hillshade image was generated using Canadian Digital Surface Model (Natural Resources Canada, 2015). Abbreviations: NW, northwest; SW, southwest.*

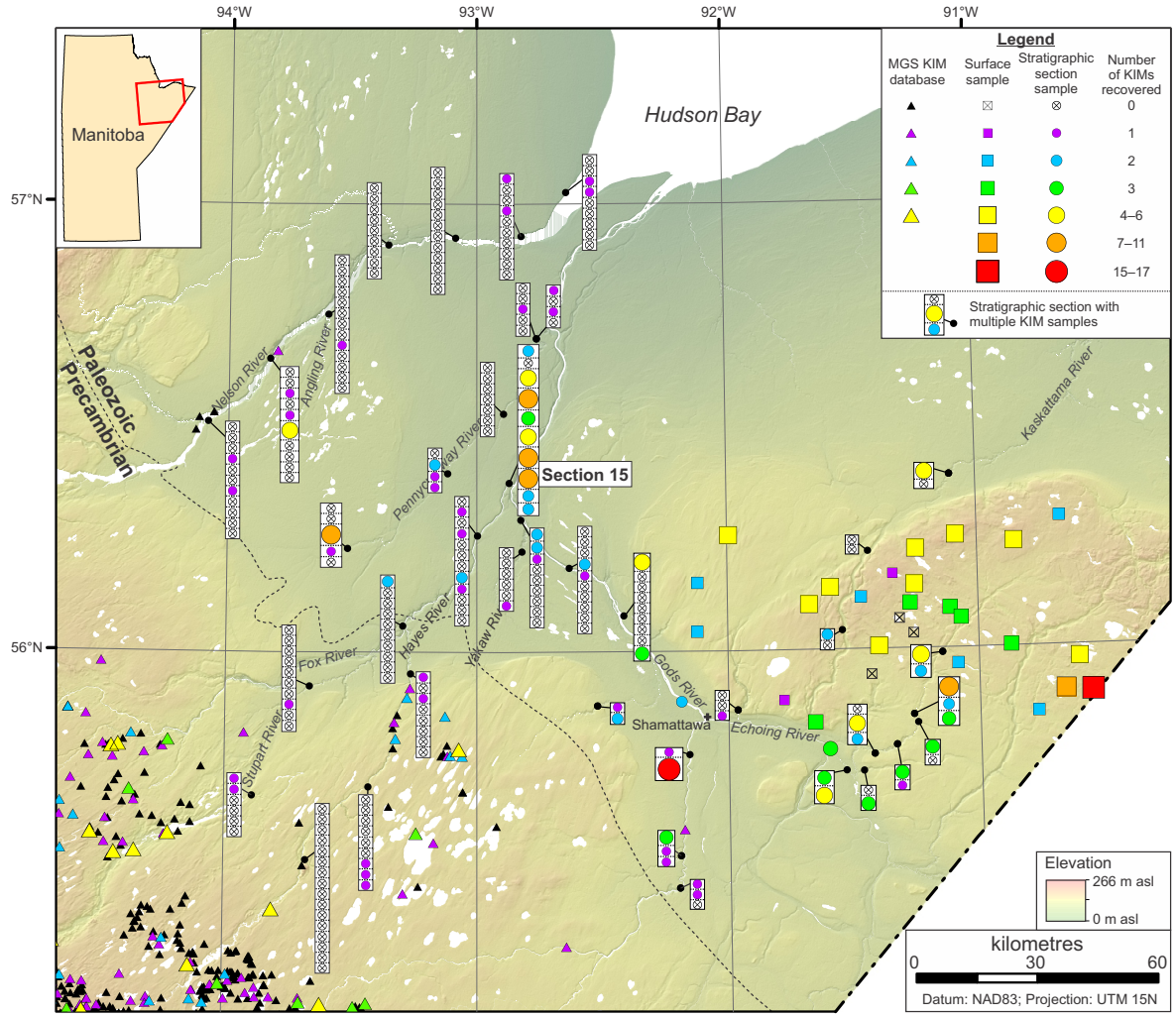

Figure GS2018-13-11: *Kimberlite-indicator mineral (KIM) results for MGS surveys conducted in northeastern Manitoba (this study; Nielsen and Fedikow, 2002; Hodder et al., 2017) and results from the MGS KIM database (Keller et al., 2004). Note, data from the KIM database is not separated into stratigraphic and surficial samples or separated by material sampled (e.g., beach versus till). Where multiple samples are present at the same location, the highest KIM count is shown. Background hillshade image was generated using Canadian Digital Surface Model (Natural Resources Canada, 2015).*

Kleman, J. and Borgstrom, I. 1996: Reconstruction of palaeo-ice sheets: the use of geomorphological data; Earth Surface Processes and Landforms, v. 21, p. 893–909.

Manitoba Department of Mines, Natural Resources and Environment 1979: Geological map of Manitoba; Manitoba Department of Mines, Natural Resources and Environment, Mineral Resources Division, Geological Report GR79-2, scale 1:1 000 000.

Matile, G.L.D. and Keller, G.R. 2007: Surficial geology of Manitoba; Manitoba Science, Technology, Energy and Mines, Manitoba Geological Survey, Surficial Geology Compilation Map Series SG-MB, scale 1: 1 000 000.

McMartin, I. and Paulen, R.C. 2009: Ice-flow indicators and importance of ice-flow mapping for drift prospecting; *in* Application of Till and Stream Sediment Heavy Mineral and Geochemical Methods to Mineral Exploration in Western and Northern Canada, R.C. Paulen and I. McMartin (eds.), Geological Association of Canada Short Course Notes, v. 18, p. 15–34.

Natural Resources Canada 2015: Canadian Digital Surface Model; Natural Resources Canada, URL <https://open.canada.ca/data/en/dataset/768570f8-5761-498a-bd6a-315eb6cc023d> [September 2015].

Nicolas, M.P.B. and Armstrong, D.K. 2017: Update on Paleozoic stratigraphic correlations in the Hudson Bay Lowland, northeastern Manitoba and northern Ontario; *in* Report of Activities 2017, Manitoba Growth, Enterprise and Trade, Manitoba Geological Survey, p. 133–147.

Nielsen, E. and Fedikow, M.A.F. 2002: Kimberlite indicator-mineral surveys, lower Hayes River; Manitoba Industry, Trade and Mines, Manitoba Geological Survey, Geological Paper GP2002-1, 11 p.

Nimis, P. 2002: The pressures and temperatures of formation of diamond based on thermobarometry of chromian diopside inclusions; The Canadian Mineralogist, v. 40, p. 871–884.

Nowicki, T.E., Moore, R.O., Gurney, J.J. and Baumgartner, M.C. 2007: Diamonds and associated heavy minerals in kimberlite: a review of key concepts and applications; Developments in Sedimentology, v. 58, p. 1235–1267.

Prest, V.K., Donaldson, J.A. and Mooers, H.D. 2000: The Omar story: the role of Omars in assessing glacial history of west-central North America; Géographie physique et Quaternaire, v. 54, no. 3, p. 257–270.

Rainbird, R.H., Hadlari, T., Aspler, L.B., Donaldson, J.A., LeCheminant, A.N. and Peterson, T.D. 2003: Sequence stratigraphy and evolution of the Paleoproterozoic intracontinental Baker Lake and Thelon basins, western Churchill Province, Nunavut, Canada; Precambrian Research, v. 125, p. 21–53.

Ramsay, R.R. and Tompkins, L.A. 1994: The geology, heavy mineral concentrate mineralogy, and diamond prospectivity of the Boa Esperança and Cana Verde pipes, Corrego D'anta, Minas Gerais, Brazil; *in* Kimberlites, Related Rocks and Mantle Xenoliths, H.O.A. Meyer and O.H. Leonardos (ed.), Proceedings of the 5th International Kimberlite Conference, Araxá, Brazil, Companhia de Pesquisa de Recursos Minerais (CRPM), Special Publication, v. 2, p. 329–345.

Schreiner, B.T. 1984: Quaternary geology of the Precambrian Shield, Saskatchewan; Saskatchewan Geological Survey, Report 221, 106 p.

Stott, G.M., Buse, S., Davis, D.W. and Hamilton, M.A. 2010: The Sutton inliers—a Paleoproterozoic succession in the Hudson Bay Lowland; *in* Summary of Field Work and Other Activities 2010, Ontario Geological Survey, Open File Report 6260, p. 19-1–19-14.

Syme, E.C., Bezys, R.K., Bogdan, D.J., Böhm, C.O., Kaszycki, C.A., Keller, G.R., Lenton, P.G. and Matile, G.L.D. 2004: Kimberlite potential in Manitoba: an update; *in* Report of Activities 2004, Manitoba Industry, Economic Development and Mines, Manitoba Geological Survey, p. 309–319.

Thorleifson, L.H., Garrett, R.G. and Matile, G. 1994: Prairie kimberlite study - indicator mineral geochemistry; Geological Survey of Canada, Open File 2875, 15 p.

Trommelen, M.S., Ross, M. and Campbell, J.E. 2013: Inherited clast dispersal patterns: implications for paleoglaciology of the southeast Keewatin Sector of the Laurentide Ice Sheet; Boreas, v. 42, no. 3, p. 693–713.

Wang, Y. 2018: Statistical analysis of till geochemistry in the Nelson River area, northeastern Manitoba: implications for Quaternary glacial stratigraphy; M.Sc. thesis, University of Waterloo, Waterloo, Ontario, 162 p.

Wyatt, B.A., Baumgartner, M., Anckar, E. and Grütter, H.S. 2004: Compositional classification of 'kimberlitic' and 'non-kimberlitic' ilmenite; Lithos, v. 77, p. 841–857.

GS2018-14

Till composition of the Kaskattama Kimberlite No. 1 drillcore, Kaskattama highland region, northeastern Manitoba (part of NTS 54B7)

by T.J. Hodder

In Brief:

- Four till units were identified in drillcore KK1 based on composition data
- Shale and siltstone clast concentrations in till suggest that this bedrock unit is more extensive in this region than previously realized, corroborating recent magnetotelluric geophysical interpretations

Citation:
Hodder, T.J. 2018: Till composition of the Kaskattama Kimberlite No. 1 drillcore, Kaskattama highland region, northeastern Manitoba (part of NTS 54B7); *in* Report of Activities 2018, Manitoba Growth, Enterprise and Trade, Manitoba Geological Survey, p. 166–174.

Summary

Drillhole Kaskattama Kimberlite No. 1 (KK1) intersected a thick sequence of Quaternary sediments in the Kaskattama highland area of northeastern Manitoba. Permafrost conditions allowed for excellent recovery of till during diamond drilling and this study focuses on documenting till composition through till-clast–lithology counts and till-matrix geochemistry.

Interpretation of till-composition data identified a minimum of four till units. The undifferentiated greenstone and greywacke clast concentration (17.8–20.4 count [ct.] %) present in two surficial till samples is elevated relative to till sampled in drillcore KK1 (maximum 6.4 ct. %), which suggests a stronger eastern provenance influence for the surficial till in this region. The concentration of black to grey shale and siltstone (BSS) clasts is elevated (maximum of 16.3 ct. %) within till from KK1, and far exceeds concentrations present in surficial and shallowly buried (<30 m) till samples in the region (maximum of 1.1 ct. %). The highest concentration of BSS clasts is present from 83.0 to 102.0 m true vertical depth. This interval of elevated concentration of BSS clasts is >100 m above local shale strata, which was observed at depths below 223.0 m. This would suggest that these BSS clasts have undergone some glacial transport into the area and are not simply sourced directly from the underlying bedrock. This is a significant observation and corroborates recent interpretations from a magnetotelluric geophysical survey, which suggest that the shale unit present in drillcore KK1 is likely more extensive in this region than previously understood.

Introduction

The Kaskattama Kimberlite No.1 (KK1) drillhole was drilled by Foran Mining Corporation during the summer of 2004 near Bouchard Lake in the Kaskattama highland region of northeastern Manitoba (Figure GS2018-14-1; Assessment File 74223, Manitoba Growth, Enterprise and Trade, Winnipeg). Drillhole KK1 tested a circular magnetic anomaly and was drilled to a total depth of 332.0 m true vertical depth (TVD; Assessment File 74223). The drillcore intersected a thick sequence of Quaternary sediments (up to 223.0 m) overlying a black shale of possible Cretaceous-age, underlain by Paleozoic carbonate rocks of the Hudson Bay Basin (Nicolas and Armstrong, 2017). Apart from Quaternary sediments exposed along river sections, this drillcore is the only subsurface observation for the entire highland region and represents a valuable source of Quaternary and Paleozoic stratigraphic data (Nicolas and Armstrong, 2017). The purpose of this study is to examine the composition of till recovered from drillcore KK1 through clast-lithology counts and till-matrix (<63 µm size-fraction) geochemistry, to contribute to ongoing regional investigations into the Quaternary geology (Hodder and Kelley, 2016; Hodder, 2017; Hodder and Kelley, GS2018-13, this volume) and subsurface structure (Craven et al., 2017) of the Kaskattama highland region.

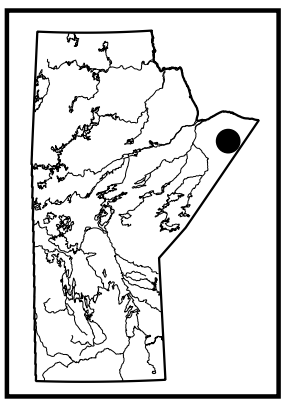

Methods

In 2017, the KK1 drillcore was pulled from archive and examined in detail to verify previous core descriptions and sample the till. The KK1 drillcore was obtained by diamond drilling and the recovery of Quaternary sediments was poor until permafrost conditions were encountered. Recovery of sand and gravel sediments was minimal, but diamict

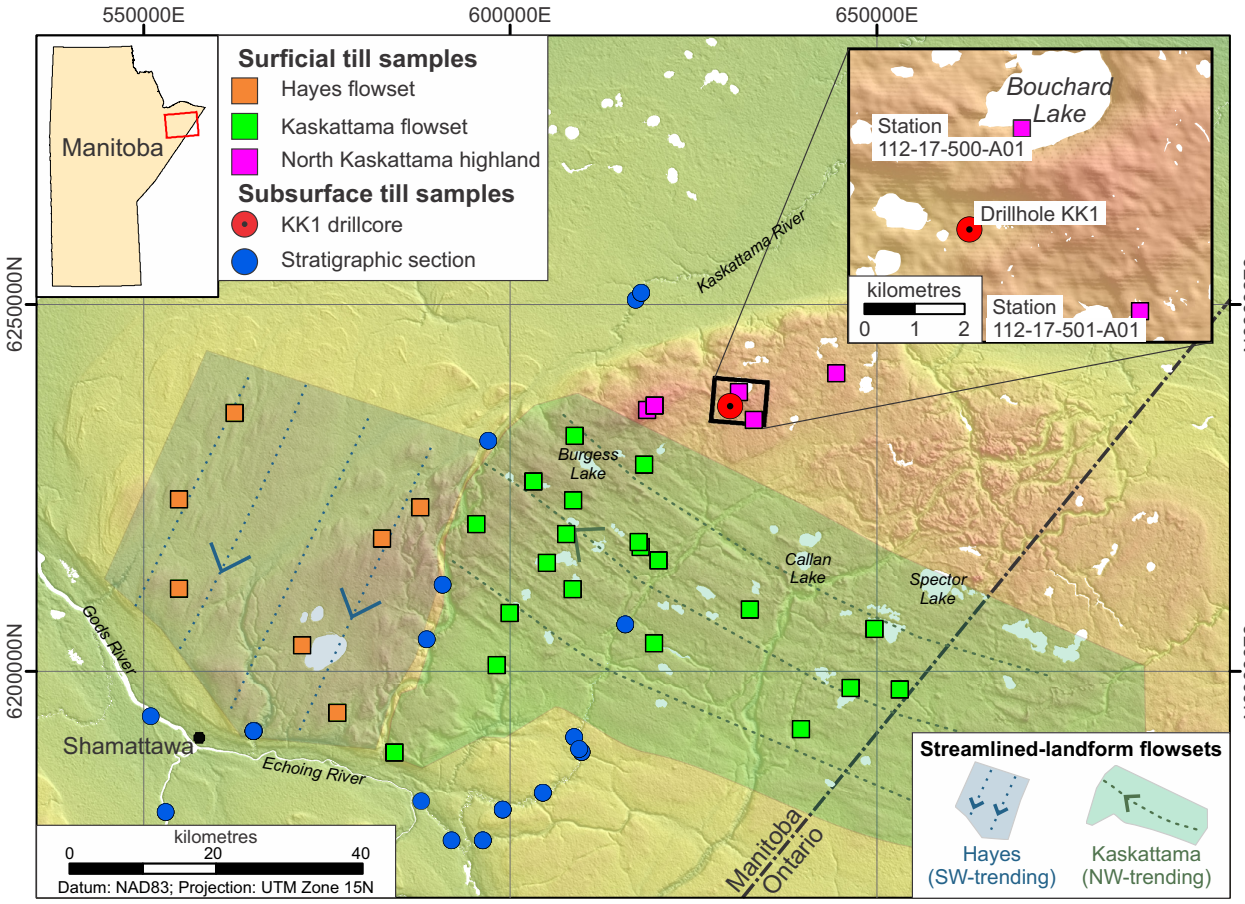

Figure GS2018-14-1: *Location of the Foran Mining Kaskattama Kimberlite No.1 (KK1) drillhole and till samples collected nearby during the 2016 and 2017 field seasons in the Kaskattama highland region of northeastern Manitoba. Background hillshade image was generated using Canadian Digital Surface Model (Natural Resources Canada, 2015). Abbreviations: NW, northwest; SW, southwest.*

recovery was good (e.g., Figure GS2018-14-2a, b), and sediment and rock were recovered from 16.8 to 332.2 m TVD. Original observations made in the field (Assessment File 74223) were compiled and verified. Till was sampled at approximately 5 m intervals, where appropriate material was present, totalling 15 samples. The 5 cm (2-in.) diameter drillcore was first halved to maintain an archived record and till was sampled over 0.5–0.8 m intervals to obtain a sufficient amount of material for till-matrix geochemistry and clast-lithology analysis. Two surficial till samples were collected nearby the KK1 drillhole location during the 2017 field season (Figure GS2018-14-1) and are discussed in this report. These till samples were collected from C-horizon material in hand-dug pits and/or auger holes (Figure GS2018-14-2c–e).

Drillcore till samples were submitted to Saskatchewan Research Council Geoanalytical Laboratories (SRC; Saskatoon, Saskatchewan) and surficial till samples to Activation Laboratories Ltd. (Actlabs; Ancaster, Ontario) for initial processing. Till samples were wet sieved at SRC and dry sieved at Actlabs to obtain <0.063, 0.063–2 and >2 mm size-fractions. Following initial sieving, the >2 mm size-fraction was further sieved into 2–4, 4–8 and >8 mm size-fractions at the laboratory of the Manitoba Geological Survey Midland Sample and Core Library (Winnipeg, Manitoba) and submitted for clast-lithology counts internally. Clasts from the 2–4, 4–8 and >8 mm size-fractions were separated into 15 detailed lithology classes with the assistance of a 10 times optical microscope (e.g., Figure GS2018-14-3). These 15 detailed classes were grouped into six simplified classes for interpretation purposes (Table GS2018-14-1). An average of 353 clasts was counted for each sample (range of 323–381) and results are expressed as a count percentage. The <63 µm size-fraction was partially digested in an aqua regia (1:3, HNO_3:HCl) solution and analyzed for 63 elements by inductively coupled plasma–mass spectrometry (ICP-MS) and –emission spectrometry (ES) at Actlabs. The <63 µm size-fraction was also submitted to Actlabs for near-total digestion (HF:HNO_3:$HClO_4$:HCl) and analyzed for 58 elements by ICP-MS. Carbonate content was determined by the Ca/Mg method on the <63 µm size-fraction at Actlabs. Till-matrix geochemistry and clast-lithology count

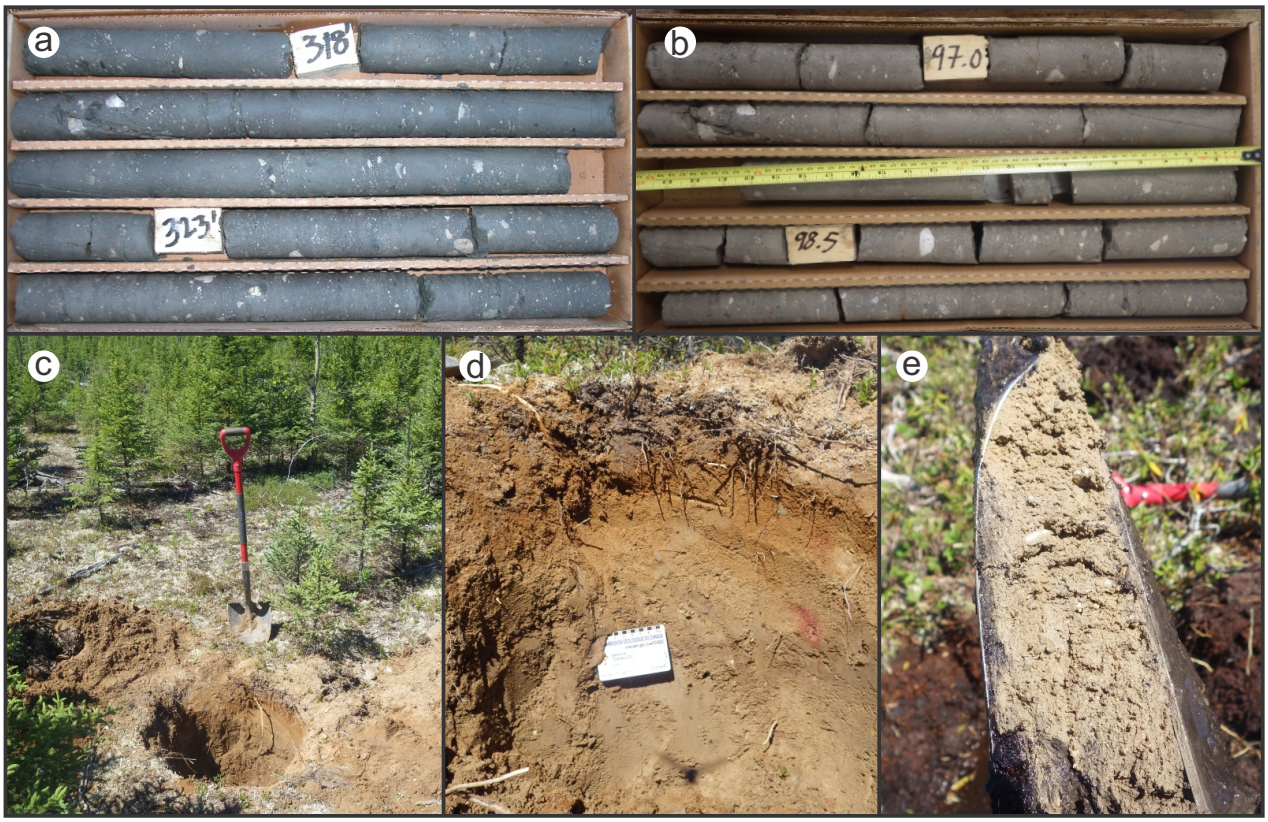

Figure GS2018-14-2*: Examples of till sampled as part of this study:* ***a)*** *till from the Foran Mining Kaskattama Kimberlite No.1 (KK1) drillcore when first drilled (2004) and* ***b****) when sampled by this study;* ***c, d****) hand-dug pit exposing C-horizon till at station 112-17-501-A01; and* ***e)*** *auger of till at station 112-17-500-A01.*

data are published as data repository item (DRI2018002[1]) in co-ordination with this report (Hodder, 2018).

Results

Till stratigraphy

Drillcore KK1 intersected a thick sequence of Quaternary sediments (Figure GS2018-14-4). Insufficient core recovery from 2.7 to 12.2 m and 25.9 to 29.3 m inhibited sampling of the diamict observed in these intervals. Two nearby surficial till samples (Figure GS2018-14-1) are likely representative of the composition of the uppermost till unit observed in drillcore KK1 (2.7–12.2 m depth). Excellent core recovery allowed for the sampling of diamict from 80.0 to 170.1 m (Figure GS2018-14-4). This diamict, interpreted as a till based on the presence of striated clasts, is remarkably homogeneous in appearance throughout this entire interval. The diamict is dark grey (blackish-grey when wet), matrix supported and contains 10–15% clasts.

Till-clast–lithology composition

Analysis of clasts within till can assist with the delineation of glacial transport directions and distances, as well as identify unmapped, drift-covered bedrock units. Glacial dispersal can be mapped at varying scales from continental (hundreds of kilometres) to regional (tens of kilometres) to local (<10 km). Four till units are identified based on the clast-lithology count concentrations (Figure GS2018-14-5).

The surficial till (Till-1) near KK1 is characterized by high concentrations of undifferentiated greenstone and greywacke (UGG) clasts (Figure GS2018-14-5), which range from 17.8–20.4 ct. %. This contrasts with till sampled from drillcore KK1, which has a maximum of 6.4 ct. % (Figure GS2018-14-5). Till-2 (Figure GS2018-14-5) is characterized by high concentrations of black to grey shale and siltstone (BSS) clasts (8.5–16.3 ct. %) and low concentrations of UGG clasts (0.8–2.8 ct. %). Till-3 (Figure GS2018-14-5) is characterized by the presence of BSS clasts (1.2–6.5 ct. %) and increased concentrations

[1] MGS Data Repository Item DRI2018002 containing the data or other information sources used to compile this report is available online to download free of charge at https://www.gov.mb.ca/iem/info/library/downloads/index.html, or on request from minesinfo@gov.mb.ca, or by contacting the Resource Centre, Manitoba Growth, Enterprise and Trade, 360–1395 Ellice Avenue, Winnipeg, Manitoba R3G 3P2, Canada.

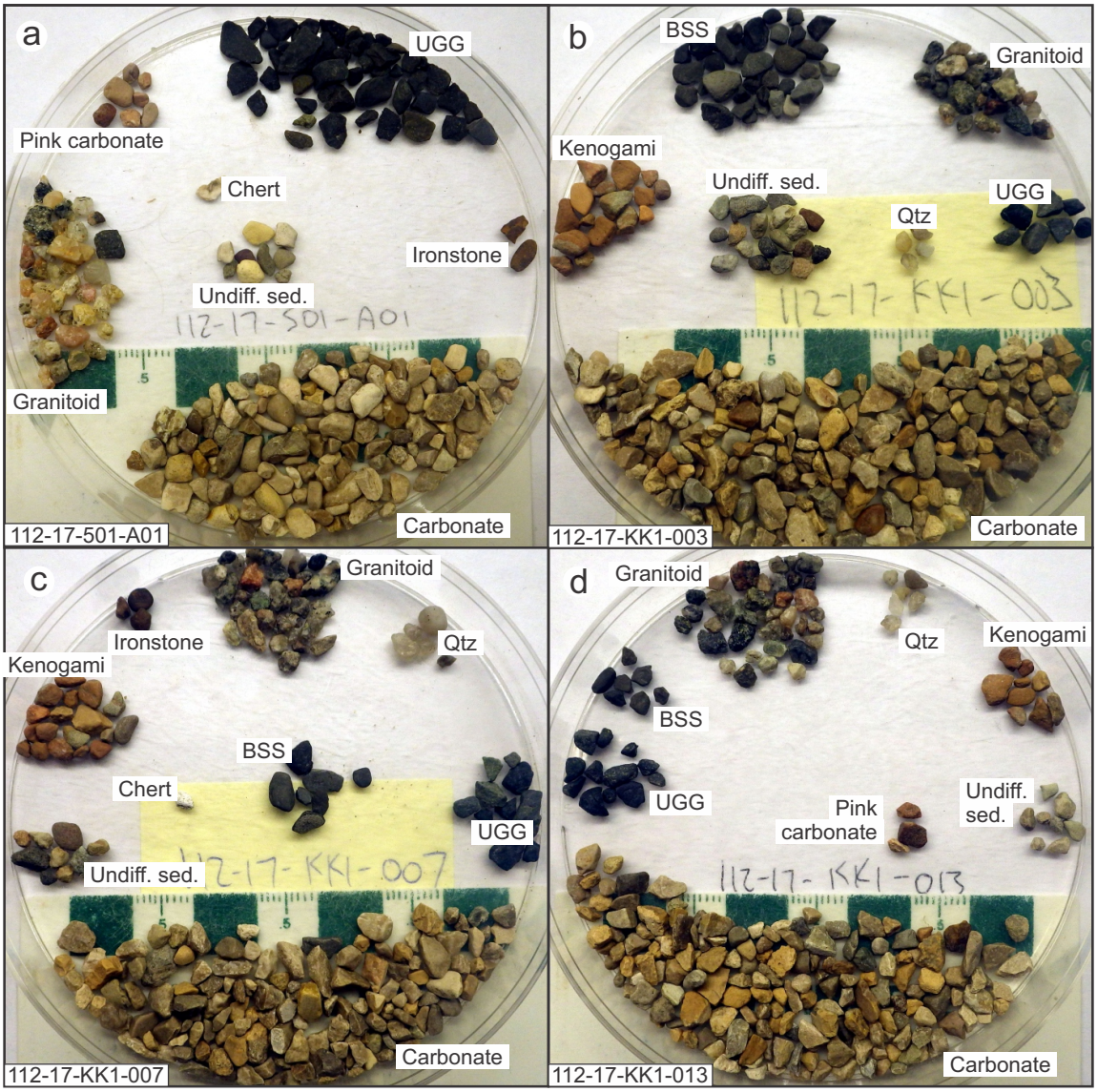

Figure GS2018-14-3*: Examples of 2–4 mm size-fraction clasts from till samples, separated by lithology:* ***a)*** *sample 112-17-501-A01 (till-1);* ***b)*** *sample 112-17-KK1-003 (till-2);* ***c)*** *sample 112-17-KK1-007 (till-3);* ***d)*** *sample 112-17-KK1-013 (till-4). Abbreviations: BSS, black to grey shale and siltstone; Carbonate, grey, tan, white carbonate; Kenogami, Kenogami Formation; Qtz, quartz; UGG, undifferentiated greenstone and greywacke; Undiff. sed., undifferentiated sandstone and siltstone.*

Table GS2018-14-1: Detailed and simplified clast-lithology classes for till samples from the Foran Mining Kaskattama Kimberlite No.1 (KK1) drillcore.

Simplified class	Undifferentiated Hudson Bay Basin	Total carbonate	Total granitoid	Undifferentiated greenstone and greywacke	Kenogami Formation	Black to grey shale and siltstone
Detailed classes	Ironstone	Grey, tan, white carbonate	Granitoid	Undifferentiated greenstone and greywacke	Fine-grained red sandstone	Black to grey shale and siltstone
	Oolitic jasper	Paleozoic fossil	Quartz			
	Chert	Pink carbonate		Quartzite		Sulphides
	Shell fragment					
	Undifferentiated sandstone and siltstone					

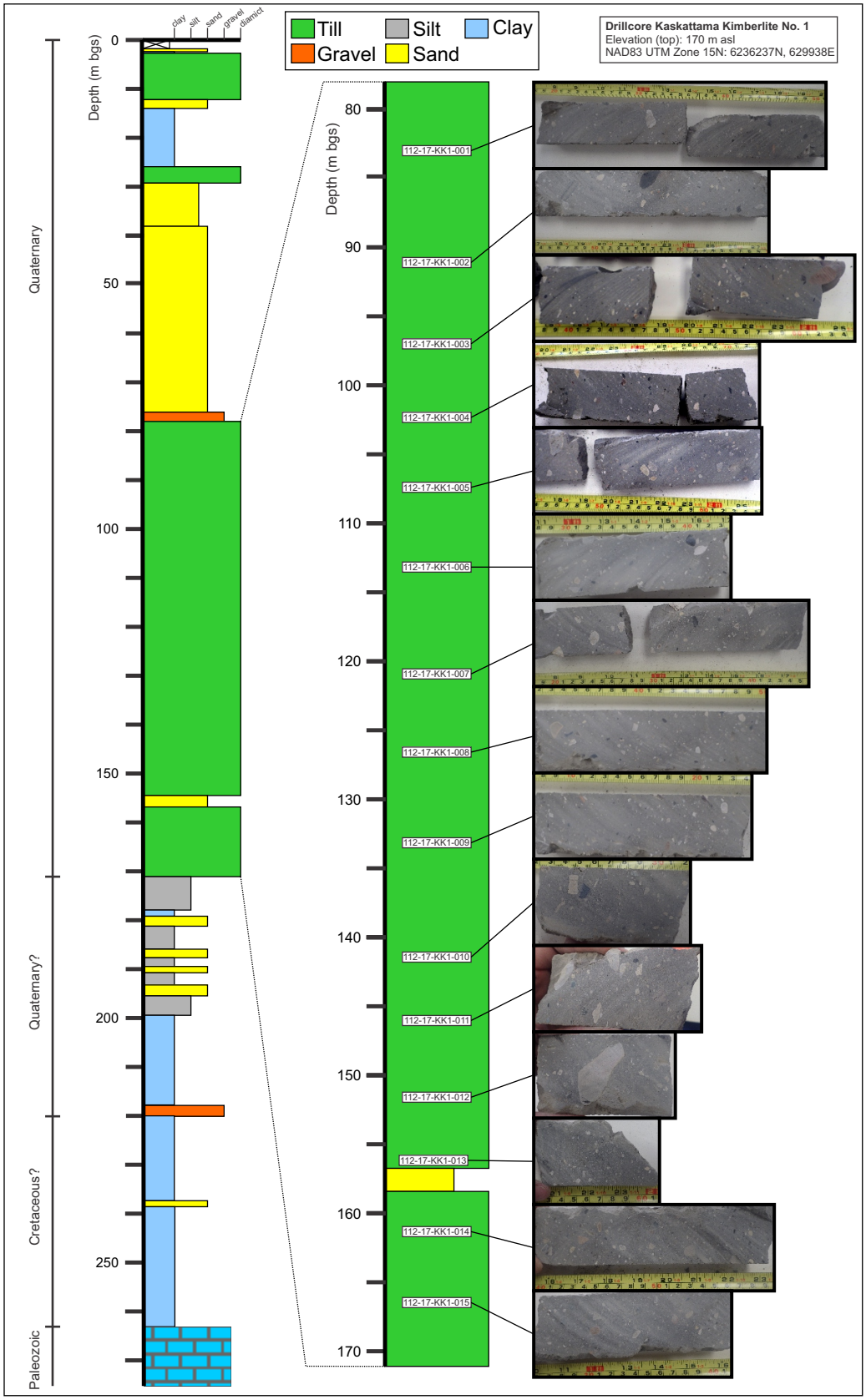

Figure GS2018-14-4*: Simplified Quaternary stratigraphy of the Foran Mining Kaskattama Kimberlite No.1 (KK1) drillcore. Till sample numbers are denoted by the white boxes, which indicate the depths at which the samples were taken. A photo of the interval sampled is displayed along the right side of the figure. Abbreviation: bgs, below ground surface.*

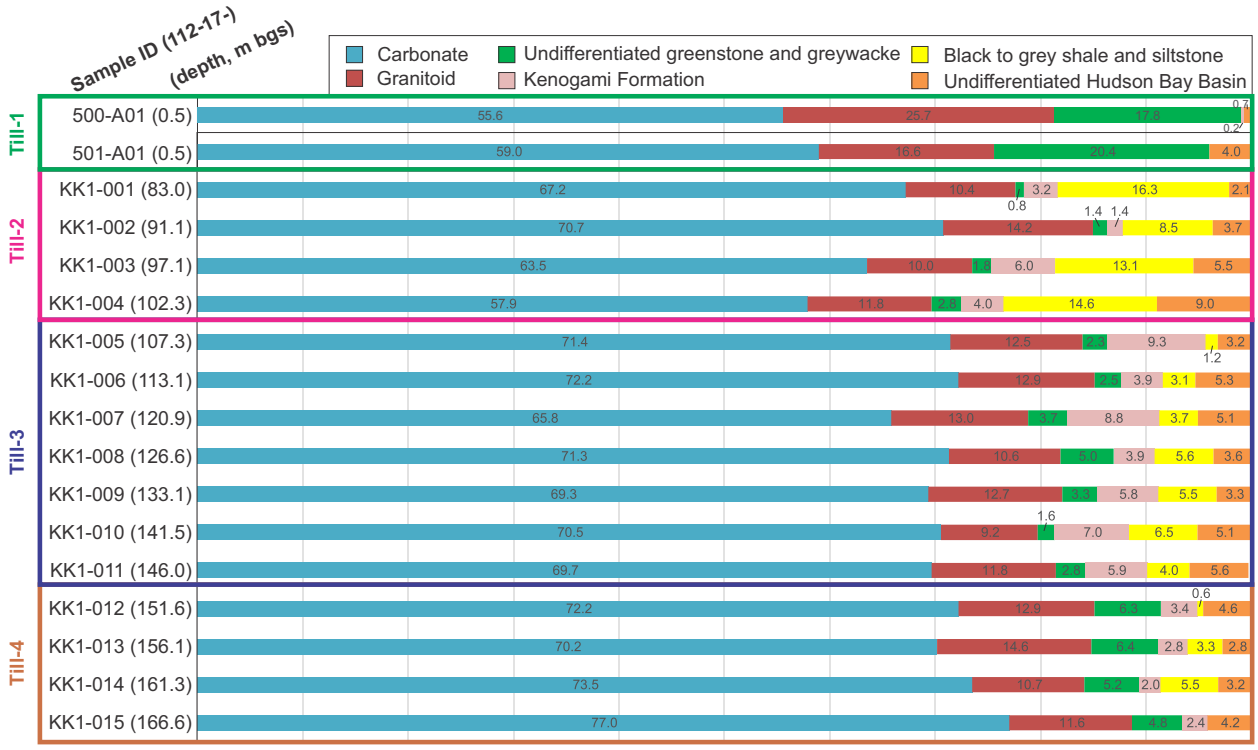

***Figure GS2018-14-5**: Simplified clast-lithology count results (in ct. %) for till samples from the Foran Mining Kaskattama Kimberlite No.1 (KK1) drillcore and two nearby surficial sample sites. Abbreviation: bgs, below ground surface.*

of Kenogami Formation clasts (3.9–9.3 ct. %). Till-4 (Figure GS2018-14-5) is characterized by an increased concentration of UGG clasts (4.8–6.4 ct. %) and decreased concentration of Kenogami Formation clasts (2.0–3.4 ct. %).

Comparing the till-clast–lithology count results from KK1 with a regional dataset (n=116; Hodder and Kelley, GS2018-13, this volume) indicates that till-clast composition of the surficial till has significantly higher UGG concentration compared to subsurface tills in the area (Figure GS2018-14-6a). This would suggest a strong influence of west-trending ice flow for the surficial till (Hodder and Kelley, GS2018-13, this volume) compared to ice-flow events that deposited till sampled in drillcore KK1. Drillcore KK1 samples have a significantly higher concentration of Kenogami Formation clasts than all surficial till samples and most of the shallow subsurface (<30 m TVD) stratigraphic till samples in the region (Figure GS2018-14-6b). The Kenogami Formation of the Hudson Bay Basin is mapped 20 km to the northeast of KK1 drillcore, striking northwest-southeast (Nicolas and Armstrong, 2017).

Till-matrix geochemistry

The carbonate content of till matrix (<63 µm size-fraction) is a proxy for the proportion of Paleozoic carbonate detritus present within till. Carbonate content of till matrix from the KK1 drillcore varies from 23.99 to 31.73%; vertical variations of the carbonate content correspond to the till classes derived from clast-lithology interpretations (Figure GS2018-14-7a). The surficial till is unique from subsurface till and has an increased carbonate content (33.26–39.39%). Till-2 carbonate content ranges from 23.99 to 26.95% and the upper two samples have a higher carbonate content. This decrease in content down unit is similar to carbonate-clast–lithology counts that indicate a decrease in the concentration of carbonate clasts downward within this interval. The carbonate content and clast-lithology count composition indicates a sharp compositional variation between till sampled at 102.0 and 107.0 m TVD, where the boundary for till-2 and till-3 has been placed. Till-3 exhibits a consistent carbonate content throughout the unit ranging from 28.05 to 31.73%. Till-4 has a consistent carbonate content ranging from 25.46 to 26.50%, which is similar to the upper part of till-2 (82.7–91.4 m TVD).

The total rare earth element (TREE) concentration in till matrix is inversely correlated to the carbonate concentration of till (Figure GS2018-14-7a). The TREE concentrations are often used as a proxy for the granitoid content of till (e.g., Trommelen, 2015), but in this specific geological context (where granitoid content of till is minimal),

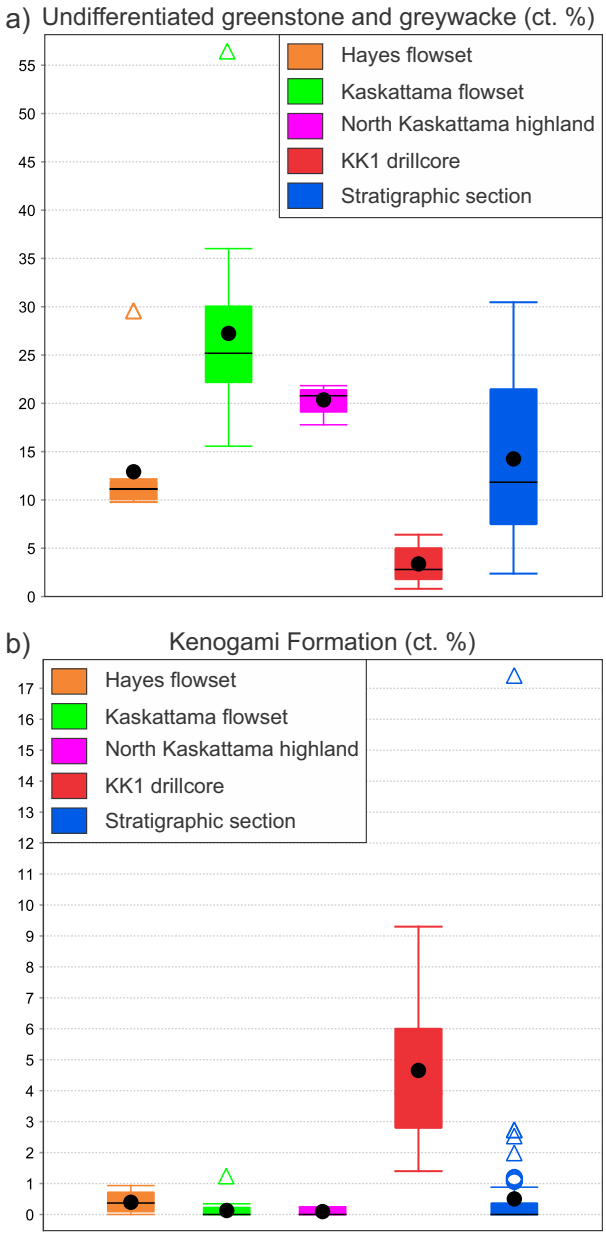

***Figure GS2018-14-6**: Box plots for **a)** undifferentiated greenstone and greywacke and **b)** Kenogami Formation clast concentrations in till sampled in the Kaskattama highland region and the Foran Mining Kaskattama Kimberlite No.1 (KK1) drillcore.*

the highest TREE concentrations are not associated with granitoid detritus. The highest TREE concentrations are in till samples 112-17-KK1-003 and -004. These samples have among the lowest carbonate (63.5 and 57.9 ct. %) and the highest BSS (13.1 and 14.6 ct. %) clast concentrations (Figure GS2018-14-5) in the dataset. Although this is a small sample size, it would broadly appear TREE concentrations are influenced by BSS lithologies (Figure GS2018-14-7b). These relationships should be investigated further with a larger dataset.

Discussion

Implications of shale content in till

The concentration of BSS clasts within KK1 till samples ranges from 0.0 to 16.3 ct. %. No BSS clasts were recovered within the surficial till samples from near drillhole KK1. Additionally, BSS concentrations in surficial and shallowly buried (<30 m TVD) till in the region do not exceed 1.1 ct. % (n=116). The relatively high proportion of BSS clasts in till from the KK1 drillcore is intriguing because there is no known bedrock source mapped in the region (Nicolas and Armstrong, 2017). A black shale unit was observed in drillcore KK1 at 223.0–257.0 m TVD (Figure GS2018-14-4; Nicolas and Armstrong, 2017) and preliminary results from a magnetotelluric geophysical survey in the region indicate that this unit is more extensive in the subsurface than previously suspected (Craven et al., 2017). Considering the highest concentration of BSS clasts was present in till-2 (83.0–102.0 m TVD; Figure GS2018-14-5), which is >100 m above the black shale encountered in KK1, it would suggest that these clasts were not directly incorporated from the observed underlying shale. These clasts have most likely been glacially transported from additional shale sources in the region. The lack of BSS clasts in the regional surficial and shallow subsurface samples (<30 m TVD) indicates that clasts in this till are likely locally sourced. These additional shale and/or siltstone sources are likely part of the same unit described from drillcore KK1 and interpreted from the magnetotelluric survey, which lends credence to the notion of a more significant and extensive shale bedrock unit in this region. The BSS clasts recovered from KK1 tills have variable lithology and include coarse siltstone (Figure GS2018-14-8a) to laminated shale (Figure GS2018-14-8b) and can contain fish scales (Figure GS2018-14-8c, d). Prior to this study, till observed in the KK1 drillcore was collectively grouped based on qualitative characteristics as a 'black till'. This study has quantitatively shown there are variations with depth, which have provided insight into till provenance.

Previous Quaternary stratigraphy investigations along river sections in the Hudson Bay Lowland have only encountered one site with a black till that contained black to grey shale and siltstone clasts. This section (14115MT405; 58.002°N, 94.930°W) is located 312 km northwest of the KK1 drillcore on the Churchill River (M. Gauthier, work in progress). At this site, a two till stratigraphy was observed with a dark grey-black till situated beneath a light brown to grey-brown till. The dark black to grey till contains 4.0–7.0 ct. % black to grey shale clasts (M. Gauthier, work in progress). The source of these clasts is also unknown and could indicate additional shale

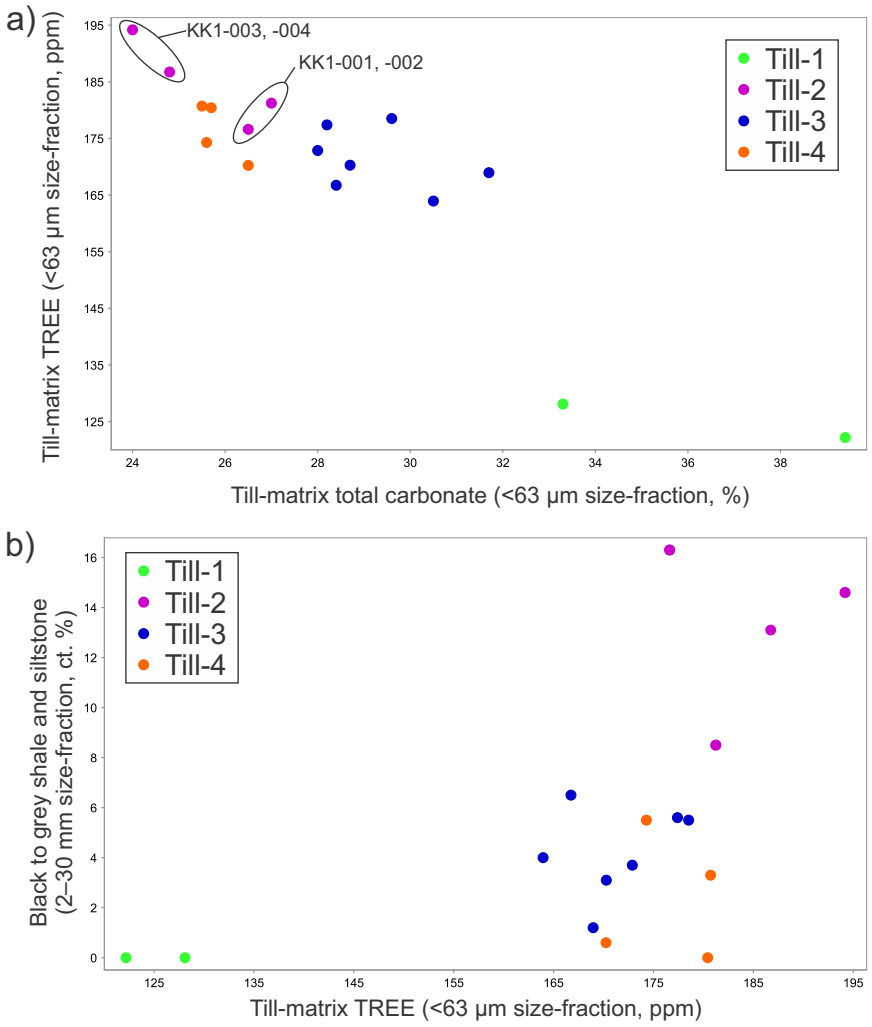

***Figure GS2018-14-7**: Total rare earth element relationship to **a)** total carbonate content of the till-matrix and **b)** black to grey shale and siltstone clast concentrations (2–30 mm size-fraction), from the Foran Mining Kaskattama Kimberlite No.1 (KK1) drillcore and two nearby surficial sample sites. Abbreviation: KK1-, sample number 112-17-KK1-; TREE, total rare earth elements (sum of La+Ce+Pr+Nd+Sm+Eu+Gd+Tb+Dy+Ho+Er+Tm+Yb+Lu).*

sources in the Hudson Bay Basin of northeastern Manitoba.

Economic considerations

The subsurface in the Kaskattama highland region is largely unexplored. This drillcore provides the only source of information on the subsurface and has changed the understanding of the bedrock geology. Further understanding of the subsurface is paramount to understanding the origin of the highland, as well as elucidating the economic potential of this region. The study area has historically been a target for diamond exploration and recent indicator-mineral studies have hinted at kimberlite potential for this region. This study directly contributes to the understanding of the Quaternary stratigraphy in this region and corroborates the notion of a local shale and/or siltstone source.

Acknowledgments

N. Clarke is thanked for compiling stratigraphic information. C. Epp is thanked for preparing drillcore KK1 for viewing and providing logistical support. K. Lapenskie and M. Nicolas are thanked for their review of this publication.

References

Craven, J.A., Ferguson, I.J., Nicolas, M.P.B., Zaprozan, T., Hodder, T.J., Roberts, B.R. and Clarke, N. 2017: Report of activities for the ground geophysical survey across the Kaskattama highlands, Manitoba: GEM-2 Hudson-Ungava Project; Geological Survey of Canada, Open File 8321, 30 p.

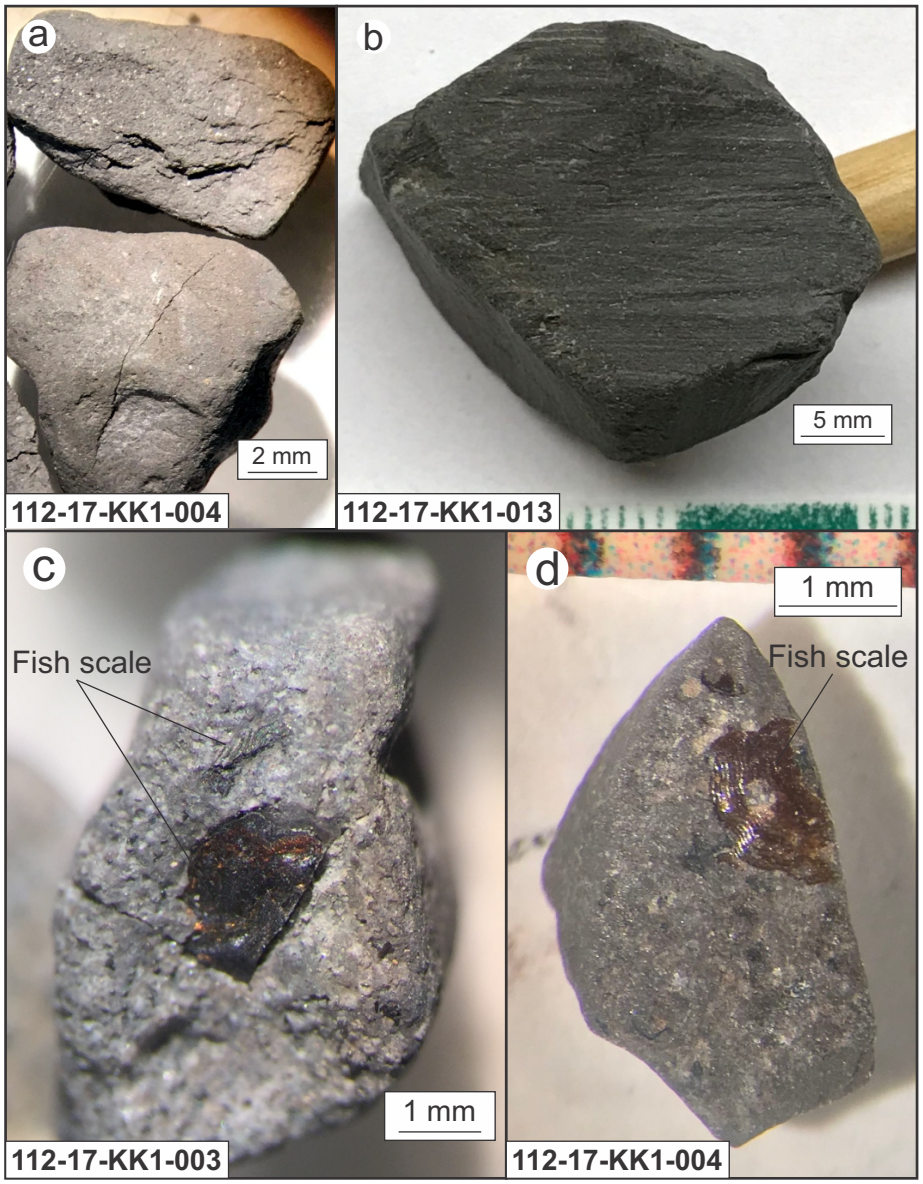

Figure GS2018-14-8*: Example of black to grey shale and siltstone clasts recovered in till from the Foran Mining Kaskattama Kimberlite No.1 (KK1) drillcore:* ***a)*** *light grey siltstone;* ***b)*** *laminated shale; and* ***c, d)*** *siltstone clasts with fish scale(s).*

Hodder, T.J. 2017: Quaternary stratigraphy and till sampling in the Kaskattama highland region, northeastern Manitoba (parts of NTS 53N, O, 54B, C): year two; *in* Report of Activities 2017, Manitoba Growth, Enterprise and Trade, Manitoba Geological Survey, p. 205–214.

Hodder, T.J. 2018: Till-matrix geochemistry and clast-lithology count data from drillcore Kaskattama Kimberlite No. 1 (629938E, 6236237N, UTM Zone 15N [NAD83]), Kaskattama highland, northeastern Manitoba (part of NTS 54B7); Manitoba Growth, Enterprise and Trade, Manitoba Geological Survey, Data Repository Item DRI2018002, Microsoft® Excel® file.

Hodder, T.J. and Kelley, S.E. 2016: Quaternary stratigraphy and till sampling in the Kaskattama highland region, northeastern Manitoba (parts of NTS 53N, O, 54B, C); *in* Report of Activities 2016, Manitoba Growth, Enterprise and Trade, Manitoba Geological Survey, p. 187–195.

Natural Resources Canada 2015: Canadian Digital Surface Model; Natural Resources Canada, URL <https://open.canada.ca/data/en/dataset/768570f8-5761-498a-bd6a-315eb6cc023d> [September 2015].

Nicolas, M.P.B. and Armstrong, D.K. 2017: Update on Paleozoic stratigraphic correlations in the Hudson Bay Lowland, northeastern Manitoba and northern Ontario; *in* Report of Activities 2017, Manitoba Growth, Enterprise and Trade, Manitoba Geological Survey, p. 133–147.

Trommelen, M.S. 2015: Till composition and glacial history, Gauer Lake – Wishart Lake, Manitoba (NTS 64H4, 5, 12, 13); Manitoba Mineral Resources, Manitoba Geological Survey, Geoscientific Paper GP2014-1, 32 p.

PUBLICATIONS

Data Repository Items

DRI2018001

Kimberlite-indicator–mineral data derived from glacial sediments (till) in the Kaskattama highland area of northeastern Manitoba (parts of NTS 53N, O, 54B, C)

by T.J. Hodder

Microsoft® Excel® file supplements:
Hodder, T.J. and Kelley, S.E. 2018: Kimberlite-indicator minerals and clast-lithology composition of till, Kaskattama highland region, northeastern Manitoba (parts of NTS 53N, O, 54B, C); *in* Report of Activities 2018, Manitoba Growth, Enterprise and Trade, Manitoba Geological Survey, p. 150–165.

DRI2018002

Till-matrix geochemistry and clast-lithology count data from drillcore Kaskattama Kimberlite No. 1 (629938E, 6236237N, UTM Zone 15N [NAD83]), Kaskattama highland, northeastern Manitoba (part of NTS 54B7)

by T.J. Hodder

Microsoft® Excel® file supplements:
Hodder, T.J. 2018: Till composition of the Kaskattama Kimberlite No. 1 drillcore, Kaskattama highland region, northeastern Manitoba (part of NTS 54B7); *in* Report of Activities 2018, Manitoba Growth, Enterprise and Trade, Manitoba Geological Survey, p. 166–174.

DRI2018003

Geochemistry data of selected samples of volcanic and volcaniclastic rocks of the North Star assemblage, the West Reed–North Star shear zone and the Fourmile Island assemblage, Flin Flon belt, west-central Manitoba (parts of NTS 63K10, 15)

By S. Gagné, S.D. Anderson, M. Hamilton, R.-L. Simard and M. Lazzarotto

Microsoft® Excel® file supplements:
Gagné, S., Anderson, S.D., Hamilton, M., Simard, R.-L. and Lazzarotto, M. 2018: Geochemistry, Sm-Nd isotopes and U-Pb geochronology of volcanic rocks from the North Star assemblage and the West Reed–North Star shear zone, Flin Flon belt, west-central Manitoba (parts of NTS 63K10, 15): implications for VMS prospectivity; *in* Report of Activities 2018, Manitoba Growth, Enterprise and Trade, Manitoba Geological Survey, p. 48–63.

DRI2018004

Whole-rock lithogeochemistry, Sm-Nd isotope geochemistry, NORMAT alteration indices and normative mineral estimates, and thin section point count results for samples from the Tower Cu-Zn-Ag-Au deposit (part of NTS 63G14)

By C.G. Couëslan

Microsoft® Excel® file supplements:
Couëslan C.G. 2018: Geology of the Tower Cu-Zn-Ag-Au deposit, sub-Phanerozoic Superior boundary zone, central Manitoba (part of NTS 63G14); Manitoba Growth, Enterprise and Trade, Manitoba Geological Survey, Open File OF2018-4, 38 p.

Open Files

OF2018-1

Ice-flow history and till composition of the Southern Indian Lake area, north-central Manitoba (parts of NTS 64G1, 2, 7–10, 64B15)

by T.J. Hodder

OF2018-2

Gravity gradiometer survey of the Creighton area, Saskatchewan and Manitoba, parts of NTS 63-L/8 and 63-K/5

by O. Boulanger, F. Kiss and M. Coyle

Also released as Geological Survey of Canada Open File 8440 and Saskatchewan Geological Survey Open File 2018-7

OF2018-3

Till composition of a sampling transect in the Lynn Lake area, northwest Manitoba (parts of NTS 64B12, 64C9, 11, 12, 14–16, 64F3, 4)

by T.J. Hodder and M.S. Gauthier

OF2018-4

Geology of the Tower Cu-Zn-Ag-Au deposit, sub-Phanerozoic Superior boundary zone, central Manitoba (part of NTS 63G14)

by C.G. Couëslan

Preliminary Maps

PMAP2018-1

Sub-Phanerozoic geology of the south Wekusko Lake-Mitishto River area, eastern Flin Flon belt, west-central Manitoba (parts of NTS 63J5, 12 and 63K8, 9)

by K.D. Reid (scale 1:50 000)

PMAP2018-2

Bedrock geology of the Wekusko Lake pegmatite field (northeastern block), central Manitoba (part of NTS 63J13)

by D. Benn, T. Martins, R.L. Linnen, J. Ziehlke and J. Singh (scale 1:4 000)

EXTERNAL PUBLICATIONS

Armstrong, D.K., Nicolas, M.P.B., Hahn, K.E., Lavoie, D. 2018: Stratigraphic synthesis of the Hudson Platform in Manitoba, Ontario, and Nunavut: Ordovician-Silurian; Geological Survey of Canada, Open File 8378, 2018, 48 p., URL <https://doi.org/10.4095/308418> [November 2018].

Gauthier, M.S., Hodder, T.J., Ross, M. and Kelley, S.E. 2018: Glacial record of the southwestern Hudson Bay region and its significance for long-term ice sheet behaviour; CANQUA/AMQUA 2018, Ottawa, Ontario, August 7–11, 2018, poster presentation.

Guevara, V.E., Dragovic, B., Caddick, M.J., Couëslan, C.G., Kylander-Clark, A.K.C., Maclennan, S.A., Schoene, B. and Baxter, E.F. 2018: Ultrahigh temperature metamorphism of Archean continental crust: insights from the petrochronology arsenal; Geological Society of America, 53rd annual northeastern section meeting, Burlington, Vermont, March 18–20, 2018, paper no. 16-1, URL <https://gsa.confex.com/gsa/2018NE/meetingapp.cgi/Paper/310491> [May 2018].

Hollings, P.N., Baker, M.J., Orovan, E.A. and Rinne, M.L. 2018: A special issue devoted to porphyry and epithermal deposits of the Southwest Pacific: an introduction; Economic Geology, v. 113, p. 1–6.

Kelley, S.E., Gauthier, M.S. Ross, M. and Hodder, T.J. 2018: Laurentide ice margin retreat and marine incursion: a view from western Hudson Bay; CANQUA/AMQUA 2018, Ottawa, Ontario, August 7–11, 2018, oral presentation.

Kelley, S.E., Ross, M., Hodder, T.J., Gauthier, M.S., Elliott, B. and Normandeau, P. 2018: A mosaic of subglacial processes: examining the geological record of subglacial landscape evolution; Geological Society of America Annual Meeting, Indianapolis, Indiana, November 4–7, 2018, oral presentation.

Lawley, C.J.M., Schneider, D., Yang, E., Davis, W.J., Jackson, S.E., Yang, Z., Zhang, S. and Selby, D. 2018: Age relationships and preliminary U-Pb zircon geochronology results from the Lynn Lake greenstone belt; *in* Targeted Geoscience Initiative: 2017 report of activities, volume 1, N. Rogers (ed.), Geological Survey of Canada, Open File 8358, p. 133–137, URL <http://doi.org/10.4095/306459> [November 2018].

Rinne, M.L., Cooke, D.R., Harris, A.C., Finn, D.J., Allen, C.M., Heizler, M.T. and Creaser, R.A. 2018: Geology and geochronology of the Golpu porphyry and Wafi epithermal deposit, Morobe Province, Papua New Guinea; Economic Geology, v. 113, p. 271–294.

Ross, M., Trommelen, M.S., Hodder, T.J., Kelley, S.E., Scott, S. and Bustard, A. 2018: Pleistocene drumlins of the Canadian Shield and their implications for recently proposed theories of drumlin formation; International Sedimentological Congress, Québec City, Québec, August 13–17, 2018, oral presentation.

Yang, X.M., Drayson, D. and Polat, A. in press: S-type granites in the southwestern Superior Province: a marker of Archean terrane boundaries; Canadian Journal of Earth Sciences, URL <https://doi.org/10.1139/cjes-2018-0056> [November 2018].